New scalars at the origin of dark matter and anomalies in magnetic moments

PhD dissertation by

CARLOS FAUBEL ALAMÁ

under the supervision of

ARCADI SANTAMARIA I LUNA

JORGE VIDAL PERONA

JUAN ANDRÉS HERRERO GARCÍA

Programa de Doctorat en Física
Facultat de Física, Universitat de València

June, 2022

VNIVERSITAT DE VALÈNCIA Facultat de Física

Arcadi Santamaria i Luna, catedrático del Departamento de Física Teórica de la Universidad de Valencia,

Jorge Vidal Perona, catedrático del Departamento de Física Teórica de la Universidad de Valencia, y

Juan Andrés Herrero García, investigador distinguido (CIDEGENT) de la Universidad de Valencia

Certifican:

Que la presente memoria **"New scalars at the origin of dark matter and anomalies in magnetic moments"** ha sido realizada bajo su dirección en el Departamento de Física Teórica de la Universidad de Valencia por **Carlos Faubel Alamá**, y constituye su Tesis para optar al grado de Doctor en Ciencias Físicas.

Y para que así conste, en cumplimiento de la legislación vigente, presentan en el Departamento de Física Teórica de la Universidad de Valencia la referida Tesis doctoral, y firman el presente certificado.

Valencia, a 2 de Junio de 2022.

Fdo. : Arcadi Santamaria i Luna

Fdo. : Jorge Vidal Perona

Fdo. : Juan Andrés Herrero García

A la meua família

List of publications

This PhD thesis is based on the following publications:

- *Dark matter from a complex scalar singlet: the role of dark CP and other discrete symmetries* [1]
  L. Coito, C. Faubel, J. Herrero-Garcia and A. Santamaria
  JHEP **11** (2021) 202

- *Sterile neutrino portals to Majorana dark matter: effective operators and UV completions* [2]
  L. Coito, C. Faubel, J. Herrero-Garcia, A. Santamaria and A. Titov
  accepted for publication in JHEP

and the following contributions to proceedings:

- *Dark matter from a complex scalar singlet and the role of dark CP* [3]
  C. Faubel, L. Coito, J. Herrero-Garcia and A. Santamaria
  J. Phys. Conf. Ser. **2156** (2021) 012031

- *Dark matter from a complex scalar singlet and preservation of its stabilising symmetry* [4]
  L. Coito, C. Faubel, J. Herrero-Garcia and A. Santamaria
  PoS **PANIC2021** (2022) 055

Other works not included in this thesis:

- *Composite Higgs bosons from neutrino condensates in an inverted seesaw scenario* [5]
  L. Coito, C. Faubel and A. Santamaria
  Phys. Rev. D **101** (2020) 7, 075009

Abbreviations

The following abbreviations have been used throughout the text:

AMM	Anomalous magnetic moment
BBN	Big Bang Nucleosynthesis
BSM	Beyond the Standard Model
CC	Charged current
CKM	Cabbibo-Kobayashi-Maskawa matrix
DCP	Dark CP
DD	Direct detection
DM	Dark matter
EDM	Electric dipole moment
EFT	Effective Field Theory
EoM	Equation of motion
EW	Electroweak
FCNC	Flavour changing neutral current
FDM	Forbidden dark matter
ID	Indirect detection
LHC	Large Hadron Collider
LNC	Lepton number conserving
MDM	Magnetic dipole moment
NC	Neutral current

NP	New physics
PMNS	Pontecorvo-Maki-Nagakawa-Sakata matrix
pNGB	pseudo-Nambu-Goldstone boson
QCD	Quantum Chromodynamics
QED	Quantum Electrodynamics
QFT	Quantum field theory
SDM	Secluded dark matter
SM	Standard Model
SSB	Spontaneous symmetry breaking
VEV	Vacuum expectation value

Resum

En aquesta part anem a resumir breument la investigació realitzada en la tesi doctoral, començant pels objectius principals de la mateixa, seguint per la metodologia utilitzada i finalitzant amb les principals conclusions obtingudes. Bàsicament, la tesi doctoral consta de tres parts clarament diferenciades que sintetitzarem en les següents línies, així com la connexió que hem intentat establir entre aquestes.

A la Part I presentarem breument conceptes bàsics que seran d'utilitat al llarg del text. Concretament, al Capítol 1 introduirem el Model Estàndard, marc teòric emprat per tal de descriure els fenòmens relacionats amb la Física de partícules a altes energies. Encara que es puguen explicar una gran quantitat d'observacions experimentals, el Model Estàndard no pot ser considerat com la teoria "definitiva" ja que no proporciona cap solució a una sèrie de qüestions teòriques i experimentals, les quals presentarem també en aquest primer capítol. Entre aquestes, farem una breu discussió sobre les masses dels neutrins i els models que poden generar-les. Finalment, explicarem breument els conceptes bàsics que donen suport a les Teories de Camps Efectives, molt útils a l'hora de parametritzar els efectes que la (possible) Nova Física, present a escales energètiques inaccessibles per als experiments actuals com el Gran Col·lisionador d'Hadrons (LHC), puga tenir sobre els diferents observables.

La Part II està dedicada a una de les qüestions que fan pensar en l'existència de Nova Física més enllà del Model Estàndard: les actuals discrepàncies en el moment magnètic anòmal (MMA) dels leptons carregats,[1] concretament electrons i muons. Al Capítol 2 farem una breu revisió dels esdeveniments històrics que van portar a la introducció del concepte d'espí, i la seua relació amb el MMA. També repassarem les diferents contribucions del Model Estàndard al MMA dels leptons carregats, entre elles la provinent de l'Electrodinàmica Quàntica (QED) i el paper fonamental que té en aquesta la constant d'estructura fina, α. Al Capítol 3 estudiarem la contribució al MMA de l'electró d'un nou escalar lleuger, i analitzarem si la seua presència pot modificar l'extracció del valor d'α que s'obté a partir del MMA de l'electró. També considerarem els efectes de nous escalars i pseudoescalars que s'acoblen a leptons carregats com a possible explicació de les anomalies al MMA de l'electró i del muó.

En la Part III, el darrer bloc de treball de la tesi, ens centrarem en la Matèria Fosca,

[1] Entenem discrepàncies del MMA dels leptons carregats com la diferència entre el valor predit pel Model Estàndard i la seua mesura experimental.

una altra de les qüestions obertes dintre de la Física de partícules actual. Al Capítol 4 resumirem breument les evidències experimentals més importants que tenim de la seua presència, així com les seues propietats. Es ben conegut que un escalar neutre pot ser un possible candidat a Matèria Fosca si té les simetries adequades que el fan estable a escales cosmològiques. Es per això que, motivats també pels escalars introduïts a l'anterior part de la tesi, al Capítol 5 analitzarem el possible candidat a Matèria Fosca que s'obté a partir d'un singlet escalar complex, fent èmfasi en les simetries discretes que aquest posseeix i poden ser responsables de la seua estabilitat. Finalment, al Capítol 6 augmentarem la complexitat respecte al nombre de noves partícules, i analitzarem un fermió de Majorana, χ, com a candidat a Matèria Fosca que proporciona l'abundància de densitat relíquia observada gràcies a les seues aniquilacions en neutrins de quiralitat dextrogira, N, també anomenats neutrins estèrils. En aquest cas, considerarem escalars més pesats que als capítols anteriors i que serviran com a mediadors d'aquesta interacció. Primerament, abordarem el problema des d'un punt de vista completament independent de cap teoria, escrivint els operadors efectius de dimensió $D \leqslant 6$ que relacionen els nous fermions χ i N. Després, analitzarem els possibles models que donen lloc a aquests operadors efectius i farem ús del procediment conegut com *matching* per tal de connectar els paràmetres físics de la teoria a altes energies amb els coeficients dels operadors efectius que descriuen perfectament la teoria a baixes energies, concretament a energies menors que l'escala associada amb la Nova Física, en aquest cas els mediadors més pesats.

Finalment, a la Part IV presentarem els resultats obtinguts i les conclusions més important. Així mateix, proporcionarem una serie d'apèndixs amb els detalls de diferents càlculs realitzats durant aquesta tesi.

Punt de partida i objectius

El Model Estàndard és el marc teòric que descriu les partícules a nivell subatòmic, així com les seues interaccions. Aquesta es tracta d'una Teoria Quàntica de Camps basada en els principis de localitat, causalitat i renormalitzabilitat. A més, el Lagrangià que podem escriure en aquesta teoria que descriu les interaccions entre els diferents camps ha de ser invariant sota la simetria de Lorentz i la simetria local (també anomenada *gauge*) $\mathcal{G}_{\text{SM}} = SU(3)_c \times SU(2)_L \times U(1)_Y$. La simetria $SU(3)_c$ està associada a les forces de la Cromodinàmica Quàntica (QCD), mentre que $SU(2)_L \times U(1)_Y$ representa la interacció feble, sent Y la hipercàrrega. En principi, la simetria *gauge* impedeix que els mediadors de les forces electrofebles, els bosons gauge W i Z, tinguen massa. Però les evidències experimentals allà per la dècada dels 80 apuntaven a tot el contrari. Així, era necessari introduir un mecanisme que dotara de massa a aquestes partícules (i també a la resta). Finalment, R. Brout, F. Englert i P.W. Higgs van resoldre el problema mitjançant el conegut com mecanisme de Brout-Englert-Higgs, explicat breument a la Secció 1.1.1. Era necessari, però, introduir un nou camp que dotara de massa a la resta de partícules del Model Estàndard, el bosó de Higgs. Finalment, aquest va ser descobert al LHC l'any 2012, constituint un dels esde-

veniments històric més rellevants de la Física en aquest incipient segle XXI. Tornant a les interaccions mencionades anteriorment, quan el camp de Higgs adquireix un valor d'expectació al buit, la simetria es trenca espontàniament de la següent manera: $SU(3)_c$ associada a QCD roman inalterada mentre que $SU(2)_L \times U(1)_Y$ dona pas a QED, $U(1)_{\text{em}}$.

Com hem comentat anteriorment, el Model Estàndard proporciona una teoria robusta a l'hora d'explicar una gran quantitat de fenòmens físics que tenen lloc a altes energies. A més a més, permet reproduir tota una serie de resultats experimentals amb gran precisió. Una mostra d'aquest poder predictiu és el MMA de l'electró, un dels protagonistes d'aquesta tesi. Com veurem més endavant, el Model Estàndard prediu fins un total de 12 xifres significatives de la mesura experimental que s'obté d'aquest. No obstant això, existeixen algunes qüestions (teòriques i experimentals) que ens fan pensar en la necessitat d'introduir nous ingredients al Model Estàndard. Així, les proves experimentals més evidents de Física més enllà del Model Estàndard son:

- **Les masses dels neutrins.** Al Model Estàndard, els neutrins tenen massa zero, fet que entra en contradicció amb les evidències experimentals, i més concretament amb les oscil·lacions de neutrins. Seguint la mateixa lògica que per a la resta de fermions, al Model Estàndard es podria generar la massa dels neutrins introduint un company de quiralitat dextrogira, ν_R. Farem una breu discussió sobre mecanismes que generen massa per als neutrins a la Secció 1.3, on també presentarem les principals diferències entre fermions de Dirac i de Majorana. Saber si els neutrins son camps de Dirac o de Majorana continua sent una de les principals preguntes sense resposta de la Física actual.

- **Les anomalies relacionades amb el sabor.** Trobem diferents anomalies relacionades amb el sabor que podrien ser explicades amb Nova Física. Concretament, a la Part II analitzarem les discrepàncies en el MMA de l'electró i del muó. A banda d'aquestes anomalies relacionades amb el sabor, també hi ha d'altres que involucren la desintegració semi-leptònica de mesons B. Aquestes pareixen distingir entre els diferents sabors dels leptons (e, μ, τ), i les discrepàncies experimentals en diferents observables podrien ser explicades amb Nova Física.

- **Asimetria matèria-antimatèria.** El Model Estàndard prediu que la quantitat de matèria i antimatèria que es va crear a l'Univers primitiu era idèntica. No obstant, l'Univers en el que vivim està constituït per matèria (afortunadament per a nosaltres!), així que l'actual marc teòric s'ha de modificar.

- **Matèria Fosca i Energia Fosca.** D'acord amb les observacions cosmològiques, el Model Estàndard solament representa el 5% del contingut energètic de l'Univers. La resta es distribueix de la següent manera: un 26% correspon a l'anomenada Matèria Fosca, de caràcter no-bariònic i que no interacciona electromagnèticament; i un 69% en forma d'Energia Fosca, associada a l'expansió accelerada de l'Univers.

Respecte a la Matèria Fosca, repassarem breument les seues evidències experimental i propietats a la Secció 4.1, mentre que als Capítols 5 i 6 buscarem possibles candidats.

D'altra banda, els aspectes teòrics que fan pensar en Nova Física son:

- **El problema del sabor.** Per què hi ha tres famílies al Model Estàndard? Aquest marc teòric no dona cap resposta a esta simple pregunta, així com tampoc a l'estructura observada per a les masses o les mescles dels leptons i quarks. Tant les masses dels quarks i els leptons carregats com els elements de la matriu de mescla CKM presenten un patró molt jeràrquic. No ocorre el mateix amb les masses dels neutrins i la seua matriu de mescla PMNS, molt més anàrquiques. Referim ací a les Figures 1.2 i 1.3. El Model Estàndard no pot explicar les anterior particularitats relacionades amb al sabor, les quals constitueixen l'anomenat problema del sabor.

- **Problema fort de CP.** El grup de simetria del Model Estàndard permet afegir un terme del tipus $\theta\epsilon^{\mu\nu\rho\sigma}G_{\mu\nu}G_{\rho\sigma}$ que violaria CP. No obstant això, experimentalment no tenim evidències de tal fet. En particular, mesurant el moment dipolar elèctric del neutró s'obté que $\theta \lesssim 10^{-9}$. En principi, hom esperaria, basant-se en arguments anomenats de naturalitat, que els paràmetres del Lagrangià del Model Estàndard foren d'$\mathcal{O}(1)$, a no ser que estigueren protegits per alguna simetria. No es este el cas al Model Estàndard, que per tal de reproduir els resultats experimentals relacionats amb el moment dipolar elèctric del neutró hauria d'introduir aquest paràmetre θ molt xicotet.

- **El problema de les jerarquies.** La massa del bosó de Higgs és sensible a la (possible) presència de Nova Física a escales energètiques més elevades, Λ. Aquesta, a diferència de la dels fermions i els bosons gauge, no està protegida per cap simetria i podria rebre correccions que serien proporcionals a Λ^2. Per tant, assumint la presencia de Nova Física a altes energies, necessitaríem introduir de manera poc natural un gran ajust (*fine-tuning*) per tal de poder reproduir el valor observat de la massa del bosó de Higgs, $m_h \simeq 125\,\text{GeV}$. Cal remarcar, però, que aquest no és un problema com a tal del Model Estàndard, i més bé està associat a possibles efectes que la Nova Física produiria en ell.

- **Gran Unificació de les interaccions.** En Teoria Quàntica de Camps sabem que el valor dels acoblaments d'una determina teoria varia en funció de l'energia a la qual es mesuren (aquesta variació en funció de l'energia rep el nom de *running* de l'acoblament). Així, les Teories de Gran Unificació (GUT) busquen la unificació de les forces del Model Estàndard a altes energies. De fet, el *running* dels tres acoblaments de les interaccions del Model Estàndard apunta a un origen comú a escales $\sim 10^{15}\,\text{GeV}$. De manera similar al que ocorre amb les forces febles i electromagnètiques, es possible que esta nova escala d'unificació indique la presència de Nova Física. No obstant això, el Model Estàndard necessita de Nova Física entre les escales electrofebles i la de gran unificació per tal d'aconseguir una convergència perfecta dels acoblaments.

- **Gravetat.** Incloure la gravetat dintre del marc teòric del Model Estàndard és un dels majors problemes amb què els físic han hagut de barallar-se durant els darrers anys. La gravetat té associada una escala de Nova Física a energies $\sim 10^{19}$ GeV, l'escala de Planck. Hom pot parametritzar els seus efectes als observables utilitzant, com a primera aproximació, Teories de Camps Efectives. No obstant, aquest procediment serà solament vàlid en un determinat rang,[2] concretament a energies menors que l'escala de Planck. Així, a partir d'aquesta escala necessitarem una teoria completa de la gravetat quàntica, i el principal problema és que partint de Teoria Quàntica de Camps, intentar quantitzar la gravetat condueix a una teoria no renormalitzable.

Una vegada presentades diferents qüestions tant teòriques com experimentals que posen de manifest la necessitat de seguir escodrinyant més enllà del Model Estàndard, l'objectiu d'aquesta tesi serà tractar d'abordar dos d'aquests problemes. En particular, al Capítol 2 ens centrarem en el MMA dels leptons carregats, presentarem la seua estimació teòrica al Model Estàndard i els valors experimentals més recents, i podrem definir així les discrepàncies entre ambdues quantitats. Al Capítol 3 analitzarem els possibles efectes que un nou escalar lleuger que s'acoble a electrons pogués tenir sobre la determinació de la constant d'estructura fina a partir del MMA de l'electró. En la darrera part d'aquest capítol abordarem conjuntament les discrepàncies del MMA d'electrons i muons, estudiant l'espai de paràmetres associat a nous escalars i pseudoescalars que s'acoblen als leptons carregats i puguen explicar ambdues anomalies.

D'altra banda, els Capítols 5 i 6 estaran dirigits a la cerca d'un possible candidat a Matèria Fosca. En el primer d'aquests estudiarem com un singlet escalar complex pot generar un candidat a Matèria fosca, centrant-nos en les simetries discretes que pot tenir l'escalar i que podran ser responsables de l'estabilitat de la partícula de Matèria Fosca. Finalment, al darrer capítol analitzarem com un fermió de Majorana χ pot ser responsable de l'abundància de densitat relíquia observada gràcies a les seues aniquilacions en neutrins estèrils N. Aquest estudi estarà basat en Teories de Camps Efectives ja que assumirem que els nous mediadors entre els fermions χ i N són molt més massius que aquests.

Metodologia i conclusions

Tractarem de resumir a continuació la metodologia emprada i els principals resultats obtinguts en aquesta tesi doctoral. Com hem argumentat a l'inici del resum, el Model Estàndard necessita d'ingredients addicionals per tal d'explicar una sèrie de qüestions teòriques i experimentals que a dia de hui romanen sense resposta, entre elles les discrepàncies del MMA de l'electró i (especialment) del muó, i també la Matèria Fosca.

[2]Com discutirem a la Secció 1.4, cada Teoria de Camp Efectiva té associat un determinat rang de validesa.

D'una banda, al Capítol 2 hem repassat breument els esdeveniments històrics que conduïren al concepte de l'espí. Després, s'ha introduït el MMA dels leptons carregats, a_l. Concretament, hem analitzat les seus principals contribucions dintre del Model Estàndard, les quals es poden classificar en tres tipus en funció del seu origen. Així tenim, per ordre d'importància: i) la contribució de QED (involucra leptons carregats i fotons), ii) la contribució hadrònica o de QCD (involucra quarks o hadrons), i finalment la contribució electrofeble (involucra als bosons gauge, W i Z, i també al bosó de Higgs). S'ha fet especial èmfasi en el paper principal que juga la constant d'estructura fina en la determinació de la contribució que prové de QED, la qual es pot escriure com una sèrie de potències en α. Bàsicament, podem considerar la constant d'estructura fina com un paràmetre d'entrada per a la determinació teòrica al Model Estàndard del MMA dels leptons carregats. En el cas de l'electró, l'estimació teòrica a_e^{SM} i la seua incertesa estan dominades per la contribució de QED. No ocorre el mateix per als muons, on la contribució de QCD domina la incertesa de l'estimació teòrica a_μ^{SM}. Cal remarcar que la contribució hadrònica no es pot calcular pertorbativament, i son necessàries tècniques complexes que inclouen *lattice* QCD, analitzades actualment amb molt de detall per tal de veure si poden ser la clau per tal d'entendre millor la discrepància del MMA del muó.

Encara al Capítol 2, hem analitzat les discrepàncies en el MMA de l'electró i del muó, i la seua relació amb el valor de la constant d'estructura fina que s'utilitza per tal d'obtindre les estimacions teòriques al Model Estàndard. De fet, si prenem l'última mesura experimental d'α obtinguda pel grup de treball del Laboratoire Kastler Brossel (LKB) utilitzant atoms de rubidi, veure $\alpha_{\mathrm{Rb}}^{(\mathrm{LKB},\,2020)}$ a la Taula 2.2, la discrepància del MMA de l'electró es situa en $\Delta a_e = (0.48 \pm 0.30) \times 10^{-12}$, al nivell de $1.6\,\sigma$. El signe positiu d'aquest valor ens ha motivat per tal d'analitzar l'impacte de nous escalars (lleugers), ρ, que s'acoblen als electrons i donen contribucions rellevants al MMA. Com ja hem comentat anteriorment, la constant d'estructura fina serveix com a paràmetre d'entrada per a la determinació teòrica dels MMAs. No obstant això, podem plantejar-nos el problema a la inversa, i obtindre un valor per a la constant d'estructura fina a partir del MMA de l'electró. Situant-nos en aquest darrer escenari, al Capítol 3 hem estudiat com de robusta pot ser l'extracció d'α assumint nous escalars que s'acoblen a electrons. Després d'imposar diferents restriccions experimentals sobre l'acoblament de l'escalar a l'electró, h_e, hem conclòs que hi ha dues regions de l'espai de paràmetres dels escalars que poden ser rellevants en el sentit de que la presència d'aquests podria afectar al valor extret de la constant d'estructura fina a partir del MMA de l'electró. Concretament, acoblaments en l'interval $10^{-4} \lesssim h_e \lesssim 10^{-2}$ per masses m_ρ entre 1 i 60 MeV, i acoblaments $h_e \gtrsim 0.2$ per $m_\rho > 100\,\mathrm{GeV}$. Així, serà important comprovar si futurs experiments poden testar aquestes regions d'interés. Si s'aconseguira "tancar" completament l'espai de paràmetres que mostrem a la part inferior de la Figura 3.2, hom podria concloure que l'extracció de la constant d'estructura fina a partir del MMA de l'electró és robusta, en el sentit de que nous escalars que s'acoblen a electrons no podrien modificar l'extracció d'α.

A l'última part del Capítol 3, però, hem utilitzat el valor de la constant d'estructura fina mesurat pel grup de Berkeley utilitzant atoms de cesi, veure $\alpha_{\mathrm{Cs}}^{(\mathrm{Berkeley},\,2018)}$ a la

Taula 2.2, a partir del qual s'obté $\Delta a_e = -(0.88 \pm 0.36) \times 10^{-12}$, al nivell de $-2.4\,\sigma$. En aquesta part hem decidit adoptar aquest valor per a la discrepància del MMA de l'electró, ja que la darrera mesura d'α obtinguda pel LKB no acabava de ser consistent amb mesures anteriors realitzades pel mateix grup experimental, veure per exemple el valor i les barres d'error dels punts en color blau a la Figura 2.3, i també $\alpha_{\rm Rb}^{(2010)}$ i $\alpha_{\rm Rb}^{(2020)}$ a la Taula 2.2. Així, hem estudiat l'espai de paràmetres associat a nous escalars (ρ) i pseudoescalars (θ) que s'acoblen a leptons carregats i poden explicar simultàniament les discrepàncies del MMA de l'electró i del muó. Primerament, hem considerat que aquesta Nova Física genera contribucions als MMAs a un *loop*, i hem obtingut que ambdues anomalies es poden explicar per masses m_ρ i m_θ entre 10 i 100 MeV, i acoblaments $h_e \sim \mathcal{O}(10^{-4})$ i $h_\mu \sim \mathcal{O}(10^{-3})$, veure per exemple la Figura 3.6. Seguidament, hem considerat que el MMA de l'electró també podia rebre contribucions a dos *loops* (solament tenint en compte al leptó tau dintre del loop), i hem conclòs que l'espai de paràmetres on es possible explicar ambdues anomalies s'amplia considerablement a regions de masses i acoblaments més altes, veure per exemple la Figure 3.9.

D'altra banda, resumirem a continuació els resultats obtinguts a la Part III relacionada amb possibles candidats a Matèria Fosca. Al Capítol 4 hem revisat breument les seues evidències experimentals i propietats principals. Es ben conegut que escalars neutres poden ser candidats a Matèria Fosca si tenen les simetries adequades per tal de previndre la seua desintegració. Així, i motivats pel treball relacionat amb nous escalars a la Part II de la tesi, al Capítol 5 hem analitzat el possible candidat a Matèria Fosca que s'obté a partir d'un singlet escalar complex. Hem considerat que aquest posseeix una simetria global $U(1)$ que es trenca tant explícita com espontàniament. En aquest escenari, es genera un pNGB que resulta ser un bon candidat a Matèria Fosca. A més a més, els termes de ruptura explícita del Lagrangià han de preservar la simetria discreta que hem anomenat *dark* CP (DCP), responsable de l'estabilitat de la partícula de Matèria Fosca. En la primera part del capítol hem analitzat les possibles simetries discretes que pot tenir un escalar complex. Després, hem considerat diferents models amb un sol terme de ruptura explícita de simetria al Lagrangià, els quals hem anomenat *models mínims*. Concretament, hem estudiat quatre models (lineal, quadràtic, cubic i quàrtic) motivats, o bé per incloure el terme de ruptura més *soft*, o bé per preservar diferents simetries discretes, en particular $\mathcal{Z}_2$, $\mathcal{Z}_3$ i $\mathcal{Z}_4$ per al model quadràtic, cubic i quàrtic, respectivament. Així mateix, tots aquests models preserven la simetria DCP.

Des d'un punt de vista fenomenològic, els *models mínims* es caracteritzen per quatre paràmetres: les masses de la part real i imaginària de l'escalar complex, m_ρ i m_θ, l'angle de mescla entre la part real de l'escalar complex i el bosó de Higgs, s_α, i el valor d'expectació al buit de l'escalar complex, v_s. Cal remarcar que el candidat a Matèria Fosca, dictat per la simetria DCP, és la part imaginària de l'escalar complex, θ. La regió de paràmetres on podem reproduir l'abundància de densitat relíquia s'amplia considerablement si la comparem amb models on solament introduïm un singlet escalar real. Concretament, hem obtingut l'abundància de densitat relíquia observada als següents canals d'aniquilació: i) a la resonancia del bosó de Higgs, h, i/o del ρ, ii) FDM (de l'anglés *forbidden dark matter*), on els parells h i/o ρ a l'estat final son

lleugerament més pesats que les partícules de Matèria Fosca, i iii) aniquilacions a parells h i/o ρ més lleugers. El cas $m_\theta \gtrsim m_\rho$ és un exemple de SDM (de l'anglés *secluded dark matter*). Els diagrames de Feynman corresponents als canals d'aniquilació de Matèria Fosca esmentats anteriorment es poden veure representats a la Figura 5.2.

Seguint amb la fenomenologia dels *models mínims*, i després de l'anàlisi numèric realitzat, concloem que aquests es poden diferenciar si s'observara un senyal en experiments de detecció directa de Matèria Fosca. Així mateix, si s'obtinguera el valor de la massa de la partícula de Matèria Fosca (per exemple, gràcies a l'observació d'una línia de raigs gamma en experiments de detecció indirecta) es podria tractar de conéixer la simetria que hi ha darrere del model en qüestió.

Més enllà dels *models mínims*, hem analitzat també l'escenari en el qual s'introdueix al Lagrangià més d'un terme de ruptura explícita de simetria. En aquest cas, s'ha de continuar demanant que la DCP es preserve després de la ruptura espontània de simetria, la qual cosa genera una sèrie de condicions sobre totes les possibles combinacions per parells de termes de ruptura explícita de simetria que defineixen cadascun dels *models mínims*. Hem conclòs que, prendre dos termes de ruptura explícita de simetria al Lagrangià bàsicament amplia l'espai de paràmetres permés, "omplint-se" la regió intermedia que hi ha entre les regions de paràmetres permeses per cadascun dels *models mínims*.

En la darrera part del Capítol 5 hem considerat que el terme de ruptura explícita de simetria dels *models mínims* és molt menor que l'escala de ruptura espontània de simetria de $U(1)$, v_s. En aquest cas, es pot fer ús de la Teoria de Camps Efectiva i integrar de l'espectre de partícules l'escalar més massiu, ρ. D'aquesta manera, hem obtingut un Lagrangià efectiu que conté el terme d'interacció del Higgs amb la Matèria Fosca, l'anomenat *Higgs portal*, i també un nou *Higgs portal* però derivatiu.

Finalment, al Capítol 6 hem analitzat la fenomenologia relacionada amb la Matèria Fosca partint del Model Estàndard al qual afegim un nou neutrí de quiralitat dextrogira (neutrí estèril), N_R, i un fermió de Majorana, χ, carregat sota una simetria discreta $\mathcal{Z}_2$, la qual permet que no es desintegre i puga ser un bon candidat de Matèria Fosca. L'abundància de densitat relíquia s'obté mitjançant el mecanisme usual de *freeze-out* del χ, gràcies a les aniquilacions $\chi\chi \to NN$. En la primera part del capítol hem estudiat els possibles operadors de quatre fermions que relacionen la partícula de Matèria Fosca i els neutrins estèrils, als quals hem anomenat *portal operators*: l'operador $\mathcal{O}_1$ preserva número leptònic, mentre que els operadors $\mathcal{O}_2$ i $\mathcal{O}_3$ el preservaran o no en funció de com assignem el número leptònic als nous fermions. Referim ací a la Taula 6.1 amb les definicions del operadors. Cal remarcar que per a $\mathcal{O}_1$, la part de la secció eficaç d'aniquilació de Matèria Fosca corresponent a l'ona s és proporcional a m_N^2, i per tant estarà suprimida per a masses xicotetes del neutrí estèril.

Després de presentar els tres operadors efectius, hem estudiat els possibles models a altes energies que generen els *portal operators*, classificant-los en funció del canal que domina la secció eficaç d'aniquilació de Matèria Fosca. En concret, als Models A el mediador pesat és un escalar real o complex, carregat sota la simetria $\mathcal{Z}_2$, i que es propaga al canal t. Contràriament, als Models B i C els mediadors pesats son escalars reals o complexos i també bosons vectorials, els quals es propaguen al canal s. Dintre

de cada categoria, A, B i C, hem considerat diferents casos. Per exemple, al Model A2a, $m_N = 0$ i els neutrins lleugers son de Dirac. A més, la secció eficaç d'aniquilació de Matèria fosca rep majoritàriament contribució de l'ona p, i es poden evitar les restriccions experimentals de detecció indirecta d'aniquilacions de la Matèria Fosca. Aquest model, encara que molt difícil de validar experimentalment degut a que els neutrins son de Dirac i els senyals de detecció directa i indirecta estaran suprimits, és interessant ja que podria generar candidats de Matèria Fosca tèrmica lleugers, $m_\chi \sim \mathcal{O}(100)$ MeV. D'altra banda, els Models A2b i A2c contenen un escalar complex, σ, però el primer d'ells té un terme de massa de Majorana per als neutrins estèrils que viola en dos unitats el número leptònic. Per contra, el segon model té $m_N = 0$, i el número leptònic es viola *softly* per el terme $\mu_\sigma^2 \sigma^2$ al Lagrangià. Aquest model té com a peculiaritat que es genera la massa dels neutrins estèrils de manera radiativa. Finalment, el Model B2 (C2) conté un escalar complex que adquireix un valor d'expectació al buit que trenca espontàniament la simetria global (local) $U(1)_{B-L}$ del Lagrangià en dos unitats.

Per a tots els possibles models que poden generar els operadors efectius $\mathcal{O}_{1,2,3}$ hem detallat en diferents apèndixs el càlcul de les condicions de *matching*. En concret, hem anomenat als Models A1 i A2 com a *genuïns* ja que solament generen els *portal operators*, però la resta de models estudiats produeixen més operadors de dimensió $D \leqslant 6$, veure les Taules 6.1 i 6.3 per a la definició de tots els operadors i els operadors generats en cadascun del models, respectivament.

Pel que fa a la fenomenologia associada a la Matèria Fosca, en l'última part del Capítol 6 ens hem centrat en els Models A2b, A2c i B1 amb acoblaments (entre els fermions χ i N, i els mediadors) reals i imaginaris. Al Model A2b (A2c) es pot reproduir l'abundància de densitat relíquia observada per masses m_χ entre 100 i 300 (800) GeV. Cal remarcar que al Model A2c la massa dels neutrins estèrils generada radiativament està fixada en termes de la resta de paràmetres del model, i la regió de l'espai de paràmetres on es reprodueix l'abundància de densitat relíquia correspon a m_N entre 2 i 10 GeV. Al Model B1, la secció eficaç d'aniquilació de Matèria Fosca rep majoritàriament contribució de l'ona p quan l'acoblament de la partícula de Matèria Fosca a l'escalar que actua com a mediador és real. En este cas, les restriccions que provenen d'experiments de detecció indirecta és poden evitar, i l'abundància de densitat relíquia observada s'obté per masses m_χ entre 2 GeV i 10 TeV. Per contra, quan l'acoblament és imaginari, la secció eficaç d'aniquilació de Matèria Fosca rep contribució de l'ona s, i l'abundància de densitat relíquia observada es reprodueix per masses m_χ entre 30 GeV i 50 TeV.

En resum, nous escalars neutres, com els que han sigut analitzats en aquesta tesi doctoral, poden explicar les discrepàncies als MMAs dels leptons carregats així com també proporcionar un possible candidat a Matèria Fosca. Per tant, serà interessant considerar escenaris més general en què aquests puguen explicar simultàniament ambdues qüestions (així com també intentar explicar la massa dels neutrins actius).

Overview

In the next paragraphs we will present the main goals of this doctoral thesis, and will try to guide the reader through the concepts that will be discussed in what follows. Basically, we have focused on two topics: the interplay between neutral scalars and the anomalous magnetic moment (AMM) of charged leptons, and dark matter (DM). Let us begin by summarising the full structure of the thesis, which is basically divided into four parts, namely:

- **Part I: Introductory concepts.** In Chapter 1, we will briefly review the construction and main ingredients of the Standard Model (SM) of particle physics. Despite the fact that its predictions have been tested with a great accuracy, see *e.g.* the electron AMM, computed at the level of parts-per-billion (ppb), there are still several open questions that call for solutions beyond the SM (BSM). Therefore, we will motivate the need for new physics (NP) presenting the most relevant unsolved problems in the theoretical framework of the SM, including a brief review on neutrino masses in the last part of the chapter.

  If NP involves energy scales much larger than the current energy thresholds reached at the high-energy particle colliders such as the Large Hadron Collider (LHC), one important tool for parameterising its effects on experimental observables are effective field theories (EFTs), which will also be revisited in the last part of Chapter 1.

- **Part II: Anomalous Magnetic Moments of charged leptons.** In this part, we will give an introduction to the AMM of charged leptons. In particular, we will start with a historical review of the events that led to the concept of spin in the first section of Chapter 2. After this, we will analyse the AMM of charged leptons, focusing on its different contributions in the SM. Namely, it gets corrections from Quantum Electrodynamics (QED), Electroweak (EW) theory and Quantum Chromodynamics (QCD) or hadronic corrections. We will also present the current values of the SM prediction and the experimental measurements of the AMM of charged leptons. Related to this, the last measurement of the fine-structure constant leads to discrepancies[3] at the level of $1.6\,\sigma$ and $4.2\,\sigma$ for elec-

[3] Discrepancy should be understood as the difference between the theoretical prediction and the measured value.

tron and muon AMM, respectively. For the latter (and also for both anomalies), we will review possible explanations that are available in the literature.

After the discussion about the discrepancies, we will focus on the electron AMM in Chapter 3, and how the presence of NP, in particular light neutral scalars, can pollute the extraction of the fine-structure constant from the electron AMM. We will revisit experimental bounds that constrain the parameter space of the NP, *i.e.* its coupling to electrons and its mass. Moreover, in the last section of the chapter, we will analyse the parameter space of new scalars and pseudo-scalars that couple to charged leptons and are able to reproduce the observed discrepancies in both the electron and the muon AMM.

- **Part III: Scalars in Dark Matter scenarios.** In this part, we will study the other important topic of the thesis, DM. First, we will motivate the need for DM and present its main properties in Chapter 4.

  Encouraged by the analysis of light neutral scalars in the framework of the AMM, in Chapter 5 we will investigate the possibilities of obtaining a suitable DM candidate from a complex scalar singlet. By doing so, we will analyse the possible discrete symmetries the complex scalar should have for yielding a good (stable) DM candidate. This will provide us with several scenarios (which will be referred to as *minimal models*) that will be discussed in detail. In addition, we will apply the EFT approach in the last part of the chapter, where the radial part of the complex scalar will be integrated out, yielding a pseudo-Nambu-Goldstone boson (pNGB) DM candidate.

  Following with the connection between neutral scalars and DM, in Chapter 6 we will analyse a Majorana DM candidate that yields the correct relic abundance thanks to its annihilations into right-handed neutrinos (sterile neutrinos). In this scenario, scalars will play the role of mediators between the dark sector and sterile neutrinos, but contrary to the case of light scalars analysed in the context of AMM, here we will consider heavy scalars, whose effects will be parameterised by means of EFTs. In particular, we will list all the possible four-fermion operators at dimension six that describe the interactions between the DM candidate and sterile neutrinos, and will discuss their UV completions. We will find several UV models in which the mediators of the interactions are scalars and vector bosons. In addition, we will provide details of the matching for the considered models in dedicated appendices. Finally, we will analyse the phenomenology of the most promising UV models. In particular, one of them will generate a Majorana mass for sterile neutrinos at one loop, which will also be discussed in a dedicated appendix.

- **Part IV: Final remarks and conclusions.** In this part, we will summarise the interpretation of the results from the different chapters of the thesis and the conclusions that can be extracted from them. As has been mentioned in the previous paragraphs, we will give details of the relevant calculations in several appendices.

Contents

Part I

Introductory concepts

CHAPTER 1

A short review of the Standard Model and beyond

In the present chapter, we introduce the main ingredients of the Standard Model (SM) and present some of its relevant features, which explain to a high degree of accuracy almost the full phenomenology of the known interactions in particle physics. However, as we will also discuss, there are several open problems that point us to discard the idea of accepting the SM as the "final" theory: new physics (NP) is needed.

In particular, we review the construction of the SM, describe the mechanism that generates particle masses and discuss the SM flavour structure. In addition, we summarise the possible hints of physics Beyond the Standard Model (BSM). Moreover, in this introductory part we will fix the notation for the SM fields.

We also briefly discuss on neutrino masses and review some models that can account for them. Finally, we present the basic concepts behind effective field theories (EFTs). The EFT approach will be useful for deriving some of the relevant results that will be presented in the next chapters of the thesis.

1.1 Elements of the Standard Model: its Lagrangian and particle content

The SM is a quantum field theory (QFT) that basically encodes all our current knowledge of modern particle physics. It successfully describes the electromagnetic, the weak and the strong interactions of the zoo of particles that, since the 20th century, have been predicted and discovered by the physicists through experimental observations at particle colliders such as the Large Hadron Collider (LHC). We refer the reader to the original work leading to the consolidation of the SM in Refs. [6–17], together with modern reviews in [18, 19].

As we have already mentioned, the SM is a QFT which is rooted on the principles of locality, causality and renormalisability. Moreover, it is based on the invariance under the gauge group $\mathcal{G}_{\rm SM} = SU(3)_c \times SU(2)_L \times U(1)_Y$. The interactions are mediated

by the well-known gauge bosons of the SM. These are:

- **i)** Eight massless gluons, G^a_μ, responsible of mediating the strong interactions or Quantum Chromodynamics (QCD), based on the $SU(3)_c$ gauge group, with the associated strong coupling constant g_s.
- **ii)** Three massive gauge bosons, mediators of the weak interactions, which are the neutral Z_μ and the charged $W^\pm_\mu$ gauge bosons.
- **iii)** The massless photon, A_μ, associated with the electromagnetic interaction.

In the SM, the mediators listed in ii) and iii) are generated by the product group $SU(2)_L \times U(1)_Y$, known as the Electroweak (EW) symmetry. The weak and the electromagnetic forces are then unified, and the associated couplings of the $SU(2)_L$ and $U(1)_Y$ interactions are the g and the g', respectively.

Another ingredient of the SM which constitutes the observed matter content in the Universe are the fermions, which we summarise in Table 1.1 together with the Higgs field, ϕ, and their representations under the SM gauge group $\mathcal{G}_{\rm SM}$. There are three different copies (the so called families or flavours) for the quarks and leptons, denoted by Q and l, respectively, although we only include one family in the table. For completeness, we also present the usual notation for the three different families of leptons and quarks, namely:

$$e = \begin{pmatrix} e \\ \mu \\ \tau \end{pmatrix}, \quad \nu = \begin{pmatrix} \nu_e \\ \nu_\mu \\ \nu_\tau \end{pmatrix}, \quad u = \begin{pmatrix} u \\ c \\ t \end{pmatrix}, \quad d = \begin{pmatrix} d \\ s \\ b \end{pmatrix}. \tag{1.1}$$

Notice also that the only difference among the flavours are their Yukawa interactions, whereas they have the same gauge interactions.

Once we have introduced the SM fermions, one can write its free Lagrangian like

$$\mathcal{L}_f = \sum_\alpha \overline{\psi}^\alpha i \not{\partial} \psi_\alpha \,, \tag{1.2}$$

where we use the notation $\psi_\alpha = (l, e_R, Q, u_R, d_R)$. Of course, this Lagrangian is invariant under the global $SU(3)_c \times SU(2)_L \times U(1)_Y$, but we need to promote the derivative in Equation (1.2) to a covariant derivative in order to get a Lagrangian interaction which is invariant under local transformations.

This covariant derivate, which is fixed by the symmetry transformation, when acting on a field takes into account the transformation properties of that field under the SM gauge group. For a general field with hypercharge Y and non-trivially transformations under $SU(3)_c$ and $SU(2)_L$, the covariant derivative has the following form:[1]

$$D_\mu = \partial_\mu - i g_s \frac{\lambda_a}{2} G^a_\mu - i g T_a W^a_\mu - i g' Y B_\mu \,, \tag{1.3}$$

[1] See the transformation properties of the particle content of the SM under $SU(3)_c \times SU(2)_L \times U(1)_Y$ in Table 1.1.

	$l = \begin{pmatrix} \nu_L \\ e_L \end{pmatrix}$	e_R	$Q = \begin{pmatrix} u_L \\ d_L \end{pmatrix}$	u_R	d_R	ϕ
$SU(3)_c$	1	1	3	3	3	1
$SU(2)_L$	2	1	2	1	1	2
$U(1)_Y$	$-1/2$	-1	$+1/6$	$+2/3$	$-1/3$	$+1/2$

Table 1.1: *The SM matter content including the Higgs field, ϕ, and their gauge transformations. The chirality of the fields is denoted by L and R, where $\psi_L = \frac{1}{2}(1-\gamma_5)\psi$ and $\psi_R = \frac{1}{2}(1+\gamma_5)\psi$. The $SU(2)_L$ is called the weak isospin T. The SM left-handed doublets, l and Q, have isospin $1/2$, and the third component is $T_3 = +(-)1/2$ for the up (down) components of the doublet. The right-handed components of the SM fermions, which are singlets, do not transform under $SU(2)_L$. Finally, the hypercharge is $Y = Q - T_3$, where Q has to be identified now with the electric charge.*

where T_a and $\lambda_a/2$ are the generators of $SU(2)_L$ and $SU(3)_c$, respectively. For SM $SU(2)_L$ doublets $T_a = \sigma_a/2$. Here, σ_a with $a = 1,2,3$, are the Pauli matrices. On the other hand, λ_a with $a = 1,...,8$ are the Gell-Mann matrices.

So far, we have presented the gauge bosons and the fermions of the SM, together with the form of the covariant derivative that yields an interaction Lagrangian which is invariant under local $SU(3)_c \times SU(2)_L \times U(1)_Y$. We also need to include the kinetic terms for the gauge bosons, so they can freely propagate as a field, which are

$$\mathcal{L}^{\text{kin}}_{\text{gauge}} = -\frac{1}{4} G^a_{\mu\nu} G^{\mu\nu}_a - \frac{1}{4} W^a_{\mu\nu} W^{\mu\nu}_a - \frac{1}{4} B_{\mu\nu} B^{\mu\nu} \,. \tag{1.4}$$

Here, the field strength tensors are given by

$$G^a_{\mu\nu} = \partial_\mu G^a_\nu - \partial_\nu G^a_\mu + g_s f^{abc} G^b_\mu G^c_\nu \,, \tag{1.5}$$

$$W^a_{\mu\nu} = \partial_\mu W^a_\nu - \partial_\nu W^a_\mu + g \epsilon^{abc} W^b_\mu W^c_\nu \,, \tag{1.6}$$

$$B_{\mu\nu} = \partial_\mu B_\nu - \partial_\nu B_\mu \,, \tag{1.7}$$

with the structure constants of $SU(3)_c$ and $SU(2)_L$ defined by f^{abc} and ϵ^{abc}, respectively. The generators of the symmetry groups $SU(3)_c$ and $SU(2)_L$ obey the following relations:

$$\left[\frac{\lambda^a}{2}, \frac{\lambda^b}{2}\right] = i f^{abc} \frac{\lambda^c}{2} \quad \text{and} \quad \left[T^a, T^b\right] = i \epsilon^{abc} T^c \,. \tag{1.8}$$

Moreover, the kinetic terms for the fermions are given by Equation (1.2) after replacing the derivative by the covariant derivative given in Equation (1.3). Therefore, they read

$$\mathcal{L}^{\text{kin}}_{\text{fermions}} = \sum_\alpha \overline{\psi}^\alpha i \not{D} \psi_\alpha \,. \tag{1.9}$$

It is interesting to note that, when we take the covariant derivative in Equation (1.2), interactions among the gauge and the fermion fields are generated. In addition, the

kinetic terms for the gauge bosons in Equation (1.4) generate self-interactions due to the non-abelian nature of the $SU(2)_L$ and $SU(3)_c$ symmetry groups. The strength of these interactions is given by the gauge couplings g_s, g and g'.

Finally, due to the gauge symmetry principles, we can not explicitly write mass terms for the gauge bosons and the fermions in the SM. However, as pointed out by experimental observations, we need somehow a mechanism that could allow us to give masses to the SM content without spoiling the renormalisability of the theory. We review this procedure in the following section.

1.1.1 The Brout-Englert-Higgs mechanism

As we have already mentioned, the Lagrangian including the pieces $\mathcal{L}^{\text{kin}}_{\text{gauge}}$ and $\mathcal{L}^{\text{kin}}_{\text{fermions}}$ given in Equations (1.4) and (1.9) is not able to account for the mass terms of bosons and fermions due to gauge invariance of the symmetry group. However, this problem was solved by R. Brout, F. Englert and P.W. Higgs by means of the so called Brout-Englert-Higgs mechanism [7, 8].

This mechanism introduces a complex scalar doublet under $SU(2)_L$, $\phi = (\phi^+, \phi^0)^T$, and the process of generating mass to the fermions and the gauge bosons in the SM is achieved via spontaneous symmetry breaking (SSB) of the EW symmetry. The most general renormalisable Lagrangian for the Higgs field is:

$$\mathcal{L}_{\text{Higgs}} = \left(D_\mu \phi\right)^\dagger D^\mu \phi - V(\phi)\,, \tag{1.10}$$

where the scalar potential is given by

$$V(\phi) = \mu^2(\phi^\dagger \phi) + \lambda(\phi^\dagger \phi)^2\,. \tag{1.11}$$

The covariant derivative defined in Equation (1.3) guarantees that the Lagrangian is locally invariant under the SM gauge group $SU(3)_c \times SU(2)_L \times U(1)_Y$, and acting on the Higgs field yields[2]

$$D_\mu \phi = \left(\partial_\mu - ig\frac{\sigma^a}{2}W^a_\mu - ig'\frac{1}{2}B_\mu\right)\phi\,. \tag{1.12}$$

Moreover, one needs to minimise the scalar potential for the Higgs field in Equation (1.11) in order to find the minimum of the theory and do perturbations around it. This is done by means of

$$\frac{\partial V}{\partial \phi}\Big|_{\phi=\langle\phi\rangle} = 0\,. \tag{1.13}$$

We denote by $\langle\phi\rangle = |\langle 0|\phi|0\rangle|$ the vacuum expectation value (VEV) of the Higgs field, which is defined by $\langle\phi\rangle \equiv v/\sqrt{2}$. Depending on the sign of the μ^2 term in the scalar potential in Equation (1.11), we can get different scenarios. However, we are

[2]Remember that we are using the convention for the hypercharge $Y = Q - T_3$, where Q is the electric charged and T_3 the third component of isospin.

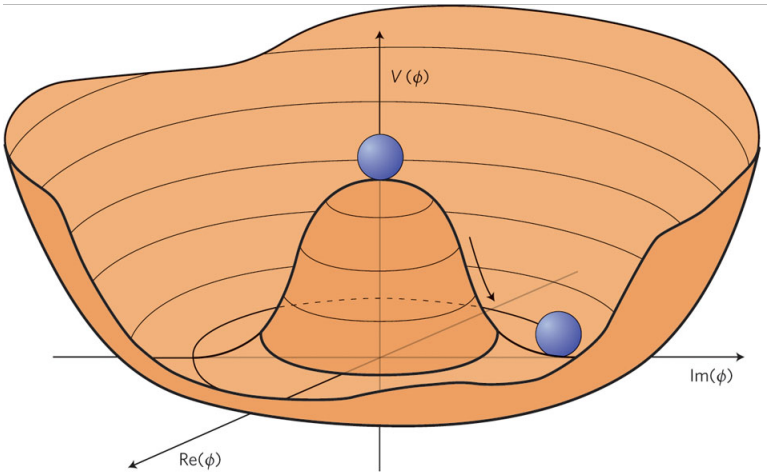

Figure 1.1: *Higgs potential for $\mu^2 < 0$. There is a set of degenerate vacua related to the would-be Goldstone bosons. The Higgs boson is associated to an excitation in the radial direction.*

interested in the case where $\mu^2 < 0$ and the scalar potential has the Mexican-hat type form shown in Figure 1.1.[3] Then, in this particular case, we have two extrema

$$v = 0\,, \quad v = \sqrt{\frac{-\mu^2}{\lambda}}\,. \tag{1.14}$$

In addition, we have to take into account that the potential should be bounded from below, which translates into the condition for the Higgs quartic coupling $\lambda > 0$. Keeping that in mind, and looking at the form of the potential in Figure 1.1, we can clearly see that $v = 0$, which corresponds to $\phi = 0$, is a local maximum, whereas $v = \sqrt{-\mu^2/\lambda}$ is a global minimum. Moreover, it can be seen that there is an infinite number of degenerate vacua, all of them with identical properties. The main point here is that, when we choose one of them, there is a SSB of the EW symmetry

$$SU(2)_L \times U(1)_Y \xrightarrow{\text{SSB}} U(1)_{\text{em}}\,, \tag{1.15}$$

being the unbroken $U(1)$ associated with the symmetry related to the electromagnetic force. Moreover, from the Goldstone theorem [20] we know that whenever we have a continuous global symmetry which is spontaneously broken, a set of massless bosons (Goldstone bosons), one for each of the broken generators, appears as a consequence of the breaking of the symmetry. If the broken symmetry is a gauge symmetry, the Goldstone bosons are absorbed or "eaten" by the gauge fields and become the longitudinal components of these fields. This is how these gauge bosons obtain a mass.

Once we have analysed the minimum of the scalar potential, we can parameterise

[3] For $\mu^2 > 0$ we just get one extremum at $v = 0$ after minimising the scalar potential by means of Equation (1.13).

the Higgs field as an excitation around the minimum as

$$\phi(x) = \frac{1}{\sqrt{2}} e^{i\sigma^a \theta^a(x)/(2v)} \begin{pmatrix} 0 \\ v + H(x) \end{pmatrix}, \tag{1.16}$$

where $a = 1, 2, 3$. The θ^a, isolated in the exponential, are the would-be Goldstone bosons, which become the longitudinal part of the massive gauge bosons, *i.e.* the Z and the W. The Goldstone bosons θ^a can be eliminated performing a rotation using the local $SU(2)_L$ invariance. This specific rotation is equivalent to the choice of the so-called unitary gauge. In addition, H will be identified with the Higgs boson.

Now, we can substitute back the expression for the Higgs field in Equation (1.16) in the Lagrangian given in Equation (1.10), focusing on the term with the covariant derivatives, which is responsible for generating the masses of the gauge bosons. On the one hand, the physical W boson, which appears as a linear combination of the ones that were introduced in Equation (1.3) as $W^{\pm} \equiv (W_1 \mp iW_2)/\sqrt{2}$, has a mass given by $m_W^2 = g^2 v^2/4$.

On the other hand, in the case of the Z boson, there is mixing between B_μ and W_μ^3. The related mixing matrix reads:

$$\frac{v^2}{4} \begin{pmatrix} W_\mu^3 & B_\mu \end{pmatrix} \begin{pmatrix} g^2 & -g\,g' \\ -g\,g' & g'^2 \end{pmatrix} \begin{pmatrix} W^{3,\mu} \\ B^\mu \end{pmatrix}. \tag{1.17}$$

In order to obtain the physical masses of the gauge bosons, we have to diagonalise this mixing matrix by means of the rotation

$$\begin{pmatrix} W_\mu^3 \\ B_\mu \end{pmatrix} = \begin{pmatrix} \cos\theta_W & \sin\theta_W \\ -\sin\theta_W & \cos\theta_W \end{pmatrix} \begin{pmatrix} Z_\mu \\ A_\mu \end{pmatrix}, \tag{1.18}$$

where $\tan\theta_W \equiv g'/g$, and θ_W is the so-called Weinberg angle. After the diagonalisation, we get a zero eigenvalue corresponding to the massless photon, and a non-zero one which is related to the mass of the physical Z boson, $m_Z^2 \equiv g^2 v^2/\left(4\cos^2\theta_W\right)$. The photon is the only massless gauge boson associated with the SSB of the EW symmetry.

Finally, we get from Equation (1.10) the following terms:

$$\mathcal{L}_{\text{Higgs}} \supset \frac{1}{2}\partial_\mu H \partial^\mu H + (v+H)^2 \left(\frac{g^2}{4} W_\mu^\dagger W^\mu + \frac{g^2}{8\cos^2\theta_W} Z_\mu Z^\mu\right). \tag{1.19}$$

In addition, we can derive the connection between the electric charge Q, the third component of isospin T_3 and the hypercharge Y using the expression for the covariant derivative, and assuming that it is acting on a SM $SU(2)_L$ doublet φ as:

$$\begin{aligned} D_\mu \varphi \supset \Bigg(& -i\frac{g}{\sqrt{2}}\left(\sigma^+ W_\mu + \sigma^- W_\mu^*\right) - i\left(g\cos\theta_W T_3 - g' Y \sin\theta_W\right) Z_\mu \\ & - i\frac{g\,g'}{\sqrt{g^2+g'^2}}\left(T_3 + Y\right) A_\mu \Bigg)\varphi, \end{aligned} \tag{1.20}$$

with $\sigma^+ = \sigma^1 + i\sigma^2$ and $\sigma^- = (\sigma^+)^\dagger$. From Quantum Electrodynamics (QED) we know that the photon couples to the electron with strength e for $Q = -1$, and in view of the last line in Equation (1.20) we get the relations $Q = T_3 + Y$ and $e = g\,g'/\sqrt{g^2 + g'^2}$ for the electron charge and coupling, respectively.

Before moving to the next section, which will be related with the flavour in the SM, let us summarise some interesting remarks from the analysis of the scalar potential and the Brout-Englert-Higgs mechanism:

- It predicts the existence of a new scalar, the Higgs boson, which was discovered at the LHC in 2012 by the ATLAS [21] and CMS [22] experiments.
- The masses of the W and the Z gauge bosons are connected by the tree-level relation
$$\rho \equiv \frac{m_W^2}{m_Z^2\,\cos^2\theta_W} = 1\,. \tag{1.21}$$
The ρ parameter has been experimentally tested to a great precision. In particular, a global fit to EW precision data yields [23]
$$\rho = 1.00038 \pm 0.00020\,, \tag{1.22}$$
which is in agreement with the SM prediction, once radiative corrections are taken into account.
- From Equation (1.19), we can see that the tree-level couplings between the gauge bosons $W^\pm$, Z and the Higgs boson are fixed by the rest of parameters. In particular, they are proportional to m_W^2 and m_Z^2, respectively.

1.1.2 Flavour in the Standard Model: masses and mixings

As we have mentioned before when introducing the Brout-Englert-Higgs mechanism, the gauge symmetry forbids a mass term for both the gauge bosons and the SM fermions. However, the same mechanism that generates the mass of the $W^\pm$ and Z gauge bosons, can also give a mass to the fermions.

To generate the mass of the gauge bosons, we added to the SM content the Higgs doublet. Therefore, we can now write the following Yukawa interactions that are allowed by the symmetries:

$$\mathcal{L}_{\text{Yukawa}} = \bar{l} Y_e e_R \phi + \overline{Q} Y_u u_R \tilde{\phi} + \overline{Q} Y_d d_R \phi + \text{H.c.}\,. \tag{1.23}$$

Here, we use the definition $\tilde{\phi} \equiv i\sigma_2\phi^*$, which is also a doublet of $SU(2)_L$ with opposite hypercharge. The Yukawa couplings Y_e, Y_u and Y_d are general 3×3 complex matrices in flavour space. After SSB (and using the unitary gauge), we get from $\mathcal{L}_{\text{Yukawa}}$ the following terms for each fermion f:

$$\mathcal{L}^{\text{mass}}_{\text{fermions}} = \sum_f \left(1 + \frac{H}{v}\right) \overline{f_L} M_f f_R + \text{H.c.}\,, \tag{1.24}$$

where $f = e,\ u,\ d$,[4] and the mass matrices are $M_f = vY_f/\sqrt{2}$. In general, the fermion fields in the last equation have to be understood as a vector in flavour space, as it is explicitly written in Equation (1.1). Note also that here the mass matrices are not diagonal in general, but they can be diagonalised by means of a bi-unitary transformation of the fields

$$f_{L,R} = V_{fL,R}\hat{f}_{L,R}\,, \tag{1.25}$$

such that

$$V_{fL}^{\dagger} M_f V_{fR} = D_f\,, \tag{1.26}$$

where D_f is a diagonal matrix with the mass of the different flavours in its diagonal. For instance, for the up-type quarks, $D_u = \text{diag}\,(m_u, m_c, m_t)$; and similarly for the down-type quarks, $D_d = \text{diag}\,(m_d, m_s, m_b)$, and the lepton sector, $D_e = \text{diag}\,\left(m_e, m_\mu, m_\tau\right)$. In Equation (1.25), the mass eigenstates are denoted by $\hat{f}_{L,R}$ to differentiate them from the gauge ones, $f_{L,R}$. Using the last two equations, one can write the Lagrangian in (1.24) in the fermion mass-diagonal basis as

$$\mathcal{L}^{\text{mass}}_{\text{fermions}} = \sum_f \left(1 + \frac{H}{v}\right) \overline{\hat{f}_L} D_f \hat{f}_R + \text{H.c.}\,. \tag{1.27}$$

It is obvious from the last equation that the Higgs boson coupling to the SM fermions is diagonal in flavour, and proportional to the fermion masses.

Once we have explicitly written the kinetic term for the SM fermions in Equation (1.9), one can derive the expressions for the neutral current (NC) and charged current (CC) interactions associated with a generic field Ψ_L, which we assume that is a $SU(2)_L$ doublet with a non-trivial representation under $SU(2)_L$. We use for this generic field

$$\Psi_L = \begin{pmatrix} U_L \\ D_L \end{pmatrix}\,, \tag{1.28}$$

where U_L and D_L stand for the up and down components of the doublet. Then, the expressions for the NC and CC interactions are:

$$\mathcal{L}_{\text{NC}} = e\overline{\psi}\gamma_\mu \left[\frac{T^3_\psi}{2\sin\theta_{\text{W}}\cos\theta_{\text{W}}}(1-\gamma_5) - Q_\psi \tan\theta_{\text{W}}\right]\psi Z^\mu + eQ_\psi\overline{\psi}\gamma_\mu\psi A^\mu\,, \tag{1.29}$$

$$\mathcal{L}_{\text{CC}} = \frac{e}{\sqrt{2}\sin\theta_{\text{W}}}\overline{U_L}\gamma_\mu D_L W^\mu + \text{H.c.}\,. \tag{1.30}$$

In the case of the NC in Equation (1.29), $\psi = U_L + U_R$ and $\psi = D_L + D_R$, and the last term is basically the QED interaction Lagrangian.

As has been commented before, in order to diagonalise the mass matrices we need to perform a rotation in flavour space, which has important implications in the phenomenology of the NC and CC interactions in the SM. After this diagonalisation by means of the bi-unitary transformations in Equation (1.25), we find that the CC is

[4]Notice that these fields are not mass eigenstates. Moreover, we consider that neutrinos are massless.

not diagonal due to the misalignment between rotations in the up- and down-quark sectors:

$$\mathcal{L}_{\rm CC}^{\rm quarks} = \frac{e}{\sqrt{2}\sin\theta_{\rm W}}\overline{\hat{u}_L}\gamma_\mu V_{\rm CKM}\hat{d}_L W^\mu + \text{H.c.}\,, \tag{1.31}$$

where $V_{\rm CKM} = V_{uL}^\dagger V_{dL}$ is the so-called Cabbibo-Kobayashi-Maskawa (CKM) quark mixing matrix. The elements of this unitary matrix have to be determined experimentally, and introduce a source of CP-violation in the SM. However, the measured values for the elements of the CKM matrix, which is usually written in the Wolfenstein parameterisation [24], show that the matrix is almost diagonal, whereas the off-diagonal elements generate the flavour-changing transitions in the CC which are, therefore, suppressed (see results from the global fits to flavour observables by the CKMfitter Group [25, 26] and the UTfit Collaboration [27, 28]). See *e.g.* Figure 1.2.

Let us remark that, in the SM, there are not flavour violations at tree level in the NC, as can be seen from Equations (1.25) and (1.29). These currents involve fermions of the same type, and the bi-unitary transformations cancel due to unitarity. Therefore, in the SM there are no tree-level flavour changing neutral currents (FCNC). However, FCNC are generated at one loop in the SM.

For the lepton sector, one can have different situations depending on how neutrinos are described. Originally, the SM was built when neutrinos were thought to be massless. In that case, one can redefine the neutrino field in order to absorb the rotation in the charged lepton sector. However, experimental evidences such as neutrino oscillations tell us that these particles have a very tiny mass. Therefore, we can not compensate the rotation in the charged lepton sector with the redefinition commented before, and for massive neutrinos we have an equivalent situation to the one described for the quark sector, but now the role of the CKM matrix is played by the Pontecorvo-Maki-Nagakawa-Sakata (PMNS) matrix:

$$\mathcal{L}_{\rm CC}^{\rm leptons} = \frac{e}{\sqrt{2}\sin\theta_{\rm W}}\overline{\hat{e}_L}\gamma_\mu U_{\rm PMNS}\hat{\nu}_L W^\mu + \text{H.c.}\,. \tag{1.32}$$

Contrary to the hierarchy shown by the elements of the CKM matrix, the PMNS matrix has most of its entries of the same order, see *e.g.* Figure 1.2.

So far, in this section we have presented the different renormalisable terms for the Lagrangian of the SM that are allowed by the gauge symmetry and the particle content, which after SSB generate charged and neutral currents, and also give mass to the fermions and the gauge bosons. Therefore, the Lagrangian of the SM reads:

$$\mathcal{L}_{\rm SM} = \mathcal{L}_{\rm gauge}^{\rm kin} + \mathcal{L}_{\rm fermions}^{\rm kin} + \mathcal{L}_{\rm Yukawa} + \mathcal{L}_{\rm Higgs}\,. \tag{1.33}$$

The expressions for the different terms in $\mathcal{L}_{\rm SM}$ are given in Eqs. (1.4), (1.9), (1.23) and (1.10), respectively.

1.2 Hints for physics Beyond the Standard Model

The SM has proven to be an amazing theory that is able to explain almost all the physics at the high-energy scale. If we consider energies below the EW scale, *i.e.*

$$|V_{\rm CKM}| \sim \begin{pmatrix} 0.974 & 0.227 & 0.004 \\ 0.226 & 0.973 & 0.041 \\ 0.009 & 0.040 & 0.999 \end{pmatrix} \qquad |U_{\rm PMNS}| \sim \begin{pmatrix} 0.82 & 0.55 & 0.15 \\ 0.32 & 0.60 & 0.74 \\ 0.48 & 0.58 & 0.66 \end{pmatrix}$$

Figure 1.2: *Absolute values of the CKM and the PMNS matrix elements [23]. We see a hierarchical structure in the CKM matrix, whereas the elements of the PMNS matrix are of the same order.*

$\mathcal{O}(100)$ GeV, this theory provides a good understanding of a wide range of all known interactions among the particles that constitute the SM. Moreover, the fact that the SM is (in some sense) a complete theory was reinforced by the discovery of the Higgs boson in 2012 [21, 22], the missing piece responsible for the generation of fermion and gauge boson masses.

However, the current energy range of the particle physics colliders like the LHC can not provide us with a full understanding of the physics beyond a given energy threshold, and in order to confirm or disprove a theory, we need to compare experimental data with what is predicted by that theory. In the meantime, how can we parameterise our ignorance? Well, we can think that the SM is just a low energy EFT, which is valid for energies smaller than a certain scale Λ, associated with the NP. In the next section we will review the concept of EFT.

Although the SM has been experimentally tested with a great accuracy, there are several hints that call for an extension of this theoretical framework. On the one hand, from the experimental point of view, one can list different issues that illustrate the fact that the SM can not be the end point:

- **Neutrino masses.** In the SM, neutrinos are massless particles. However, experimental data coming from neutrino oscillations shows that these particles do have a mass. The SM, however, can easily be extended with right-handed companions, ν_R, which account for neutrino masses (we need at least two right-handed neutrinos). Related to this question, there are different mechanisms that can generate neutrino masses, see *e.g.* Section 1.3, where we also briefly discuss the main differences between Dirac and Majorana fermions. Nevertheless, the Dirac or Majorana nature of neutrinos is still an open question.

- **Flavour anomalies.** There are several flavour anomalies that can be understood as hints of BSM physics. For instance, discrepancies in the so-called anomalous magnetic moment (AMM) of charged leptons, namely of the muon, but also there is some tension in the case of the electron. We will analyse this topic in detail in Chapters 2 and 3.

  In addition, there is experimental evidence regarding processes that seem to distinguish between lepton flavours in semi-leptonic B meson decays. In the SM, lepton flavours are identical except for their Yukawas, that break the accidental (approximate) symmetry associated to lepton flavour universality. The decay

rate of $B \to K^{(*)} l^+ l^-$ in the SM is a $b \to s$ FCNC process [29–32], and therefore one-loop suppressed. Its amplitude involves EW loops through the well-known penguin (and box) diagrams, and the existence of virtual particles related to NP could potentially affect the decay rates.

Note that the decay rate of $b \to s l^+ l^-$ for $l = e,\ \mu$ is expected to show universality regarding lepton flavour due to the fact that electrons and muons have the same EW coupling in the SM, and only differences from kinematics appear in the calculation. In view of that, the interesting observable from the experimental side is $R_{K^{(*)}} = \text{BR}(B \to K^{(*)} \mu\mu)/\text{BR}(B \to K^{(*)} ee)$, whose predicted value in the SM is unity. Similarly, we can consider other related observables like $R_{D^{(*)}} = \text{BR}(B \to D^{(*)} \tau\nu)/\text{BR}(B \to D^{(*)} l\nu)$. Deviations from the SM prediction in these observables could indicate violation of the lepton flavour universality: in the case of $R_{K^{(*)}}$ the discrepancy is at $4\,\sigma$ [33, 34], whereas for $R_{D^{(*)}}$ the deviation is in the range of $(3.1\text{–}3.6)\,\sigma$ [35, 36].

Many solutions have been introduced from the theoretical point of view to solve these problems related to anomalies in the flavour sector, see *e.g.* Ref. [37].

- **Matter-antimatter asymmetry.** The SM predicts that, in the Early Universe, the amount of matter and antimatter that was created should be the same. However, the observed Universe is made of matter, so annihilations have not erased all particles. Therefore, extra ingredients are required in the SM to successfully address this question.

- **Dark matter and dark energy.** As we will briefly discuss in Section 4.1, there are strong experimental evidences for the existence in the Universe of non-baryonic matter which does not have electromagnetic interactions. This exotic type of matter is the so-called dark matter (DM). Moreover, there are also experimental hints that show the accelerated expansion of the Universe, namely the data from Type Ia Supernovae [38, 39]. This expansion is associated to dark energy (DE), whose nature is not well-understood. Then, according to cosmological observations, we conclude that the SM can only account for $\sim$ 5% of the energy in the Universe, whereas the rest should be distributed in the form of $\sim$ 26% of DM and $\sim$ 69% of DE.

  We will study possible DM candidates in Chapters 5 and 6.

On the other hand, from the theoretical point of view, there are also reasons for arguing that the SM is not satisfactory:

- **The flavour puzzle.** The fact that the SM has (three) families has no explanation at all. Moreover, the particular structure followed by the masses or the mixings of the SM leptons and quarks is also not well understood. In particular, the masses of the quarks and the charged-leptons have very hierarchical structure, as well as the CKM matrix elements. This is not the case for the neutrino masses and PMNS matrix elements. See *e.g.* Figures 1.2 and 1.3.

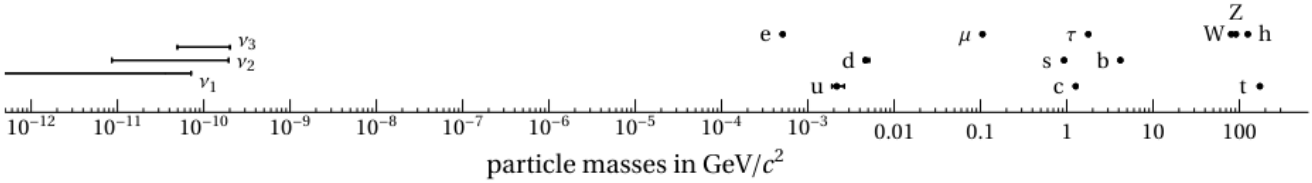

Figure 1.3: *Masses of the SM particles. As can be seen, they span several orders of magnitude. Figure extracted from Ref. [37].*

Regarding possible solutions to explain the observed pattern in fermion masses and mixings, an interesting approach is to consider a new symmetry acting on flavour space, which can constrain the couplings in this sector yielding differences among flavours. See *e.g.* some interesting reviews in Refs. [40–42].

- **The strong CP problem.** Regarding the SM symmetry group, the inclusion of a term like $\theta\epsilon^{\mu\nu\rho\sigma}G_{\mu\nu}G_{\rho\sigma}$ is allowed, and a source of CP violation is added through its presence. However, there is no experimental evidence for such source of CP violation (for instance, bounds from neutron electric dipole moments show that $\theta \lesssim 10^{-9}$). Moreover, using naturality arguments one expects that the parameters in the SM Lagrangian should be $\mathcal{O}(1)$, unless a symmetry protects them. Then, since the SM does not have a mechanism to forbid this new term in the Lagrangian, in order to account for the experimental evidence one needs to assign a (rather unnatural) small number to the parameter θ. A possible solution is to consider θ as a field, the axion, with a charge under the so-called Peccei-Quinn symmetry [43–46].

- **The hierarchy problem.** The Higgs boson mass can be very sensitive to the presence of high-energy NP at scale Λ, which would correspond to possible extensions of the SM. This is due to the fact that its mass is not protected by any symmetry, and receives radiative corrections proportional to Λ^2. This is not the case for fermions and gauge bosons, whose masses are protected by the chiral and gauge symmetries, respectively. Therefore, in the presence of NP one would need to introduce a fine-tuning in order to account for the observed value of the Higgs boson mass, $m_H \simeq 125$ GeV, being rather unnatural. As can be understood from these lines, the hierarchy problem is not a problem of the SM *per se*, but it is related to problems that the presence of NP would generate in the SM.

- **Grand Unification of interactions.** We know that in QFT, couplings evolve (run) with energy, and the main idea behind the Grand Unified Theories (GUTs) is the unification of forces at a high-energy scale. In fact, the running of the three SM gauge couplings seems to point to a similar high-energy scale around $\sim 10^{15}$ GeV, the so-called GUT scale. Just as in the case of the weak and the

electromagnetic forces, maybe this scale at which the SM gauge couplings unify indicates the presence of NP. However, the SM requires some NP between the EW and the GUT scale in order to help the forces to converge.

- **Gravity.** From the theoretical point of view, the unification of the SM interactions with gravity is one of the biggest problems. Gravity involves an associated NP scale at $\sim 10^{19}$ GeV, the Planck scale, and their effects could be parameterised, as a first attempt, by means of EFTs. As we will see in Section 1.4, each EFT has associated a validity range, which will be below the Planck scale in the case of gravity. However, for larger scales we need the full theory of quantum gravity. From QFT, the problem is that trying to quantise gravity leads us to a non-renormalisable theory. A possible solution beyond QFT is, for instance, String Theory.

1.3 Brief review on neutrino masses

The fact that neutrinos are massive particles follows from experimental evidences, namely neutrino oscillations, one of the most important discoveries in particle physics. In view of that, the three left-handed flavour neutrinos, ν_e, ν_μ and ν_τ, are mixtures of the neutrinos with definite mass.

But first, let us briefly summarise the history of neutrinos, originally proposed in 1930 by W. Pauli, who wrote his famous letter to the Tübingen Conference addressed to the "Dear Radiactive Ladies and Gentlemen" [47]. He suggested the existence of spin-1/2 neutral particles as a solution to save the conservation of energy and angular momentum in nuclear β decay. The continuum energy spectrum of electrons in nuclear β decays, depicted in Figure 1.4, was then completely understood with the emission of neutrinos together with electrons in these processes.

Later on, this elusive particle was experimentally discovered by Reines and Cowan in 1956, detecting (electron anti-)neutrinos that escape from a nuclear reactor in Savannah River [49–51]. After that, a discrepancy between the neutrino flux expected from the Sun and its detected value at the Homestake experiment [52] was the first indication that, due to neutrino oscillations, those particles should be massive. In addition, oscillations in the solar neutrino flux were confirmed later by SNO and KamLAND experiments, and also there were experimental hints of oscillations in the atmospheric neutrino flux given by Super-Kamiokande.

Once we know that neutrinos are massive particles, we should try to accommodate their masses in the SM framework. Conversely to the rest of the fermions, they are electrically neutral, which allows two types of neutrino mass terms in the Lagrangian, namely Dirac or Majorana. In the following, we present the main differences between them.

- **Dirac fermions.** They have four internal degrees of freedom, and the complete Dirac field ψ is a four-component spinor. However, in QFT the fundamental fields are the two component spinors ψ_L and ψ_R, where $\psi_{L,R} = P_{L,R}\psi$ with the

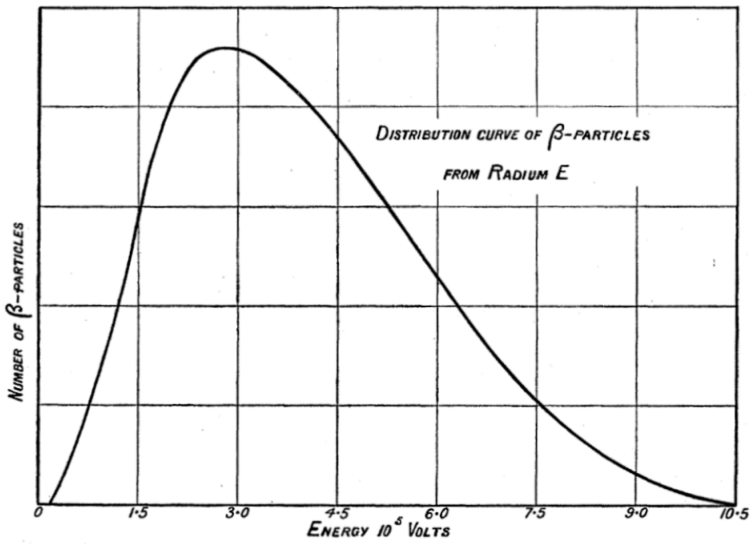

Figure 1.4: *Energy spectrum of the electron in nuclear β decay [48].*

usual definition for the chiral projectors, $P_{L,R} = (1 \mp \gamma_5)/2$. They describe particles and antiparticles, which have opposite charges. Therefore, one can write a mass term in the Lagrangian as

$$\mathcal{L}^{\text{mass}}_{\text{Dirac}} = m_{\text{D}} \overline{\psi_R} \psi_L + \text{H.c.}\,, \tag{1.34}$$

connecting fields with opposite chiralities, ψ_L and ψ_R.

- **Majorana fermions.**[5] They have only two internal degrees of freedom, and describe a fermion which is its own antiparticle. In this case, one can add a mass term in the Lagrangian of the form[6]

$$\mathcal{L}^{\text{mass}}_{\text{Majorana}} = \frac{1}{2} m_{\text{M}} \overline{\psi^c_L} \psi_L + \text{H.c.}\,. \tag{1.35}$$

The Majorana field is $\psi = \psi_L + \psi^c_L$, describing a fermion which is its own antiparticle, *i.e.* $\psi = \psi^c$. Note that $\psi_L\,(\psi_R)$ is a left (right)-handed field whereas $\psi^c_L\,(\psi^c_R)$ is a right (left)-handed field.

Conversely to the Dirac case, the Majorana mass term connects a field ψ_L with its corresponding transformed field under CP, ψ^c_L. Therefore, a Majorana mass term would violate any $U(1)$ symmetry carried by the fields.

Now, we can relate the different mass terms explained before with active neutrino masses. However, neutrinos in the SM are massless particles, and one needs an extension of this theoretical framework in order to account for neutrino masses.

[5] This possibility was introduced by E. Majorana in 1937 [53].

[6] A similar mass term can be written for ψ_R instead of ψ_L.

Related to this, one can think in a simple extension of the SM: the inclusion of three[7] families of right-handed neutrinos, ν_R, which would transform under the SM gauge group $(SU(3)_c, SU(2)_L)_{U(1)_Y}$ as $(1,1)_0$. The SM gauge symmetry allows us to write the following terms in the Lagrangian related to the right-handed neutrino:

$$\mathcal{L}_\nu = \bar{l} Y_\nu \nu_R \tilde{\phi} + \frac{1}{2}\overline{\nu_R^c} M_R \nu_R + \text{H.c.}\,, \tag{1.36}$$

where M_R is, in general, a 3×3 symmetric matrix. As mentioned before, the Majorana mass term breaks all $U(1)$ symmetries, and if we assume a particular symmetry under which all leptons are charged (the so-called lepton number, $U(1)_L$), this mass term would violate it in two units.

After the SSB of the EW symmetry, the Lagrangian in Equation (1.36) leads to

$$\mathcal{L}_\nu = m_\text{D} \overline{\nu_L} \nu_R + \frac{1}{2}\overline{\nu_R^c} M_R \nu_R + \text{H.c.} = \frac{1}{2}\overline{\chi^c} \mathcal{M}_\chi \chi + \text{H.c.}\,, \tag{1.37}$$

where $m_\text{D} = Y_\nu v/\sqrt{2}$, and we used that

$$\chi = \begin{pmatrix} \nu_L^c \\ \nu_R \end{pmatrix} \quad \text{and} \quad \mathcal{M}_\chi = \begin{pmatrix} 0 & m_\text{D} \\ m_\text{D}^T & M_R \end{pmatrix}. \tag{1.38}$$

This is the well-known Type-I Seesaw model [54–57]. In principle, M_R is a free parameter of the model, and assuming that $M_R \gg m_\text{D}$, the neutrino mass matrix $\mathcal{M}_\chi$ can be block-diagonalised, obtaining:

i) Three SM singlets heavy leptons, $\chi_\text{heavy} \simeq \nu_R$, with masses $m_\text{heavy} \simeq M_R$.

ii) Three SM singlets light leptons, $\chi_\text{light} \simeq \nu_L$, with masses $m_\text{light} \simeq -m_\text{D}^T M_R m_\text{D}$.

Therefore, light neutrino masses are given by the so-called *seesaw formula*, $m_\nu \equiv m_\text{light} \simeq m_\text{D}^2/M_R$, that in the presence of heavy SM singlet leptons could naturally explain the smallness of the observed neutrino masses.

To conclude with this short discussion on neutrino mass models, we emphasise that there are other variations of the seesaw mechanism, namely the Type-II [58–62], Type-III [63, 64] and the inverse Seesaw [65]. Moreover, there are also neutrino mass models available in the market that generate the neutrino mass term radiatively, see for instance the Zee-Babu model [66, 67], the Scotogenic model [68], or a review of models in Ref. [69]. Moreover, we will discuss in Chapter 6 a model that generates, in a similar way to the Scotogenic model, the mass term for a right-handed (sterile) neutrino at one loop.

1.4 Effective Field Theory

As we have already mentioned, the EFT approach is another of the relevant notions that will be applied in the following chapters of the thesis. The main idea behind it

[7] Notice that we need at least two extra singlets to explain neutrino data, which requires a minimum of two massive neutrinos.

is that, whenever we have a system with two (very) separated scales, the dynamics of each one basically seems to evolve independently of that of the other. Being more pragmatic, in particle physics one could ask oneself about the meaning of the aforementioned scale, which is naturally associated with the energy of a given process. Then, one can rephrase the main principle behind the EFT saying that it is based on the fact that dynamics at low energies does not depend on the details of the dynamics at high energies [70–73].

Assuming that the high-energy regime is not accessible in the facilities that we have nowadays, and taking into account the EFT principle, one could think about deriving an effective theory in the low-energy regime, which only contains the relevant degrees of freedom, *i.e.* light particles.[8] The effect of the higher degrees of freedom (or heavy particles), which are eliminated (or integrated out) from the effective description, are incorporated in the theory as an expansion controlled by inverse powers of the high-energy scale. We will discuss this expansion below.

However, the procedure of parameterising the relevant interactions of a complete theory by means of the EFT approach has an important caveat: its range of validity. As we are supporting the construction of an effective theory in the fact that there are separated scales associated with the low and high-energy regimes, we have to consider that our effective description of the full theory will only be valid in a certain regime. If we remain within its range of validity, the EFT gives a complete description of the phenomenology we are interested in, with the same infra-red (IR) but different ultra-violet (UV) behaviour than the underlying fundamental theory. Therefore, we obtain a simplified framework without any necessity of knowing the details of the complete theory that lies behind the effective one. With its limitations regarding the validity, EFT proves to be a very useful tool for describing the low-energy dynamics of a given theory.

In order to clarify the concept of integrating out a heavy degree of freedom in particle physics, let us qualitatively explain how this mechanism works in a simplified situation. Imagine that we have a *system* with two kinds of scalar particles, ϕ and Φ, with a definite hierarchy in their masses. In particular, we assume that $m_\phi \ll m_\Phi$. Figure 1.5 represents the scattering process of light particles, $\phi\phi \to \phi\phi$, mediated by the heavy ones.[9] In addition, we consider that the energy of this process is sufficiently small compared to the mass of the heavy field, and therefore Φ can not be produced in the final state. However, it can mediate the interaction as a virtual particle, as it is the case in this example. Then, computing the amplitude for this particular process, we have a term that involves the internal propagator of Φ, which goes as[10]

$$\frac{1}{p^2 - m_\Phi^2}\,, \tag{1.39}$$

being p the momentum associated to the heavy field, Φ, which can be identified with

[8] In a scattering process, one has to compare the mass of the particles with the typical energy of the process, E, for differentiating between light and heavy particles.

[9] For simplicity, we are assuming that the process $\phi\phi \to \phi\phi$ only occurs through the s channel. In general, one can have a more complex situation involving different type of diagrams.

[10] We forget about the factor i in the propagator in order to simplify the notation.

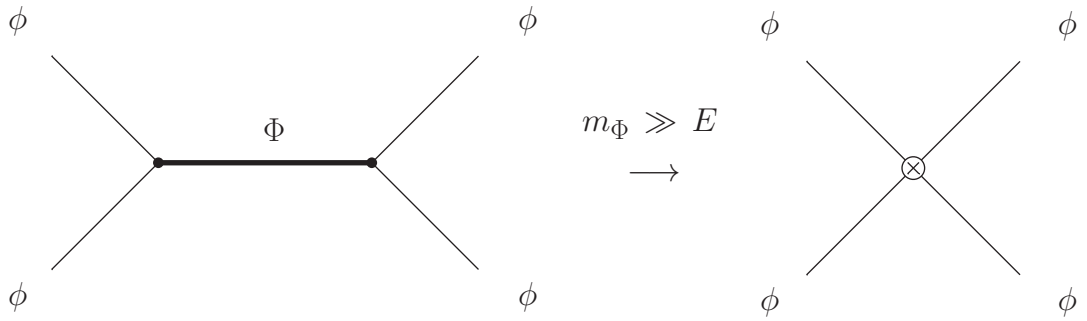

Figure 1.5: *Feynman diagrams associated with the integration out of the heavy field Φ that mediates the scattering process of light particles $\phi\phi \to \phi\phi$ in a given toy model. For typical energies of the process E much below the mass of the heavy field (mediator) m_Φ, i.e. $E \ll m_\Phi$, the internal propagator can be reduced to a factor $-1/m_\Phi^2$, and we end up with a four-point vertex effective interaction.*

the typical energy of the process, E. Then, in the limit $E \ll m_\Phi$, we can neglect the internal momentum compared to the mass, and the last equation just reduces to a numerical (and dimensionful) factor $-1/m_\Phi^2$. The remaining part in the calculation is related to the four external legs of light fields. Therefore, the process of integrating out the heavy field Φ has a final result which has the form of a factor with dimensions of inverse heavy mass squared times a four-point vertex interaction involving light fields. Diagrammatically, integrating out the heavy particle is denoted by $\otimes$ in Figure 1.5, which basically means to contract the internal propagator in $\phi\phi \to \Phi \to \phi\phi$ (non-local heavy particle exchanges) to a point in space-time (local interaction).

The general procedure when we want to construct an EFT that describes a high-energy QFT in a given range of validity and up to a certain accuracy can be described as follows. First, we have to identify the relevant fields of the theory, and also determine the symmetries they have. The relevant fields and symmetries of the theory allow us to construct its Lagrangian, $\mathcal{L}$, which at this point is renormalisable, *i.e.* with dimension four or less. Now, by means of the EFT one can parameterise the effects of any high-energy physics at a high-energy scale, Λ, which can be identified with the scale associated to NP. We proceed by adding all the effective operators that must respect Lorentz invariance and gauge symmetries of the fundamental theory. As we will see in Chapter 6, we can also add to the set of non-renormalisable operators specific cases that do not respect accidental global symmetries which are preserved (at some level) by the fundamental theory, like the lepton number in the SM.

The effective Lagrangian of the theory contains the original Lagrangian $\mathcal{L}$, which is renormalisable and has operators up to dimension four, and the tower of local interactions described by non-renormalisable operators. Therefore, the effective Lagrangian reads:

$$\mathcal{L}_{\text{eff}} = \mathcal{L} + \sum_{n=5}^{\infty} \sum_{i} \left(\frac{C_i^{(n)}}{\Lambda^{n-4}} \mathcal{O}_i^{(n)} + \text{H.c.} \right) . \tag{1.40}$$

Here, n denotes the dimensionality of the operator, and i labels the different operators that share the same dimension. As we already know, Lagrangians have dimensions of energy to the fourth power, E^4. Therefore, in order to saturate the dimensionality, the effective operators in the expansion must be multiplied by a dimensionful quantity with dimensions of inverse mass to a certain power. In the simple case schematically depicted in Figure 1.5 one can see that this factor, namely $1/m_\Phi^2$, arises from the contraction of the internal propagator of the heavy field.

On general grounds, the dimensionality of the coupling of the effective operators is controlled by the NP scale Λ, which has dimensions of mass. Then, by looking at Equation (1.40), the operators of dimension n have associated couplings with dimensions of inverse mass to the power $(n-4)$, whereas the coefficients $C_i^{(n)}$ are dimensionless. The separation between Λ and C is arbitrary, of course, and the general approach when we do not know anything about the heavy particles and their properties is to assume that the dimensionless coefficients are $\mathcal{O}(1)$, $C_i^{(n)} \sim 1$. Notice also that, in specific situations or processes that one has to analyse using EFTs, these dimensionless coefficients may not be order one because of some suppression factor that could come, for instance, from a numerical factor $1/(4\pi)^2$ if the operator is generated at one loop.

As we have commented through this section, every EFT has associated some range of validity where its parameterisation of the complete underlying theory is a good procedure to hide our lack of knowledge of the high-energy dynamics. In that sense, the expansion in Equation (1.40) in terms of non-renormalisable operators is restricted to energies smaller than the NP scale, *i.e.* $E \ll \Lambda$. Moreover, regarding the predictivity of a given EFT, we can not consider the infinite number of effective operators that should be taken into account in the expansion. Then, we need to stop at some operator of dimension n, which translates into a certain accuracy in the results that we can extract by means of the EFT approach. Moreover, one can also reduce the number of effective operators that have to be considered in the Lagrangian in Equation (1.40). For instance, one can include only the effective operators that are generated at tree level, arguing that the loop-generated ones are suppressed with respect to the former.

In addition, it is interesting to note that whenever one has complete information about the dynamics of the full theory, *i.e.* we know the physics of the heavy-energy regime, we may be interested in calculating the effects of the heavy particles in the process that we are considering. In order to do that, we start from the complete theory and compute the full process that gives rise to the effective interaction, including all the fields (also the heavy ones; remember that now, working with the underlying complete theory under control, we assume that the physics of heavy particles is understood). Once this has been done, we match the full process calculation with the one obtained in the effective theory. This procedure, also known as *matching*, allows us to compute the effective coupling of the non-renormalisable operators in the EFT. We will apply this technique in Chapter 6, allowing us to test the range of validity of the EFT.

In view of what has been commented in this section, we can now summarise the general principles that support the construction of an EFT [73]:

- Dynamics at low energies does not depend on details of dynamics at high energies.
- Whenever we have a theory with separated scales, we can integrate out the heavy degrees of freedom if there are large energy gaps, *i.e.* $m_{\text{light}} \ll E \ll m_{\text{heavy}}$.
- Non-local heavy particle exchanges are replaced by a tower of local interactions that involve the light particles.
- There is some range of validity where the EFT can describe, to a given accuracy, the low-energy dynamics of a theory. Then, associated with this validity range, the EFT has the same IR but different UV behaviour than the full theory.
- The only remnants of the high-energy dynamics are in the low-energy couplings and in the symmetries of the EFT.

Part II

Anomalous Magnetic Moments of charged leptons

CHAPTER 2

Introduction to the Anomalous Magnetic Moment

In this chapter we will review the current status of the anomalous magnetic moment of charged leptons, in particular for electrons and muons.

In the first part we will briefly summarise the historical events that led to the concept of spin, and how it is related with the anomalous magnetic moment. Moreover, we will discuss the different contributions to the SM prediction of the anomalous magnetic moment, in particular the one from QED, which can be expressed as a perturbation series with the fine-structure constant as the expansion parameter. Finally, we will present the most recent values for the SM prediction and the experimental measurements of electron and muon anomalous magnetic moments. In addition, we will give the current discrepancy between the theoretical and experimental values.

2.1 Spin: a historical review

Historically, the beginning of the 20th century was a revolutionary period of time regarding physics, where unexpected experimental observations led to develop new ideas from the theoretical point of view.

In particular, there was not a clear explanation for the structure of atoms until Rutherford proposed his theory in 1911 [74]. Basically, the positive charge of the atom is concentrated in the nucleus, whereas the electrons, with negative charge, orbit around it. The net result is a neutral atom, but unstable from the classical point of view. Electrons, when orbiting around the nucleus, would emit radiation and loss part of their energy, leading to a collapse of the atom. In some sense, Rutherford's model was self-destructive. Then, trying to solve the problems of this model, Bohr presented his quantum theory in 1913 [75].

Later on, Stern proposed in 1921 an experiment to disprove[1] the Bohr-Sommerfeld model of the atomic orbits, and therefore rule out the associated space quantisa-

[1] See a historical review of the Stern-Gerlach experiment in Ref [77].

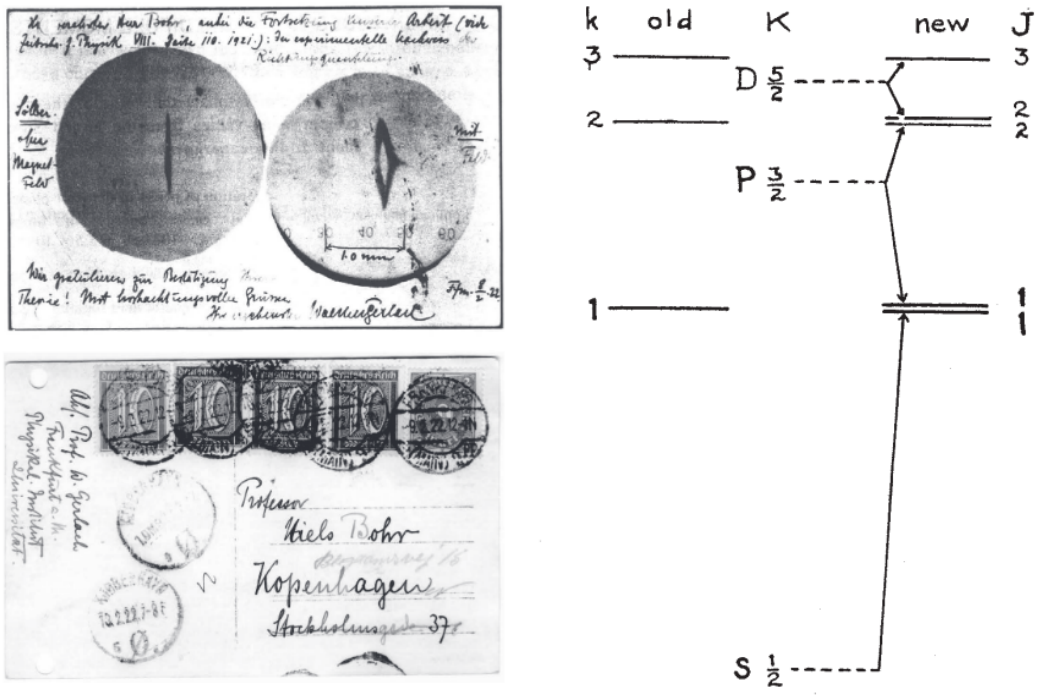

Figure 2.1: *Left: Postcard sent by Gerlach to Bohr with the tow-band structure observed in the experiment. Right: Original figure from Ref [76] where Uhlenbeck and Goudsmit showed the difference between the Sommerfeld's theory (left) and their "new theory" (right) with respect to the fine-structure of the hydrogen-like spectra.*

tion [78–81]. From the experimental side, the so-called Stern-Gerlach experiment consists in a region of the space where a gradient magnetic field is applied. Then, when an atomic beam of silver atoms passes through this region, there is a net force on the magnetic dipole of the atoms that separates the different magnetic quantum states. Classically, one would not expect any separation because the dipole moment could have any value. However, the result from the experiment was the observation of two bands, see *e.g.* the left panel of Figure 2.1 , and therefore Stern and Gerlach concluded that the magnetic moment for the silver atoms was one Bohr magneton[2] to within 10 % of accuracy [82]. A similar experiment was repeated with a hydrogen beam by Phipps and Taylor in 1927 finding also a two-band structure, therefore the magnetic moment of the hydrogen was also one Bohr magneton [83].

Regarding the concept of spin,[3] it appeared in 1925 when Uhlenbeck and Goudsmit proposed a solution to the fine-structure observed in hydrogen-like atoms [85]. As can be seen on the right panel of Figure 2.1, the splitting in the energy levels of hydrogen-

[2]The Bohr magneton is defined by $e\hbar/2m_e$. Here, e and m_e are the charge and the mass of the electron, respectively, and $\hbar \equiv h/2\pi$, where h is the Planck constant.

[3]The idea of a quantised spinning of the electron was already proposed in 1921 by Compton related to a possible explanation to ferromagnetism [84].

like atoms can be explained thanks to the interaction of the magnetic dipole moment of the electron with the magnetic field generated by the motion of the nucleus.

The magnetic dipole moment (MDM) of an electron is

$$\vec{\mu} = g_s \left(\frac{q}{2m_e} \right) \vec{s}, \tag{2.1}$$

with $q = \pm e$ being the charge of the particle in terms of the electron charge, e, m_e is the mass of the electron, and g_s is the so-called Landé g-factor. If there is no external electric or magnetic field, the spin $\vec{s}$ gives a preferred direction in space, so the MDM of a charged particle should be along its spin. Going back to the Stern-Gerlach experiment, today we know that the observed value for the magnetic moment was indeed related to an un-paired atomic electron, and the two-band structure indicates that the z-component of the spin (of the electron) should have two discrete values, namely $s_z = \pm\hbar/2$. Therefore, the result for the magnetic moment of one Bohr magneton implies that for the electron $g_s = 2$, see *e.g.* Equation (2.1).

Then, the next (and very important) step in this brief historical review of the spin was taken by Dirac when he introduced in 1928 the relativistic wave equation for the electron, the well-known Dirac equation [86, 87]. Dirac showed that in the presence of an external magnetic and electric fields, the wave function of an electron has two extra terms that represent the interactions of the magnetic and electric dipole moments with the external magnetic and electric fields, respectively. In his theory, the predicted value for the magnetic moment of the electron is one Bohr magneton (and therefore $g_s = 2$), which is in agreement with the experimental observations from Stern and Gerlach. For completeness, we show in the following the Dirac equation of an electron in a weak magnetic field $\vec{B}$ in the non-relativistic limit:[4]

$$i\hbar \frac{\partial \psi}{\partial t} = \left[\frac{\vec{p}^2}{2m_e} - \frac{e}{2m_e c} \left(\vec{L} + 2\vec{S} \right) \cdot \vec{B} \right] \psi, \tag{2.2}$$

where $\vec{L}$ and $\vec{S}$ are the orbital angular momentum and the spin, respectively, and c is the speed of light. From the last equation we see that the predicted values for the g-factors are $g_s = 2$ for the spin, and $g_l = 1$ for the corresponding g-factor associated to the orbital angular momentum.

Let us also reproduce here an interesting comment done by Dirac regarding his equation: "It was found that this equation gave the particle a spin of half a quantum. And also gave it a magnetic moment. It gave just the properties that one needed for an electron. That was an unexpected bonus for me, completely unexpected" [89].

2.2 Anomalous Magnetic Moment of charged leptons

Now, we can write the Hamiltonian for a particle of spin $\vec{s}$ in presence of both an external electric and magnetic field as

$$\mathcal{H} = -\vec{\mu} \cdot \vec{B} - \vec{d} \cdot \vec{E}, \tag{2.3}$$

[4] See *e.g.* page 13 on Ref. [88].

	$\vec{E}$	$\vec{B}$	$\vec{\mu}, \vec{d}$	$\vec{\mu} \cdot \vec{B}$	$\vec{d} \cdot \vec{E}$
C	$-$	$-$	$-$	$+$	$+$
P	$-$	$+$	$+$	$+$	$-$
T	$+$	$-$	$-$	$+$	$-$

Table 2.1: *Transformation properties under C, P and T symmetries of the terms in Equation* (2.3).

where $\vec{\mu}$ is the MDM, already introduced in Equation (2.1), and $\vec{d}$ is the electric dipole moment (EDM) given by

$$\vec{d} = \eta \left(\frac{q}{2mc} \right) \vec{s}, \tag{2.4}$$

with η being a dimensionless constant that plays a similar role than that of the g-factor in the MDM. Here, m denotes the mass of the particle that is considered.

We can now analyse the transformation properties of both terms in Equation (2.3) under C, P and T symmetries. As can be seen from Table 2.1, the first term is even under P and T, whereas the second is odd under the same symmetries. Therefore, the presence of a non-zero EDM indicates that both P and T are violated by the Hamiltonian in Equation (2.3). Moreover, assuming that CPT is preserved, T violation implies that CP is not conserved, and one concludes that an EDM different from zero indicates CP violation. Regarding this, in the SM the CKM matrix is the only source of CP violation. However, it is not enough to explain the matter-antimatter asymmetry in the Universe, and therefore additional CP-violating sources would contribute to solve this question.

Of course, we know that P and T symmetries are violated in the SM by weak interactions [90], therefore, one should expect a non-zero value for the EDM of leptons. However, in the SM it is generated at the four-loop level, and therefore very suppressed. In particular, the value for the electron EDM is [91]:

$$|d_e^{\mathrm{SM}}| \simeq 10^{-41}\, e\,\mathrm{cm}\,. \tag{2.5}$$

Charged leptons in the SM basically differ by their masses. Then, from the last equation, we can also derive an estimation for $|d_\mu^{\mathrm{SM}}| = |d_e^{\mathrm{SM}}| m_\mu / m_e \simeq 10^{-39}\, e\,\mathrm{cm}$, and $|d_\tau^{\mathrm{SM}}| = |d_e^{\mathrm{SM}}| m_\tau / m_e \simeq 10^{-38}\, e\,\mathrm{cm}$. However, the experiments can not be sensitive to these predicted values for the EDMs, see *e.g.* the current experimental upper bounds [23]:

$$|d_e| < 10^{-29}\, e\,\mathrm{cm}\,, \qquad |d_\mu| < 10^{-19}\, e\,\mathrm{cm}\,, \qquad |d_\tau| < 10^{-17}\, e\,\mathrm{cm}\,. \tag{2.6}$$

Conversely to the SM contribution, the presence of NP could enter in the EDMs of charged leptons, for instance, at the one- or two-loop level, yielding a much more relevant contribution than the one given by the SM prediction. Therefore, EDM can be used to obtain strong constraints on the energy scale associated to NP, see *e.g.* Ref.[92].

With respect to the MDM, it is usually written as

$$\mu = (1+a)\frac{q\hbar}{2m} \quad \text{with} \quad a = \frac{g-2}{2}\,, \tag{2.7}$$

where a is the so-called anomalous magnetic moment (AMM). It basically measures the difference with respect to the classical value predicted by Dirac theory, $g = 2$.

In general, both the AMM and the EDM of charged leptons are calculated from the matrix element of the electromagnetic current,

$$J^{\mu}_{\text{em}} = e\sum_{f} Q_f \overline{f}\gamma^{\mu} f\,, \tag{2.8}$$

between an initial state (charged lepton f) with momentum p, and a final state (same f) with momentum p', given by

$$\langle\, f(p') \,|\, J^{\mu}_{\text{em}} \,|\, f(p)\,\rangle = \overline{u}_f(p')\Gamma^{\mu}u_f(p)\,, \tag{2.9}$$

where $\overline{u}_f$, u_f are the Dirac spinor fields of the charged leptons, and Γ_{μ} is dictated by Lorentz invariance. In general, one can write

$$\begin{aligned} e\Gamma^{\mu} = \;& \gamma^{\mu} eF_1(q^2) + \frac{i\sigma^{\mu\nu}q_{\nu}}{2m_f} eF_2(q^2) - \gamma_5\,\sigma^{\mu\nu}q_{\nu}eF_3(q^2) \\ & + F_A(q^2)\left(\gamma^{\mu}q^2 - 2m_f q^{\mu}\right)\gamma_5\,, \end{aligned} \tag{2.10}$$

where we have defined $q \equiv p' - p$, γ^{μ} are the gamma matrices and $\sigma^{\mu\nu} = i\left[\gamma^{\mu},\gamma^{\nu}\right]/2$. In addition, $F_i(q^2)$ with $i = 1, 2, 3$ are the so-called charge, anomalous magnetic dipole and electric dipole form factors, respectively, whereas $F_A(q^2)$ is called the anapole form factor, which will not be discussed here.

Since gauge invariance requires the charge of the leptons $f = e,\ \mu,\ \tau$ to be (minus) one at all orders, the normalization of $F_1(q^2)$ is fixed. Moreover, in the limit where $q^2 \to 0$, the form factors F_2 and F_3 are related to the AMM and EDM, respectively. Therefore, we have:

$$F_1(0) = 1\,, \qquad F_2(0) = a_f\,, \qquad F_3(0) = \frac{d_f}{e}\,. \tag{2.11}$$

Focusing now on the NP contributions to the AMM of charged leptons due to a high-energy scale Λ, we can use an EFT approach to parameterise its effects. Regarding this, there are contributions to the AMM of charged leptons from operators of dimension $D \geqslant 6$. In particular, one can write the $D = 6$ operator

$$\frac{e\,Cv}{16\pi^2\Lambda^2\sqrt{2}}\overline{e_L}\sigma_{\mu\nu}e_R F^{\mu\nu} + \text{H.c.}\,, \tag{2.12}$$

which generates this kind of contributions. The dipole operator in the last equation arises from a combination of the gauge invariant operators

$$\bar{l}\sigma_{\mu\nu}e_R H B^{\mu\nu} \quad \text{and} \quad \bar{l}\sigma_{\mu\nu}\vec{\sigma}e_R H\vec{W}^{\mu\nu}\,, \tag{2.13}$$

once the Higgs field develops a VEV, and the EW symmetry is spontaneously broken. Here, we use the same notation as in Chapter 1, except for the fact that now, the usual Higgs $SU(2)_L$ doublet is denoted by H. On general grounds, one can show that this operator can only be generated at the loop level [72]. Therefore, we include a factor $1/(4\pi)^2$. Moreover, it is interesting to note that the operator $\bar{l}\sigma_{\mu\nu}iD\!\!\!/ lB^{\mu\nu}$ can be related to the first operator in Equation (2.13) after using the equation of motion. Then, the same operator is generated, but with an additional suppression factor $\sqrt{2}m_f/v$.

The dipole operator in Equation (2.12) gives the following contribution to the AMM of charged leptons:

$$a_f^{\rm NP} = \frac{m_f C v}{4\pi^2 \Lambda^2 \sqrt{2}}\,. \tag{2.14}$$

Let us remark that the coefficient of the dipole operator in Equation (2.12) can be expressed as $a_f^{\rm NP} e/(4m_f)$. In addition, this operator connects left- and right-handed fermions, which has associated a chirality flip. Therefore, one expects that, in the chiral limit ($m_f \to 0$), NP contributions to $a_f^{\rm NP} e/(4m_f)$ must vanish. In view of that, we get:

$$a_f^{\rm NP} = C' \left(\frac{m_f}{\Lambda}\right)^2\,, \tag{2.15}$$

where, in general, the C' coefficient could be $\mathcal{O}(1)$, or even smaller if the NP contribution is generated at loops or it has extra suppression factors such as masses of light leptons. Nevertheless, in Section 3.1.1 in the next chapter, we will analyse different scenarios for the coefficient of the dipole operator, and the kind of NP that could generate it.

2.2.1 Theoretical computation

On the one hand, regarding the theoretical computation of the AMM of charged leptons in the SM, there are three types of contributions, namely:

$$a_f^{\rm SM} = a_f^{\rm QED} + a_f^{\rm had} + a_f^{\rm EW}\,. \tag{2.16}$$

They are the QED, the hadronic and the EW contributions, respectively. In the following, we present them in order of relevance.

- **The QED contribution.** It involves charged leptons and photons. At tree level we have the Dirac contribution that gives $g = 2$, see Figure 2.2 (a). Then, several corrections to this result have been calculated. In particular, the most famous one is the leading quantum correction computed by Schwinger and depicted in Figure 2.2 (b). It yields [93]:

$$\left(a_f^{\rm QED}\right)_{1-\rm loop} = \frac{\alpha}{2\pi} \simeq 0.00116\ldots\,, \quad \text{with} \quad \alpha = \frac{e^2}{4\pi}\,. \tag{2.17}$$

  This contribution is independent of the mass of the charged lepton, and therefore it is the same for electrons, muons and taus. From this point, one can start

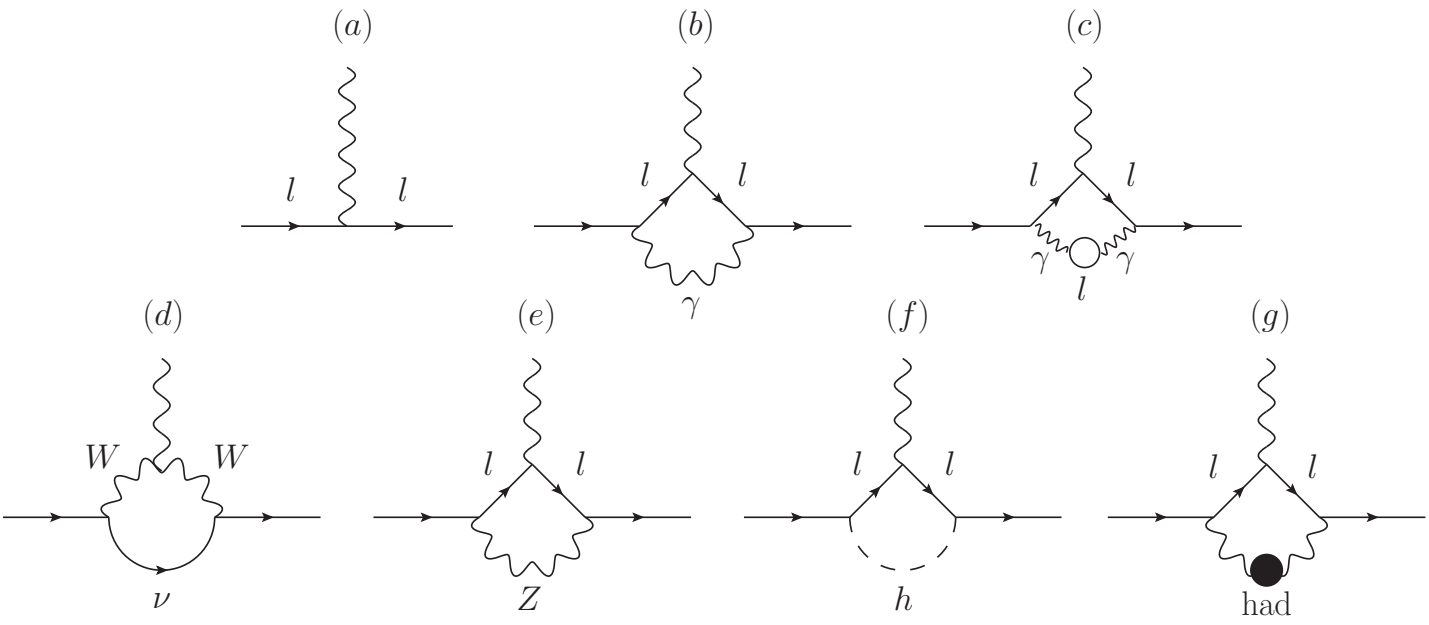

Figure 2.2: *Feynman diagrams for: (a) Dirac computation, $g = 2$; (b) the first QED correction to the AMM computed by Schwinger; (c) the vacuum polarization contribution up to two loops; (d), (e) and (f) the first EW contributions of the gauge bosons and the Higgs boson; and (g) the first QCD correction by the hadronic vacuum polarization.*

to compute corrections at higher order, as depicted in Figure 2.2 (c) for the vacuum polarization contribution, which is one of the terms of $\mathcal{O}(\alpha/\pi)^2$. Nowadays, the QED contribution of the AMM has been computed up to $\mathcal{O}(\alpha/\pi)^5$. We will discuss in detail the expansion in α of the QED contribution in the next paragraphs.

- **The hadronic contribution.** It takes into account the contribution from quarks or hadrons without a weak boson. In Figure 2.2 (g) we show the first QCD correction associated to the hadron vacuum polarization (HVP), but there are also higher-order terms. For instance, the hadronic light-by-light contribution, which occurs at three loops. However, these QCD corrections can not be computed perturbatively and they are mainly obtained by means of lattice QCD. For a recent review on the lattice QCD calculations for the muon AMM see Ref. [94]. Note that the main contribution to the leading-order HVP comes from light quarks, see *e.g.* Refs. [95, 96].

- **The EW contribution.** It contains the loop contributions involving the gauge bosons $W^{\pm}$, Z and also the Higgs boson, as can be seen at leading order in Figure 2.2 (d), (e) and (f), respectively. It could be the case where higher-order

corrections become more relevant that the lower ones. In particular, the one-loop correction due to the Higgs boson involves two couplings of the scalar to the (light) charged lepton, namely m_f, whereas there could be two-loop contributions with only one of those couplings (if the Higgs boson couples once to the lepton). In this case, there is no relative suppression with respect to the one-loop calculation because one factor of the lepton mass is needed for the chirality-flipping in AMMs. See a detailed calculation of the EW contribution to the AMM of the muon in Refs. [97, 98].

Now, let us focus on the most important contribution to the AMM of charged leptons, the QED term, particularised for the electron. In general, it can be split into different pieces according to their dependence on the mass of the charged leptons, namely:

$$a_e^{\text{QED}} = A_1 + A_2\left(\frac{m_e}{m_\mu}\right) + A_2\left(\frac{m_e}{m_\tau}\right) + A_3\left(\frac{m_e}{m_\mu}, \frac{m_e}{m_\tau}\right) . \tag{2.18}$$

From the definition of the AMM given in Equation (2.7) we see that this quantity is dimensionless. Therefore, any possible dependence on lepton masses should enter as ratios.

The A_i terms (for $i = 1, 2, 3$) can be calculated perturbatively and expressed as an expansion in the coupling constant of QED, the charge of the electron, e. As can be seen, for instance, from Figure 2.2 (b), the coupling e will enter in the computation of the AMM in even powers, therefore it is useful to take the fine-structure constant α given in Equation (2.17) as the expansion parameter. In view of that, the A_i terms can be written as

$$A_i = \left(\frac{\alpha}{\pi}\right) A_i^{(2)} + \left(\frac{\alpha}{\pi}\right)^2 A_i^{(4)} + \left(\frac{\alpha}{\pi}\right)^3 A_i^{(6)} + \dots . \tag{2.19}$$

The superscript $A_i^{(2n)}$ indicates that a Feynman diagram with n-loops enters in the $2n$th-order of the perturbation series in the QED coupling. Regarding this, it is interesting to note that the $A_1^{(2)}$ is the lepton-mass independent term associated with the Schwinger's calculation, and therefore $A_1^{(2)} = 1/2$. Moreover, the QED is a renormalisable theory, and then it yields to finite results for the coefficients $A_i^{(2n)}$. In particular, coefficients up to $\mathcal{O}(\alpha/\pi)^4$ have been computed both numerically and analytically, whereas the 10th-order terms (or equivalently $\mathcal{O}(\alpha/\pi)^5$ coefficients) have been determined numerically in Ref. [99]. In addition, one can find in Table 2 of the aforementioned reference the hadronic and EW contributions to the AMM of the electron.

Apart from the lepton masses that are used as input parameters in A_2 and A_3 in Equation (2.18), the other relevant ingredient for the determination of the electron AMM is the fine-structure constant, see *e.g.* Equation (2.19). Basically, α is an input parameter for the computation of a_e, and it must be derived from other experimental measurements. In particular, its best determination is based on atomic recoil measurements. This kind of experiments use matter-wave interferometry to first, determine the recoil velocity of an atom that absorbs a photon, calculate the quotient h/m_X,

	α^{-1}	$a_e^{\rm SM} \times 10^{12}$	$\delta a_e^{\rm SM}/a_e^{\rm SM}$ (ppb)	$\Delta a_e \times 10^{12}$
$\alpha_{\rm Rb}^{(\rm LKB,2010)}$ [101]	137.035 999 037(91)	1 159 652 182.032(720)	0.62	-1.30 ± 0.77 $[-1.7\,\sigma]$
$\alpha_{\rm Cs}^{(\rm Berkeley,2018)}$ [102]	137.035 999 046(27)	1 159 652 181.61(23)	0.19	-0.88 ± 0.36 $[-2.4\,\sigma]$
$\alpha_{\rm Rb}^{(\rm LKB,2020)}$ [103]	137.035 999 206(11)	1 159 652 180.252(95)	0.08	0.48 ± 0.30 $[\ \ 1.6\,\sigma]$

Table 2.2: *Values of the fine-structure constant extracted from atomic recoil measurements, see details in the text. Also the SM computation of the electron AMM moment given in Equation* (2.16) *is listed, in addition to its precision in parts-per-billion (ppb). Finally, the difference between the SM prediction and the experimental measurement of the electron AMM given in Equation* (2.22) *is also presented.*

where m_X is the mass of an atom X, and finally obtain α by means of

$$hcR_\infty \equiv \frac{1}{2} m_e c^2 \alpha^2 \quad \rightarrow \quad \alpha^2 = \frac{2R_\infty}{c}\frac{h}{m_e} = \frac{2R_\infty}{c}\frac{m_X}{m_e}\frac{h}{m_X}\,, \tag{2.20}$$

which is taken as a definition and extracted from spectroscopy of hidrogen-like atoms (with just one electron, and in some cases muon or antiproton). Here, R_∞ is the Rydberg constant, which is obtained from hydrogen spectroscopy, and m_e is the electron mass. With respect to the Rydberg constant, one has to consider QED corrections, see *e.g.* [100], so in some sense the determination of the fine-structure constant based on Equation (2.20) is not independent of QED. However, the uncertainty from the quantity h/m_X that enters in the full computation is the dominant one, and this extraction of α can be understood as independent of QED.

We summarise in Table 2.2 the last values of the fine-structure constant obtained from experiments based on atomic recoil measurements. In particular, the subscript and the superscript in α in the first column indicate the atoms which have been used, the year of the experimental result and the experimental collaboration, respectively. In addition, we also present the $a_e^{\rm SM}$ given in Equation (2.16) which is obtained using these particular values for α, see *e.g.* Equations (2.16), (2.18) and (2.19). The main source of the uncertainty for $a_e^{\rm SM}$ is the QED contribution.

2.2.2 Experimental results

So far, we have investigated the different terms that contribute to the theoretical estimation in the SM of the AMM of charged leptons, in particular of the electron. On the other hand, from the experimental point of view we can also obtain a determination of this quantity. In particular, the most recent experimental result for the electron AMM is [104]:

$$a_e^{\rm exp} = 1\,159\,652\,180.73(28) \times 10^{-12} \quad (0.24\,\text{ppb})\,. \tag{2.21}$$

Now, the roles of a_e and the fine-structure constant can be reversed, and it is possible to derive a value for α from the experimental determination of the AMM. Regarding

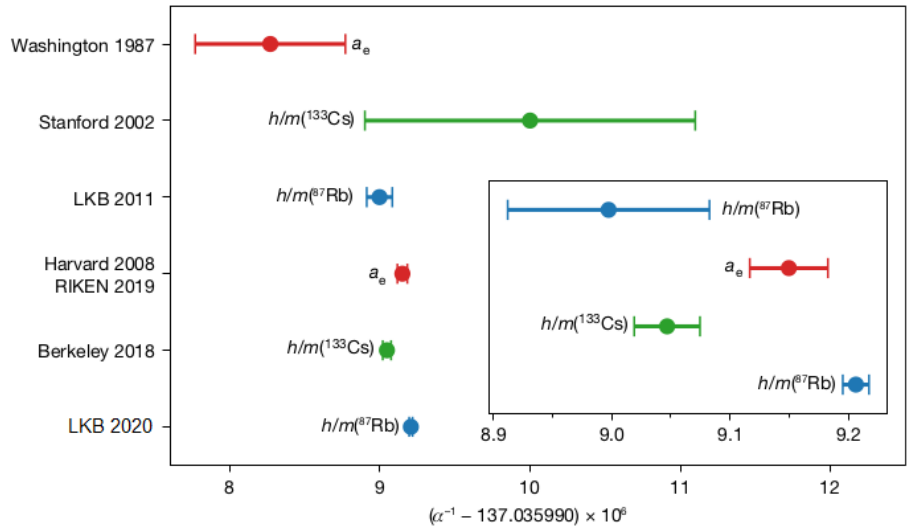

Figure 2.3: *Comparison of the values of the fine-structure constant extracted from experimental measurements and QED computations (red points) and atomic recoil measurements (green and blue points). Error bars are associated to* $\pm 1\,\sigma$ *uncertainty. The inset shows a zoomed-in region with the most accurate values. In this particular region, the values of* α *labelled as LKB 2011, Berkeley 2018 and LKB 2020 are given in Table 2.2. In addition, the value of the fine-structure constant labelled as Harvard 2008 is extracted from the experimental determination in Equation* (2.21)*, see Ref. [104]. Figure extracted from Ref. [103].*

this, in Figure 2.3 we show different values of the fine-structure constant obtained from i) experimental determination of the electron AMM and QED calculations (red points) and ii) atomic recoil measurements (green and blue points).

At this point, we can compute the difference of the experimental result and the theoretical estimation of the electron AMM by means of

$$\Delta a_e \equiv a_e^{\text{exp}} - a_e^{\text{SM}}\,, \tag{2.22}$$

and complete the Table 2.2. In the last column of this table we give this quantity, where we use for a_e^{exp} the value in Equation (2.21), and for a_e^{SM} the different estimations by means of the determination of α also given in the same table, in particular in the third column.

With respect to the other charged leptons, let us mention that due to the short lifetime of taus, namely $\tau_\tau = 2.903 \times 10^{-13}\,\text{s}$, it is very difficult to get a precise experimental determination of its AMM. In particular, its theoretical prediction in the SM [105] and the experimental estimation [23] are:

$$a_\tau^{\text{SM}} = 117\,721(5) \times 10^{-8}\,, \tag{2.23}$$

$$a_\tau^{\text{exp}} \;\epsilon\; [-0.052,\, 0.013] \quad (95\,\%\,\text{C.L.})\,. \tag{2.24}$$

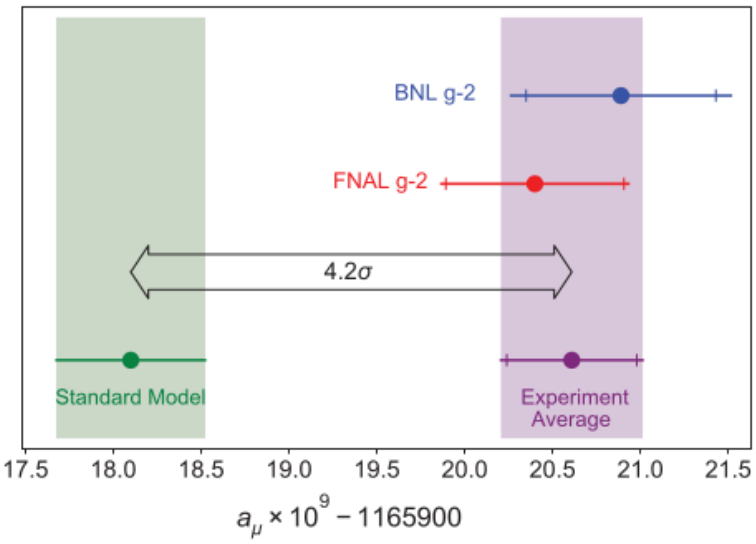

Figure 2.4: *Different values of the muon AMM, namely its SM prediction (green) and the experimental measurements from both BNL E821 (blue), and the recent FNAL E989 (red). In addition, it is also shown the combined average of the experimental values (purple). Figure extracted from Ref. [107].*

On the other hand, muons live sufficiently long and can be copiously produced. Therefore, we can obtain precise measurements of its AMM. The values for the theoretical prediction in the SM [106] and the experimental determination [107] are:

$$a_\mu^{\mathrm{SM}} = 116\,591\,810(43) \times 10^{-11} \quad (0.37\,\mathrm{ppm})\,, \tag{2.25}$$

$$a_\mu^{\mathrm{exp}} = 116\,592\,061(41) \times 10^{-11} \quad (0.35\,\mathrm{ppm})\,. \tag{2.26}$$

The main source of the uncertainty in the SM prediction is related to hadronic effects, namely the leading order hadronic vacuum polarization contribution and the hadronic light-by-light scattering contribution. Related to this, for a recent review of the prospects for improving the precison of these contributions see Ref. [108]. Moreover, the current status of the experimental measurement of the muon AMM has been reviewed in Ref. [109].

With respect to the experimental value of the AMM of the muon, it is about 1500 times less precise than a_e^{exp}, see *e.g.* Equations (2.21) and (2.26). However, the muon AMM is still much more sensitive to EW and hadronic contributions or NP effects than the electron one. In general, these contributions are proportional to m_l^2 (naive scaling, see *e.g.* Equation (2.15)), and the enhancement due to $(m_\mu/m_e)^2 \simeq 43000$ can compensate the experimental precision, making the muon AMM a better candidate to study the effects of NP.

As in the case of the electron, now we can compute the difference between the SM prediction and the experimental measurement of the muon AMM in Equations (2.25)

and (2.26):

$$\Delta a_\mu \equiv a_\mu^{\rm exp} - a_\mu^{\rm SM} = (2.51 \pm 0.59) \times 10^{-9} \ \ [4.2\,\sigma] \ . \tag{2.27}$$

We show in Figure 2.4 different values for the muon AMM: the SM calculation given in Equation (2.25) in green, and the experimental results from i) Brookhaven National Laboratory E821 Experiment (BNL) [110] and ii) Fermilab Muon $g-2$ Experiment E989 (FNAL) [107] in blue and red, respectively. Also, the average value for the experimental measurements given in Equation (2.26) is depicted in purple.

As can be seen from both Equation (2.27) and Figure 2.4, there is a discrepancy between the theoretical value and the experimental measurement of the muon AMM at the level of $4.2\,\sigma$. This can be understood as a hint of NP, and a lot of effort has been made during the last years by the theoretical community in order to address this question [111–113].

We know that AMM is generated, at least, at one loop, and requires a chirality flip. Therefore, one can have two scenarios depending on where the chirality flip occurs, either on the internal NP line in the loop or on the external (muon) line. In the latter case, there is a suppression due to the muon mass insertion, which flips chirality. Therefore, the NP in the loop must be light, see e.g. Ref. [114] where the new particle that explains the muon anomaly is a vector boson.[5] There are other examples of light NP that could explain the anomaly, for instance models with axion-like particles (ALPs) [116–121]. On the other hand, if the chirality flip occurs on the internal NP line in the loop, the mass of the new particle can be larger (in the TeV range). For instance, see Refs. [122, 123] and [113] for models with singlet scalars and ALPs that couple to heavy vector-like leptons, respectively.

However, by means of the naive scaling mentioned before, see *e.g.* Equation (2.15), one can infer the contribution to the electron AMM, if it is generated by the same NP responsible for the muon anomaly. Therefore, from the value in Equation (2.27) one can estimate

$$\Delta a_e \sim \left(\frac{m_e}{m_\mu}\right)^2 \Delta a_\mu \simeq (0.060 \pm 0.014) \times 10^{-12} \, . \tag{2.28}$$

With this kind of (naive scaling) arguments, we conclude that reaching a good accuracy in the determination of the electron AMM, either excluding or observing a discrepancy between its theoretical and experimental values, could play an important role for studying the origin of the muon anomaly.

In the next chapter, we will assume the last value for the electron AMM given in Table 2.2, which has been obtained by the experimental group from Laboratoire Kastler Brossel (LKB). In particular, it reads [103]:

$$\Delta a_e^{\rm (LKB)} = (0.48 \pm 0.30) \times 10^{-12} \ \ [1.6\,\sigma] \ . \tag{2.29}$$

The positive sign of this discrepancy will motivate us to consider scalars as a possible explanation of the result. In particular, we will analyse whether the presence of light

[5] In Ref. [115] the vector boson, which is a gauge boson from an anomaly-free $U(1)_X$, can explain the discrepancy in the muon AMM for masses $\mathcal{O}(100)$ MeV.

scalars could spoil the extraction of the fine-structure constant from the AMM of the electron.

Conversely, one can adopt a different strategy in view of the tension between the recent values for Δa_e, see *e.g.* the results from 2018 and 2020 in Table 2.2. As we have discussed along this chapter, the fine-structure constant serves as an input for the AMMs, and regarding its determination, the latest result from LKB in 2020 seems to be incompatible with older measurements of α done by the same experimental group, see *e.g.* the value and the error bars of the points in blue in Figure 2.3.

In view of what has been commented in the last paragraph, one can take for the discrepancy in the electron AMM the value obtained by the Berkeley group in 2018, namely [102]:

$$\Delta a_e^{(\text{Berkeley})} = -\,(0.88 \pm 0.36) \times 10^{-12} \;\; [-2.4\,\sigma] \; . \tag{2.30}$$

We will adopt this point of view in Section 3.2 of the next chapter, where we will try to explain the discrepancy in both the electron and the muon AMM by adding new scalars and pseudo-scalars that couple to charged leptons.[6] For the muon anomaly, we will assume the value given in Equation (2.27). Let us mention that a lot of effort has been done in order to provide possible explanations to both discrepancies, see *e.g.* Refs. [116–118, 124–139].

[6] As we will see in the next chapter, scalars (pseudo-scalars) give a positive (negative) one-loop contribution to the AMM of charged leptons.

CHAPTER 3

Light scalars and the Anomalous Magnetic Moment of charged leptons

As we have already discussed in the previous chapter, AMM of charged leptons can be used to obtain the value of the fine-structure constant. In view of that, in the first part of the present chapter we will consider whether the presence of NP, in particular neutral scalars that couple to electrons, could affect the extraction of the fine-structure constant from the electron AMM.

Moreover, in the last part of the chapter we will analyse the parameter space of new scalars and pseudo-scalars that couple to charged leptons and can explain both the electron and the muon AMM.

3.1 Robustness of the extraction of α from a_e

The prediction of the g-factor of the electron using QFT and its precise measurement is considered one of the best successes of physics, given that the incredible precision achieved by experiments, which has been matched by precise calculations in the SM, as we already discussed in Chapter 2. This success has led in the last years to use the electron AMM to extract one of the most important parameters of the SM, the fine-structure constant, α, which measures the strength of electromagnetic interactions.

However, α and a_e are quite different objects. As it is well known the photon-electron vertex, given in Equation (2.10), contains two form factors, $F_1(q^2)$ and $F_2(q^2)$, which at $q^2 = 0$ give the electron charge and the AMM, respectively; see *e.g.* Equation (2.11). Since gauge invariance requires the charge of the electron to be (minus) one at all orders, the normalization of $F_1(q^2)$ is fixed, $F_1(0) = 1$. This is independent on the details of the theory (it would apply equally well to a proton) as long as electromagnetic gauge invariance is preserved. On the other hand, $F_2(0)$ is a derived quantity (calculable in renormalisable theories) and depends on the details of the the-

ory. In fact, any NP added to the SM will have an impact on a_e but will have no impact on $F_1(0)$. This fact makes, in principle, the computation of α from the measurement of $F_1(0)$ a much more robust determination of the fine-structure constant. The fact that the determinations of α from a_e and other methods based on $F_1(0)$ agree quite well can be used to set limits on the possible NP that could affect a_e, see *e.g.* Refs. [140, 141].

Alternatively, one may be worried about the fact that the possible NP beyond the SM could pollute the extraction of α from a_e. Here we will take this last point of view and will study some NP designed "ad hoc" in order to give large contributions to a_e. Then, we will try to bound its parameter space from the experimental results. Finally, once the experimental constraints have been applied, we will conclude if the NP can affect the determination of α from a_e.

3.1.1 The effective Lagrangian below the muon mass

For scales much below the muon mass ($E \ll m_\mu$), and assuming there are no new light particles at this scale, physics can be described by the QED Lagrangian plus some non-renormalisable interactions

$$\mathcal{L} = \mathcal{L}_{\text{QED}} + \mathcal{L}_{\nu K} + \mathcal{L}_5 + \mathcal{L}_6 + \cdots , \tag{3.1}$$

with

$$\mathcal{L}_{\text{QED}} = \bar{e} i \not{D} e - m \bar{e} e , \tag{3.2}$$

and $\mathcal{L}_{\nu K}$ the neutrino kinetic and mass terms we will not discuss any more. The dimension six Lagrangian $\mathcal{L}_6$ in Equation (3.1) contains four-fermion weak interactions involving electrons and neutrinos which are not relevant for our discussion. The only dimension five operator one can write in $\mathcal{L}_5$ is just the electron (also neutrino) magnetic moment:[1]

$$\mathcal{L}_{\text{eff}} = \frac{e}{(4\pi)^2} \frac{C}{M} \left(\bar{e} \sigma_{\mu\nu} e \right) F^{\mu\nu} . \tag{3.3}$$

Note that in this expression we use the same letter for the electron charge and the electron field. This effective Lagrangian contains all kind of contributions from the SM particles with masses larger than the muon mass (i.e. muon, tau, quarks, weak gauge bosons), but also contributions from new particles with masses $\geqslant m_\mu$. Here, M is a mass which sets the scale of these contributions (in principle the mass of the lightest particle that give a contribution to this operator). On general grounds one can show that this effective Lagrangian can only be generated at the loop level [72], that is why we have included a factor $1/(4\pi)^2$. Finally, C, which is real,[2] contains the rest of the factors. As we already mentioned in Chapter 2, AMM change chirality. And note that in the SM (an many of its extensions), the only source of chirality breaking are fermion masses, then C should be proportional to m_e and then one expects further suppressions in C order m_e/M. For the sake of generality we will allow other sources of chirality breaking. Finally, there is also the possibility that this dimension five

[1] In this thesis we do not study EDMs. However, see a brief discussion about them in Section 2.2.

[2] If the Lagrangian in Equation (3.3) is hermitian, C must be real.

operator obtains contributions from some kind of non-perturbative physics (as for instance proton and neutron magnetic moment obtain the dominant contributions from QCD). This case can also be taken into account with this parametrization by allowing C to be as large as $(4\pi)^2$.

In general, C can be split in two terms, namely the SM contributions and the NP contributions

$$C = C_{\rm SM} + C_{\rm NP}\,, \tag{3.4}$$

where we will always assume that $C_{\rm NP}$ is small compared with $C_{\rm SM}$. Therefore, the effective Lagrangian in Equation (3.3) gives the following contribution to the AMM of the electron:

$$a_e^{\rm eff} = \frac{4m_e\,C}{(4\pi)^2 M}\,. \tag{3.5}$$

The complete contribution to a_e will then be the pure QED contribution[3] plus the contribution from the effective Lagrangian, *i.e.*

$$a_e = a_e^{\rm QED} + a_e^{\rm eff} = a_e^{\rm QED} + \frac{4m_e\,C_{\rm SM}}{(4\pi)^2 M} + \frac{4m_e\,C_{\rm NP}}{(4\pi)^2 M} = a_e^{\rm SM} + a_e^{\rm NP}\,, \tag{3.6}$$

with

$$a_e^{\rm NP} = \frac{4m_e\,C_{\rm NP}}{(4\pi)^2 M}\,. \tag{3.7}$$

From Equation (3.6) and the difference Δa_e defined in Equation (2.22), one can set bounds on the contribution from NP that could explain the current discrepancy in the electron AMM. In particular, using that[4]

$$\Delta a_e^{\rm (LKB)} = (0.48 \pm 0.30) \times 10^{-12}\ \ [1.6\,\sigma]\,, \tag{3.8}$$

we obtain

$$-0.11 < a_e^{\rm NP} \times 10^{12} < 1.07 \quad (95\,\%\,\text{C.L.})\,. \tag{3.9}$$

Then, assuming that the NP contribution can not be large, namely $\left|a_e^{\rm NP}\right| < 10^{-12}$, we obtain a lower bound on the NP mass scale:

$$M > 10^7\,C_{\rm NP}\ \text{GeV}\,. \tag{3.10}$$

In fact, if we assume the highest possible value of the coupling coming from some non-perturbative physics, $C_{\rm NP} \simeq (4\pi)^2$ and we get $M > 10^9\,\text{GeV}$; if the physics is perturbative, $C_{\rm NP} \simeq 1$ and one finds $M > 10^7\,\text{GeV}$. However, we mentioned before that in many extensions of the SM the only source of chirality breaking are fermion masses. In those cases one expects $C_{\rm NP} \propto m_e/M$. Then, if the couplings of NP are order one, we get that the masses of new particles could be around the EW scale, namely $M > 70\,\text{GeV}$. But the couplings of new particles could be much smaller than

[3] We already know from Chapter 2 that AMMs in the SM have three contributions, namely the QED, the EW and the hadronic ones. However, here we only write the most relevant contribution for the electron AMM, the QED contribution, in order to simplify the notation.

[4] See Table 2.2 for the evolution of the values of Δa_e.

Assumptions	C_{NP}	$M >$ (GeV)
Non-perturbative	$(4\pi)^2$	10^9
Perturbative	$C_{NP} \simeq 1$	10^7
Chirality Suppressed	$C_{NP} \simeq m_e/M$	70
Small couplings	$C_{NP} \ll 1$	Anything

Table 3.1: *The scales of NP that are obtained assuming that the NP contribution to the electron AMM from the effective operator in Equation* (3.3) *is* $|a_e^{NP}| < 10^{-12}$ *depending on the assumptions on* C_{NP}*, see e.g. Equations* (3.7) *and* (3.10).

one and therefore, the masses of new particles could take any value, even below the muon mass. In that case our effective Lagrangian description is not appropriate and we should give more details of the type of NP. Then, it makes sense to study the type of physics that could generate the dimension five operator in Equation (3.3). We summarise in Table 3.1 the lower bound on M depending on the assumptions on the coefficient C_{NP}.

3.1.2 Opening the magnetic moment operator at one loop

We will leave on a side non-perturbative physics which, as commented earlier, suggests scales which are much above any scale that can be tested in the near future. Then, the dimension five operator in Equation (3.3) can be generated at one loop by exchange of a boson and a fermion. One of the two (or the two) should be charged. However, new charged particles are bounded by LEP experiment to have a mass larger than 100 GeV, which would set the scale of the loop and the NP at $M \gtrsim 100\,\text{GeV}$, and from Equation (3.7) we obtain $a_e^{NP} \lesssim 10^{-7}$ if the loop does not give any chirality suppression.[5] This could dramatically affect the extraction of α from a_e, and it is a case to be studied. However, since the scale is above the EW scale it is compulsory to study these class of models in a full EW context not discussed here.

On the other hand, if the charged particle in the loop is a SM particle we do not have this constraint. For instance, the fermion running in the loop could be the electron and the boson could be a light neutral real scalar or pseudo-scalar, ϕ, which couples to electrons[6] as

$$\mathcal{L}_\phi = h\bar{e}e\phi \quad \text{or} \quad ih\bar{e}\gamma_5 e\phi\,. \tag{3.11}$$

In this case, we necessarily have a chirality suppression, and obtain $C_{NP} \sim h^2 m_e/M$ if $M > m_e$, which leads to[7]

$$a_e^\phi \simeq \frac{4h^2}{(4\pi)^2}\frac{m_e^2}{M^2} \lesssim \frac{4h^2}{(4\pi)^2}\,, \tag{3.12}$$

[5] This requires a heavy fermion in the loop.

[6] A similar discussion could be made with a light neutral vector boson, see *e.g.* Ref. [114].

[7] If $M < m_e$ the effective Lagrangian description cannot be used but then we can still estimate $a_e^\phi \simeq 4h^2/(4\pi)^2$.

which can be huge unless h is very small. Of course, the coupling h and the mass M of such a scalar will be strongly constrained by experiment, but it is important to check that, after imposing all those constraints, there is no region allowed that could affect the determination of α from a_e. That is what we will discuss in the following from a phenomenological point of view, assuming that the new scalar only couples to electrons.

Note that the interactions in Equation (3.11) are not gauge invariant. However, they could come from the following dimension five operator:

$$\mathcal{L}_5 = \frac{C_5}{\Lambda_5}\bar{l}e_R H\sigma + \text{H.c.}\,, \tag{3.13}$$

where Λ_5 is the typical scale of NP leading to the effective interaction, l and H are the SM left-handed lepton and Higgs doublets, respectively, e_R is a right-handed charged lepton, and σ is a complex scalar singlet. It is interesting to note that the $\bar{l}e_R H$ part in the dimension five operator in Equation (3.13) could arise from terms like $\overline{e_R} i\not{D} e_R$ or $\bar{l} i\not{D} l$, which, after using the equations of motion, will generate the same operator with an additional suppression factor $\sqrt{2}m_f/v$, that can be taken into account in the coefficient C_5. Here, m_f and v are the mass of the charged fermion that we are considering and the VEV of the Higgs field, respectively.

Now, we have two possibilities depending on whether σ gets a VEV or not. In the former case, for instance, one has to take into account that there will be corrections to the mass of the charged leptons when both H and σ develop a VEV. However, we will not analyse this complex scenario, and in the following sections we will consider a kind of "toy model" described by the interactions given in Equation (3.11).

3.1.3 Simplified model

In this part we focus on the simplest model that could give large contributions to the AMM of the electron, assuming that NP is a neutral real scalar, ρ, that couples to electrons by means of the following Lagrangian:

$$\mathcal{L}_\rho = h_e \bar{e} e \rho\,. \tag{3.14}$$

This generates a contribution to the AMM of the electron given by [140]

$$a_{e,\rho}^{(1)} = \frac{h_e^2}{(4\pi)^2}\, 2r_\rho \int_0^1 dx \frac{x^2(2-x)}{1-x+x^2 r_\rho}\,, \quad \text{with} \quad r_\rho \equiv \left(\frac{m_e}{m_\rho}\right)^2. \tag{3.15}$$

Note that the superscript in $a_{e,\rho}$ refers to the fact that it is a one-loop computation. In addition, we give in Appendix A.1 the expressions for the NP contribution to the AMM of charged leptons from different scenarios, namely scalar, pseudo-scalar and vector boson as NP.

The current status of the discrepancy for the electron AMM in Equation (3.8) shows a nice agreement (at the $1.6\,\sigma$ level) between theory and experiment, suggesting that NP contribution explaining the discrepancy can not be large, see Equation (3.9). Therefore, in order to affect the present measurement of the fine-structure

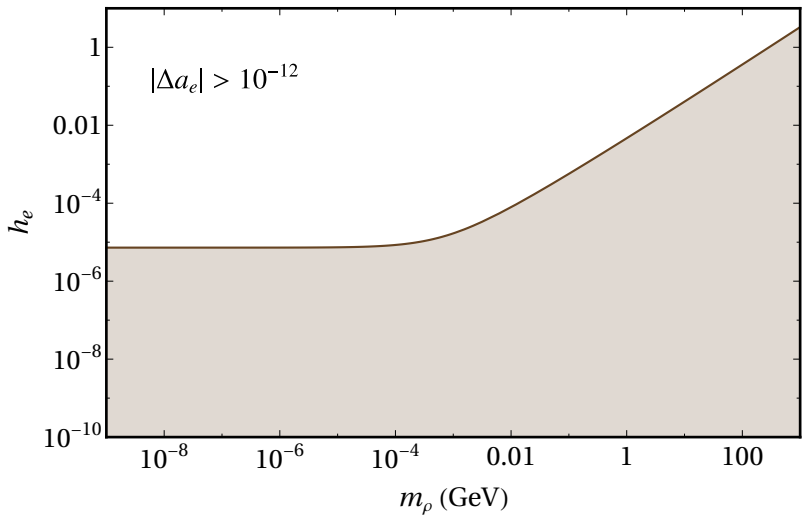

Figure 3.1: *The unshaded area corresponds to the region of the parameter space of a scalar that couples to electrons and gives a large contribution to the electron AMM, namely* $|\Delta a_e| > 10^{-12}$*. Therefore, in that region the extraction of* α *from* a_e *could be polluted by the presence of the scalar.*

constant extracted from a_e, this NP contribution should be[8] $|\Delta a_e| > 10^{-12}$, which translates into a lower bound for the coupling h_e as a function of the mass of the new particle. In Figure 3.1 we depict the parameter space where the extraction of α from a_e could be spoiled by the presence of NP in the simplest case of a scalar that couples to the electron by means of the interaction given in Equation (3.14). Note that the unshaded region corresponds to values for the discrepancy of $|\Delta a_e| > 10^{-12}$.

As has been discussed in Section 2.2.1, the fine-structure constant can be obtained mainly from two sources, i) the experimental measurement of the electron AMM (and also using QED calculations) and ii) from atomic recoil measurements. Regarding the latter, we concluded that it could be considered as (almost) independent from QED. However, it is compulsory to ask whether NP, in particular scalars, could affect the determination of α using this method. Basically, its value is obtained from Equation (2.20). Mass ratios and recoils are basically obtained from kinematic effects, and are not affected by scalars. In fact, these methods can be seen as a determination of m_e from where one obtains α once the Rydberg constant, R_∞, is known.

The only effect could come in the determination of R_∞. There is a large list of standard QED effects in R_∞, see *e.g.* Ref. [100]. From this list given in Section IV.A.1 of the aforementioned reference, there are three cases where the scalar could contribute, namely:

- Vertex electron-photon. It is assumed that the QED standard corrections are already included, and we know that the a_e contribution due to the scalar must

[8]Scalars give positive contribution to the AMM of the charged leptons whereas a negative contribution is obtained when we consider pseudo-scalars.

be very small, and probably gives a negligible correction.

- Photon self-energy. It is affected by the scalar at two loops. Since energy levels are $\mathcal{O}(\text{eV})$ we will have $q^2 \ll m_e$, therefore we assume that the scalar effects will be important only for extremely light scalars, namely $m_\rho < m_e$, and then the couplings are presumably small. In any case, this effect is an additional contribution to the Lamb shift; one can compute it but probably will be very small.

- Electron self-energy (off-shell). Scalars contribute at one loop. One should look at the calculation of the standard contribution and see how the scalars could affect.

Experimental constraints

The main purpose of this analysis is try to close the whole unshaded region of the parameter space in Figure 3.1. If this could be fulfilled, we can then safely conclude that NP contributions in the case of scalars that couple to electrons do not interfere in the extraction of α from a_e.

In the following we scrutinize the relevant experimental constraints that potentially affect the parameter space of scalars that couple to electrons, and summarise the results in Figure 3.2. Let us comment the considered experimental constraints one at a time.

- **Astrophysical constraints.** With the interaction given in Equation (3.14), there could be new processes inside stars such as $\gamma e \to e\rho$. In that case, the scalar ρ escapes an produces an extra cooling of the star [142].[9] In particular, we apply limits from extra cooling of both red giant and the so-called horizontal branch stars [143]. These constraints are shown in Figure 3.2 (top) as exclusion regions in red (RG) and orange (HB), respectively.

- **Cosmology.** For large enough coupling, scalars are in thermal equilibrium with SM particles through annihilations $ee \to \gamma\rho$, and Compton scattering $e\gamma \to e\rho$. In particular, for values of the coupling $h_e \gtrsim 5 \times 10^{-10}$ scalars can be in equilibrium with electrons before BBN, at $T \sim$ MeV. This would spoil light-nuclei abundances: any (new) light degrees of freedom in thermal equilibrium with electrons and photons will reduce, for instance, the abundance of deuterium. Comparing with observations, one can then obtain a constraint on the coupling h_e as a function of the scalar mass [143]. This experimental bound is depicted in Figure 3.2 (top) as the exclusion region in brown (BBN).

- **Precision spectroscopy.** Scalars interacting with electrons can modify theoretical predictions of spectral lines in atoms with few electrons. In addition, the high precision of current measurement of atomic spectra can be used to derive

[9] One needs to check that the particle does not decay inside or that the mean free path is larger than the size of the star.

bounds on NP that interacts with electrons (and also neutrons and protons). In particular, we depict in Figure 3.2 (top) and (bottom) the upper bound for the coupling h_e obtained from the transition $1^3S_1 - 2^3S_1$ in positronium [144], labelled as Ps in magenta.

- **Beam dump experiments.** Beam dump experiments could produce scalars via bremsstrahlung, which eventually decay back to electron pairs. The absence of this signal yields the shaded gray exclusion region in Figure 3.2 (top) and (bottom), labelled as BEAM DUMP. This exclusion region incorporates the results from E137 [145], E141 [146] and Orsay [147, 148] beam dump experiments. The JLab experiment HPS [149] future projection applied to scalars [150] is also shown as a dot-dashed cyan line.

- **Kaon decay experiments.** With respect to the constraints from kaon decay experiments,[10] we could have extra decay channels involving the new scalar, ρ, namely rare kaon decays $K \to e\nu\rho$. Therefore, current measurements of kaon decay can be used to obtain upper bounds on the coupling h_e as a function of the scalar mass. We have considered two constraints depending on m_ρ: i) $K \to e\nu\rho$ for $m_\rho < 2m_e$, and ii) $K \to e\nu\rho\,(\rho \to ee)$ for $m_\rho \geqslant 2m_e$. Note that if scalars predominantly couple to muons, one can perform a similar analysis regarding the constraints coming from rare kaon decays $K \to \mu\nu\rho$, see *e.g.* Ref. [152] where also the case of light vector bosons is studied.

  First, we assume that $m_\rho < 2m_e$. In this case, scalars can not decay into electrons and they leave the experimental setup yielding no signal.[11] The value of the branching ratio (BR) of the decay $K \to e\nu$ given by [23]

$$\mathrm{BR}(K \to e\nu) = (1.582 \pm 0.007) \times 10^{-5}\,, \tag{3.16}$$

  can then be used for getting an upper bound on h_e. In particular, we impose that the BR of rare decays $K \to e\nu\rho$ must be smaller than the uncertainty in Equation (3.16), which yields the following bound:

$$\mathrm{BR}(K \to e\nu\rho) < 0.007 \times 10^{-5}\,. \tag{3.17}$$

  In Appendix A.2 we have computed the $\mathrm{BR}(K \to e\nu\rho)$, see *e.g.* Equation (A.28). Substituting back its expression in Equation (3.17) we can obtain an upper bound on the coupling h_e, namely:

$$h_e < \left(\frac{0.007 \times 10^{-5} \times 96\,\pi^2 \omega\,(1-\omega)^2}{F(\omega, y)\,\mathrm{BR}(K \to e\nu)} \right)^{1/2}\,. \tag{3.18}$$

  Here, we have defined $\omega \equiv (m_e/M_K)^2$ and $y \equiv (m_\rho/M_K)^2$, and the expression for the function $F(\omega, y)$ is given in Appendix A.2, see *e.g.* Equation (A.25). This

[10] For a recent review of NP searches using rare kaon decays see *e.g.* Ref. [151].

[11] We consider that the signal comes from the e^+e^- pairs generated from decays of the new scalar ρ. There could be signals from $\rho \to \gamma\gamma$, although this process is one-loop suppressed.

constraint on the coupling as a function of the scalar mass is depicted in green in Figure 3.2 (top) and labelled as $K \to e\nu\rho$.

On the other hand, one can assume that the mass of the new scalar is larger than 1 MeV, *i.e.* $m_\rho \geqslant 2m_e$. In this case, e^+e^- pairs can be produced as a consequence of the decay of the scalar yielding a signal in experiments. The value of the BR of the decay $K \to e\nu\rho$ with $\rho \to ee$ can be constrained using that:[12]

$$\mathrm{BR}(K \to e\nu ee) = \mathrm{BR}(K \to e\nu\rho) \times \mathrm{BR}(\rho \to ee) < \delta_K \,. \tag{3.19}$$

In the last equation, δ_K is defined as the difference between the theoretical estimation in the SM and the experimental value of the $\mathrm{BR}(K \to e\nu ee)$, given by [153]:

$$\delta_K \equiv \mathrm{BR}(K \to e\nu ee)|_{\mathrm{theo}} - \mathrm{BR}(K \to e\nu ee)|_{\mathrm{exp}} = 0.59 \times 10^{-8} \,. \tag{3.20}$$

In Appendix A.2 we have computed the $\mathrm{BR}(K \to e\nu\rho)$, see *e.g.* Equation (A.28). One can then obtain an upper bound on the coupling h_e from Equations (3.19) and (3.20), namely:

$$h_e < \left(\frac{0.59 \times 10^{-8} \times 96\,\pi^2 \omega\,(1-\omega)^2}{F(\omega, y)\,\mathrm{BR}(K \to e\nu)} \right)^{1/2} . \tag{3.21}$$

Here we have used the same definitions for ω, y and $F(\omega, y)$ as in Equation (3.18). This constraint on the coupling as a function of the scalar mass is depicted in red in Figure 3.2 (bottom) and labelled as $K \to e\nu\rho\,(\rho \to ee)$.

- **Constraints from Z boson decay.** Additional constraints on the parameter space could be derived considering e^+e^- collider experiments.[13] In particular, the LEP experiment has studied properties of the Z boson with a very good precision, and these results can be used to constrain NP effects. If new scalars were produced via their coupling with electrons, the Z boson properties would be affected. In view of that, we have analysed three constraints related with the Z boson decay width, namely i) $Z \to ee\rho$, ii) $Z \to ee$ at next-to-leading order (NLO) and iii) $Z \to 4e$. We discuss them in detail in what follows.

  For instance, we could have the emission of scalars via the process $Z \to ee\rho$. In this case, an upper bound on h_e could be derived using the value for the $\mathrm{BR}(Z \to ee)$. Similarly to kaon decays discussed before, first we assume that $m_\rho < 2m_e$, therefore scalars can not decay into e^+e^- pairs and yield no signal in experiments. We can use the value for the BR of $Z \to ee$ given by [23]

$$\mathrm{BR}(Z \to ee) = (3.3632 \pm 0.0042)\,\% \,, \tag{3.22}$$

[12] We have used the narrow width approximation, *i.e.* $\Gamma(K \to e\nu ee) = \Gamma(K \to e\nu\rho) \times \mathrm{BR}(\rho \to ee)$. In addition, we assume that $\mathrm{BR}\,(\rho \to ee) = 1$ because ρ only couples to electrons.

[13] See a nice discussion about the effects of new light gauge bosons in electron-positron collision experiments in Ref. [154]. In addition, they apply their results to the case of light scalars in Section IV of the aforementioned reference.

to get a constraint on h_e. One has to require that the BR of the new decay channel, namely $Z \to ee\rho$, must be smaller than the uncertainty in Equation (3.22). This assumption reads

$$\mathrm{BR}(Z \to ee\rho) < 4.2 \times 10^{-5} \,. \tag{3.23}$$

In Appendix A.3 we have computed the $\mathrm{BR}(Z \to ee\rho)$, see *e.g.* Equation (A.39). Substituting back its expression in Equation (3.23) we can obtain an upper bound on the coupling h_e, namely:

$$h_e < \left(\frac{4.2 \times 10^{-5} \times 32\,\pi^2\,(1-4\omega)^{3/2}}{[G(\omega,y) + I(\omega,y)]\ \mathrm{BR}(Z \to ee)} \right)^{1/2} . \tag{3.24}$$

Here, we have defined $\omega = (m_e/M_Z)^2$ and $y = (m_\rho/M_Z)^2$, and the expressions for the functions $G(\omega,y)$ and $I(\omega,y)$ are given in Appendix A.3, see *e.g.* Equations (A.33) and (A.34). This constraint on the coupling as a function of the scalar mass is depicted in blue in Figure 3.2 (top) and labelled as $Z \to ee\rho$.

Moreover, loop corrections due to scalars can affect the leptonic decay width of the Z boson. In particular, the NLO correction to the decay width $Z \to ee$ is approximately given by [155]:[14]

$$\delta\Gamma(Z \to ee) \simeq -\Gamma_0 \frac{h_e^2}{8\pi^2} \left(\log\left(\frac{M_Z^2}{m_\rho^2} \right) - 2 \right) , \tag{3.25}$$

where Γ_0 is the leading order contribution given by (dropping m_e against M_Z):

$$\Gamma_0 = \frac{\alpha}{12 s_W^2 c_W^2} (g_V^2 + g_A^2) M_Z \,. \tag{3.26}$$

We can get an upper bound on the coupling h_e imposing that the NLO correction to the Z boson decay into electrons should be smaller than the uncertainty in the experimental measured value of the BR of the process $Z \to ee$ given in Equation (3.22), namely:

$$\frac{|\delta\Gamma(Z \to ee)|}{\Gamma_Z} < 4.2 \times 10^{-5} \,. \tag{3.27}$$

In the last equation, Γ_Z is the full Z boson decay width, $\Gamma_Z = 2.5\,\mathrm{GeV}$. Using Equations (3.25–3.27) we get an upper bound on the coupling h_e as a function of the scalar mass depicted in olive in Figure 3.2 (bottom), and labelled as $Z \to ee$ (NLO).

Finally, we can derived a constraint for the coupling h_e coming from the fact that the final scalar in the process $Z \to ee\rho$ could decay into e^+e^- pairs if it

[14] In Ref. [155] they neglect m_e in the loops, and keep m_ρ only as an IR regulator, which is justified for $m_\rho \gg m_e$ where this bound is mostly relevant.

had enough mass, *i.e.* $m_\rho \geqslant 2m_e$.[15] In this scenario, the final state of the Z boson decay involves four electrons, and one can then use the value for the $\mathrm{BR}(Z \to 4l)$, namely [23]

$$\mathrm{BR}(Z \to 4l) = (4.63 \pm 0.21) \times 10^{-6}\,, \tag{3.28}$$

to derive a constraint for the coupling h_e by means of[16]

$$\mathrm{BR}(Z \to 4l) = \mathrm{BR}(Z \to ee\rho) \times \mathrm{BR}(\rho \to ee) < \delta_Z\,. \tag{3.29}$$

In the last equation, δ_Z is the uncertainty in Equation (3.28), $\delta_Z = 0.21 \times 10^{-6}$. In Appendix A.3 we have computed the $\mathrm{BR}(Z \to ee\rho)$, see *e.g.* Equation (A.39). Substituting back its expression in Equation (3.29) we can obtain an upper bound on the coupling h_e, namely:

$$h_e < \left(\frac{\delta_Z \times 32\,\pi^2\,(1-4\omega)^{3/2}}{[G(\omega,y) + I(\omega,y)]\ \mathrm{BR}(Z \to ee)} \right)^{1/2}\,. \tag{3.30}$$

Here we have used the same definitions for ω, y, $G(\omega,y)$ and $I(\omega,y)$ as in Equation (3.24). This constraint on the coupling as a function of the scalar mass is depicted in blue in Figure 3.2 (bottom) and labelled as $Z \to 4e$.

- **KLOE experiment.** Basically, the KLOE experiment studies processes like $ee \to \gamma\, A'$ with the later decay of A' into e^+e^- pairs. Here, A' stands for light vector boson mediators, the so-called "dark photons". They talk to the SM photon through a mixing term in the interaction Lagrangian such as $\epsilon F_{\mu\nu} F'^{\mu\nu}$, where $F_{\mu\nu}$ and $F'_{\mu\nu}$ are the electromagnetic and the "dark" field strength tensor, respectively.

  In this experiment, a resonant peak in the e^+e^- invariant mass distribution has not yet been observed, and then the KLOE collaboration sets un upper bound on the mixing parameter ϵ as a function of the dark photon mass [157]. However, in the model that we are considering, the NP candidate that couples to electrons is a scalar instead of a vector boson (through the mixing), and this constraint should be re-interpreted into bounds on the scalar coupling h_e, see Refs. [128, 158]. Finally, the excluded region from this re-interpretation of the KLOE experimental data is depicted in green in Figure 3.2 (bottom) and labelled as KLOE2.

- **BABAR collaboration.** Similarly to the KLOE experiment, the BABAR collaboration analyses dark photons, A', through the process $ee \to \gamma\, A'$ with the later decay of A' into lepton pairs, namely electrons and muons. They obtain upper bounds on the mixing strentgh between the photon and the dark

[15] See *e.g.* Ref. [156] where stringent limits on NP (in particular scalars and vector boson) are set from the experimental measurement on the BR of the Z boson decay into four leptons.

[16] We have used the narrow width approximation, *i.e.* $\Gamma(Z \to 4e) = \Gamma(Z \to ee\rho) \times \mathrm{BR}(\rho \to ee)$. In addition, we assume that $\mathrm{BR}\,(\rho \to ee) = 1$ because ρ only couples to electrons.

photon as a function of the mass of the latter [159, 160]. These results can be re-interpreted to get a constraint on the scalar coupling h_e via the process $e^+e^- \to \gamma(\rho \to l^+l^-)$ [143].

The BABAR dark photon searches assume that A' has democratic branching ratios between electrons and muons, and therefore the muon channel is more sensitive than the electron one. In particular, Ref. [143] provides an upper bound for the scalar coupling from BABAR data that applies for $\mathrm{BR}(\rho \to \mu\mu) \gg \mathrm{BR}(\rho \to ee)$, which is the case where the scalar couples to leptons proportional to their masses. If the scalar does not couple to muons, as in our simplified model, the limit derived in [143] will be weaker by an order one factor. However, in a conservative way, we depict in Figure 3.2 (bottom) the upper bound from [143] on the coupling h_e as a function of the scalar mass. It corresponds to the orange region labelled as BABAR.

In addition, it is interesting to note that the BABAR collaboration has analysed light leptophilic scalars, ϕ_L, with masses in the MeV to GeV range, that couples to charged leptons (predominantly to taus) [161]. They search for processes like $e^+e^- \to \tau^+\tau^-\phi_L\,(\phi_L \to l^+l^-)$ with $l = e,\ \mu$, using data collected by the BABAR experiment at SLAC.

- **Belle-II experiment.** As we have already mentioned before, the process $e^+e^- \to \gamma\rho$ can be used to derive constraints on the scalar coupling h_e. In particular, the Belle II experiment [162, 163] located at the Super-KEKB e^+e^- collider could set bounds on this coupling. Related to this, we depict in Figure 3.2 (bottom) the projected sensitivity to the scalar coupling as a function of the scalar mass [150]. It corresponds to the dot-dashed black line labelled as Belle-II.

With respect to the constraints for light scalars that couple to charged leptons,[17] we encourage the interested reader to follow the analysis done in Refs. [143, 150, 165] (and references therein) with respect to new proposals and future sensitivity projections for beam dump, collider searches and cosmology constraints. In addition, it is interesting to remark the analysis done in Ref. [166] with data from the NA64 experiment at CERN. They study the contributions to the electron AMM from light bosons (namely scalar, pseudo-scalar, vector and axial vector particles, in the mass range between 1 MeV and 1 GeV), which are assumed to decay into invisible states, *e.g.* dark sector particles. On the other hand, searches for (heavy) leptophilic scalars in the mass range of 10 GeV to 1 TeV have been analysed in Ref. [167], using data from the future high-luminosity LHC runs and the high-energy lepton colliders including the Circular Electron Positron Collider (CEPC) and the muon collider.

Let us remark that the main goal in our analysis is try to close the unshaded region in Figure 3.1, and, if this could be realised, we can conclude that the extraction of the fine-structure constant from the electron AMM can not be spoiled by the presence of new scalars that couple to electrons.

[17] See Ref. [164] for a recent analysis of light bosons (vector and scalar particles) that couple to both neutrinos and quarks using current data of the COHERENT CEνNS experiment.

The experimental constraints on the parameter space of the scalar (coupling h_e and mass m_ρ) discussed in this section are plotted in Figure 3.2. On the one hand, in the low mass region ($m_\rho < 1\,\mathrm{MeV}$) depicted in the top panel, the parameter space is fully constrained by astrophysical (RG, HB) and cosmological (BBN) bounds, precision spectroscopy (Ps), beam dump experiments (BEAM DUMP), kaon decay ($K \to e\nu\rho$) and Z boson decay ($Z \to ee\rho$).

On the other hand, we plot in the bottom panel in Figure 3.2 the parameter space for $m_\rho \geqslant 1\,\mathrm{MeV}$. We can see that there are two region of interest or "open windows" in the parameter space, namely: i) couplings in the interval $10^{-4} \lesssim h_e \lesssim 10^{-2}$ for m_ρ between 1 and 60 MeV, and ii) couplings $h_e \gtrsim 0.2$ for $m_\rho > 100\,\mathrm{GeV}$.

In view of that, it will be interesting to see whether future experiments can constrain the coupling of new scalars to electrons in the "open windows" discussed in the previous paragraph. If this is the case, and the parameter space depicted in the bottom panel in Figure 3.2 is completely ruled out by experiments, one can safely ensure that the extraction of the fine-structure constant from the electron AMM will be robust in the sense that new scalars that couple to electrons could not pollute the extraction of α.

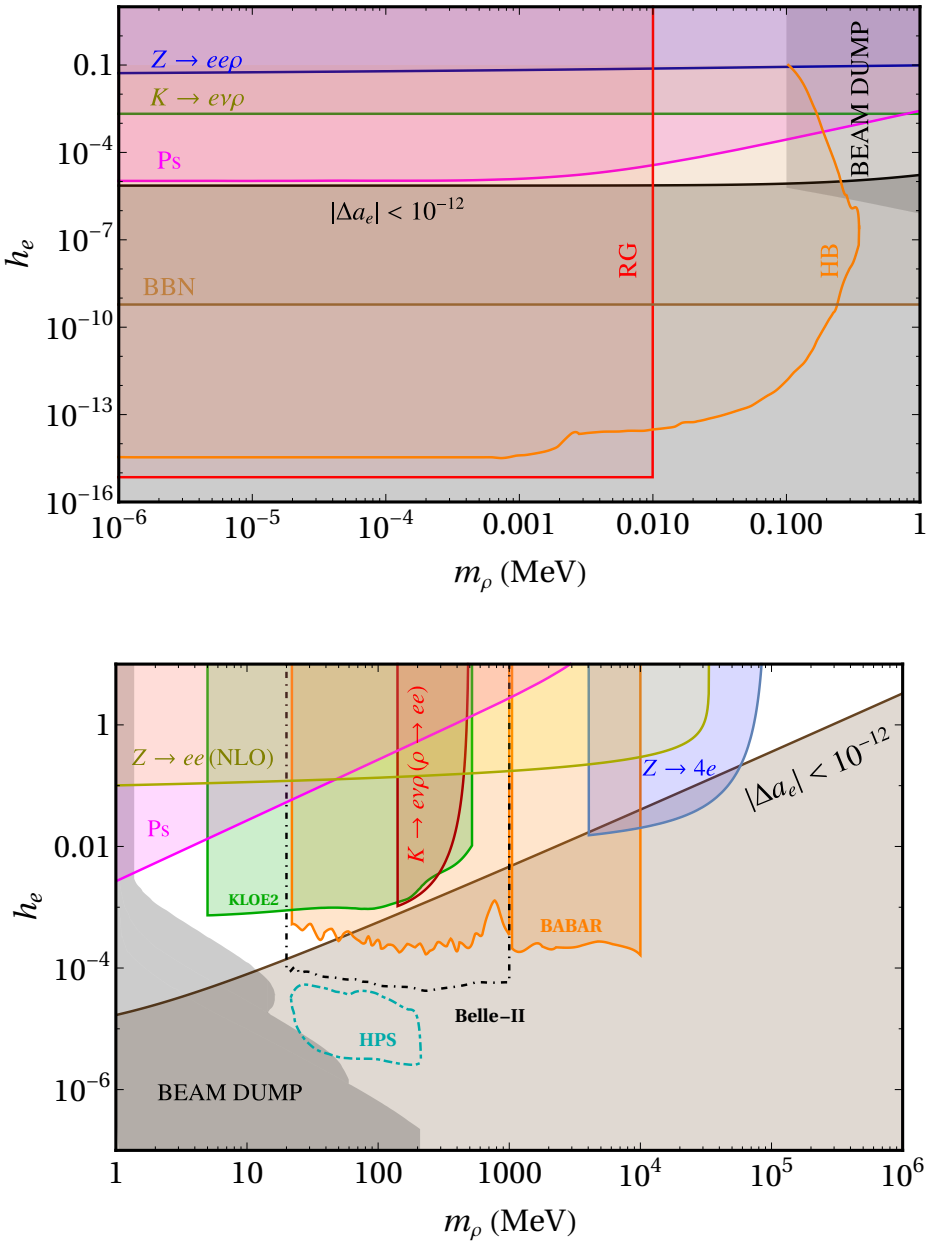

Figure 3.2: *Region of interest of the parameter space where a scalar could pollute the extraction of α from a_e. As in Figure 3.1, the unshaded region corresponds to $|\Delta a_e| > 10^{-12}$. Shaded areas represent excluded regions by the experimental constraints discussed in the text. Top: Low scalar mass region, namely $m_\rho < 1\,\text{MeV}$. The parameter space is fully constrained by different experimental bounds. Bottom: Parameter space for scalar mass $m_\rho > 1\,\text{MeV}$. There are two regions of interest, namely $1\,\text{MeV} \lesssim m_\rho \lesssim 60\,\text{MeV}$ and $m_\rho > 100\,\text{GeV}$.*

3.2 Bonus: explaining Δa_e and Δa_μ

In the previous section we have analysed how the presence of NP could spoil the extraction of the fine-structure constant from the electron AMM. In particular, we have assumed the value for Δa_e given in Equation (3.8), which is obtained using the last experimental determination of the fine-structure constant with rubidium atoms at Laboratoire Kastler Brossel (LKB). The positive sign of this contribution has motivated the analysis performed in the last section regarding scalars that couple to electrons.

However, the recent value for the discrepancy in the electron AMM has originated some debate due to the tension with the old measurement of α done by the same experimental group, see *e.g.* Table 2.2 and the value and the error bars of the blue points in Figure 2.3. Conversely, using the experimental determination of the fine-structure constant obtained by the Berkeley group[18] with cesium atoms the discrepancy reads:

$$\Delta a_e^{(\text{Berkeley})} = -\,(0.88 \pm 0.36) \times 10^{-12} \;\; [-2.4\,\sigma]\;. \tag{3.31}$$

In view of the ambiguity with respect to Δa_e depending on the chosen value of α for its determination, now we take the Equation (3.31) as the discrepancy for the electron AMM. Moreover, we also consider the anomaly in the muon case given in Equation (2.27), and try to explain both results by means of scalars and pseudo-scalars that couple to charged leptons.[19] Therefore, on general grounds we consider the following interactions[20]

$$\mathcal{L}_{\rho,\theta} = h_f \overline{f} f \rho + i h_f \overline{f} \gamma_5 f \theta\,, \tag{3.32}$$

with $f = e,\, \mu$. This Lagrangian generates one-loop contributions to electron and muon AMMs given by

$$a_f^{(1)} = \frac{h_f^2}{(4\pi)^2}\, I_f^{(1)}(m_f, m_\rho, m_\theta)\,, \tag{3.33}$$

where the superscript denotes that this contribution is generated at one loop, and the function $I_f^{(1)}(m_f, m_\rho, m_\theta)$ is defined in Appendix A.1, see *e.g.* Equations (A.5–A.7).

In what follows we present the numerical analysis performed in the parameter space of scalars and pseudo-scalars that couple to electrons and muons and can explain both discrepancies. Therefore, we consider the NP contributions to the AMMs given in Equation (3.33), and scan in the following ranges for scalar and pseudo-scalar masses and couplings:

$$m_\rho, m_\theta \,\epsilon\, \left[1, 10^5\right] \text{ MeV}, \quad h_e \,\epsilon\, \left[5 \times 10^{-6}, 10^{-1}\right], \quad h_\mu \,\epsilon\, \left[10^{-4}, 10^{-1}\right]\,. \tag{3.34}$$

[18] Note that in this section of the chapter we do not include references for any experiment. However, we refer the reader to Section 2.2.2 where we discussed in detail the experimental measurements of the AMM of charged leptons.

[19] Note that scalars give a positive one-loop contribution to AMM of charged leptons and pseudo-scalars generate a negative one.

[20] For simplicity, we assume that scalars and pseudo-scalars have the same coupling to charged leptons.

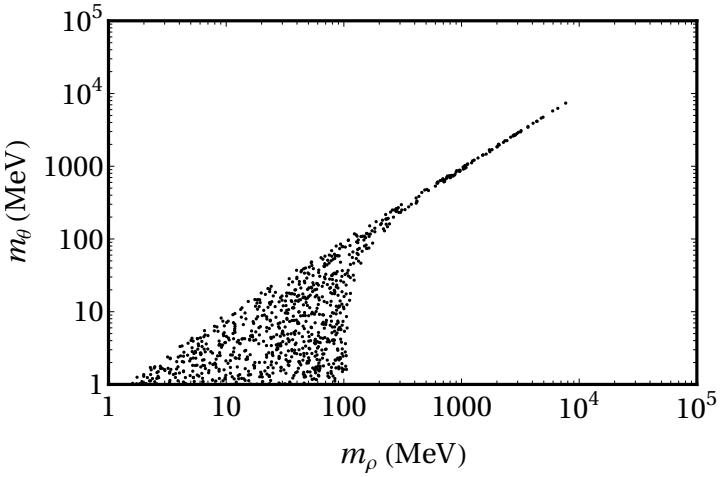

Figure 3.3: *Numerical scan of scalar (ρ) and pseudo-scalar (θ) masses that explain Δa_e and Δa_μ, i.e. the points fulfil the conditions in Equation* (3.35)*. We consider NP contributions to the AMM generated at one loop given in Equation* (3.33)*. The values of the masses and the couplings that have been used in the numerical scan are given in Equation* (3.34)*.*

Moreover, we require that the points in the parameter space explain both anomalies within $2\,\sigma$, *i.e.*:

$$-16 \leqslant a_e^{(1)} \times 10^{13} \leqslant -1.7 \qquad \text{and} \qquad 1.3 \leqslant a_\mu^{(1)} \times 10^{9} \leqslant 3.7\,. \tag{3.35}$$

We depict in Figure 3.3 the results of the scan in the scalar and pseudo-scalar masses that fulfil the conditions in the last equation. Let us try to understand these results.

The Lagrangian in Equation (3.32) gives the one-loop contribution to the AMM of charged leptons described in Equation (3.33). Moreover, the function $I_f^{(1)}(m_f, m_\rho, m_\theta)$ contains the scalar and the pseudo-scalar contributions as given in Equation (A.5), which yield the following results:

$$I_\theta^{(1)}(r_f) \simeq -\begin{cases} 1 & \text{for} \quad m_\theta \ll m_f\,, \\ -2r_f\left(\log r_f + 11/6\right) & \text{for} \quad m_\theta \gg m_f\,, \end{cases} \tag{3.36}$$

$$I_\rho^{(1)}(r_f) \simeq \begin{cases} 3 & \text{for} \quad m_\rho \ll m_f\,, \\ -2r_f\left(\log r_f + 7/6\right) & \text{for} \quad m_\rho \gg m_f\,. \end{cases} \tag{3.37}$$

Here, we have defined $r_f = (m_f/m_{\rho,\theta})^2$. We can see that there is a partial cancellation between the scalar and the pseudo-scalar contributions, but it is not complete even if the masses m_ρ and m_θ are exactly the same. In that case, $m_\rho = m_\theta = m_\phi$, and we have the following scenarios: in the limit $m_\phi \ll m_f$, the result for $I_f^{(1)}(m_f, m_\rho, m_\theta)$ is 2, whereas for $m_\phi \gg m_f$, the log-enhanced part exactly cancels, and the result is

$4/3\,(m_f/m_\phi)^2$. Therefore, we conclude that $a_f^{(1)}$ is always positive as long as the scalar and the pseudo-scalar masses are equal.[21]

If the masses of scalars and pseudo-scalars are different, we can have other combinations, and the contribution $a_f^{(1)}$ can be either positive or negative depending on the masses. Let us assume, for instance, that the pseudo-scalar is the lighter one. Then, if $m_\theta \ll m_f$ and $m_\rho \gg m_f$, the total contribution is negative. In this scenario, the scalar contribution basically "decouples". Then, as long as we take m_ρ lighter, it will start to cancel the pseudo-scalar contribution, and at some point, $a_f^{(1)}$ will become positive.

Now, if we consider $m_\theta \ll m_e \ll m_\rho \ll m_\mu$, it is clear that $a_e^{(1)}$ is negative and $a_\mu^{(1)}$ is positive, and we can explain the discrepancies in both the electron and the muon AMM taking different values for the couplings h_e and h_μ. However, if the interactions in Equation (3.32) come from an effective operator as the one given in Equation (3.13), one expects the ratio C_5/Λ_5 to be the same for electrons and muons, and therefore $a_\mu^{(1)} = -2a_e^{(1)}$. Remember that $m_\theta \ll m_e \ll m_\rho \ll m_\mu$, therefore the electron has only the pseudo-scalar contribution in Equation (3.36), -1, and the muon has both contributions from Equations (3.36) and (3.37), which add to 2. In addition to the correct sign, it would be nice to explain the magnitude of the suppression in $\Delta a_e/\Delta a_\mu$. From the experimental results given in Equations (3.31) and (2.27) we get:

$$\frac{\Delta a_e}{\Delta a_\mu} = (-3.5 \pm 1.7) \times 10^{-4}\,. \tag{3.38}$$

This result can be translated into the following range for the ratio:

$$-6.7 \leqslant \frac{\Delta a_e}{\Delta a_\mu} \times 10^4 \leqslant -0.3 \quad (95\,\%\,\text{C.L.})\ . \tag{3.39}$$

In this respect, we would like to notice that $(m_e/m_\mu) \simeq 5 \times 10^{-3}$, and $(m_e/m_\mu)^2 \simeq 2.5 \times 10^{-5}$, which are both in one order of magnitude of the result in Equation (3.38). Therefore, a natural way to explain $\Delta a_e/\Delta a_\mu$ in the regime $m_\theta \ll m_e \ll m_\rho \ll m_\mu$ would be to assume that scalar couplings are chirality suppressed, *i.e.* $C_5 \sim m_f/v$. In that case, $a_e^{(1)}/a_\mu^{(1)} \simeq -1/2(m_e/m_\mu)^2 \simeq -1.25 \times 10^{-5}$, which is off by about one order of magnitude. It would also be interesting to generate the effective operator in Equation (3.13) but with derivatives, which, after using the equations of motion, would lead to a chirality suppressed effective operator.

In view of what has been discussed in the previous paragraphs, we can first, analyse the possibility of obtaining $a_e^{(1)}/a_\mu^{(1)} < 0$ with $a_e^{(1)} < 0$, and second, try to explain the value $\Delta a_e/\Delta a_\mu$ given in Equation (3.38). From Equation (3.33) one gets

$$\frac{a_e^{(1)}}{a_\mu^{(1)}} = \left(\frac{h_e}{h_\mu}\right)^2 \frac{I_e^{(1)}(m_e, m_\rho, m_\theta)}{I_\mu^{(1)}(m_\mu, m_\rho, m_\theta)}\,, \tag{3.40}$$

[21] We have also checked that $I_f^{(1)}(m_f, m_\rho, m_\theta)$ is always positive for intermediate values of $m_\rho = m_\theta = m_\phi$, *i.e.* for scenarios between $m_\phi \ll m_f$ and $m_\phi \gg m_f$.

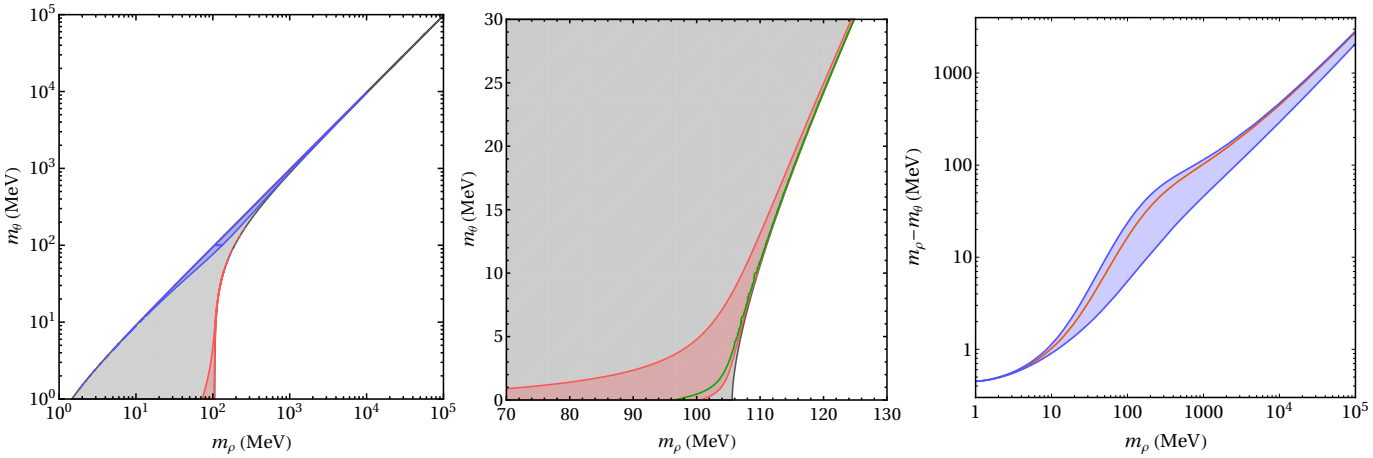

Figure 3.4: *Left: Region of the parameter space for the scalar and the pseudo-scalar masses that reproduces* $a_e^{(1)}/a_\mu^{(1)} < 0$ *with* $a_e^{(1)} < 0$*, depicted in gray. In addition, we plot in red (blue) the region that fulfils the condition in Equation* (3.39) *assuming that* $h_e/h_\mu = m_e/m_\mu$ (1)*. Middle: Parameter space that fulfils the same conditions as before for* $h_e/h_\mu = m_e/m_\mu$*, but for scalar masses between* 70 *and* 130 MeV*. Moreover, we show in green the central value of the ratio* $\Delta a_e/\Delta a_\mu$ *given in Equation* (3.38)*. Right: The orange line corresponds to the mass splitting* $m_\rho - m_\theta$ *as a function of* m_ρ *that reproduces the central value* $\Delta a_e/\Delta a_\mu$ *in Equation* (3.38)*, assuming* $h_e/h_\mu = 1$*. The blue band stands for the mass splitting that yields the values of the ratio* $\Delta a_e/\Delta a_\mu$ *given in Equation* (3.39)*.*

where the relevant part to get the correct sign is the ratio $I_e^{(1)}/I_\mu^{(1)}$. Regarding this, in the left panel in Figure 3.4 we depict in gray the region of the parameter space that yields $a_e^{(1)}/a_\mu^{(1)} < 0$ with $a_e^{(1)} < 0$. Moreover, we plot in red (blue) the region that fulfils the condition in Equation (3.39) assuming that $h_e/h_\mu = m_e/m_\mu$ (1). In the middle panel, we focus on m_ρ between 70 and 130 MeV, and show the parameter space that fulfils the same conditions as before for $h_e/h_\mu = m_e/m_\mu$. In addition, we depict in green the central value of the ratio $\Delta a_e/\Delta a_\mu$ given in Equation (3.38). Finally, in the right panel, the orange line corresponds to the mass splitting $m_\rho - m_\theta$ as a function of m_ρ that reproduces the central value $\Delta a_e/\Delta a_\mu$ in Equation (3.38), assuming that $h_e/h_\mu = 1$. Moreover, the blue band stands for the mass splitting that yields the values of the ratio $\Delta a_e/\Delta a_\mu$ given in Equation (3.39).

From the results depicted in Figure 3.4, we obtain the regions of the parameter space that can explain the discrepancies in both the electron and the muon AMM assuming either $h_e/h_\mu = m_e/m_\mu$ or 1. However, in the numerical scan we take arbitrary values for the couplings, see *e.g.* Equation (3.34). Therefore, one expects that the region of the parameter space that accounts for the discrepancies extends in all the area depicted in gray in the aforementioned figure, which is in agreement with the results of the numerical scan shown in Figure 3.3. Moreover, as we already know from the

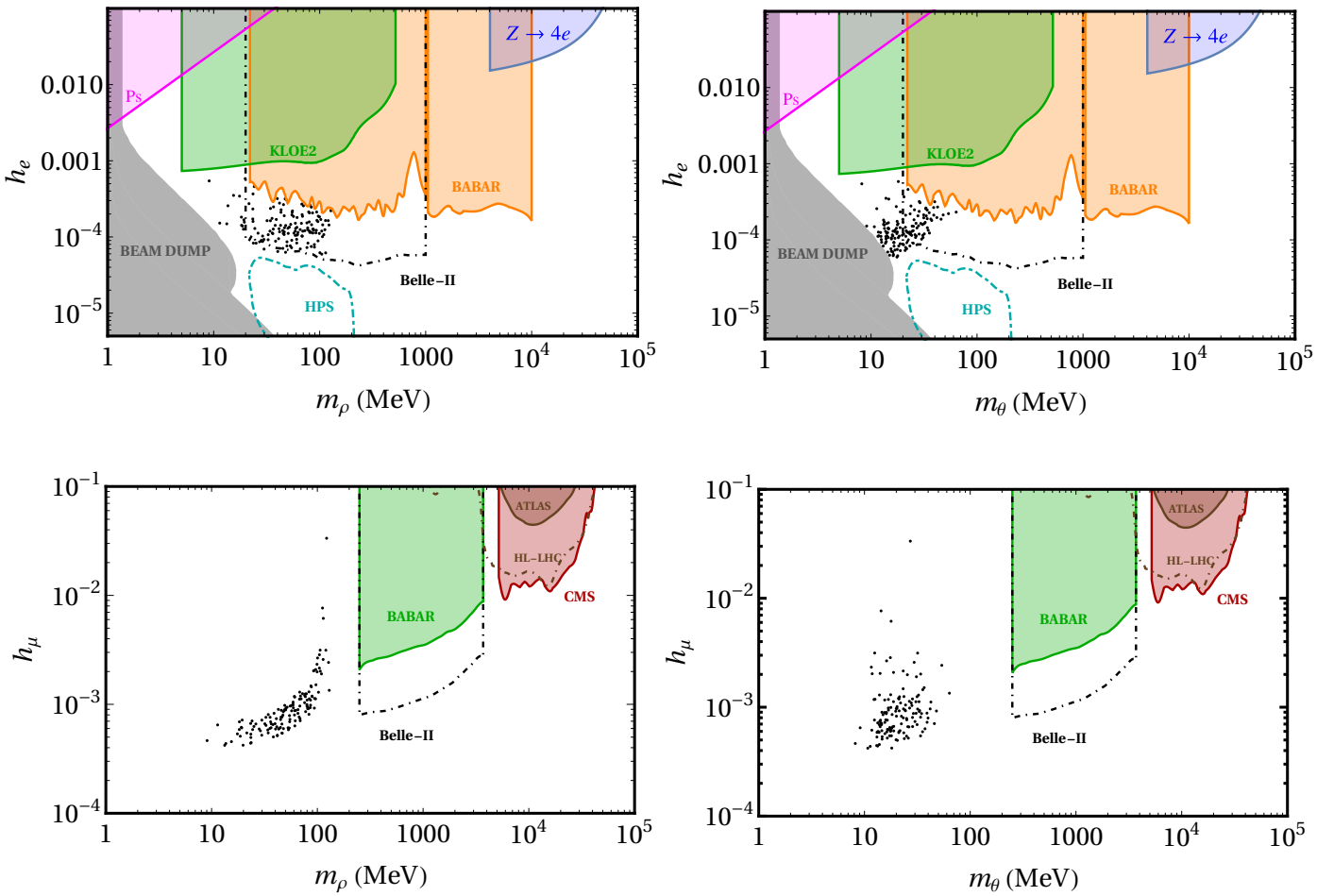

Figure 3.5: *Results of the numerical scan with points that fulfil the conditions in Equation* (3.35)*. In addition, the experimental constraints discussed in the text are imposed. Top: We depict the coupling of electrons to scalars (ρ) and pseudo-scalars (θ), h_e, as a function of m_ρ and m_θ in the left and right panels, respectively. Bottom: Similar plots for the muon case.*

discussion in Section 3.1.3, (light) scalars and pseudo-scalars that couple to charged leptons are strongly constrained from different experimental bounds. Therefore, in Figure 3.5 we plot the results of the scan that satisfies Equation (3.35) after imposing several experimental constraints. In the top panels, we show the coupling to electrons as a function of scalar (left) and pseudo-scalar (right) masses. In this case, when NP (scalars and pseudo-scalars) couples to electrons,[22] we consider the experimental constraints discussed in Section 3.1.3.

On the other hand, in the bottom panels in Figure 3.5 we present similar plots for

[22]We assume that the same experimental constraints apply for scalars as well as for pseudo-scalars. A detailed analysis is beyond the current work, however we expect minimal changes in the results.

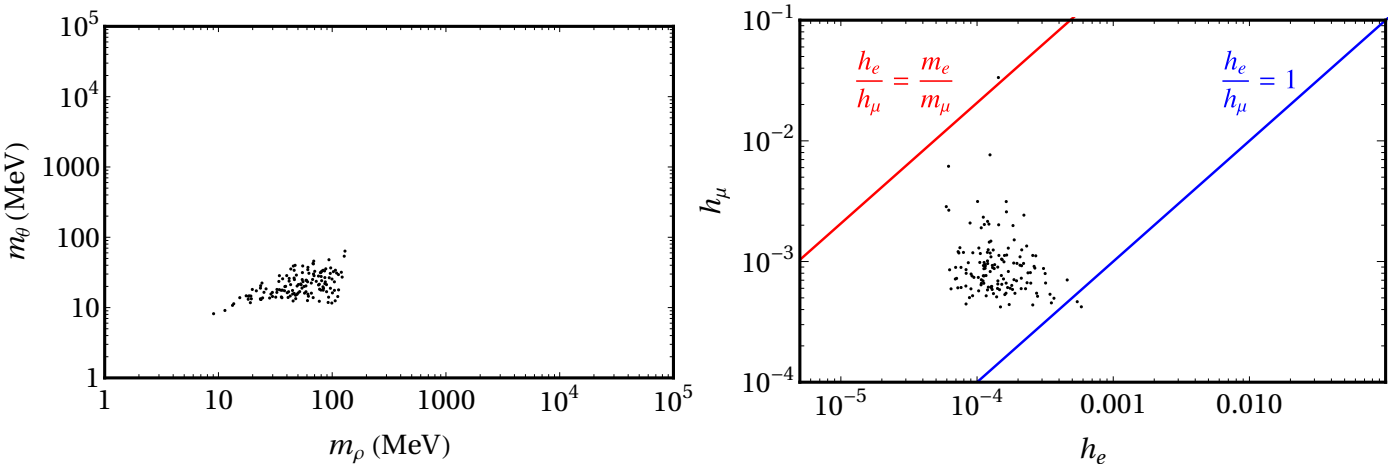

Figure 3.6: *Results of the numerical scan with points that fulfil the condition in Equation* (3.35) *and are allowed by the experimental constraints discussed in the text. Left: Results for scalar (ρ) and pseudo-scalar (θ) masses. Note the reduction of the allowed parameter space compared to Figure 3.3. Right: Results for the coupling of electrons and muons to scalars and pseudo-scalars. The red and the blue lines stand for $h_e/h_\mu = m_e/m_\mu$ and $h_e/h_\mu = 1$, respectively.*

the muon case. Regarding its coupling to scalars and pseudo-scalars, we can obtain an upper bound using dark photon searches performed by the BABAR collaboration. They analysed the process $e^+e^- \to \mu^+\mu^- A'$, where $A' \to \mu^+\mu^-$ [168], and the results can be applied after reinterpreting them in terms of scalars [150, 165]. The region of the parameter space excluded by BABAR is depicted in green. In addition, we also plot the Belle-II projected sensitivity [163, 165] as dot-dashed black line. In the high NP mass regime, the results from the ATLAS collaboration searches for the process $Z \to 4\mu$ with the 7 and 8 TeV data [169] can be recast to $Z \to \mu^+\mu^-\rho$, and interpreted as a constraint for the coupling to muons [165]. This upper bound for the coupling as a function of the NP mass is depicted in brown and labelled as ATLAS. In addition, the high luminosity LHC (HL-LHC) projection [165] is also shown as the dot-dashed brown line. Moreover, the CMS collaboration has studied the process $Z \to Z'\mu^+\mu^-$, with Z' being a gauge boson [170]. This analysis presents the $\mathrm{BR}(Z \to Z'\mu^+\mu^-)$ as a function of $m_{Z'}$ and can be reinterpreted as a constraint for scalars [128]. This upper bound for the coupling as a function of the NP mass is depicted in red and labelled as CMS.

Finally, in the left panel of Figure 3.6 we show the results of the scan in the scalar and pseudo-scalar masses that fulfil the condition in Equation (3.35) after imposing the experimental constraints discussed before. Note the reduction of the parameter space compared with Figure 3.3. Moreover, we present in the right panel of Figure 3.6 the results of the scan in the couplings of the NP (scalars and pseudo-scalars) to electrons and muons after imposing the experimental constraints, where we also plot in red (blue) the line which corresponds to constant value of the ratio

$h_e/h_\mu = m_e/m_\mu\,(1)$.

In view of the results from Figure 3.6, we conclude that the discrepancies in both the electron and the muon AMM can be explained for m_ρ and m_θ between 10 and 100 MeV, and couplings $h_e \sim \mathcal{O}(10^{-4})$ and $h_\mu \sim \mathcal{O}(10^{-3})$. It is interesting to note that, in view of the results depicted in Figure 3.5, a large region of the allowed parameter space can be tested by the Belle-II experiment.

Adding Barr-Zee effects to the electron AMM

In the last part we have analysed the parameter space of NP (scalars and pseudo-scalars) that couples to charged leptons and generates one-loop contributions to AMMs, which are able to reproduced the observed electron and muon anomalies.

Now, we try to extend the parameter space adding the effect of the two-loop contribution to the electron AMM. For simplicity, we assume that only taus enter in the loop, and therefore the new ingredient in the numerical analysis is their coupling to scalars and pseudo-scalars, h_τ. In Appendix A.1 we give the two-loop contribution to the AMM of charged leptons in Equation (A.9), and also depict the corresponding Feynman diagram in the right panel of Figure A.1. Finally, the total contribution to the electron AMM up to two loops is given in Equation (A.13).

In what follows, we present the numerical analysis performed in the parameter space of scalars and pseudo-scalars that couple to electrons and muons and can explain both discrepancies. We consider the NP contributions to the AMMs discussed in the previous paragraph, *i.e.* up to two loops for the electron and at one loop for the muon. We scan in the following ranges for scalar and pseudo-scalar masses and couplings:

$$m_\rho, m_\theta\, \epsilon\, \left[1, 10^6\right]\ \text{MeV}, \quad h_e\, \epsilon\, \left[5\times 10^{-6}, 10\right], \quad h_\mu\, \epsilon\, \left[10^{-4}, 10\right]. \tag{3.41}$$

Regarding the tau coupling to NP, we take the value $h_\tau = 8\times 10^{-2}$ from Ref. [117].[23] Moreover, the points of the scan must fulfil the conditions in Equation (3.35). In Figure 3.7 we plot the result of the scan in the scalar and pseudo-scalar masses. Comparing it with the result shown in Figure 3.3 we conclude that the two-loop contribution to the electron AMM opens the region of higher scalar and pseudo-scalar masses.

Similarly to what has been done in the previous part, where only the one-loop contribution to the AMM of electrons and muons was considered, now we have to impose the same experimental constraints on the parameter space in order to get the region of interest. Regarding this, we present in Figures 3.8 and 3.9 the points in the parameter space that are allowed by the experimental bounds discussed before. These figures are analogous to the ones presented in the last section, in particular Figures 3.5

[23] We take the value $h_\tau = 8\times 10^{-2}$ from Ref. [117]. However, they mention that a detailed analysis of the experimetal constraints on the parameter space of the scalar that couples to taus is required for this value of the coupling. Regarding this, from Ref. [155] we can estimate an upper bound $h_\tau \lesssim m_\tau \times 0.01\ \text{GeV}^{-1}$, which translates into $h_\tau \lesssim 2\times 10^{-2}$. However, in the numerical analysis we use the first value for h_τ.

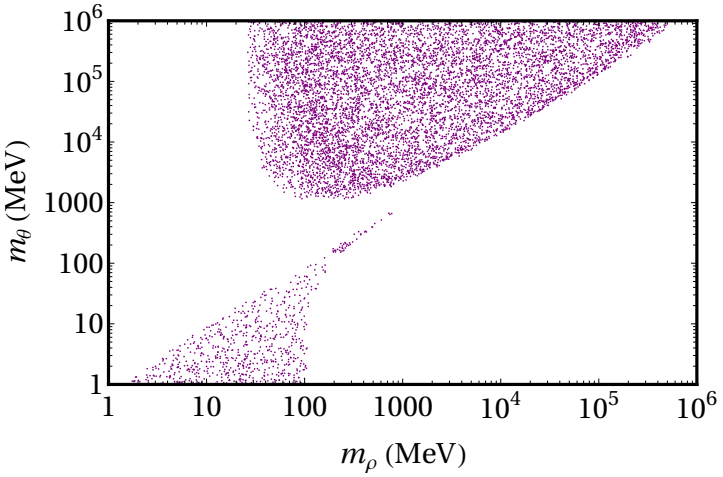

Figure 3.7: *Numerical scan of scalar (ρ) and pseudo-scalar (θ) masses that explain Δa_e and Δa_μ at two-loop and one-loop level, respectively. Therefore, the points fulfil the conditions in Equation* (3.35)*. The values of the masses and the couplings that have been used in the numerical scan are given in Equation* (3.41)*.*

and 3.6. Therefore, here we do not repeat the explanation for the parameter space that is depicted in each figure.

In view of the results from Figure 3.9, we conclude that adding Barr-Zee effects to the electron AMM enlarges the region of the parameter space where one can explain the discrepancies in both the electron and the muon AMM with respect to the case where only one-loop contributions are considered. In particular, higher scalar and pseudo-scalar masses and couplings are allowed, see *e.g.* the comparison between Figures 3.6 and 3.9.

It is interesting to note that, in view of the results depicted in Figures 3.5 and 3.8, there are several regions of the allowed parameter space that can be tested by the Belle-II experiment.

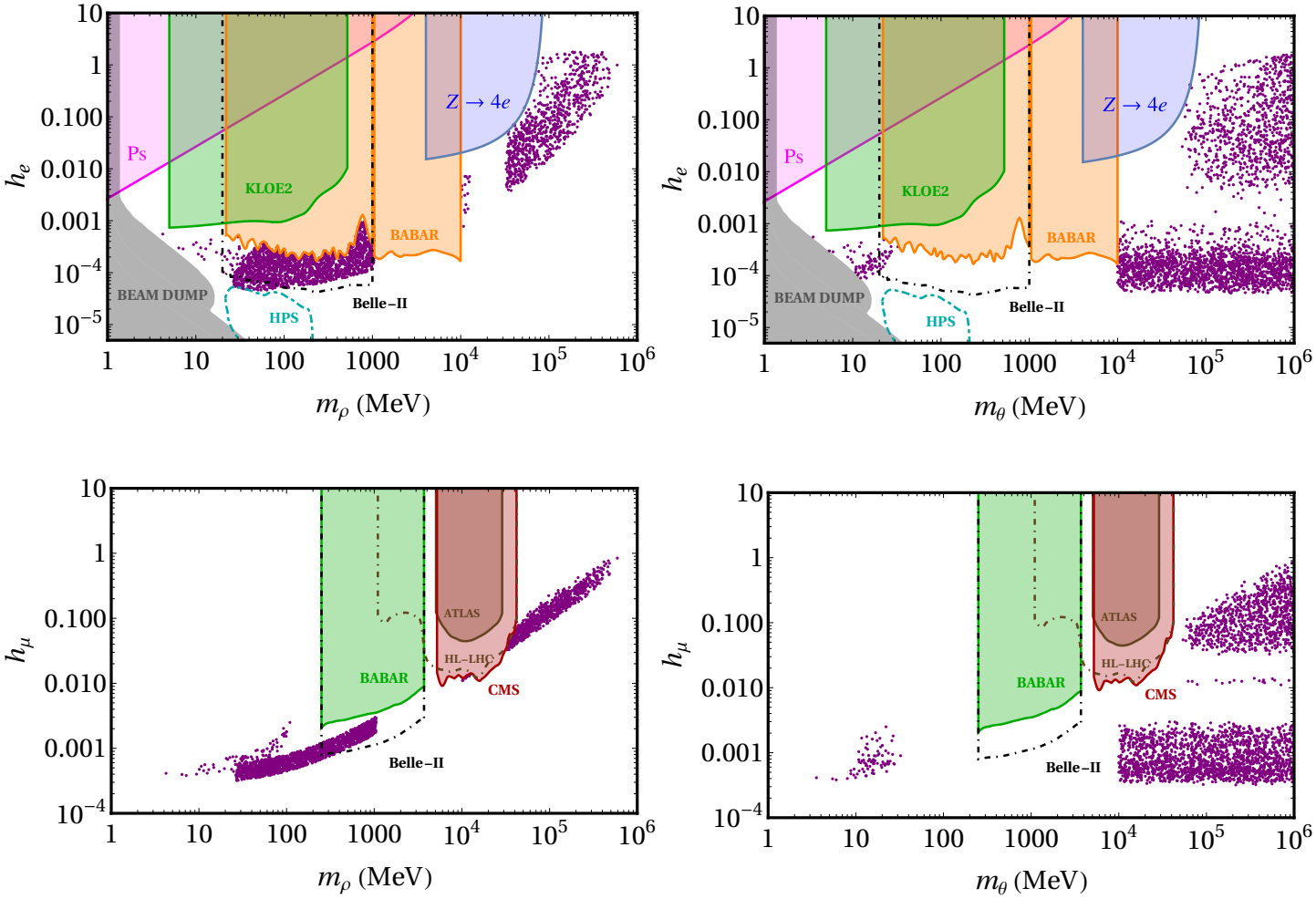

Figure 3.8: *Results of the numerical scan with points that fulfil the conditions in Equation* (3.35). *We consider two and one-loop NP contributions to the electron and muon AMM, respectively. In addition, the experimental constraints discussed in the text are imposed. Top: We depict the coupling of electrons to scalars (ρ) and pseudo-scalars (θ), h_e, as a function of m_ρ and m_θ in the left and right panels, respectively. Bottom: Similar plots for the muon case.*

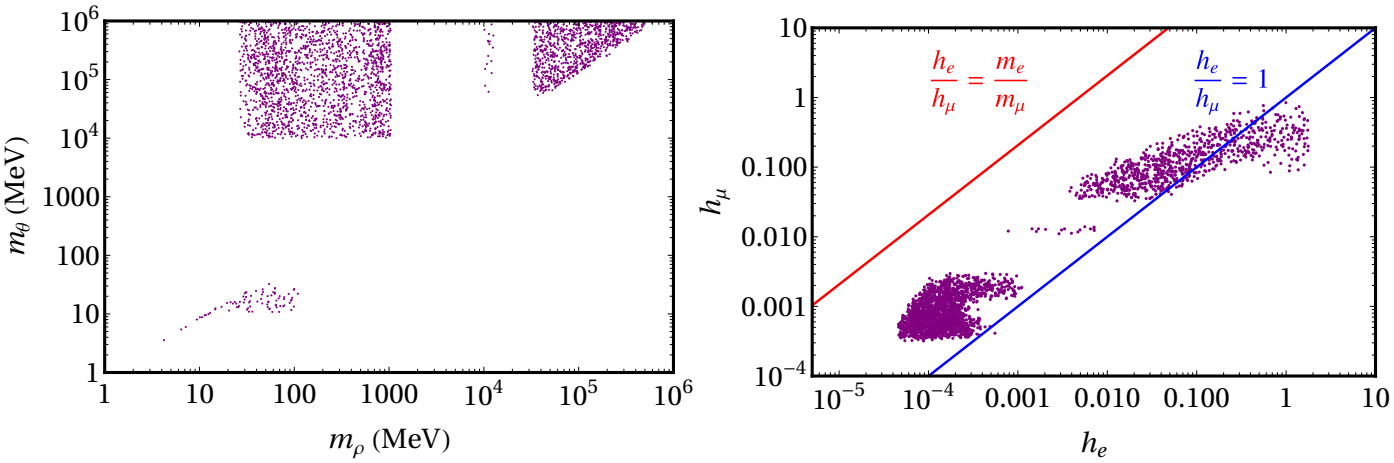

Figure 3.9: *Results of the numerical scan with points that fulfil the condition in Equation* (3.35) *and are allowed by the experimental constraints discussed in the text. We consider two and one-loop NP contributions to the electron and muon AMM, respectively. Left: Results for scalar (ρ) and pseudo-scalar (θ) masses. Note the reduction of the allowed parameter space compared to Figure 3.7. Right: Results for the coupling of electrons and muons to scalars and pseudo-scalars. The red and the blue lines stand for $h_e/h_\mu = m_e/m_\mu$ and $h_e/h_\mu = 1$, respectively.*

Part III

Scalars in Dark Matter scenarios

CHAPTER 4

Brief introduction to Dark Matter

In this part of the thesis, we address one of the most important unsolved issues of the SM: the absence of a suitable DM candidate. So far, in Chapters 2 and 3 we tackled the AMM of charged leptons and, in particular, we analysed the discrepancy in the $(g-2)$ of the electron between the theoretical value predicted in the SM framework and the experimental measurements. In doing so, we have studied the consequences of adding to the SM particle content light scalars which basically interact with electrons. A (neutral) scalar could be a good DM candidate if it has the convenient symmetries, namely the ones that prevent it from decaying, yielding a stable particle. Therefore, driven by the fact that we have started with the study of scalars and its relation with the electron AMM, a reasonable procedure from this point could be trying to provide a suitable DM candidate based on neutral scalars.

In Chapter 5, we will analyse the discrete symmetries that a complex scalar has, and how these can be used to provide a suitable DM candidate. For that, first we will review in Section 4.1 of the present chapter the experimental evidences that indicate the existence of DM, and briefly outline its main properties.

As a next step in our analysis, in Chapter 6 we will consider a scalar that couples to two different electrically neutral fermions. In this scenario, with an increased complexity regarding the number of particles that we are dealing with, one of the new fermions could be the DM candidate, whereas the scalar would play the role of mediator of the DM annihilations. One needs to require a set of conditions on the masses and symmetries these particles must have. In particular, we will consider interactions of new scalars with Majorana fermions, see *e.g.* Section 1.3 where we briefly discussed the main differences between Dirac and Majorana fermions.

4.1 Dark Matter: evidences and its properties

In view of experimental observations, we know that there must be some kind of "exotic" extra matter in the Universe with well defined properties. In the following, we briefly summarise the most relevant experimental observations that allow us to predict the existence of this "exotic" matter, that we will identify with the so-called DM.

- **Rotation curves of spiral galaxies.** As a first (and reasonable) approximation, one can assume that spiral galaxies have a spherical distribution of matter in the bulge, forgetting about the contribution coming from their spiral arms. Then, considering objects that orbit around the galaxy, one can obtain a correspondence between their velocity of rotation and their distance to the galactic center, which basically reads

$$v_{\rm rot} = \sqrt{\frac{G\,M(r)}{r}}\,, \tag{4.1}$$

  where $M(r)$ is the total mass which is contained within a sphere of radius r. Therefore, one would expect that in the outer part of the galaxy, where there is no luminous matter, the rotation speed decrease with the distance to the galactic center as $v_{\rm rot} \sim 1/\sqrt{r}$. However, the results obtained by V. Rubin in [171, 172] showed that the rotation velocity remains practically constant, as can be seen in Figure 4.1. This behaviour can be explained if we introduce a new component with a mass distribution $M(r) \propto r$.[1]

- **Mass-to-light ratio of galaxy clusters.** Taking the galaxy cluster as an isolated system, one can apply the Virial theorem $(2T + V = 0)$ to relate the average velocity of the baryons in the gas (obtained through their temperature from X-rays observations) with the total mass of the system. However, this determination of the mass does not rely on the fact that the components of the system either emit light or not. In particular, F. Zwicky analysed the peculiar motions of galaxies in the Coma cluster [173], and obtained a large mass-to-light ratio, indicating the presence of missing non-luminous matter.

- **Collision of clusters: the Bullet Cluster.** The Bullet Cluster consists of two galaxy clusters which suffered a collision, as can be seen in Figure 4.2. Weak-lensing analysis has shown that the most of the matter that constitute the cluster is located in the blue regions, whereas the visible luminous matter, which is the gas of the clusters that collided, is in the red areas. This visible component is inferred via X-ray observations. The interpretation of these observations from the Bullet Cluster is that its non-luminous matter (the DM component) has crossed the interaction point almost with no interacting at all.

- **Large scale structure: Dark Matter filaments.** At large scales, the luminous matter in the Universe tends to follow a particular structure in filaments, and this pattern has been reproduced by means of N-body numerical simulations

[1] This is the expected profile for a self-gravitational gas of non-interacting particles.

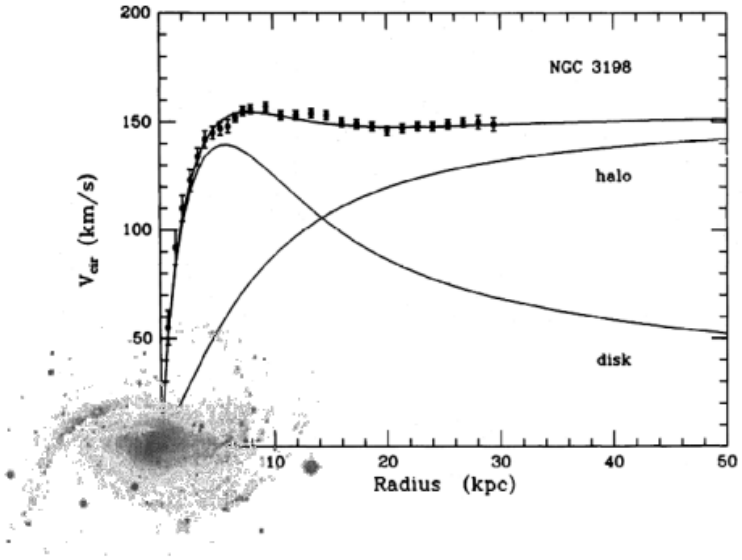

Figure 4.1: *Rotation curve of a spiral galaxy, which explicitly shows that the sum of the contributions from both the luminous disc and the dark matter halo gives the observed final constant speed as a function of the distance to the galactic center.*

if one includes non-relativistic (cold) DM. This ingredient, which bounds by gravitational effects the luminous matter, has a relevant impact on the growth of structures in the Universe. Then, a hierarchical structure formation happens: from smaller-scale structures (stars and galaxies) to larger structures (clusters of galaxies).

- **The anisotropies of the Cosmic Microwave Background (CMB).** Observations done by the COBE, WMAP and Planck satellites in the past decades show, with a high precision, that we live in a flat Universe ($\Omega_{\text{total}} = 1$) dominated by DM and DE. In particular, the CMB peaks (more precisely their position, shape and height) vary as a function of the Universe content, basically the relative fraction of baryons, DM and DE.

  The relic abundance of DM is given in terms of $\Omega_{\text{DM}}h^2 = \rho_{\text{DM}}/\rho_c$, where ρ_c is the critical density necessary to recover a flat Universe, and h is the dimensionless Hubble parameter $H = 100\,h$ km/s/Mpc. From the latest results driven by the Planck Collaboration [175] we get

$$\Omega_{\text{DM}}h^2 = 0.120 \pm 0.001\,, \tag{4.2}$$

  and given that $\Omega_{\text{total}} = \Omega_{\text{baryons}} + \Omega_{\text{DM}} + \Omega_{\text{DE}} = 1$, one infers that DM is responsible for $\sim 26\%$ of the Universe energy density nowadays. The rest is distributed in the form of DE $\sim 69\%$, and visible matter (atoms) $\sim 5\%$.

In view of the experimental evidences listed above, one can infer the main properties that a suitable DM candidate should have, namely:

Figure 4.2: *Image of the Bullet Cluster [174]. Regions in blue are the matter component of the cluster determined via gravitational lensing, whereas the red ones are the luminous component, which has been experimentally observed by the Chandra X-ray satellite.*

- **Non-Baryonic.** Using the results from the CMB analysis, we know that the baryonic matter corresponds to $\sim 5\%$ of the total energy density of the Universe, and therefore DM should be non-baryonic.

- **Collision-less.** Experimental observations from cluster collisions, such as the Bullet Cluster, yield an upper bound to the DM self-interaction cross-section, $\sigma/m_{\rm DM} = 1.25\ {\rm cm}^2{\rm g}^{-1}$ [176]. Therefore, one can infer that the DM counterpart in the cluster does not (basically) interact between itself, in contrast to the behaviour of ordinary matter.

  Related to this, it is interesting to note that self-interacting DM could alleviate some discrepancies in small scale structure observations, see *e.g.* Ref. [177].

- **Neutral.** DM does not scatter light (this is why people called it dark). Therefore, it should not interact with photons. There are also strong constraints on (mili)charged DM particles [178–180], which would interact with electrons and protons at the recombination epoch modifying the CMB power spectrum [178].

- **Non-relativistic.** Thanks to numerical simulations of structure formation, we know that DM particles must be non-relativistic (cold, or warm) at the epoch of structure formation. Otherwise, relativistic (hot) DM would erase the smaller structures due to its larger free-streaming length.

  On top of that, numerical simulations assuming cold DM yield a large number of subhaloes at the Galactic scale. This problem could be mitigated if DM was warm, with a mass ~ 2 KeV [181].

- **Stable or long-lived.** DM particles need to be stable, or at least long-lived with

respect to the age of the Universe. If not, they would have disappeared. Nevertheless, the stability condition for DM particles is not strictly required in the sense that, there can be decaying DM particles if their lifetime is longer than the age of the Universe. A possible long-lived DM candidate is the axion, see *e.g.* Ref. [182].

CHAPTER 5

Dark Matter from a complex scalar singlet: from symmetries to phenomenology

In this chapter, we will study how the inclusion of a complex scalar singlet in the SM could yield a suitable DM candidate, which must have a discrete symmetry responsible for its stability. After discussing different possibilities, we will conclude that what we call *dark* CP is the only symmetry that stabilises the DM candidate. Moreover, we will analyse the phenomenology associated with several models that break both explicitly and spontaneously a global $U(1)$ symmetry under which the scalar singlet is also charged.

First, we will refer to models with just one explicit symmetry breaking term (the *minimal models*), and, after that, we will also consider a more general situation with more than one explicit symmetry breaking term.

In the first case, we will find several regions of the parameter space where the observed DM abundance can be explained: the resonances of the two scalars (the Higgs boson and the CP-even part of the complex scalar), the forbidden or secluded DM regions, and through non-resonant Higgs-mediated DM annihilations.

In the second case, the *dark* CP symmetry responsible for the stability of the DM candidate may be spontaneously broken. Therefore, requiring that this does not happen will give us certain constraints on the allowed parameter space.

In the last part of the chapter, we will discuss an EFT approach that provides a pNGB as a DM candidate if the explicit symmetry breaking term is much smaller than the $U(1)$ symmetry breaking scale, which will be considered much larger than the EW scale.

5.1 The Lagrangian and its symmetries

In Section 4.1 we reviewed some of the strongest evidences for the existence of non-baryonic cold DM, one of the clearest manifestations of physics BSM. The simplest extension of the SM that contains a suitable DM candidate is based on a real scalar singlet, ϕ, equipped with a discrete symmetry, $\phi \to -\phi$, that yields a stable particle if this symmetry is not spontaneously broken [183, 184].[1] The general scalar potential for this model is

$$V_\phi = V_{\rm SM} + \Delta V(H,\phi)\,, \tag{5.1}$$

where

$$V_{\rm SM} = m_H^2|H|^2 + \lambda_H|H|^4\,, \tag{5.2}$$

is the SM scalar potential,[2] H is the Higgs doublet, and

$$\Delta V(H,\phi) = m_\phi^2\phi^2 + \lambda_{H\phi}|H|^2\phi^2 + \lambda_\phi\phi^4\,, \tag{5.3}$$

is the extra piece associated with the new singlet scalar, where terms odd in ϕ are absent due to the discrete symmetry.

The DM phenomenology associated to this simplified model is very predictive, and it is basically driven by the Higgs portal coupling, $\lambda_{H\phi}$, which controls: i) the DM pair annihilation into SM states, ii) DM scatterings in direct detection (DD) experiments [185], and iii) invisible Higgs boson decay into DM particles, $h \to \phi\phi$, if $m_\phi < m_h/2$ [186–188]. The parameter space for this model is very constrained, and the observed relic abundance can be reproduced via freeze-out for DM masses either in the Higgs boson resonance or for large values, $m_\phi \gtrsim 500$ GeV [189–192].

Now, one can try to minimally extend this setup considering a second scalar singlet with certain symmetries that yields a suitable DM candidate [193–198]. Therefore, the most general potential one can write with two real scalar singlets, ϕ_1 and ϕ_2, is:

$$\begin{aligned} V(H,\phi_1,\phi_2) =& \frac{|H|^2}{\sqrt{2}}(\omega_1\phi_1 + \omega_2\phi_2) + \frac{|H|^2}{2}(\alpha_1\phi_1^2 + \alpha_{12}\phi_1\phi_2 + \alpha_2\phi_2^2) \\ &+ V_{\rm I} + V_{\rm II} + V_{\rm III} + V_{\rm IV}\,, \end{aligned} \tag{5.4}$$

where

$$V_{\rm I} = \frac{1}{\sqrt{2}}\left(\delta_1\phi_1 + \delta_2\phi_2\right)\,, \tag{5.5}$$

$$V_{\rm II} = \frac{1}{2}\left(m_1^2\phi_1^2 + 2m_{12}^2\phi_1\phi_2 + m_2^2\phi_2^2\right)\,, \tag{5.6}$$

$$V_{\rm III} = \frac{1}{2\sqrt{2}}\left(\mu_1\phi_1^3 + \mu_{12}\phi_1^2\phi_2 + \mu_{21}\phi_2^2\phi_1 + \mu_2\phi_2^3\right)\,, \tag{5.7}$$

$$V_{\rm IV} = \frac{1}{4}\left(\lambda_1\phi_1^4 + \beta_{12}\phi_1^3\phi_2 + \lambda_{12}\phi_1^2\phi_2^2 + \beta_{21}\phi_2^3\phi_1 + \lambda_2\phi_2^4\right)\,. \tag{5.8}$$

[1] Generalisation of this scenario for the case of N complex scalar singlets was analysed in Ref. [184].

[2] For practical reasons, we have changed the notation for the SM scalar potential with respect to the one used in Equation (1.11).

It is interesting to count the number of parameters of the potential in Equation (5.4). In principle, it has 19 real parameters. But some of them are redundant, in the sense that they can be removed by means of the symmetries that the kinetic terms of the new scalars have, namely a shift symmetry and an $\mathcal{O}(2)$ rotation. In particular, the former can be used to eliminate the linear terms in the fields, V_I or $|H|^2(\omega_1\phi_1 + \omega_2\phi_2)$, whereas the latter can remove the m_{12}^2 term. Therefore, we end up with 16 real parameters in the potential.

As we have already mentioned, a suitable DM candidate should have an associated symmetry responsible for its stability, in general. In this scenario, the parameter counting of the potential is slightly different, and the general procedure is:

1. Start from the most general Lagrangian compatible with the symmetry.
2. Use the symmetries of the kinetic terms to eliminate redundant parameters.
3. Check if the global minimum of the potential is invariant under the symmetry. Then, we can have a good DM candidate.

In the case of two scalars, and starting from the potential in Equation (5.4), there are different symmetries one can impose that lead to a suitable DM candidate. For instance, $\phi_1 \to -\phi_1$ and $\phi_2 \to -\phi_2$, which would remove linear terms in the new scalar fields and V_{III}. In addition, if the discrete symmetry is not spontaneously broken, the DM candidate will be the lightest of the two scalars, see *e.g.* [194]. Similar analysis can be done with other symmetries such as i) $\phi_1 \to \phi_1$, $\phi_2 \to -\phi_2$, ii) $\phi_1 \leftrightarrow \phi_2$, iii) complete invariance under the symmetry of the kinetic term.

The point here is that the symmetries of the kinetic term of the scalar can be understood as a $U(1)$ times a reflection, or in other words, the $\mathcal{O}(2)$ is isomorphic to $U(1)$ times a reflection. Then, it is convenient for the analysis of the different symmetries that could yield suitable DM candidates to use the complex parameterisation for the two real fields. In view of that, we can write the complex scalar S as

$$S \equiv \frac{1}{\sqrt{2}}(\phi_1 + i\phi_2)\,, \tag{5.9}$$

and the most general Lagrangian of the SM extended by this complex scalar reads

$$\mathcal{L} = \mathcal{L}_{\rm SM} + |\partial_\mu S|^2 - V(H,S)\,. \tag{5.10}$$

Here, $\mathcal{L}_{\rm SM}$ contains the SM potential in Equation (5.2), and $V(H,S)$ takes into account all the interactions of the scalar sector, which contains the Higgs field and the complex scalar. The stability condition for a suitable DM candidate requires that this potential has to preserve, at least, a discrete symmetry. Then, let us analyse which are the possible discrete symmetries one can impose.

Basically, the available options are the discrete subgroups of the kinetic term symmetry group, namely

$$S \to e^{i\alpha}S \quad \text{and} \quad S \to S^*\,, \tag{5.11}$$

compatible with a polynomial Lagrangian. Therefore, there are four possibilities:

- $\mathcal{Z}_2$ ($S \to -S$)
- $\mathcal{Z}_3$ ($S \to e^{i2\pi/3}S$)
- $\mathcal{Z}_4$ ($S \to iS$)
- The reflection ($S \to S^*$), which can be identified with a *dark* CP (DCP).[3]

Once we have listed the possible symmetries, it is useful to separate the scalar potential $V(H,S)$ in the terms that preserve the global $U(1)$ symmetry, V_0, and the ones that break it explicitly, labelled according to the discrete symmetry they preserved, namely $V_{1,\text{full}}$, $V_{\mathcal{Z}_2,\text{full}}$, $V_{\mathcal{Z}_3}$ and $V_{\mathcal{Z}_4}$. In view of that, we can write the potential $V(H,S)$ in Equation (5.10) as

$$V(H,S) = V_0 + V_{1,\text{full}} + V_{\mathcal{Z}_2,\text{full}} + V_{\mathcal{Z}_3} + V_{\mathcal{Z}_4}\,, \tag{5.12}$$

with

$$V_0 = m_S^2|S|^2 + \lambda_S|S|^4 + \lambda_{HS}|H|^2|S|^2\,, \tag{5.13}$$

and

$$V_{1,\text{full}} = \frac{1}{2}\mu^3 S + \frac{1}{2}\mu_{H1}|H|^2 S + \frac{1}{2}\mu_1|S|^2 S + \text{H.c.}\,, \tag{5.14}$$

$$V_{\mathcal{Z}_2,\text{full}} = \frac{1}{2}\mu_S^2 S^2 + \frac{1}{2}\lambda_{H2}|H|^2 S^2 + \frac{1}{2}\lambda_2|S|^2 S^2 + \text{H.c.}\,, \tag{5.15}$$

$$V_{\mathcal{Z}_3} = \frac{1}{2}\mu_3 S^3 + \text{H.c.}\,, \tag{5.16}$$

$$V_{\mathcal{Z}_4} = \frac{1}{2}\lambda_4 S^4 + \text{H.c.}\,. \tag{5.17}$$

Let us proceed with the parameter counting of the potential given in Equation (5.12). It has 3 real parameters from V_0, which also is invariant under DCP, and 8 complex parameters from the terms that explicitly break the $U(1)$, given in Equations (5.14–5.17). Therefore, we have 19 real parameters, which agrees with the starting number of parameters in the real parameterisation. We list in Table 5.1 the correspondence among the couplings of the scalar potential in Equations (5.4) and (5.12). Moreover, after re-phasing S one of the couplings can be rendered real, for instance μ_S^2 (which corresponds to $m_{12}^2 = 0$ in the real parameterisation, see *e.g.* Table 5.1). Finally, by means of the minimisation of the scalar potential, the linear terms in S can be rewritten in terms of the other couplings.

To sum up, we started with 19 real parameters (3 real and 8 complex), changed a complex coupling by a real one, and eliminated another complex coupling. Therefore, we get 4 real and 6 complex couplings, or equivalently 16 real parameters. Then, the parameter counting of the potential in the complex parameterisation agrees with the counting in the real parameterisation, as it should. It is interesting to note that from

[3]We can refer to this *dark* charge conjugation as DCP due to the fact that the kinetic term of S in Equation (5.10) also preserves parity.

(ϕ_1, ϕ_2)	Complex S
ω_1	$\mathrm{Re}\,\mu_{H1}$
ω_2	$-\,\mathrm{Im}\,\mu_{H1}$
α_1	$\mathrm{Re}\,\lambda_{H2} + \lambda_{HS}$
α_{12}	$-2\,\mathrm{Im}\,\lambda_{H2}$
α_2	$-\,\mathrm{Re}\,\lambda_{H2} + \lambda_{HS}$
δ_1	$\mathrm{Re}\,\mu^3$
δ_2	$-\,\mathrm{Im}\,\mu^3$

(ϕ_1, ϕ_2)	Complex S
m_1^2	$m_S^2 + \mathrm{Re}\,\mu_S^2$
m_{12}^2	$-\,\mathrm{Im}\,\mu_S^2$
m_2^2	$m_S^2 - \mathrm{Re}\,\mu_S^2$
μ_1	$\mathrm{Re}\,(\mu_1 + \mu_3)$
μ_{12}	$\mathrm{Im}\,(-\mu_1 - 3\mu_3)$
μ_{21}	$\mathrm{Re}\,(\mu_1 - 3\mu_3)$
μ_2	$\mathrm{Im}\,(-\mu_1 + \mu_3)$

(ϕ_1, ϕ_2)	Complex S
λ_1	$\mathrm{Re}\,(\lambda_2 + \lambda_4) + \lambda_S$
λ_2	$\mathrm{Re}\,(-\lambda_2 + \lambda_4) + \lambda_S$
β_{12}	$\mathrm{Im}\,(-2\lambda_2 - 4\lambda_4)$
λ_{12}	$-6\,\mathrm{Re}\,\lambda_4 + 2\lambda_S$
β_{21}	$\mathrm{Im}\,(-2\lambda_2 + 4\lambda_4)$

Table 5.1: *Relation among the couplings of the scalar potential in Equations* (5.4) *and* (5.12)*, which correspond to the real and the complex parameterisation of the scalar fields, ϕ_1 and ϕ_2, and $S = (\phi_1 + i\phi_2)/\sqrt{2}$, respectively.*

the 16 independent parameters in the potential, 3 of them preserve the global $U(1)$ symmetry whereas 13 break it.

In general, the complex scalar could take a VEV different from zero,[4] $v_s \neq 0$, and there would be SSB of the global $U(1)$. In that case, also the $\mathcal{Z}_2$, $\mathcal{Z}_3$ and $\mathcal{Z}_4$ symmetries will be broken by the VEV. Conversely, DCP will be preserved if one chooses real couplings in the potential in Equation (5.12), together with a real v_s. Regarding this, we can see from Table 5.1 that if all the couplings are real in the complex parameterisation of the scalar field, 8 couplings in the real parameterisation vanish, namely m_{12}^2, δ_2, ω_2, α_{12}, μ_2, μ_{12}, β_{12} and β_{21}. Therefore, if one of them is present in the potential in Equation (5.4), DCP is explicitly broken.

On the one hand, considering the simplest Lagrangian with only one $U(1)$ symmetry breaking term, both its coupling and v_s can be taken real [205], and then one ensures that DCP is preserved also by the vacuum. On the other hand, if one considers several symmetry breaking terms in the potential, there could be DCP violation depending on the values of the couplings even if they are considered real, because the VEV v_s could become complex. We will discuss this scenario in Section 5.4.

In view of what has been discussed in this section, we can conclude that if there is SSB of the global $U(1)$, only the DCP symmetry is able to yield a suitable DM candidate regarding its stability.

[4]This case is useful to avoid DD constraints [199–203], and also to mitigate the instability problems of the SM scalar potential, see *e.g.* Ref. [204]. Moreover, notice that if the scalar does not get a VEV, all the discussed symmetries can ensure the stability of the DM candidate (see *e.g.* Ref. [194], where the $\mathcal{Z}_2$ symmetry has been imposed).

5.2 Mass spectrum and couplings

If one allows for the general scenario, *i.e.* SSB of the global $U(1)$ and the full potential in Equation (5.12), there are many (free) parameters and the predictability of the model is reduced. Then, it is more useful to analyse scenarios with just one explicit symmetry breaking term, and then see how the inclusion of other terms modify these setups.

However, for the time being we will take all the possible real explicit symmetry breaking terms in the scalar potential, assume that S takes a VEV, v_s, and derive the expressions for the masses of the particles that are present in the model, together with the relevant couplings.

The complex scalar singlet can be written in the linear parameterisation as

$$S = \frac{1}{\sqrt{2}}\left(v_s + \rho' + i\theta\right) , \tag{5.18}$$

and the minimisation of the potential in Equation (5.12) yields the following conditions on the bare masses written in terms of the couplings and VEVs:[5]

$$-m_H^2 = \frac{1}{2}(\lambda_{H2} + \lambda_{HS})v_s^2 + \lambda_H v^2 + \frac{\sqrt{2}}{2}\mu_{H1}v_s \,, \tag{5.19}$$

$$\begin{aligned} -m_S^2 = {} & \mu_S^2 + (\lambda_2 + \lambda_S + \lambda_4)v_s^2 + \frac{1}{2}(\lambda_{H2} + \lambda_{HS})v^2 + \frac{\sqrt{2}}{4}\mu_{H1}\left(\frac{v}{v_s}\right)v \\ & + \frac{3\sqrt{2}}{4}(\mu_1 + \mu_3)v_s + \frac{\sqrt{2}}{2}\frac{\mu^3}{v_s} \,. \end{aligned} \tag{5.20}$$

One can always take the VEV of the Higgs field, v, real, but in addition, v_s must also be real to preserve the DCP symmetry, as discussed in the previous section. It is interesting to note that when we write the scalar as in Equation (5.18), the Lagrangian of the model is invariant under $\theta \to -\theta$, which is the manifestation of the DCP symmetry. Therefore, the pseudo-scalar θ is the DM candidate, which do not mix with the CP-even scalars if all the couplings in the potential and the VEVs are real. Moreover, the mass of θ reflects the pNGB nature of the pseudo-scalar, *i.e.* it is zero if the explicit symmetry breaking couplings are absent:[6]

$$\begin{aligned} m_\theta^2 = {} & -2\mu_S^2 - \frac{\sqrt{2}}{2}\frac{\mu^3}{v_s} - (\lambda_2 + 4\lambda_4)v_s^2 - \lambda_{H2}v^2 - \frac{v_s}{2\sqrt{2}}(\mu_1 + 9\mu_3) \\ & - \mu_{H1}\frac{v}{2\sqrt{2}}\left(\frac{v}{v_s}\right) . \end{aligned} \tag{5.21}$$

[5] Note that we write the Higgs field in the unitary gauge, see Equation (1.16) with the corresponding change in the notation, namely $\phi \to H$ and $H \to h'$.

[6] If the global $U(1)$ symmetry is spontaneously but not explicitly broken, there is a massless Goldstone boson which can not be the DM candidate. It would contribute to dark radiation.

This expression is obtained when we substitute back the minimisation conditions in Equations (5.19) and (5.20) in the scalar potential $V(H,S)$ in Equation (5.12). Moreover, we get that the CP-even parts (h',ρ') do mix with the following mass matrix:

$$M_S^2 = \begin{pmatrix} (M_S^2)_{11} & (M_S^2)_{12} \\ (M_S^2)_{21} & (M_S^2)_{22} \end{pmatrix}, \tag{5.22}$$

where the entries of the matrix are given by

$$(M_S^2)_{11} = 2\lambda_H v^2\,, \quad (M_S^2)_{12} = (M_S^2)_{21} = (\lambda_{H2} + \lambda_{HS})\, v_s v + \frac{\mu_{H1} v}{\sqrt{2}}\,, \tag{5.23}$$

$$(M_S^2)_{22} = 2\,(\lambda_2 + \lambda_S + \lambda_4)\, v_s^2 + \frac{3 v_s}{2\sqrt{2}}\,(\mu_1 + \mu_3) - \frac{\mu_{H1} v}{2\sqrt{2}}\left(\frac{v}{v_s}\right) - \frac{\sqrt{2}\mu^3}{2 v_s}\,. \tag{5.24}$$

In order to get the physical masses of the CP-even scalars, we can diagonalise the matrix M_S^2 by means of an orthogonal rotation of angle α given by

$$\begin{pmatrix} h \\ \rho \end{pmatrix} = R \begin{pmatrix} h' \\ \rho' \end{pmatrix}, \quad R \equiv \begin{pmatrix} c_\alpha & -s_\alpha \\ s_\alpha & c_\alpha \end{pmatrix}, \quad R M_S^2 R^T = \begin{pmatrix} m_h^2 & 0 \\ 0 & m_\rho^2 \end{pmatrix}, \tag{5.25}$$

where we use $s_\alpha \equiv \sin\alpha$ and $c_\alpha \equiv \cos\alpha$ to simplify the notation. We will identify the observed Higgs boson as the eigenstate h.

Regarding the couplings in the potential, we can trade-off three of them, λ_H, λ_S and λ_{HS}, in terms of the physical masses of the scalars and the mixing angle, namely:

$$\lambda_H = \frac{c_\alpha^2 m_h^2 + s_\alpha^2 m_\rho^2}{2v^2}\,, \tag{5.26}$$

$$\lambda_S = \frac{s_\alpha^2 m_h^2 + c_\alpha^2 m_\rho^2}{2 v_s^2} - \frac{3}{4\sqrt{2}}\frac{(\mu_1 + \mu_3)}{v_s} - (\lambda_2 + \lambda_4) + \frac{\mu_{H1}}{4\sqrt{2} v_s}\left(\frac{v}{v_s}\right)^2 + \frac{\sqrt{2}}{4}\frac{\mu^3}{v_s^3}\,, \tag{5.27}$$

$$\lambda_{HS} = \frac{s_\alpha c_\alpha (m_\rho^2 - m_h^2)}{v v_s} - \frac{\mu_{H1}}{\sqrt{2} v_s} - \lambda_{H2}\,. \tag{5.28}$$

5.2.1 *Minimal models*

In this part we introduce the concept of *minimal models*. They basically emerge by taking just one symmetry breaking term in the scalar potential in Equation (5.12), with real coupling. In this scenario, DCP is automatically preserved and yields a suitable DM candidate, the CP-odd scalar θ.

From the general potential in Equation (5.12) we get four *minimal models*:

- **Linear model.** Choosing the softest term from $V_{1,\text{full}}$:

$$V_1 = \frac{1}{2}\mu^3 S + \text{H.c.}\,. \tag{5.29}$$

- **Quadratic model.** Choosing the softest term from $V_{\mathcal{Z}_2,\text{full}}$:

$$V_{\mathcal{Z}_2} = \frac{1}{2}\mu_S^2 S^2 + \text{H.c.}\,. \tag{5.30}$$

- **Cubic model.** It is given in Equation (5.16).

- **Quartic model.** It is given in Equation (5.17).

As can be seen from Equation (5.21), the DM mass, m_θ, is proportional to the explicit symmetry breaking term that characterises each model. Having this in mind, the expressions for the couplings in Equations (5.26–5.28) can be written as

$$\begin{aligned}\lambda_H =& \frac{c_\alpha^2 m_h^2 + s_\alpha^2 m_\rho^2}{2v^2}\,, \quad \lambda_{HS} = \frac{s_\alpha c_\alpha (m_\rho^2 - m_h^2)}{v v_s}\,,\\ \lambda_S =& \frac{1}{2v_s^2}\left(s_\alpha^2 m_h^2 + c_\alpha^2 m_\rho^2 + A\, m_\theta^2\right)\,,\end{aligned} \tag{5.31}$$

with $A = -1,\ 0,\ 1/3,\ 1/2$ for the linear, quadratic, cubic and quartic models, respectively. One concludes that in the *minimal models* there are only four relevant parameters, namely m_θ, m_ρ, v_s and s_α. The remaining ones are the well-known mass and VEV of the Higgs boson, m_h and v.

In Section 5.3 we will study the DM phenomenology of the *minimal models*, and in the numerical analysis we must require several theoretical constraints on the models: perturbativity, stability of the potential and checking that the minimum at $(v \neq 0, v_s \neq 0)$ is also the global minimum of the potential [199]. From perturbativity and stability we get

$$\lambda_H > 0\,, \quad \lambda_S > 0\,, \quad \lambda_{HS} > -2\sqrt{\lambda_H \lambda_S}\,, \tag{5.32}$$

and

$$\lambda_H \leqslant 4\pi\,, \quad |\lambda_{HS}| \leqslant 4\pi\,, \quad \lambda_S \leqslant 4\pi + B\,, \tag{5.33}$$

where $B = 0$ for the linear, quadratic and cubic model, and $B = -3\left(m_\theta/(2v_s)\right)^2$ for the quartic model. Regarding these conditions, $\lambda_S > 0$ is automatically fulfilled in the *minimal models* except for the linear case, see *e.g.* Equation (5.31). In this particular model, the condition $\lambda_S > 0$ translates into $m_\theta^2 \lesssim m_\rho^2$ for the values of the mixing that we will consider in our numerical scan, namely $s_\alpha \,\epsilon\, [10^{-5},\, 10^{-1}]$.

5.2.2 Radiative corrections

Even if we consider the *minimal models* defined before, other explicit symmetry breaking terms may be radiatively generated in the Lagrangian, as can be seen for the quadratic model in Figure 5.1.[7] Its potential induces one-loop finite contributions to

[7] Note that the rest of the models do not generate radiative corrections: the linear case in Equation (5.29) is not an interaction, and the cubic and quartic models in Equations (5.16) and (5.17) contain all the interactions that preserve the $\mathcal{Z}_3$ and $\mathcal{Z}_4$ symmetries, respectively, which do not generate any other terms.

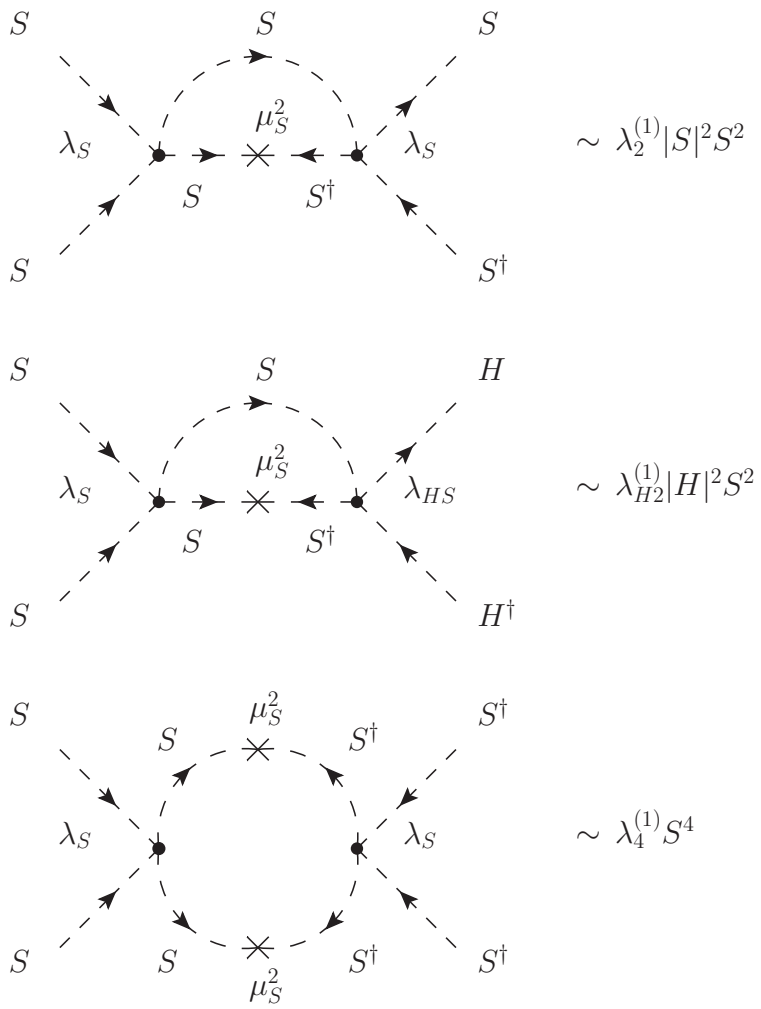

Figure 5.1: *Feynman diagrams of the radiative corrections that are generated in the quadratic model.*

the couplings in $V_{\mathcal{Z}_2,\text{full}}$ and $V_{\mathcal{Z}_4}$, given in Equations (5.15) and (5.17), respectively. In the limit $m_\rho \gg m_h$, these corrections can be estimated as[8]

$$\lambda_2^{(1)} \simeq \frac{\lambda_S^2}{(4\pi)^2}\frac{\mu_S^2}{m_\rho^2}\,, \quad \lambda_{H2}^{(1)} \simeq \frac{\lambda_{HS}\lambda_S}{(4\pi)^2}\frac{\mu_S^2}{m_\rho^2}\,, \quad \lambda_4^{(1)} \simeq \frac{\lambda_S^2}{(4\pi)^2}\frac{\mu_S^4}{m_\rho^4}\,. \tag{5.34}$$

In our numerical analysis, we have checked that contributions from radiative corrections are irrelevant.

[8]Note that $\lambda_4^{(1)}$ is parametrically suppressed by μ_S^2/m_ρ^2 compared to $\lambda_2^{(1)}$ and $\lambda_{H2}^{(1)}$. This is also the case if the couplings come from higher-dimensional operators with spurions [206].

5.3 Phenomenology of the *minimal models*

So far, we have presented all the main ingredients that need to be considered for defining what we call *minimal models*, but before starting with the analysis of the relevant parameter space associated with each one of these minimal scenarios, let us briefly summarise how can we get the correct DM relic abundance.

In the Early Universe, we ensure the thermal equilibrium of the complex scalar with the SM via the Higgs portal coupling in the potential, λ_{HS}. Moreover, the scalar gets a real VEV during the evolution of the Universe, and after that, the DCP is the only symmetry that is preserved also by the vacuum of the theory, yielding a stable DM candidate: the pseudo-scalar θ. Then, at some point, its interactions are slow enough compared to the Hubble rate, $\Gamma \lesssim H(T)$, and its number density over entropy remains constant. This is the usual freeze-out mechanism.

Therefore, we assume that the DM abundance is obtained through the non-relativistic freeze-out mechanism, and we find several regions of the parameter space where its correct value given in Equation (4.2) can be reproduced, namely:

- Resonances with the Higgs boson h or with the scalar ρ, for $m_\theta \simeq m_{h,\rho}/2$. See *e.g.* top panel in Figure 5.2.[9]

- Direct annihilations into (lighter) pairs of scalars h and/or ρ, for $m_\theta \gtrsim m_h$ and/or $m_\theta \gtrsim m_\rho$. See *e.g.* bottom panel in Figure 5.2. The latter case is known as secluded dark matter (SDM). If $\lambda_{HS} \neq 0$, for $s_\alpha \gtrsim 10^{-16}$, ρ decays via mixing into SM states, as long as $m_\rho > 2m_e$.

- Direct annihilations into (slightly) heavier pairs of $hh, h\rho, \rho\rho$. See *e.g.* bottom panel in Figure 5.2. This is known as forbidden dark matter (FDM).[10]

  In this regime, we can have two scenarios depending on the hierarchy of masses: i) $m_\theta \lesssim m_\rho \lesssim m_h$, and the DM abundance is determined by the annihilations $\theta\theta \to \rho\rho$; ii) $m_\theta \lesssim m_h \lesssim m_\rho$, with the dominant channel controlled by the mixing angle, s_α.

- Non-resonant Higgs-mediated annihilations into SM states happening for DM masses above 100 GeV and at mixings s_α larger than the previous cases. [210, 211]. See *e.g.* top panel in Figure 5.2.

In the numerical analysis of the *minimal models*, we have to consider all the experimental constraints that can potentially affect the regions of the parameter space which are able to reproduced the observed relic abundance. We briefly discuss these constraints in what follows.

[9] The assumption of kinetic equilibrium of the final states could not be a good starting point near resonances. Therefore, there is some associated uncertainty in the parameters that reproduce the DM abundance in this region, see *e.g.* [207–209].

[10] Within the FDM regime, the departure from the assumption that final states are in kinetic equilibrium at freeze-out has been analysed in Ref. [208].

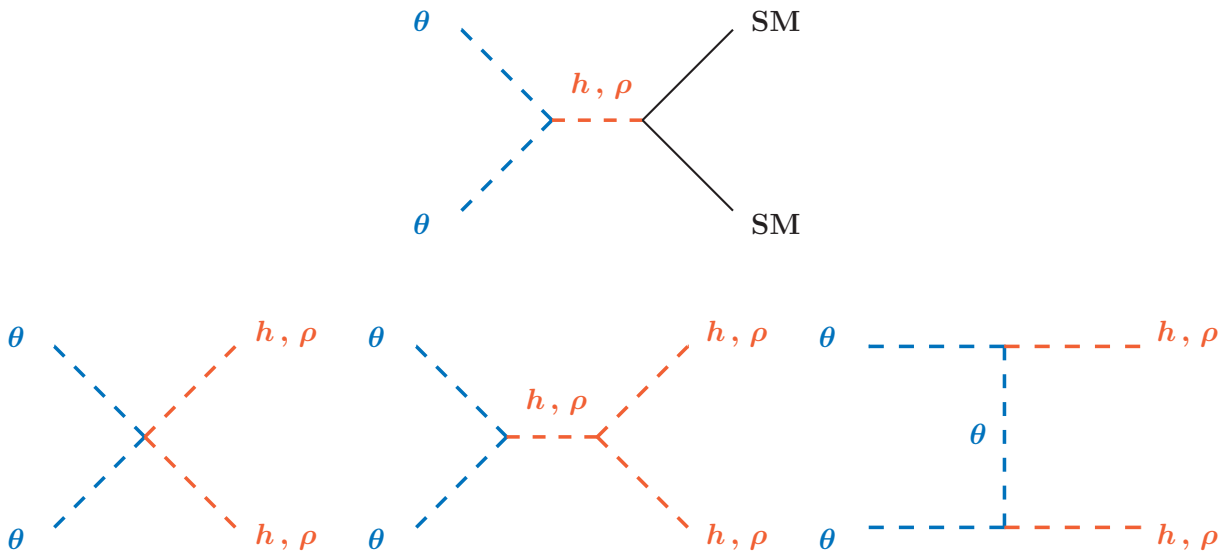

Figure 5.2: *Feynman diagrams of the DM annihilation channels described in the text. Top: DM annihilations into SM states mediated by the Higgs boson h and/or the scalar ρ. Bottom: DM annihilations into h, ρ (FDM and SDM).*

On the one hand, there are constraints coming from DD experiments due to the mixing between the CP-even scalars, discussed in Section 5.2. This mixing could produce nuclear scattering of the DM candidate.[11] At tree level, the spin-independent DD cross section reads [199, 202]:

$$\frac{d\sigma_{SI}}{d\Omega} = \frac{\lambda_{SI}^2 f_N^2 m_N^2}{16\pi^2 m_\theta^2} \left(\frac{m_\theta m_N}{m_\theta + m_N} \right)^2 , \tag{5.35}$$

where $m_N = 0.939\,\text{GeV}$ is the nucleon mass, $f_N = 0.3$ is the effective Higgs-nucleon coupling [192], and λ_{SI} is the effective DM-nucleon coupling, which depends on the transferred total momentum. In Table 5.2 we summarise the expressions for the effective coupling for the *minimal models* in the limit of small (zero) momentum, considering that the masses of the particles that are involved in nuclear scattering processes in DD experiments are larger than the transferred momentum.[12] The DD cross-section goes as λ_{SI}^2, see *e.g.* Equation (5.35), so there is no difference for the linear and cubic models, but a factor of 4 larger appears for the quartic model with respect to the others. It is interesting to note that there is a cancellation for the quadratic model, already noticed in Refs. [199, 202]. Therefore, in this model the one-loop contributions to the DD cross section should be considered, see *e.g.* [212–215].

[11] In the limit of an exact Goldstone boson, DM-nucleon scatterings are suppressed by the (small) momentum transfer due to the derivative nature of Goldstone boson's coupling.

[12] Note that the typical momentum transfer in xenon is $\mathcal{O}(\text{MeV})$.

Minimal model	$\lambda_{SI} \propto -\left(\frac{\beta_{h\theta\theta}\, c_\alpha}{m_h^2} + \frac{\beta_{\rho\theta\theta}\, s_\alpha}{m_\rho^2}\right)$
Linear	$\frac{s_\alpha c_\alpha}{v_s m_h^2 m_\rho^2} m_\theta^2 (m_h^2 - m_\rho^2)$
Quadratic	0
Cubic	$-\frac{s_\alpha c_\alpha}{v_s m_h^2 m_\rho^2} m_\theta^2 (m_h^2 - m_\rho^2)$
Quartic	$-2\frac{s_\alpha c_\alpha}{v_s m_h^2 m_\rho^2} m_\theta^2 (m_h^2 - m_\rho^2)$

Table 5.2: *Effective DM-nucleon coupling in the limit of small momentum transferred as a function of physical parameters of the models. The β_i coefficients are given in the Appendix B.*

In the numerical analysis, we use the DD constraints from the XENON1T experiment, considering only those points in the scan that fulfils the following condition:

$$\sigma_{SI,\,\mathrm{resc}} \leqslant \sigma^{\mathrm{XENON1T}}, \quad \text{with} \quad \sigma_{SI,\,\mathrm{resc}} \equiv \frac{\Omega}{\Omega_{\mathrm{DM}}}\sigma_{SI}\,. \tag{5.36}$$

Here, Ω and σ_{SI} are the DM abundance and the spin-independent DD cross section in Equation (5.35) of each point in the scan, respectively. Moreover, $\sigma^{\mathrm{XENON1T}}$ stands for the 90% confidence level upper limit on the DM-nucleon spin-independent cross section from XENON1T [216]. Finally, Ω_{DM} is the observed DM relic abundance given in Equation (4.2).

On the other hand, regarding experimental constraints, if the masses of the new scalars and pseudo-scalars are such that $m_{\theta,\rho} < m_h/2$, we can have invisible Higgs boson decays driven by the following expressions:

$$\Gamma(h \to \theta\theta) = \frac{\beta_{h\theta\theta}^2}{32\pi\, m_h}\sqrt{1 - \frac{4m_\theta^2}{m_h^2}}\,, \tag{5.37}$$

$$\Gamma(h \to \rho\rho) = \frac{\beta_{h\rho\rho}^2}{32\pi\, m_h}\sqrt{1 - \frac{4m_\rho^2}{m_h^2}}\,, \tag{5.38}$$

with the β_i coefficients defined in Appendix B. Moreover, the Higgs boson invisible branching ratio is given by

$$\mathrm{BR}(h \to \mathrm{inv}) = \frac{\Gamma(h \to \theta\theta) + \Gamma(h \to \rho\rho)}{c_\alpha^2 \Gamma_h^{\mathrm{SM}} + \Gamma(h \to \theta\theta) + \Gamma(h \to \rho\rho)}\,, \tag{5.39}$$

with Γ_h^{SM} being the SM Higgs boson decay width, $\Gamma_h^{\mathrm{SM}} = 4.1\,\mathrm{MeV}$.

From the experimental side, there are constraints on the observed Higgs boson signal strength, $\mu = c_\alpha^2(1 - \mathrm{BR}(h \to \mathrm{inv}))$. However, one should include contributions from both CP-even scalars ρ and h in the experimental analysis, which deserves

a dedicated study not covered in this thesis. Regarding this, let us remark that there are regions of the parameter space where it is a reasonable assumption to consider the current experimental bounds on the invisible Higgs boson decay. For instance, in the limit of small mixing s_α and heavy scalar ρ, we can neglect the contribution from the new CP-even scalar, which implies $c_\alpha^2 = 1$. Also when $m_\rho \sim m_h$ or below (SDM), and the mixing is small, it is still a good assumption.

In the numerical analysis we apply the 90% confidence level upper limit of $\mathrm{BR}(h \to \mathrm{inv}) < 0.16$ derived by the CMS Collaboration [217].

Numerical analysis

This subsection is devoted to the numerical analysis of different scenarios, seeking for the regions of their parameter space that reproduce the observed relic abundance in Equation (4.2). First, we consider the quadratic model as a distinctive example with suppressed DD constraints, and second, we extend the study to the rest of the *minimal models*. For that, we use the numerical code `micrOMEGAs` [218], taking into account the relevant theoretical and experimental constraints discussed in the previous section. Moreover, it is useful to introduce now the mass splitting parameter, Δ, given by

$$\Delta = \frac{(m_\rho - m_\theta)}{m_\theta} \,. \tag{5.40}$$

The quadratic model

Focusing first on the quadratic model, in Figure 5.3 the red line represents the (logarithm of the) mixing that reproduces the observed relic abundance as a function of the DM mass for different values of the mass splitting parameter, namely $\Delta = 1 + 1/10$ and $\Delta = 1 + 1/100$, and a given VEV $v_s = 100$ GeV. The relevant DM annihilation process in this region is $\theta\theta \to ff$ mediated by the new CP-even scalar, ρ, where f stands for some SM particles determined by the value of the DM mass. Therefore, in this case the DM abundance is set by the ρ resonance.

With respect to the constraints, we have considered i) being in thermal equilibrium with the SM bath in the Early Universe, exclusion region in green, ii) invisible Higgs boson decay, exclusion region in blue, and iii) rare B-meson decay from Ref. [23], exclusion region in orange. The latter basically stands for processes like $B \to K\rho \to K +$ "invisible", due to the mixing between the (light) scalar ρ and the Higgs boson. In our model, $\rho \to \theta\theta$ yields invisible final states.[13]

The red line in the aforementioned figure shows a definite behaviour in the parameter space, which can be explained as follows. For $m_\theta < m_\mu$, the relic abundance is set by the DM annihilations $\theta\theta \to ee$, which are very suppressed. Therefore, the mixing angle to reproduce the observed relic should be large, which at the same time is almost excluded by the different constraints. For $m_\theta > m_\mu$, the kinks corresponds to different hadronic and leptonic final states resulting from the DM annihilations.[14]

[13] We derived the decay rate for $B \to K\rho$ from the Appendix in Ref. [219].

[14] See *e.g.* Figure 4 from Ref. [219].

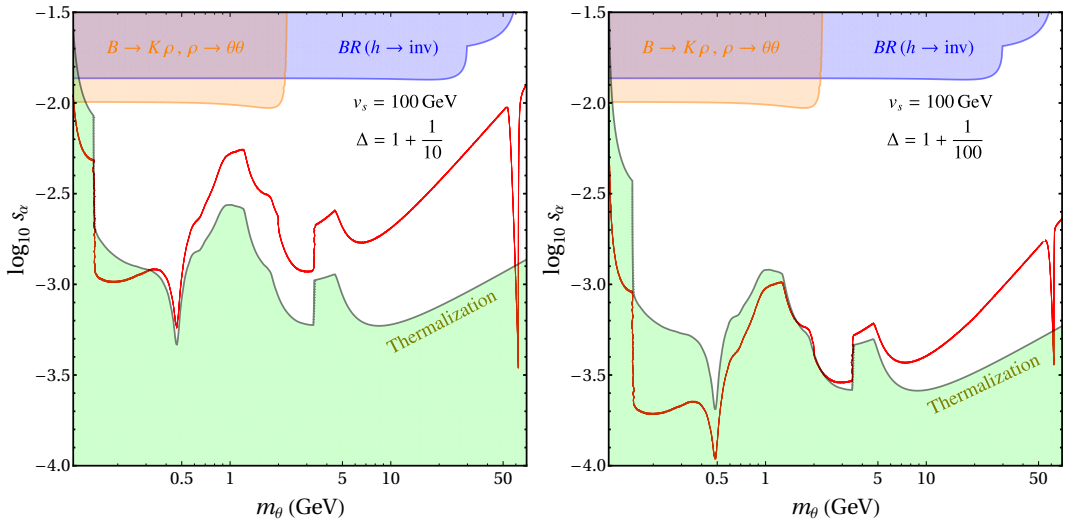

Figure 5.3: *The red curve represents the observed DM relic abundance in Equation* (4.2) *for the quadratic model. We fix* $v_s = 100\,\text{GeV}$ *and* $\Delta = 1 + 1/10$ $(1 + 1/100)$ *on the left (right) panel. Regions in blue, orange and green are excluded because of invisible Higgs boson decays, rare B meson decays into light scalars and the thermalization condition. See details in the text.*

In addition, we see the resonance due to the Higgs boson at $m_\theta \simeq m_h/2$. But, how does this figure change with the value of v_s? Basically, there are two effects one needs to consider. First, as we are on the ρ resonance, there is a cancellation that makes both the red curve and the thermalization condition (in green) independent of v_s. And second, the constraint from invisible Higgs boson decays allows for a larger mixing when we increase v_s.

It is important to stress that `micrOMEGAs` does not take into account DM annihilations into hadronic states for $m_\theta \lesssim 4$–$5\,\text{GeV}$, and therefore we can not trust the results given by the numerical code in that region. However, we solve this problem applying the results from Ref. [192]. In this regime for the DM mass, the relic abundance is set by the standard freeze-out of annihilations $\theta\theta \to$ hadrons, through the ρ resonance.[15] Here, the final state "hadrons" stands for a pair of hadronic states. Following the aforementioned reference, this cross section times the relative velocity of the DM particles can be written as

$$\sigma v_{rel} = \frac{4\beta^2_{\rho\theta\theta}}{\sqrt{s}} \left|D_\rho(s)\right|^2 \Gamma_{\rho\to\text{hadrons}}\left(\sqrt{s}\right), \tag{5.41}$$

where

$$\left|D_\rho(s)\right|^2 \equiv \frac{1}{\left(s - m_\rho^2\right)^2 + m_\rho^2\,\Gamma^2_{\rho,\text{full}}\left(m_\rho\right)}\,. \tag{5.42}$$

[15] Note that in our notation ρ is the new CP-even scalar, not the ρ-meson.

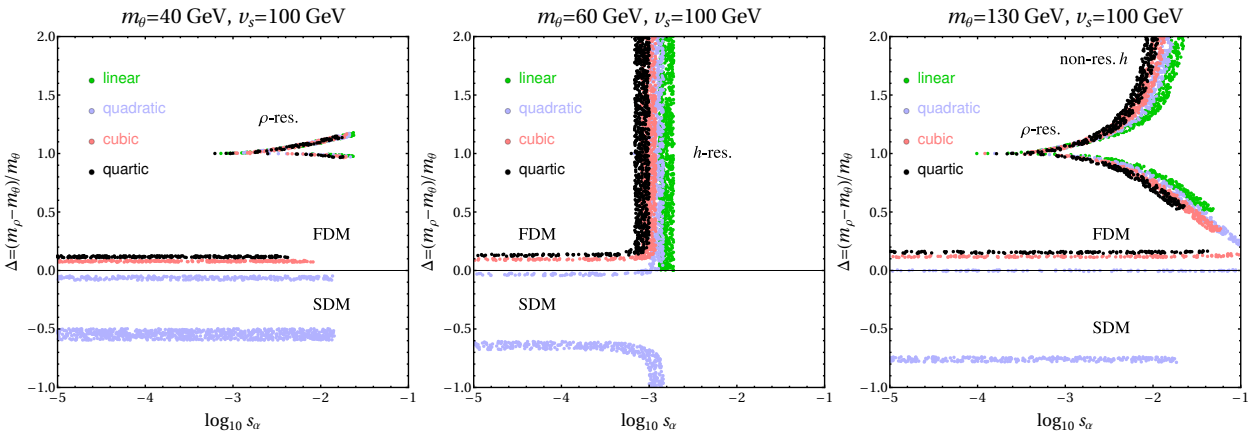

Figure 5.4: *Results from a scan in* Δ *and mixing,* s_α*, for the minimal models. We fix* $v_s = 100\,\text{GeV}$ *and* $m_\theta = 40, 60, 130\,\text{GeV}$ *from left to right, respectively. The color code is green, blue, red and black for the linear, quadratic, cubic and quartic model, respectively. The points fulfil the condition* $0.5 \leqslant \Omega/\Omega_{DM} \leqslant 1$*, where* Ω_{DM} *is the observed abundance in Equation* (4.2)*. In addition, we have considered the theoretical and experimental constraints explained in the text.*

The decay width of the new CP-even scalar into hadrons, $\Gamma_{\rho\to\text{hadrons}}$, can be extracted from Figure 4 of Ref. [219], and the $\beta_{\rho\theta\theta}$ coefficients are given in Appendix B for the *minimal models*. Moreover, in the parameter space that we are considering for the numerical analysis, the total decay width of the new scalar, $\Gamma_{\rho,\text{full}}$, is basically given by its decay width into DM particles, namely

$$\Gamma_{\rho,\text{full}} \simeq \Gamma_{\rho\to\theta\theta} = \frac{\beta^2_{\rho\theta\theta}}{32\pi\, m_\rho}\sqrt{1-\frac{4m_\theta^2}{m_\rho^2}}\,. \tag{5.43}$$

Finally, from Equation (5.41) and following the same procedure as in Appendix B of Ref. [192], we can get the DM relic abundance considering now annihilations into hadronic final states.

Comparison of the *minimal models*

So far, we have analysed the parameter space that reproduces the relic abundance for the quadratic model in the ρ resonance region. Now, we extend the numerical analysis to the *minimal models* including the full parameter space. Moreover, we also check that the thermal equilibrium of DM with SM particles in the Early Universe is satisfied,[16] and therefore we can safely use `micrOMEGAs` for the scan because the code assumes that the equilibrium condition is automatically fulfilled.

As we mentioned in Section 5.2, we have four independent parameters in the *minimal models*, namely m_θ, m_ρ, v_s and s_α. Therefore, we need to fix some of them

[16]The relevant DM interaction processes are: $\theta\theta \leftrightarrow$ SM SM in the resonance, and $\theta\theta \leftrightarrow \rho\rho, h\rho, hh$, with $\rho \leftrightarrow$ SM SM in the SDM/FDM regions.

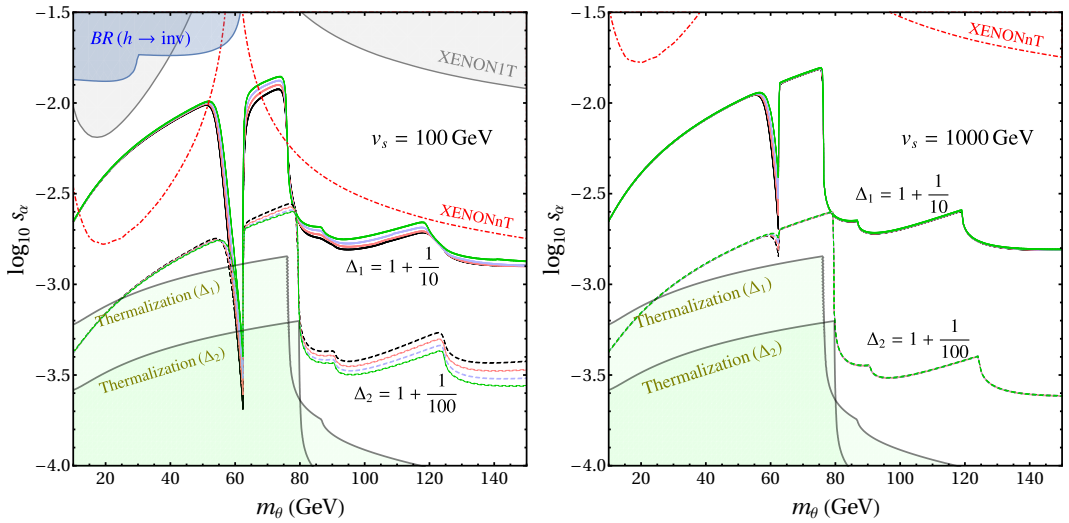

Figure 5.5: *The green, blue, red and black lines are the observed relic abundance in Equation* (4.2) *for the linear, quadratic, cubic and quartic model, respectively. We take different values for the normalized mass splitting,* $\Delta_1 = 1 + 1/10$ *(solid lines) and* $\Delta_2 = 1 + 1/100$ *(dashed lines), and fix* $v_s = 100\,(1000)$ GeV *on the left (right) panel. Regions in blue, gray and green are excluded because of invisible Higgs boson decays, XENON1T experiment [216] and the thermalization condition, respectively. Finally, the red dot-dashed line is the projection for XENONnT [220].*

to analyse the available parameter space in the remaining ones.[17] Having this in mind, in Figure 5.4 we fix $v_s = 100$ GeV and three values of the DM mass, $m_\theta = 40, 60, 130$ GeV from left to right, and plot the results from a scan in the mass splitting parameter and the (logarithm of the) mixing angle for the linear (green), quadratic (blue), cubic (red) and quartic (black) models. All these points fulfil the condition $0.5 \leqslant \Omega/\Omega_{\rm DM} \leqslant 1$. We use this range in the relic abundance to make clearly visible the available regions of the parameter space for the models.

The relic abundance is obtained in the separated regions discussed in the first part of Section 5.3, namely: for $m_\theta \simeq m_h/2$ through the Higgs boson resonance labelled as "h-res.", for $\Delta \simeq 1$ via the ρ resonance labelled as "ρ-res.", for $\Delta \gtrsim 0$ the FDM region, for $\Delta < 0$ the SDM region and finally, for $m_\theta > 100$ GeV and large values of s_α the non-resonant Higgs-mediated annihilations region labelled as "non-res. h". Let us remark that, apart from the experimental restrictions from DD and invisible Higgs boson decays, the theoretical constraints in Equations (5.32) and (5.33) also affect the parameter space. In particular, for the linear model $\lambda_S > 0$ implies that $\Delta > 0$, so there are no points in the SDM region. Moreover, for large m_ρ (or equivalently large Δ), $\lambda_S < 4\pi$ from perturbativity reduces the allowed region for each model.

From Figure 5.4 we conclude that distinguishing among the *minimal models* is dif-

[17] Another interesting option would be a global fit of the four parameters, beyond the scope of this work.

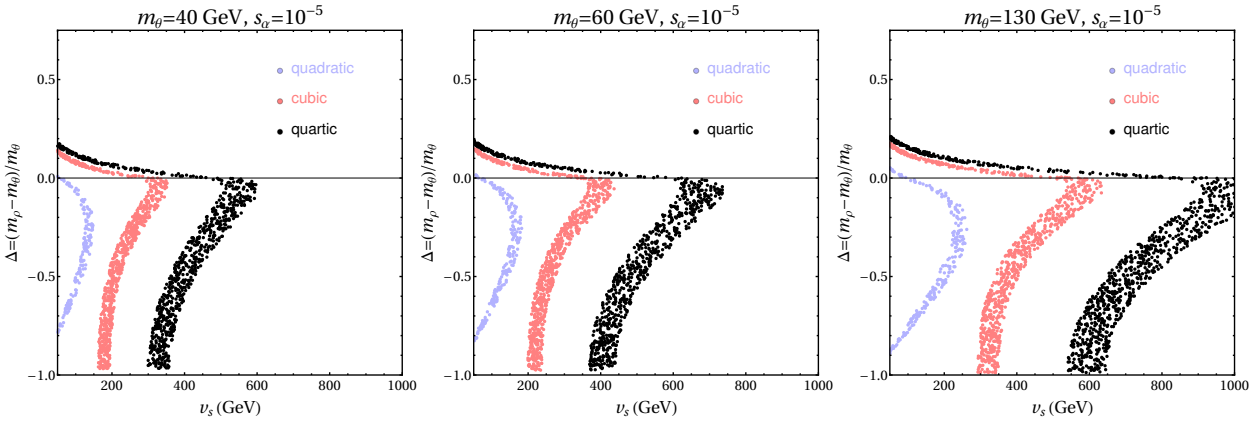

Figure 5.6: *Results from scanning in* Δ *and* v_s *for the minimal models. We fix* $s_\alpha = 10^{-5}$ *and* $m_\theta = 40$, 60, 130 GeV *from left to right, respectively. The points fulfil the condition* $0.5 \leqslant \Omega/\Omega_{DM} \leqslant 1$, *where* $\Omega_{\rm DM}$ *is the observed abundance in Equation* (4.2). *In addition, we have considered the theoretical and experimental constraints explained in the text. We apply the same color code as in Figure 5.4.*

ficult in the resonance region, but not in the SDM and FDM scenarios. To clarify this, we present the following two figures focusing on each one of these regions.

On the one hand, in Figure 5.5 we depict the mixing angle that reproduces the observed relic abundance as a function of m_θ for different values of the VEV (v_s = 100, 1000 GeV for the left and right panels, respectively) and fixed values of the mass splitting parameter close to the resonance region ($\Delta_1 = 1 + 1/10$ and $\Delta_2 = 1 + 1/100$ in solid and dashed lines, respectively). We use the same color code for the *minimal models* as in Figure 5.4. Apart from the Higgs boson resonance, the kinks in each curve are related to the opening of the new DM annihilations channels $\theta\theta \to WW, ZZ, hh$ once $m_\theta \simeq m_W$, m_Z and m_h, respectively. This figure supports the aforementioned conclusion about the difficulty to distinguish among the *minimal models* in the resonance region.

On the other hand, in Figure 5.6 we fix the mixing angle to a small value, $s_\alpha = 10^{-5}$, and we consider three values of the DM mass, $m_\theta = 40$, 60, 130 GeV from left to right, respectively. We plot the results from a scan in the mass splitting parameter and the VEV of the scalar. The resulting points satisfy that $0.5 \leqslant \Omega/\Omega_{\rm DM} \leqslant 1$. In this figure we can clearly see differences among the *minimal models* in the FDM and SDM regions.

Last but not least, in Figure 5.7 we take the VEV $v_s = 100$ GeV, and the mass splitting parameter $\Delta = 0.1$ (FDM region, left panel) and $\Delta = 1.1$ (ρ resonance region, right panel),[18] and we plot the results from a numerical scan in $s_\alpha \in \left[10^{-5}, 10^{-1}\right]$ and $m_\theta \in [10, 1000]$ GeV of the rescaled spin-independent DD cross section given in Equation (5.36). All these points fulfil the condition $0.5 \leqslant \Omega/\Omega_{\rm DM} \leqslant 1$. In addition, we

[18] In the parameter space of this scan, there is not enough DM abundance in the SDM region ($\Delta < 0$), *i.e* $\Omega/\Omega_{\rm DM} \leqslant 0.5$.

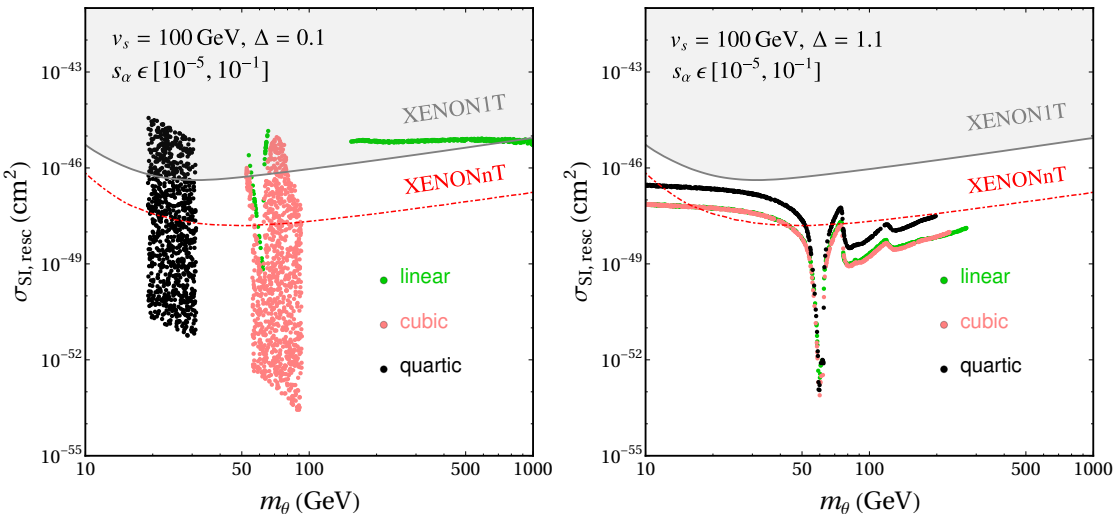

Figure 5.7: *Results from scanning in the rescaled spin-independent DD cross section given in Equation* (5.36) *and the DM mass for the minimal models. We fix* $v_s = 100\,\text{GeV}$ *and* $\Delta = 0.1\,(1.1)$ *on the left (right) panel, which corresponds to the FDM (*ρ *resonance) scenarios. The points fulfil the condition* $0.5 \leqslant \Omega/\Omega_{DM} \leqslant 1$*, where* Ω_{DM} *is the observed abundance in Equation* (4.2)*. In addition, we have considered the theoretical and experimental constraints explained in the text. In particular, the gray region is excluded by XENON1T [216]. Finally, the red dot-dashed line is the projection for XENONnT [220]. We apply the same color code as in Figure 5.4.*

also depict the current experimental limit on the spin-independent DD cross section and its future prospect from XENON1T [216, 220]. Note that for the quadratic model, the DD cross section is very suppressed because its main contribution is through one-loop processes, see *e.g.* Table 5.2.

From this figure, we conclude that the *minimal models* can yield distinguishable signals regarding DD in the FDM region, assuming that astrophysical details are under control (*i.e.* the standard halo model). Conversely, this is not the case for the ρ resonance region, where there is no significant difference among the results for the *minimal models*.

So far, we have focused on the *minimal models*, with just one explicit symmetry breaking term. In the next section, we will study how the inclusion of additional breaking terms modifies the allowed parameter space of the minimal scenarios. But before continuing with this analysis, several comments regarding the DM phenomenology of the *minimal models* are in order:

- Indirect detection bounds [221] can be evaded due to the temperature dependence of the thermally averaged DM annihilation cross section, which has also been analysed for the quadratic model in Ref. [210].

- There can be DM self-interactions, $\theta\theta \leftrightarrow \theta\theta$. In the parameter space that we are considering in this analysis, their maximum value (reached at the ρ res-

onance region) is well below the usual bound from galaxy clusters, $\sigma/m_\theta \lesssim 1\ \mathrm{cm}^2\mathrm{g}^{-1}$ [177].

- There is the possibility of light DM candidate: the lowest DM mass at the ρ resonance could be at the sub-GeV scale, with the DM relic abundance set by annihilations into hadrons and muons; the DM could be even lower for the FDM and SDM scenarios. See the dedicated section in Ref. [1].

5.4 Beyond *minimal models*

In this section, we extend the *minimal models* with an additional symmetry breaking term in their Lagrangian. This generalisation, even with real couplings for all the terms in the Lagrangian, could lead to SSB of the DCP, the symmetry which is responsible for the stability of the DM candidate.

First of all, it is useful to introduce the following notation for the potential that contains two terms with general couplings $\tilde{a}$ and $\tilde{b}$ that explicitly break the global $U(1)$ symmetry:

$$V_{\cancel{U(1)}} = \tilde{a}\, S^n + \tilde{b}\, S^{n'} + \mathrm{H.c.}\,, \tag{5.44}$$

where n, $n' = 1, 2, 3, 4$. These values for n and n' are associated to the linear, quadratic, cubic and quartic model interactions, respectively. In what follows, we assume (without loss of generality) $n < n'$. Moreover, by means of the exponential parameterisation for the scalar field

$$S = \frac{1}{\sqrt{2}}\left(v_s + \sigma'\right) e^{iG/v_s}\,, \tag{5.45}$$

one can write the potential that contains the explicit symmetry breaking terms, $V_{\cancel{U(1)}}$, in such a way that only the angular mode of the complex scalar, G, appears. Therefore, from Equation (5.44) we get

$$V_{\cancel{U(1)}} \supset V_{\mathrm{sb}} \equiv v_s^4 \left(a\, \cos\left(n\frac{G}{v_s}\right) + b\, \cos\left(n'\frac{G}{v_s}\right)\right)\,, \tag{5.46}$$

with the following definitions for the dimensionless couplings

$$a \equiv \frac{2}{v_s^4}\left(\frac{v_s}{\sqrt{2}}\right)^n \tilde{a} \quad \text{and} \quad b \equiv \frac{2}{v_s^4}\left(\frac{v_s}{\sqrt{2}}\right)^{n'} \tilde{b}\,. \tag{5.47}$$

In Table 5.3 we summarise their expressions in terms of the original couplings of the Lagrangian.

Regarding the discussion about DCP conservation, let us mention that:

i) The invariance of the Lagrangian under DCP ($S \to S^*$) requires that both $\tilde{a}$ and $\tilde{b}$ should be taken real.

ii) In order to avoid SSB of the DCP, the VEV of the scalar should also be invariant under this transformation, *i.e.* $\langle S\rangle = \langle S^*\rangle$. Therefore, $\langle S\rangle = v_s$ must be real. Note that, since the rest of the Lagrangian is invariant under phase transformations, we can always make a redefinition $S \to -S$ and take v_s real and positive.

n, n'	*Minimal model*	a, b
1	Linear	$\mu^3 / \left(\sqrt{2}\, v_s^3\right)$
2	Quadratic	$\mu_s^2 / \left(2\, v_s^2\right)$
3	Cubic	$\mu_3 / \left(2\sqrt{2}\, v_s\right)$
4	Quartic	$\lambda_4 / 4$

Table 5.3: *Effective parameters a and b defined in Equations* (5.44)*,* (5.46) *and* (5.47) *in terms of the explicit symmetry breaking couplings in the potential for the minimal models. See e.g. Equations* (5.29)*,* (5.30)*,* (5.16) *and* (5.17) *for the linear, quadratic, cubic and quartic models, respectively.*

Having these considerations in mind, we proceed with the minimisation of the potential, requiring that its global minimum is located at $\langle \sigma' \rangle = 0$ (this will fix the value of v_s in terms of all the parameters of the potential) and $\langle G \rangle = 0$. Therefore, in this case $\sqrt{2}\langle S \rangle = v_s > 0$.

In view of that, if $G = 0$ is the global minimum of the potential in Equation (5.46), the DCP will not be spontaneously violated. Clearly, the first derivative of this potential in $G = 0$ is zero, and the second derivative is $-v_s^2(n^2 a + n'^2 b)$. Then, we should impose $b \leqslant -a(n^2/n'^2)$ to have a local minimum at $G = 0$. Moreover, one has to check that it is the global minimum of $V_{\rm sb}(G)$.

Finally, we get the following conditions on the dimensionless couplings in the potential for DCP conservation:

$$a \leqslant 0 \quad \text{and} \quad \begin{cases} b \leqslant 0 & \text{for} \quad (n, n') = (2,3), (3,4)\,, \\ b \leqslant -a(n^2/n'^2) & \text{for} \quad (n, n') \neq (2,3), (3,4)\,, \end{cases} \tag{5.48}$$

which are depicted in Figure 5.8 for all the different combinations of explicit symmetry breaking terms associated to the *minimal models*. These conditions, which can be translated into restrictions on the explicit symmetry breaking parameters of the general potential in Equations (5.12–5.17) thanks to the relations in Table 5.3, have to be considered in the analysis of the parameter space for scenarios beyond the *minimal models*.

In Figure 5.9 we focus on one of those non-*minimal models*. In particular, we consider the combination of interactions from the cubic and the quartic models. On the left-hand side, we plot the results from scanning in Δ and s_α, fixing $m_\theta = 40$ GeV and $v_s = 100$ GeV. On the right-hand side, we depict the results from a scan in Δ and v_s, fixing $m_\theta = 40$ GeV and $s_\alpha = 10^{-5}$. All the points fulfil the condition on the relic abundance $0.5 \leqslant \Omega/\Omega_{\rm DM} \leqslant 1$, with the following color code: red and black for the cubic and quartic models, and gray for the non-*minimal model* that includes interactions from both the cubic and the quartic models.

We clearly see that the gray dots fill the region of the parameter space in between the *minimal models*. In addition, considering other combinations of *minimal models*

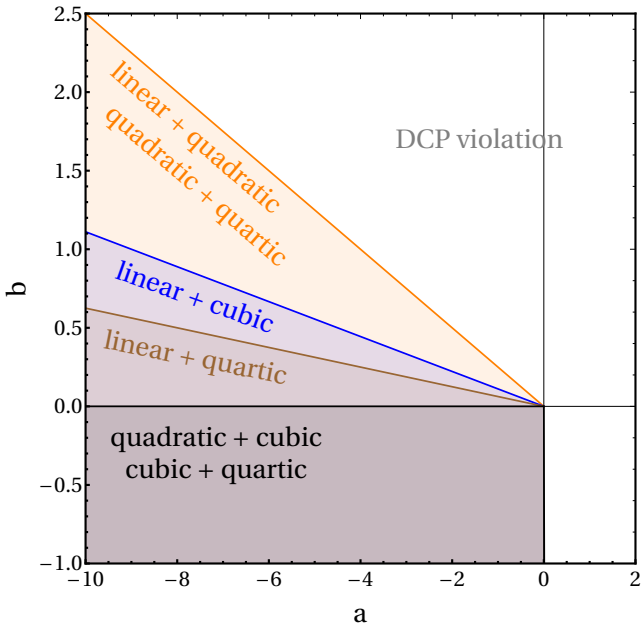

Figure 5.8: *For all the possible combinations of two minimal models, the colored regions represent the parameter space associated to the effective parameters a and b (see e.g. Table 5.3) where one has DCP conservation, as described in Equations* (5.48). *Combinations of models which appear with the same color share the same DCP conserving parameter region.*

we get similar results, and then we can conclude that having two explicit symmetry breaking terms in the Lagrangian enlarges the parameter space for a suitable DM candidate to regions bounded by the *minimal models*. This is due to the restrictions on the couplings of the Lagrangian derived in this section from not having spontaneous DCP violation, see *e.g.* Equation (5.48).

Before moving to the last section of the chapter, let us make some comments about the selection of the minimum of the potential in these non-*minimal models*. We obtain the conditions for DCP conservation in Figure 5.8 requiring that the global minimum of the potential is located at $\langle G \rangle = 0$. However, one can show that there are physically equivalent regions if one imposes the minimum at $\langle G \rangle = \pi$.

For instance, we start with the potential containing the linear and the quadratic interactions, namely

$$V^{12}_{\cancel{U(1)}} = \mu^3 S + \mu_S^2 S^2 + \text{H.c.}\,. \tag{5.49}$$

We find separated regions of the parameter space $(\mu^3,\, \mu_S^2)$ where the global minimum is either at $\langle G \rangle = 0$ or $\langle G \rangle = \pi$. But also one can check that these regions are symmetric under reversing the sign of the μ^3 term, and physically equivalent.

First, we select a specific point in the parameter space where the global minimum is at $\langle G \rangle = 0$, namely $\mu^3 = a_0$. In addition, we know that a_0 must be smaller than zero for having DCP conservation, see *e.g.* Figure 5.8. On the other hand, one can

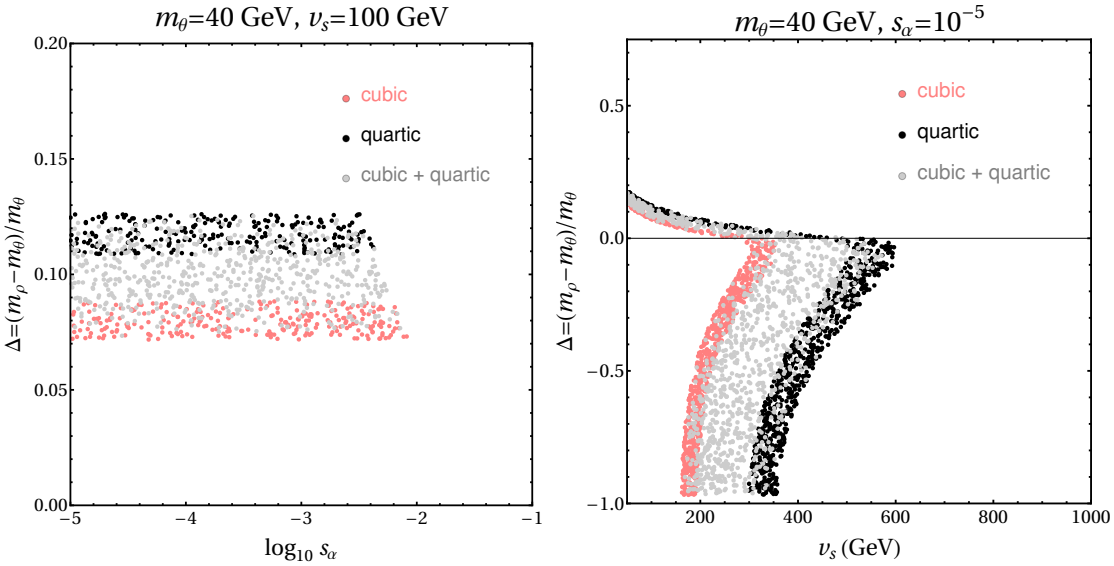

Figure 5.9: *On the left panel, we plot the results from scanning in* Δ *and mixing,* s_α*, around the FDM region* ($\Delta \gtrsim 0$) *for* $m_\theta = 40\,\text{GeV}$ *and* $v_s = 100\,\text{GeV}$*. On the right panel we depict the results from scanning in* Δ *and* v_s *for* $m_\theta = 40\,\text{GeV}$ *and* $s_\alpha = 10^{-5}$*. In both panels, we present the cubic (red) and quartic (black) model, together with the non-minimal model (gray) that combines the aforementioned models. The points fulfil the condition* $0.5 \leqslant \Omega/\Omega_{DM} \leqslant 1$*, where* Ω_{DM} *is the observed abundance in Equation* (4.2)*. In addition, we have considered the theoretical and experimental constraints explained in the text. Finally, in the non-minimal model we have also considered the constraints for having DCP conservation, see e.g. Equation* (5.48) *and Table 5.3.*

select $\mu^3 = -a_0$, which corresponds to the minimum at $\langle G \rangle = \pi$, and expand the scalar complex field around this minimum, $S \to Se^{i\pi}$. Performing this transformation in Equation (5.49), we get the same potential as in the case with $\mu^3 = a_0$ where the minimum is located at $\langle G \rangle = 0$. In view of this, we conclude that the separated points in the parameter space $(\mu^3 = a_0,\ \mu_S^2)$ and $(\mu^3 = -a_0,\ \mu_S^2)$ are physically equivalent.

We can generalise this procedure with the other possible combinations of *minimal models*. Consider now the linear and the cubic interactions

$$V^{13}_{\cancel{U(1)}} = \mu^3 S + \mu_3 S^3 + \text{H.c.}\,, \tag{5.50}$$

and select a point $(\mu^3,\ \mu_3) = (a_0,\ b_0)$ where the global minimum is at $\langle G \rangle = 0$. Moreover, we can check that in $(-a_0,\ -b_0)$ the minimum is located at $\langle G \rangle = \pi$. Then, we expand around this minimum, $S \to Se^{i\pi}$, and obtain the same potential as in the case $(a_0,\ b_0)$. Basically, we reverse both signs in the potential, μ^3 and μ_3, thanks to the transformation $S \to -S$. Therefore, the points $(a_0,\ b_0)$ and $(-a_0,\ -b_0)$ are physically equivalent.

The potential with the quadratic and the cubic interactions can be understood in a

similar way. Conversely, the potential with the quadratic and the quartic interactions deserves special attention. In this case,

$$V^{24}_{\cancel{U(1)}} = \mu_S^2 S^2 + \lambda_4 S^4 + \text{H.c.}\,. \tag{5.51}$$

We can rotate the field from 0 to π, namely $S \to -S$, and the sign of both terms in the potential does not change. Therefore, a given point in the parameter space (μ_S^2, λ_4) where the global minimum is at $\langle G \rangle = 0$ is identical to the one with the global minimum at $\langle G \rangle = \pi$.

However, in this case one can reverse the sign of the μ_S^2 term with a rotation of $\pi/2$, or equivalently a field transformation $S \to iS$. Therefore, if we select a point in the parameter space where the global minimum is at $\langle G \rangle = \pi/2$, we can show that this point is equivalent to $\langle G \rangle = 0$ by means of the aforementioned redefinition of the scalar field S. Then, for the potential in Equation (5.51) also the points in the parameter space where the minimum is located at $\langle G \rangle = \pi/2$ are physically equivalent to the ones where the minimum is at $\langle G \rangle = 0$ or π.

5.5 The pNGB limit and EFT

In this section we study the case where the explicit symmetry breaking term in the scalar potential of the *minimal models* is much smaller than the scale of SSB of the $U(1)$ symmetry, v_s. For doing that, it is useful to apply the exponential parameterisation for the scalar field in Equation (5.45).

As has been discussed in Section 5.2, the mass of the DM candidate, which is the CP-odd scalar (or the angular mode in the exponential parameterisation, G), is proportional to the explicit symmetry breaking terms, see *e.g.* Equation (5.21). Therefore, the limit that is considered in this section basically reads $m_G \ll v_s$, and G can be treated as a pNGB.

In this particular scenario, there is a gap between the energy scales of the theory, and we can make use of the EFT description, briefly reviewed in Section 1.4. From a bottom-up approach, at low energies we can construct the following (effective) Lagrangian for a pNGB, G, invariant under a discrete symmetry $G \to -G$ (which is the DCP in the exponential parameterisation), responsible for its stability. Therefore, including only operators of dimension $D \leqslant 6$ we get:

$$\begin{aligned}\mathcal{L}_{\text{eff}} =& \frac{1}{2}(\partial G)^2 + \frac{c_G}{v_s^2}\left(|H|^2 - \frac{v^2}{2}\right)(\partial G)^2 - \frac{1}{2}m_G^2 G^2 + \lambda_G G^4 \\ &+ \lambda_{HG}\left(|H|^2 - \frac{v^2}{2}\right) G^2\,.\end{aligned} \tag{5.52}$$

Note that the pNGB mass m_G, the quartic coupling λ_G and the Higgs portal λ_{HG} break the shift symmetry $G/v_s \to G/v_s + 2\pi/n$.

We can extract information about the coefficients c_G, λ_{HG} and λ_G in Equation (5.52) by means of the so-called matching: basically, we start with the full theory and parameterise the symmetry breaking terms in the potential with the charge n of the field

S, *i.e.* $V \propto S^n + \text{H.c.}$. Then, we integrate out the heavy particle (the radial part of the complex scalar, σ') and obtain the Wilson coefficients in terms of the UV parameters of the theory. We detail the computation of the matching conditions in what follows.

First, we can write the scalar potential for the *minimal models* as

$$V = V_0 + V_{\cancel{U(1)}}, \quad \text{with} \quad V_{\cancel{U(1)}} = \frac{1}{2}\lambda_n S^n + \text{H.c.}\,, \tag{5.53}$$

where V_0 given in Equation (5.13) preserves the global $U(1)$ symmetry, and $V_{\cancel{U(1)}}$ corresponds to the part that explicitly breaks the $U(1)$, with λ_n being an arbitrary coupling without loss of generality. In particular, $\lambda_n = \mu^3$, μ_S^2, μ_3, λ_4 for the linear, quadratic, cubic and quartic models, respectively. Therefore, $n = 1, 2, 3, 4$ corresponds to the linear, quadratic, cubic and quartic models, respectively.

Then, using the exponential parameterisation for the complex scalar in Equation (5.45), and after minimising the potential V, one gets the following expressions for the V_0 and the $V_{\cancel{U(1)}}$ terms:

$$V_0 = \frac{1}{2}m_{\sigma'}^2\sigma'^2\left(1 + \frac{\sigma'}{v_s} + \frac{\sigma'^2}{4v_s^2}\right) + \frac{1}{2}\lambda_{HS}v_s^2\left(1 + \frac{\sigma'}{v_s}\right)^2\left(|H|^2 - \frac{v^2}{2}\right), \tag{5.54}$$

$$\begin{aligned} V_{\cancel{U(1)}} &= \lambda_n \frac{(v_s + \sigma')^n}{2^{n/2}}\cos\left(\frac{nG}{v_s}\right) \simeq \lambda_n \frac{(v_s + \sigma')^n}{2^{n/2}}\left(1 - \frac{1}{2}\left(\frac{nG}{v_s}\right)^2\right) \\ &\supset -\frac{\lambda_n}{2}\left(\frac{nG}{v_s}\right)^2 \frac{v_s^{n-1}n}{2^{n/2}}\sigma'\,. \end{aligned} \tag{5.55}$$

Note that in the minimisation of the potential, we apply the pNGB limit (λ_n, $v \ll v_s$) and also consider that $\lambda_{HS} \ll \lambda_S$. This leads to $m_S^2 \simeq -\lambda_S v_s^2$, and furthermore we find the mass of the radial part to be $m_{\sigma'}^2 = 2\lambda_S v_s^2$.

On the other hand, from the kinetic term of the complex scalar we have:

$$|\partial S|^2 = \frac{1}{2}\left(\partial\sigma'\right)^2 + \frac{1}{2}\left(\partial G\right)^2 + \frac{\sigma'}{v_s}\left(1 + \frac{\sigma'}{2v_s}\right)\left(\partial G\right)^2, \tag{5.56}$$

and the Lagrangian of the theory, keeping only the dominant pieces, can be written as:

$$\begin{aligned} \mathcal{L} \simeq\, &\frac{1}{2}\left(\partial\sigma'\right)^2 - \frac{1}{2}m_{\sigma'}^2\sigma'^2 \\ &+ \sigma'\left(\frac{\left(\partial G\right)^2}{v_s} - \lambda_{HS}v_s\left(|H|^2 - \frac{v^2}{2}\right) + \frac{\lambda_n}{2}\left(\frac{nG}{v_s}\right)^2\frac{v_s^{n-1}n}{2^{n/2}}\right). \end{aligned} \tag{5.57}$$

Now, using the equation of motion (EoM) for σ', given by

$$\partial^2\sigma' + m_{\sigma'}^2\sigma'^2 - \left(\frac{\left(\partial G\right)^2}{v_s} - \lambda_{HS}v_s\left(|H|^2 - \frac{v^2}{2}\right) + \frac{\lambda_n}{2}\left(\frac{nG}{v_s}\right)^2\frac{v_s^{n-1}n}{2^{n/2}}\right) = 0\,, \tag{5.58}$$

we can get the following expression for the radial part:

$$\sigma' \simeq \frac{1}{m_{\sigma'}^2}\left(\frac{(\partial G)^2}{v_s} - \lambda_{HS} v_s \left(|H|^2 - \frac{v^2}{2}\right) + \frac{\lambda_n}{2}\left(\frac{nG}{v_s}\right)^2 \frac{v_s^{n-1} n}{2^{n/2}}\right). \tag{5.59}$$

In the last equation we apply that the momentum of σ', corresponding to the derivative term, is assumed to be much smaller than its mass (for the EFT approach to hold).

Substituting back the last expression for σ' in the Lagrangian in Equation (5.57), considering the EoM for σ', and neglecting the terms that go as $1/m_{\sigma'}^4$, we get an effective interaction described by the following Lagrangian:

$$\mathcal{L}_{\text{eff}} = \frac{1}{2m_{\sigma'}^2}\left(\frac{(\partial G)^2}{v_s} - \lambda_{HS} v_s \left(|H|^2 - \frac{v^2}{2}\right) + \frac{\lambda_n}{2}\frac{v_s^{n-3} n^3}{2^{n/2}} G^2\right)^2. \tag{5.60}$$

It is interesting to note that in the *minimal models*, we can express the mass of the DM candidate G as a function of the couplings that explicitly break the global $U(1)$ symmetry as:

$$m_G^2 = -\lambda_n \frac{v_s^{n-2} n^2}{2^{n/2}}. \tag{5.61}$$

This expression can be used in the effective Lagrangian $\mathcal{L}_{\text{eff}}$ to substitute the coupling λ_n in terms of m_G.

Finally, from the effective Lagrangian in Equation (5.60) one can select the terms that are interesting for the DM phenomenology associated to the theory, namely

$$\mathcal{L}_{\text{eff}} \supset \mathcal{L}_{HG} + \mathcal{L}_{GG}, \tag{5.62}$$

where $\mathcal{L}_{HG}$ and $\mathcal{L}_{GG}$ describe the interactions of the DM candidate G with the Higgs boson and its self-interactions, respectively. These Lagrangians are given by

$$\mathcal{L}_{HG} = -\frac{\lambda_{HS}}{2\lambda_S v_s^2}\left(|H|^2 - \frac{v^2}{2}\right)\left((\partial G)^2 - \frac{n}{2} m_G^2 G^2\right), \tag{5.63}$$

$$\mathcal{L}_{GG} = \frac{1}{4\lambda_S v_s^4}\left((\partial G)^4 + \frac{n^2}{4} m_G^4 G^4 - n m_G^2 G^2 (\partial G)^2\right). \tag{5.64}$$

Note that the Lagrangian $\mathcal{L}_{GG}$ includes also operators of $D = 6$ and $D = 8$, given by the $G^2 (\partial G)^2$ and the $(\partial G)^4$ terms, respectively. Now, we can compare the interactions in Equations (5.63) and (5.64) with the ones in the low-energy effective Lagrangian in Equation (5.52) to get the expressions for the Wilson coefficients in terms of the UV parameters. Therefore, we get

$$c_G = -s_\alpha \frac{v_s}{v}, \tag{5.65}$$

$$\lambda_{HG} = -c_G \frac{n}{2}\frac{m_G^2}{v_s^2}, \tag{5.66}$$

$$\lambda_G = \frac{n^2}{8}\frac{m_G^4}{m_{\sigma'}^2 v_s^2}, \tag{5.67}$$

where the mass of the pNGB is given in Equation (5.21), $m_G = m_\theta$, and there are some interesting relations among the coefficients (*e.g.* m_G and λ_G, or c_G and λ_{HG}). In addition, we have used that $m^2_{\sigma'} \simeq 2\lambda_S v_s^2$, and also the fact that in the limit $v_s \gg v$, the mixing can be written as

$$s_\alpha \simeq \frac{\lambda_{HS}}{2\lambda_S}\frac{v}{v_s}\,, \tag{5.68}$$

see *e.g.* Equation (5.28).

Apart from that, one can extract additional information regarding DD from the effective Lagrangian in Equation (5.52). In fact, after integrating by parts the derivative interaction of this Lagrangian, we obtain[19]

$$\begin{aligned}\left(|H|^2 - \frac{v^2}{2}\right)(\partial G)^2 \to &-\left(|H|^2 - \frac{v^2}{2}\right) G\partial^2 G - G\partial_\mu\left(|H|^2\right)\partial^\mu G \\ &\to m_G^2\left(|H|^2 - \frac{v^2}{2}\right) G^2 - G\partial_\mu\left(|H|^2\right)\partial^\mu G\,.\end{aligned} \tag{5.69}$$

The net result after this manipulation is an additional contribution to the Higgs portal coupling, namely

$$\lambda_{HG} \to \lambda_{HG} + m_G^2\frac{c_G}{v_s^2} = c_G\frac{m_G^2}{v_s^2}\left(1 - \frac{n}{2}\right)\,. \tag{5.70}$$

This equation shows an explicit cancellation for $n = 2$, which corresponds to the quadratic model, already noticed in Ref. [199]. Therefore, in this case, signals in DD experiments are suppressed, which is in agreement with what has been discussed during the chapter.

As a final remark, let us mention that, at low energies, one can remove the non-derivative terms in the effective Lagrangian in Equation (5.52) by means of a shift symmetry in the pNGB field like $G/v_s \to G/v_s + 2\pi/n$. Therefore, the allowed terms in the effective potential are

$$V_{\text{eff}} = \sum_{n=1}^{4} V_n + \sum_{n=1}^{2} U_n\,, \tag{5.71}$$

where

$$V_n = d_n \cos\left(n\frac{G}{v_s}\right) \quad \text{and} \quad U_n = c_n\left(|H|^2 - \frac{v^2}{2}\right)\left(1 - \cos\left(n\frac{G}{v_s}\right)\right)\,. \tag{5.72}$$

We assume a renormalisable UV completion, setting the upper limit in the sums. The d_n terms with $n = 1, 2, 3, 4$ correspond at high energy to the linear, quadratic, cubic and quartic terms in S in the complex parameterisation, which respect DCP, $\mathcal{Z}_2$, $\mathcal{Z}_3$ and $\mathcal{Z}_4$, respectively. Moreover, the c_n terms with $n = 1, 2$ correspond to the linear and quadratic terms with the Higgs doublet respecting DCP and $\mathcal{Z}_2$, respectively.

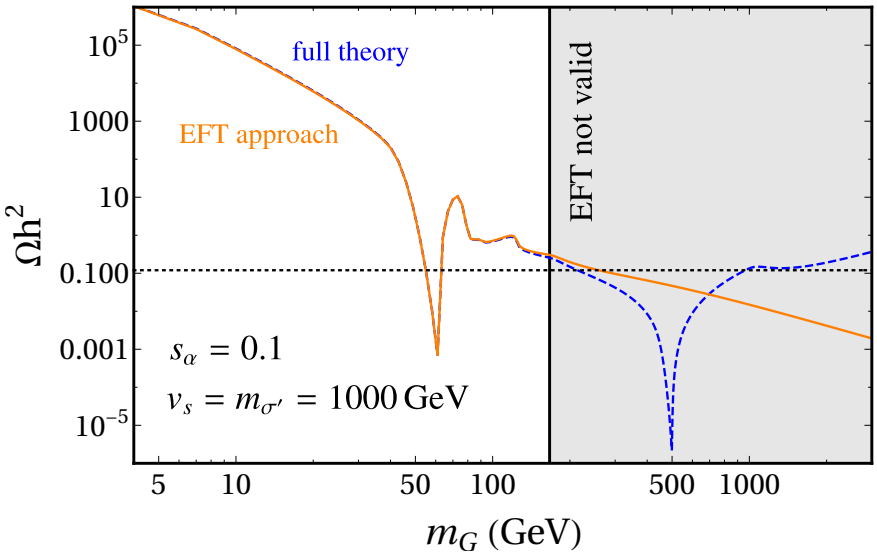

Figure 5.10: *The blue dashed line corresponds to the relic abundance as a function of the DM mass for the quadratic model, whereas the orange line corresponds to the relic abundance as a function of the DM mass for the pNGB effective Lagrangian with the Higgs field given in Equation* (5.52)*. They are labelled as full theory and EFT approach, respectively. We fix* $v_s = m_{\sigma'} = 10^3\,\text{GeV}$ *and* $s_\alpha = 0.1$*. The black dotted line is the observed DM abundance in Equation* (4.2)*, then the region above is excluded and in the region below the DM is under-abundant. We depict in gray the region where the EFT can not capture the full theory, namely* $m_G \gtrsim v_s/6$*.*

Numerical analysis

In the full theory there are basically three energy scales, namely m_G, v_s and v, associated with the angular and the radial modes of the complex scalar, and the Higgs field, respectively. And in this section, we get an EFT based on $m_G \ll v_s$, but also implicitly $v \ll v_s$. In that case, we can use the effective Lagrangian given in Equation (5.63) which contains only the Higgs field and the pNGB.[20]

Moreover, knowing the details of the underlying theory we can get the matching conditions for the coefficients of the effective operators, and then compare the EFT results regarding DM phenomenology (abundance and DD signals) with the ones that are obtained from the full theory. In Figure 5.10 we exemplify this procedure for the quadratic model. We plot the relic abundance as a function of the DM mass for a given value of the mixing, $s_\alpha = 0.1$, and the VEV, $v_s \simeq m_{\sigma'} = 10^3\,\text{GeV}$. The blue dashed line corresponds to the full model, whereas the orange line is associated to the effective Lagrangian approach, with the Wilson coefficients obtained in Equations (5.65) and (5.66) with $n = 2$, associated to the quadratic model.

[19] Note that in the last step of the integration by parts we use the Klein-Gordon equation of motion for G, which is correct for G on-shell, as in the case of DD experiments.

[20] See also related works in Refs. [222, 223].

Regarding the DM abundance curve, in the full theory we can see both the Higgs boson and the σ' resonances, and also the solution at $m_G \simeq m_{\sigma'} \simeq 1\,\text{TeV}$. The latter corresponds to the opening of the channel $GG \to \sigma'\sigma'$. On the other hand, the EFT reproduces with a high accuracy the full theory for $m_G \lesssim v_s/6$. Clearly, it can not capture the solutions at the σ' resonance, $m_G \simeq m_{\sigma'}/2$, and also at $m_G \simeq m_{\sigma'}$. Note that in both the full model and the EFT we see a small kink at $m_G \simeq m_h$, associated to the opening of the annihilation channel $GG \to hh$.

CHAPTER 6

Sterile neutrino portals to Majorana dark matter: an Effective Field Theory approach

In this chapter, we will analyse a framework where a Majorana DM candidate communicates with the SM through its coupling to sterile neutrinos, which at the same time generates the masses for active neutrinos. In this scenario, the relic abundance is set by the standard freeze-out of the annihilations of the Majorana fermions into sterile neutrinos, which are also assumed to be Majorana fermions.

First, using an EFT approach, we will list all the possible four-fermion operators at dimension six that describe interactions between the Majorana DM candidate and the sterile neutrino. As we will see, these operators can either conserve or violate lepton number, which can be related with the Dirac or Majorana nature of active neutrinos.

As a next step, we will study the possible UV completions of the effective operators. In particular, there can be UV completions of the EFT which include scalars. However, this time we consider that they are heavier than in the case of scalars that could explain the discrepancies in the AMM of charged leptons. We will also provide details of the matching for the considered models in dedicated appendices.

Finally, we will analyse the phenomenology of certain (the most promising) models. Interestingly, in a particular case the Majorana mass of the sterile neutrino is generated radiatively. We will also discuss the details of the one-loop sterile neutrino mass calculation in a dedicated appendix.

6.1 Motivation and setup

In Section 1.2 we reviewed the most important hints of physics BSM, and among them we had neutrino masses and the existence of DM. Regarding the former, many extensions of the SM can provide a solution involving the so-called sterile or right-handed neutrinos, N_R, which are SM gauge singlet fermions. See also the discussion

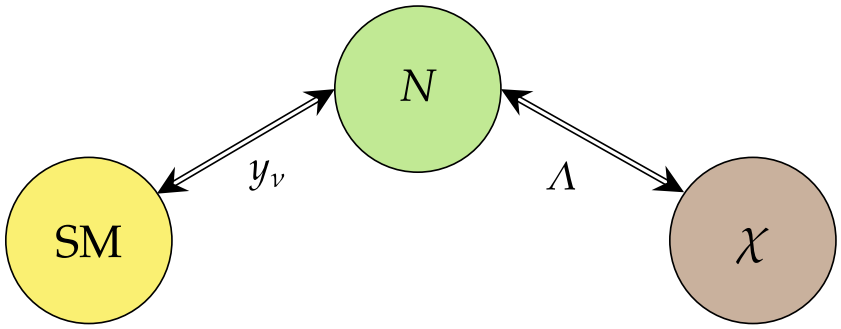

Figure 6.1: *The sterile neutrino, N, talks both to the SM via the Yukawa interaction in Equation* (6.1)*, and also to the dark sector, χ. The latter interaction is described by four-fermion operators generated at some NP scale, Λ.*

about neutrino masses in Section 1.3.

The sterile neutrinos only talk to the SM through a Yukawa interaction of the form

$$\mathcal{L} \supset \bar{l} y_\nu N_R \tilde{H} + \text{H.c.}\,, \tag{6.1}$$

where l and H are the $SU(2)_L$ lepton and Higgs doublets, respectively.[1] Moreover, sterile neutrinos could interact with a hypothetical dark sector, which contains a DM candidate. This scenario is the usual sterile neutrino portal to DM [224]. Constraints from DD, ID and collider searches on weakly interacting massive particles suggest that it is natural to assume scenarios where the SM and the dark sector interact mainly via sterile neutrinos.

Therefore, one can have several scenarios depending on the mass of the sterile neutrino, m_N, assuming that the DM abundance is obtained through the usual thermal freeze-out mechanism:

- **i)** $m_N < m_{\text{DM}}$. The relic abundance is set by DM annihilations into sterile neutrinos, which decay into SM particles, yielding ID signals in photon, charged particles and neutrino spectra. This is the secluded regime [224]. See for a phenomenological analysis of this scenario Refs. [225–228].

- **ii)** $m_N > m_{\text{DM}}$. DM annihilations into sterile neutrinos are kinematically forbidden. However, there could be annihilations into active neutrinos due to the mixing between active and sterile neutrinos. In this scenario, the observed relic abundance requires a large mixing. See for a phenomenological analysis of this scenario Refs. [229–231].

In this chapter we analyse the first regime, $m_N < m_{\text{DM}}$, assuming that the DM particle is a Majorana fermion, denoted by χ, and there is a conserved $\mathcal{Z}_2$ symmetry

[1] Note the change of notation for the Higgs doublet with respect to the one used in Section 1.1, namely $\phi \to H$.

under which it is charged, and therefore it is stable. Moreover, interactions between DM particles and sterile neutrinos are described by four-fermion operators, which are generated at some NP scale, Λ. In Figure 6.1 we schematically depict this scenario. Let us remark that usually in the literature, the so-called neutrino portal is referred to the operator $(lH) \times \mathcal{O}_{\text{dark}}$, with $\mathcal{O}_{\text{dark}}$ being a singlet of a dark symmetry group, which can be composed of a dark fermion and a dark scalar [232, 233]. This operator can be obtained after integrating out a heavy sterile neutrino, but note that our approach will be different.

There are several interesting works related to the effective description of interactions between DM particles and the SM extended with sterile neutrinos, see *e.g.* Ref. [234]. Moreover, other EFT analysis of the SM (without sterile neutrinos) extended with different types of DM candidates have been done in [235, 236].

In our analysis, we extend the SM particle content with two chiral fermions that transform under the SM gauge group $(SU(3)_c, SU(2)_L)_{U(1)_Y}$ as $(1,1)_0$. They are the sterile neutrino, N_R, and χ_L, which is charged under a discrete symmetry $\mathcal{Z}_2$ responsible for its stability, yielding a suitable DM candidate. With these ingredients, the most general renormalisable Lagrangian one can construct is

$$\mathcal{L}_4 = \mathcal{L}_{\text{SM}} + \overline{N_R} i\partial\!\!\!/ N_R + \overline{\chi_L} i\partial\!\!\!/ \chi_L - \left[\frac{1}{2} m_N \overline{N_R^c} N_R + \frac{1}{2} m_\chi \overline{\chi_L} \chi_L^c + y_\nu \bar{l} \tilde{H} N_R + \text{H.c.}\right], \tag{6.2}$$

with $\mathcal{L}_{\text{SM}}$ being the SM Lagrangian given in Equation (1.33). The mass terms of the new chiral fermions, m_N and m_χ, can always be taken real by re-phasing N_R and χ_L. One can consider a preserved global $U(1)_L$ symmetry, the lepton number, with the assignment for the fields $L(N_R) = 1$ and $L(\chi_L) = 0$. In this case, the Majorana mass term for the sterile neutrino is not allowed.

As was briefly mentioned in Section 1.3, we need at least two extra right-handed neutrinos to explain neutrino data, which requires a minimum of two massive neutrinos. However, we simplify our analysis considering that only one of the right-handed neutrinos is lighter than the DM candidate, *i.e.* $m_N < m_\chi$. Therefore, the DM abundance is set by $\chi\chi \to NN$, and the rest of the sterile neutrinos are decoupled. In our discussion, χ and N are Majorana fields, *i.e.*

$$\chi = \chi_L + \chi_L^c \qquad \text{and} \qquad N = N_R^c + N_R \,. \tag{6.3}$$

6.2 Effective Field Theory approach

So far, we have presented the main ingredients of our model, and in this section we ask for possible four-fermion effective operators that can describe interactions between the Majorana fermions χ and N. These operators connect the SM and DM via the sterile neutrinos. For the EFT approach to be valid, we assume that the masses of the new fermions are below the scale Λ associated to NP, *i.e.* $m_N < m_\chi < \Lambda$.

At dimension $D = 6$ we get the following effective Lagrangian:

$$\mathcal{L}_6 = \frac{c_1}{\Lambda^2} \mathcal{O}_1 + \left[\frac{c_2}{\Lambda^2} \mathcal{O}_2 + \frac{c_3}{\Lambda^2} \mathcal{O}_3 + \text{H.c.}\right], \tag{6.4}$$

with the operators given by

$$\mathcal{O}_1 = (\overline{N_R}\chi_L)(\overline{\chi_L}N_R) = -\frac{1}{2}(\overline{N_R}\gamma_\mu N_R)(\overline{\chi_L}\gamma^\mu\chi_L)\,, \tag{6.5}$$

$$\mathcal{O}_2 = (\overline{N_R}\chi_L)(\overline{N_R}\chi_L) = -\frac{1}{2}(\overline{N_R}N_R^c)(\overline{\chi_L^c}\chi_L)\,, \tag{6.6}$$

$$\mathcal{O}_3 = (\overline{N_R^c}N_R)(\overline{\chi_L^c}\chi_L) = -\frac{1}{2}(\overline{N_R^c}\gamma_\mu\chi_L)(\overline{\chi_L^c}\gamma^\mu N_R)\,, \tag{6.7}$$

which will be denoted as *portal operators*. The second equalities are obtained using the Fierz identities. Regarding this, note that the Fierz transformation in Equation (6.6) in general includes also a term $+1/2(\overline{N_R}\sigma_{\mu\nu}N_R^c)(\overline{\chi}\sigma^{\mu\nu}\chi)$, which vanishes for one generation of N or χ.

- **Operator $\mathcal{O}_1$.** The Wilson coefficient c_1 is real, and the operator is lepton number conserving (LNC). In this case, the Majorana mass term for the sterile neutrino is forbidden, $m_N = 0$, and we get for active neutrino masses $m_\nu = y_\nu v_h/\sqrt{2}$.[2]
- **Operators $\mathcal{O}_2$ and $\mathcal{O}_3$.** In general, the Wilson coefficients c_2 and c_3 are complex, and both operators violate lepton number in two units. If they are present, lepton number is broken and in general, one can add a Majorana mass term for the sterile neutrinos. Regarding neutrino masses, this is the usual Type-I Seesaw model, briefly discussed in Section 1.3.

In the rest of the chapter, unless stated otherwise, active neutrino masses are obtained through the standard seesaw mechanism (see *e.g.* Section 1.3). Therefore, in the limit $m_N \gg m_{\rm D}$, we get

$$m_{\rm light} \simeq \frac{m_{\rm D}^2}{m_N}\,, \qquad \nu_{\rm light} \simeq \nu_L\,, \tag{6.8}$$

$$m_{\rm heavy} \simeq m_N\,, \qquad \nu_{\rm heavy} \simeq N_R\,. \tag{6.9}$$

The mass and the weak eigenstates are equivalent due to the small value for the mixing between the light (active) and the heavy (sterile) neutrinos.[3] Moreover, in Figure 6.2 we depict the thermal decay rate of sterile neutrinos as a function of its mass compared to the Hubble parameter at the time of BBN, in red and gray lines, respectively. Sterile neutrinos should decay before BBN for not spoiling light-nuclei abundances, and we see that for $m_N \gtrsim 2\,\text{GeV}$, the decay rate is larger than the Hubble parameter at BBN [226]. The expressions for the sterile neutrino decay width are taken from Refs. [225, 237].

Of course, there are other operators at dimensions five and six which involve χ_L, see *e.g.* [234]. As we will discuss in Section 6.3, different UV models will generate different sets of effective operators at $D \leqslant 6$, which for the time being are listed in Table 6.1.

[2] In this chapter, v_h is the VEV of the Higgs field because the letter v is reserved to the relative velocity of the DM particles, as we will see in the next section.

[3] The mixing is approximately given by $\sqrt{m_{\rm light}/m_{\rm heavy}}$ and therefore very small, namely, it is smaller than 10^{-5} for $m_N \gtrsim 2\,\text{GeV}$.

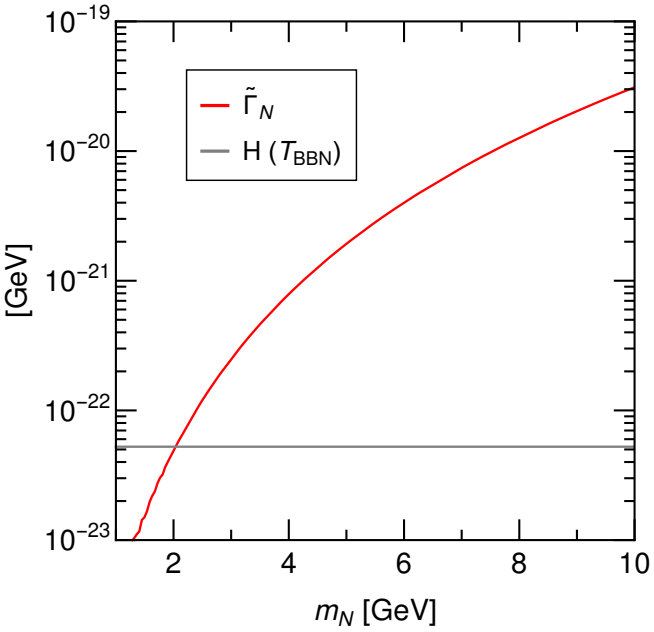

Figure 6.2: *The red line represents the thermal decay rate of sterile neutrinos, $\tilde{\Gamma}_N$, as a function of m_N compared to the Hubble parameter at the time of BBN, denoted by the gray line. BBN constraint imposes that the decay width of sterile neutrinos should be larger than the Hubble parameter at BBN, i.e. $\tilde{\Gamma}_N > H(T_{\rm BBN} \simeq 10\,\text{MeV})$. The expressions for $\tilde{\Gamma}_N$ are taken from Refs. [225, 237, 238].*

Dark matter relic abundance

As we have mentioned in Section 6.1, the relic abundance is set via the usual freeze-out of DM annihilations $\chi\chi \to NN$. And for the standard freeze-out mechanism to happen, we need that the new particles were in thermal equilibrium in the Early Universe. Regarding this condition, which process could be responsible for the thermal equilibrium of the sterile neutrino?

The only connection between sterile neutrinos and the SM particles is via the Yukawa interaction in Equation (6.1). Moreover, as we already know from the EFT review in Section 1.4, each EFT has an associated range of validity, namely energies below the NP scale Λ. This validity bound, in addition to unitarity and the conditions for the masses of new fermions to get the DM abundance via $\chi\chi \to NN$ yields:

$$m_N < m_\chi < \Lambda < \mathcal{O}(100)\,\text{TeV}\,. \tag{6.10}$$

In addition, from the seesaw formula in Equation (6.8) and imposing $m_\nu \lesssim 0.05\,\text{eV}$, we get an upper bound for the Yukawa coupling

$$y_\nu \lesssim 1.3 \times 10^{-6} \quad \text{for} \quad m_N \lesssim 1\,\text{TeV}\,. \tag{6.11}$$

Due to the small value of this coupling, DM abundance set by the freeze-in mechanism is also a well-motivated scenario, see *e.g.* Refs. [239–242]. However, in our

Notation	Operator	Dimension
	Portal operators	
$\mathcal{O}_1$	$(\overline{N_R}\chi_L)(\overline{\chi_L}N_R)$	6
$\mathcal{O}_2$	$(\overline{N_R}\chi_L)(\overline{N_R}\chi_L)$	6
$\mathcal{O}_3$	$(\overline{N_R^c}N_R)(\overline{\chi_L^c}\chi_L)$	6
	Self-interactions	
$\mathcal{O}_4$	$(\overline{N_R^c}N_R)(\overline{N_R}N_R^c)$	6
$\mathcal{O}_5$	$(\overline{\chi_L^c}\chi_L)(\overline{\chi_L}\chi_L^c)$	6
$\mathcal{O}_{\psi\psi}$	$(\overline{\psi}\gamma_\mu\psi)(\overline{\psi}\gamma^\mu\psi)$	6

Notation	Operator	Dimension
	***N*/DM–SM interactions**	
$\mathcal{O}_{NH}$	$(\overline{N_R^c}N_R)(H^\dagger H)$	5
$\mathcal{O}_{\chi H}$	$(\overline{\chi_L^c}\chi_L)(H^\dagger H)$	5
$\mathcal{O}_{N\psi}$	$(\overline{N_R}\gamma_\mu N_R)(\overline{\psi}\gamma^\mu\psi)$	6
$\mathcal{O}_{\chi\psi}$	$(\overline{\chi_L}\gamma_\mu\chi_L)(\overline{\psi}\gamma^\mu\psi)$	6
	Majoron interactions	
$\mathcal{O}_{\Psi J}$	$(\overline{\Psi}\gamma^\mu\Psi)(\partial_\mu J)$	5
$\mathcal{O}_{HJ}$	$\lvert H\rvert^2 (\partial J)^2$	6

Table 6.1: *$D \leqslant 6$ effective operators generated by the UV completions studied in Section 6.3. They are generated after integrating out at tree level scalar and/or vector mediators, except for the $\mathcal{O}_{\Psi J}$ generated in Model B2 as a consequence of the non-linear field redefinition defined in Equation* (6.46)*. For this operator, Ψ represents the fields carrying non-zero lepton number, i.e. $\Psi = N_R$, χ_L, l and e_R (see details in Section 6.3.2.). Finally, in $\mathcal{O}_{\psi\psi}$, $\mathcal{O}_{N\psi}$ and $\mathcal{O}_{\chi\psi}$, ψ stands for the SM fermions, i.e. $\psi = l$, e_R, Q, u_R, d_R. Note that for $\mathcal{O}_{\Psi J}$ and $\mathcal{O}_{HJ}$, J stands for the Majoron in Model B2, see discussion in Section 6.3.2.*

setup, there are also scalars or gauge bosons responsible for the openings of the effective portal operators. These new particles have also other interactions with the SM (through Higgs portal and/or kinetic mixing), which can help to reach the thermal equilibrium condition. In view of that, it is safe to assume that early on, N_R and χ_L were in thermal equilibrium with the SM.

Therefore, assuming thermal equilibrium of sterile neutrinos in the Early Universe, the relic abundance is given by the usual freeze-out of DM annihilations $\chi\chi \to NN$, and this cross section can be expanded as a function of the relative velocity $v = |\vec{v}_1 - \vec{v}_2|$ of DM particles as follows:[4]

$$\sigma v = a + b\frac{v^2}{4} + \mathcal{O}\left(v^4\right). \tag{6.12}$$

In this expansion, the coefficients a and b are related to the s- and p-wave contributions to the DM annihilation cross section. In order to get the value for these coefficients, we use the numerical codes FeynRules [243], FormCalc and FeynArts [244] with the effective Lagrangian interaction given in Equation (6.4). Finally, we get the

[4]The DM annihilation cross section only depends on v in the non-relativistic limit. Remember that at freeze-out, $T \simeq m_\chi/20$, and then this limit is appropriate.

following expressions:

$$a = \frac{m_\chi^2}{16\pi\Lambda^4}\sqrt{1-r_N^2}\,\left[(c_1 r_N + 2\,\mathrm{Re}\,c_2 + 4\,\mathrm{Re}\,c_3)^2 + 4\,(\mathrm{Im}\,c_2 - 2\,\mathrm{Im}\,c_3)^2\,\left(1-r_N^2\right)\right], \tag{6.13}$$

$$\begin{aligned} b = \frac{m_\chi^2}{96\pi\Lambda^4}\frac{1}{\sqrt{1-r_N^2}}\Bigg\{ & c_1^2\left(8-28r_N^2+23r_N^4\right) + 24\left[(\mathrm{Im}\,c_2 + 2\,\mathrm{Im}\,c_3)^2 + (\mathrm{Re}\,c_2 - 2\,\mathrm{Re}\,c_3)^2\right] \\ & + 12r_N^2\left[(\mathrm{Im}\,c_2)^2 + 4(\mathrm{Im}\,c_3)^2 - 20\,\mathrm{Im}\,c_2\,\mathrm{Im}\,c_3 - (\mathrm{Re}\,c_2 - 6\,\mathrm{Re}\,c_3)\,(3\,\mathrm{Re}\,c_2 - 2\,\mathrm{Re}\,c_3)\right] \\ & + 12c_1 r_N\,(\mathrm{Re}\,c_2 + 2\,\mathrm{Re}\,c_3)\,\left(-2+3r_N^2\right) \\ & + 12r_N^4\left[2\,(\mathrm{Re}\,c_2 - 2\,\mathrm{Re}\,c_3)^2 - 3\,(\mathrm{Im}\,c_2 - 2\,\mathrm{Im}\,c_3)^2\right]\Bigg\}, \end{aligned} \tag{6.14}$$

with $r_N \equiv m_N/m_\chi$. For the following discussions, it is useful to derive the limit of these expressions for $m_N \to 0$, namely

$$a = \frac{m_\chi^2}{4\pi\Lambda^4}\,\left[|c_2|^2 + 4\,|c_3|^2 + 4\,\mathrm{Re}(c_2 c_3)\right], \tag{6.15}$$

$$b = \frac{m_\chi^2}{12\pi\Lambda^4}\left[c_1^2 + 3\,|c_2|^2 + 12\,|c_3|^2 - 12\,\mathrm{Re}(c_2 c_3)\right]. \tag{6.16}$$

It is interesting to note that one can analyse DM annihilations $\chi\chi \to NN$ using arguments based on discrete symmetries and conservation of the total angular momentum. By means of that, we get results for the s- and p-wave nature of the DM annihilations which are consistent with the coefficients obtained in Equations (6.13–6.16). See full discussion in Appendix C.1. In particular, we can see that the s-wave vanishes if $c_1 = 0$ and $c_2 = -2c_3^*$, see *e.g.* Equation (6.13).

There is also the possibility that the sterile neutrino, N_R, is the right-handed companion of the left-handed neutrino in the SM, ν_L. In this scenario, ν is of Dirac type with mass $m_\nu \simeq 0.05\,\mathrm{eV}$, and only the LNC $\mathcal{O}_1$ is present. Then, the expressions for the coefficients a and b read

$$a = \frac{c_1^2 m_\nu^2}{32\pi\Lambda^4}\sqrt{1-r_\nu^2}, \tag{6.17}$$

$$b = \frac{c_1^2 m_\chi^2}{192\pi\Lambda^4}\,\frac{\left(16 - 32r_\nu^2 + 19r_\nu^4\right)}{\sqrt{1-r_\nu^2}}, \tag{6.18}$$

with $r_\nu \equiv m_\nu/m_\chi$. Due to the smallness of m_ν, these coefficients are basically given by[5]

$$a \approx 0 \qquad \text{and} \qquad b \approx \frac{c_1^2 m_\chi^2}{12\pi\Lambda^4}. \tag{6.19}$$

[5]The expression for the coefficients a and b in the Dirac case agree with those for the Majorana case in the limit $m_N \to 0$ with vanishing c_2 and c_3 coefficients. See *e.g.* Equations (6.15) and (6.16).

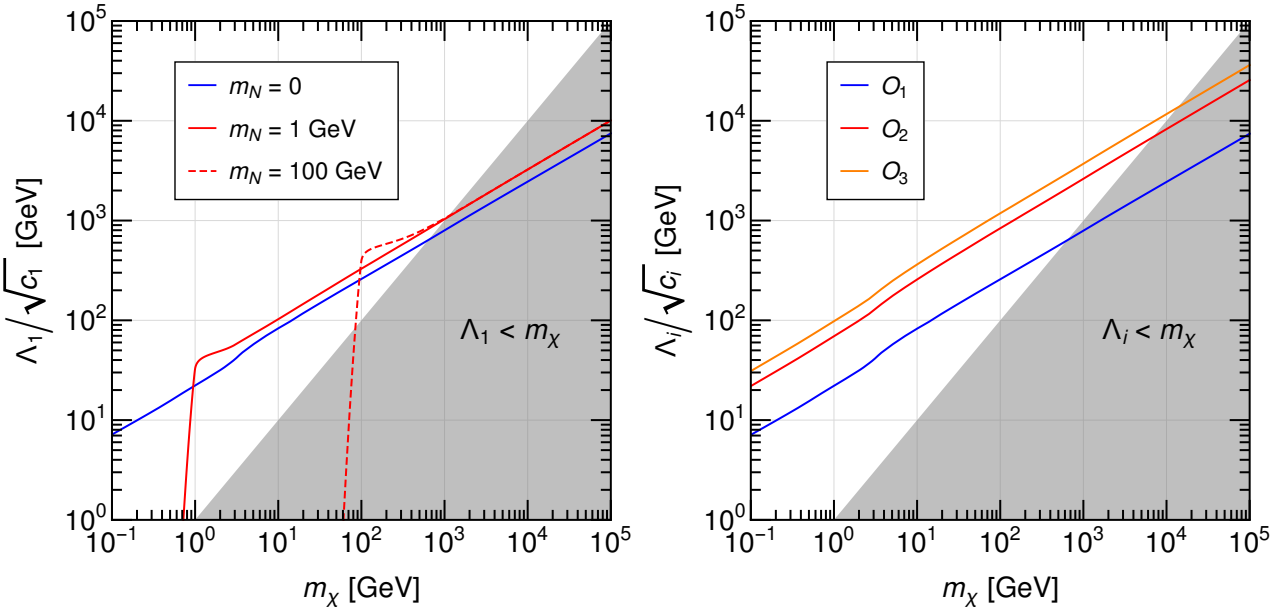

Figure 6.3: *NP scales associated to the portal operators as a function of the DM mass required to explain the observed relic abundance. Left: LNC $\mathcal{O}_1$ operator for different values of the sterile neutrino mass, m_N. Right: For $m_N = 0$, we consider only one portal operator at a time. See details in the text.*

Now, let us analyse the relic abundance obtained from the DM annihilation cross section in Equation (6.12). For that, we need to thermally average this expression yielding an expansion in (inverse) powers of $x = m_\chi/T$:

$$\langle \sigma v \rangle = a + \frac{3}{2} b\, x^{-1} + \mathcal{O}\left(x^{-2}\right). \tag{6.20}$$

For typical freeze-out temperatures, $T_{\rm fo} \simeq m_\chi/20$, we can safely keep only the first two terms in this expansion, and relativistic corrections will only enter in higher order terms [245].

Regarding the numerical analysis of the parameter space of the models that will be discussed in the following sections of this chapter, we apply the results from Ref. [246] with respect to the values for $\langle \sigma v \rangle$ that reproduce the observed relic abundance, see *e.g.* Figs. 1 and 4 of the aforementioned reference for the case of s- and p-wave DM annihilation cross section, respectively.

So far, starting from the effective interactions described by the Lagrangian in Equation (6.4), we have derived the expressions for the coefficients a and b that enter in the thermally averaged DM annihilation cross section $\chi\chi \to NN$ given in Equation (6.20). Using these results, we obtained Figure 6.3, which is described in what follows.

On the one hand, we discuss in the left panel the case where only the portal operator $\mathcal{O}_1$ is present. We plot the NP scale associated to this operator, Λ_1, as a function of

the DM mass, m_χ, that reproduces the observed relic abundance for different values of the sterile neutrino mass. For $m_N = 0$ (blue line) the cross section is p-wave (see *e.g.* Equation (6.15) with $c_{2,3} = 0$), and we extract the value for the thermally averaged DM annihilation cross section from Fig. 4 in Ref. [246]. Conversely, for $m_N = 1\,\text{GeV}$ (red line) and $m_N = 100\,\text{GeV}$ (red dashed line), the cross section is s-wave and therefore, we extract the value from Fig. 1 in the aforementioned reference. Note also that: i) the lower limit $m_\chi \simeq 100\,\text{MeV}$ for $m_N = 0$ is obtained by imposing thermal equilibrium of χ until the freeze-out, assumed at $x = 20$; ii) near the threshold $m_\chi \simeq m_N$, we use the general expression for the thermally averaged DM annihilation cross section given by [245, 247]:

$$\langle \sigma v \rangle = \frac{1}{8 m_\chi^4 T K_2^2 (m_\chi/T)} \int_{4m_\chi^2}^{\infty} ds\, \sigma(s) \left[s - 4m_\chi^2 \right] \sqrt{s}\, K_1 \left(\sqrt{s}/T \right) . \tag{6.21}$$

As argued in Ref. [245], the expansion in Equation (6.12) fails in some particular scenarios, namely near resonances and mass thresholds. Regarding the left panel of Figure 6.3, for m_χ slightly smaller than m_N, $\langle \sigma v \rangle$ is Boltzmann suppressed, and then the required Λ_1 to explain the abundance should decrease.[6]

On the other hand, we discuss in the right panel of Figure 6.3 the case for $m_N = 0$ and only one portal operator at a time. For a given DM mass, there is a factor 3 (4) in the NP scale associated to $\mathcal{O}_2$ ($\mathcal{O}_3$) for reproducing the observed DM abundance compared to the NP scale for $\mathcal{O}_1$. This is related to the fact that $\mathcal{O}_2$ and $\mathcal{O}_3$ give s-wave DM annihilation cross section, and therefore there is no $1/x$ suppression, see *e.g.* Equations (6.15) and (6.20). Finally, we plot in gray the region $\Lambda_i < m_\chi$ (assuming $c_i = 1$) excluded by EFT validity arguments.

6.3 Opening the portal operators at tree level

In this section, we present different UV completions of the portal operators given in Equations (6.5–6.7). Inspired also by their Fierz transformed versions of the operators, we can classify the models depending on the channel that governs the DM annihilations. Namely, we have:

- ***t*-channel-mediated models.** The mediator is a real or complex scalar heavier than the DM particle, therefore DM can not annihilate into a pair of mediators. These are Models A in Figure 6.4.

- ***s*-channel-mediated models.** The mediators are a real or complex scalar, and also a vector boson, all of them heavier than the DM particle, therefore DM can not annihilate into a pair of mediators. These are Models B and C in Figure 6.4.

Before continuing, we list in Table 6.2 the transformations under the $\mathcal{Z}_2$ and the global $U(1)_{B-L}$ symmetries of the dark sector for the UV models that will be discussed in what follows. Note that in Models A, the mediator is also charged under

[6] The DM abundance is inversely proportional to $\langle \sigma v \rangle$, while σ is also inversely proportional to Λ. Then, if one wants to keep constant the value for the relic abundance, reducing $\langle \sigma v \rangle$ implies smaller values for Λ.

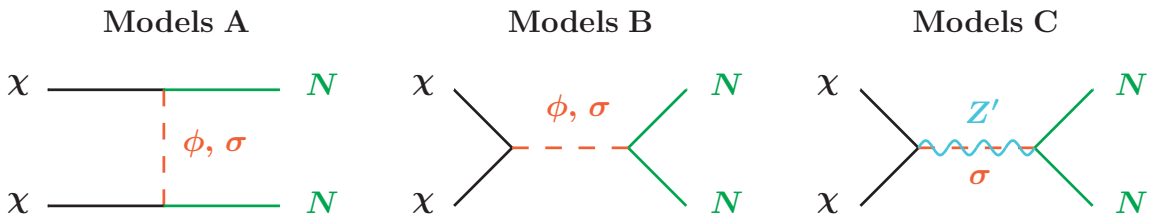

Figure 6.4: *Feynman diagrams for DM annihilation into sterile neutrinos in the different UV models. The mediators ϕ and σ represent a real and complex singlet scalar, respectively, whereas Z' is a vector boson. Note that the mediators in Models A are charged under the $\mathcal{Z}_2$. We also refer to Models A as genuine because they only generate the portal operators.*

$\mathcal{Z}_2$, and precisely we will refer to these models as *genuine* in the sense that they only generate at $D \leqslant 6$ the portal operators (or at least one of them). In addition, the full set of matching conditions at tree level for the coefficients of the effective operators are summarised in Table 6.3.

6.3.1 Models A

Model A1

The Lagrangian of the model reads[7]

$$\mathcal{L}_{\text{A1}} = \mathcal{L}_4 + \frac{1}{2}\left(\partial_\mu \phi\right)\left(\partial^\mu \phi\right) - V(\phi, H) - \left[f\overline{N_R}\chi_L\phi + \text{H.c.}\right], \tag{6.22}$$

with $\mathcal{L}_4$ given in Equation (6.2) and the following scalar potential:

$$V(\phi, H) = \frac{1}{2}m_\phi^2\phi^2 + \lambda_{\phi H}\phi^2\left|H\right|^2 + \lambda_\phi\phi^4\,. \tag{6.23}$$

This model contains an additional real scalar, ϕ, also charged under the same discrete symmetry $\mathcal{Z}_2$ responsible for the stability of the DM candidate χ. $V(\phi, H)$ is the most general potential preserving the discrete symmetry. The coupling f is complex, in general: we already re-phased the fields of the new chiral fermions yielding their mass terms real and positive, and ϕ, as a real field, can not absorb the phase of the Yukawa coupling.

As the new Yukawa interaction among the scalar mediator and the fermions violates lepton number, we also expect portal operators that break the global $U(1)_L$ symmetry after integrating out the heavy mediator ϕ. We give in Table 6.3 the Wilson coefficient of the generated effective operators and detail the computation of the matching conditions in what follows.

[7] We assume only one generation of each of the new chiral fermions, therefore the new Yukawa couplings are numbers.

Model	Dark sector particles	κ	$U(1)_{B-L}$
A1	Majorana fermion χ	-1	0
	real scalar ϕ	-1	0
A2	Majorana fermion χ	-1	0
	complex scalar σ	-1	-1
B1	Majorana fermion χ	-1	0
	real scalar ϕ	$+1$	0
B2	chiral fermion χ_L	-1	$+1$
	complex scalar σ	$+1$	$+2$
C1	Majorana fermion χ	-1	0
	massive vector boson Z'	$+1$	0
C2	chiral fermion χ_L	-1	$+1$
	complex scalar σ	$+1$	$+2$
	gauge boson Z'	$+1$	0

Table 6.2: *Transformations under $\mathcal{Z}_2$ and $B-L$ charges of the particles that constitute the dark sector in the considered UV models. Under $\mathcal{Z}_2$, a generic field φ undergoes $\varphi \to \kappa\varphi$, with $\kappa = \pm 1$. For $\kappa = -1$ we say that the field is charged under $\mathcal{Z}_2$. Note also that each model contains, apart from the particles listed in this table, i) the SM particle content, and ii) right-handed neutrinos, N_R, which are not charged under $\mathcal{Z}_2$ and have $B-L$ charge equal to -1.*

The relevant part of the Lagrangian in Equation (6.22) for integrating out the heavy mediator ϕ can be written as

$$\mathcal{L}_{\text{A1}} \supset \frac{1}{2}\left(\partial_\mu\phi\right)\left(\partial^\mu\phi\right) - \frac{1}{2}m_\phi^2\phi^2 - \phi\overline{N}\left[fP_L + f^*P_R\right]\chi\,, \tag{6.24}$$

where $P_{L,R}$ are the usual chiral projectors

$$P_L = \frac{1}{2}\left(1-\gamma_5\right) \quad \text{and} \quad P_R = \frac{1}{2}\left(1+\gamma_5\right)\,, \tag{6.25}$$

and N and χ are the Majorana fields given in Equation (6.3). Note that we have not included the λ_ϕ and $\lambda_{\phi H}$ terms in the scalar potential in Equation (6.23) since they would lead to higher-dimensional operators we are not interested in.

Now, using the equation of motion (EoM) for the scalar ϕ we get

$$\left(\partial^2 + m_\phi^2\right)\phi + \overline{N}\left[fP_L + f^*P_R\right]\chi = 0\,. \tag{6.26}$$

In addition, assuming that the momentum of the real scalar, corresponding to the derivative, is much smaller than its mass (for the EFT approach to hold), we obtain

Model	c_1/Λ^2	c_2/Λ^2	c_3/Λ^2	c_4/Λ^2	c_5/Λ^2	c_{NH}/Λ	$c_{\chi H}/\Lambda$
A1	$\frac{\lvert f\rvert^2}{m_\phi^2}$	$\frac{f^2}{2m_\phi^2}$	✗	✗	✗	✗	✗
A2a	$\frac{f^2}{m_g^2}$	✗	✗	✗	✗	✗	✗
A2b	$\frac{f^2}{m_g^2}$	✗	✗	✗	✗	✗	✗
A2c	$\frac{f^2}{m_\sigma^2}$	$-\frac{f^2\mu_\sigma^2}{2m_\sigma^4}$	✗	✗	✗	✗	✗
B1	✗	$-\frac{2f^*g}{m_\phi^2}$	$\frac{fg}{m_\phi^2}$	$\frac{\lvert f\rvert^2}{m_\phi^2}$	$\frac{\lvert g\rvert^2}{m_\phi^2}$	$\frac{f\mu_{\phi H}}{m_\phi^2}$	$\frac{g\mu_{\phi H}}{m_\phi^2}$
B2	✗	$-\frac{fg}{m_s^2}$	$\frac{fg}{2m_s^2}$	$\frac{f^2}{2m_s^2}$	$\frac{g^2}{2m_s^2}$	$\frac{f\lambda_{\sigma H}v_\sigma}{\sqrt{2}m_s^2}$	$\frac{g\lambda_{\sigma H}v_\sigma}{\sqrt{2}m_s^2}$
C1	$\frac{2g_Ng_\chi}{m_{Z'}^2}$	✗	✗	$-\frac{g_N^2}{m_{Z'}^2}$	$-\frac{g_\chi^2}{m_{Z'}^2}$	✗	✗
C2	$\frac{2g'^2Q_NQ_\chi}{m_{Z'}^2}$	$-\frac{fg}{m_s^2}$	$\frac{fg}{2m_s^2}$	$\frac{f^2}{2m_s^2}-\frac{g'^2Q_N^2}{m_{Z'}^2}$	$\frac{g^2}{2m_s^2}-\frac{g'^2Q_\chi^2}{m_{Z'}^2}$	$\frac{f\lambda_{\sigma H}v_\sigma}{\sqrt{2}m_s^2}$	$\frac{g\lambda_{\sigma H}v_\sigma}{\sqrt{2}m_s^2}$

Table 6.3: *Matching conditions for the Wilson coefficients of the effective $D \leqslant 6$ operators generated in renormalisable models by integrating out a scalar and/or vector mediator at tree level. The operators are given in Table 6.1. Note that in Model B1 with real g and Model B2, the relation $c_2 = -2c_3^*$ is satisfied and therefore annihilations are p-wave, see e.g. Equation* (6.13).

the following expressions for the scalar field:

$$\phi \simeq -\frac{1}{m_\phi^2}\overline{N}\left[fP_L + f^*P_R\right]\chi\,. \tag{6.27}$$

It is interesting to note that we can rewrite the Lagrangian in Equation (6.24) as:

$$\begin{aligned}\mathcal{L}_{\text{A1}} \supset\ & \frac{1}{2}\partial_\mu\left(\phi\partial_\mu\phi\right) - \frac{1}{2}\phi\overline{N}\left[fP_L + f^*P_R\right]\chi \\ & -\frac{1}{2}\phi\left[\left(\partial^2 + m_\phi^2\right)\phi + \overline{N}\left[fP_L + f^*P_R\right]\chi\right]\,.\end{aligned} \tag{6.28}$$

Moreover, in the last equation we can omit the total derivative term in the first line, whereas the second line is zero by Equation (6.26). Therefore we get the Lagrangian

$$\mathcal{L}_{\text{A1}} \supset -\frac{1}{2}\phi\overline{N}\left[fP_L + f^*P_R\right]\chi\,, \tag{6.29}$$

which after substituting back the expressions for the real scalar field in Equation (6.27)

yields the following effective interactions:

$$\mathcal{L}_{\rm A1}^{\rm eff} = \frac{|f|^2}{m_\phi^2}\left(\overline{N}P_L\chi\right)\left(\overline{\chi}P_R N\right) + \frac{f^2}{2m_\phi^2}\left(\overline{N}P_L\chi\right)\left(\overline{N}P_L\chi\right) + \frac{f^{*2}}{2m_\phi^2}\left(\overline{N}P_R\chi\right)\left(\overline{N}P_R\chi\right) . \tag{6.30}$$

Finally, this effective Lagrangian can be expressed in terms of the portal operators as:

$$\mathcal{L}_{\rm A1}^{\rm eff} = \frac{|f|^2}{m_\phi^2}\mathcal{O}_1 + \left[\frac{f^2}{2m_\phi^2}\mathcal{O}_2 + \text{H.c.}\right] . \tag{6.31}$$

From the last equation one can directly obtain the matching conditions for the coefficients of the portal operators $\mathcal{O}_1$ and $\mathcal{O}_2$:

$$\frac{c_1}{\Lambda^2} = \frac{|f|^2}{m_\phi^2} \quad \text{and} \quad \frac{c_2}{\Lambda^2} = \frac{f^2}{2m_\phi^2} . \tag{6.32}$$

Model A2

The Lagrangian of the model reads

$$\mathcal{L}_{\rm A2} = \mathcal{L}_4 + \left(\partial_\mu\sigma\right)^*\left(\partial^\mu\sigma\right) - V(\sigma, H) - \left[f\overline{N_R}\chi_L\sigma + \text{H.c.}\right] , \tag{6.33}$$

with the following scalar potential:

$$V(\sigma, H) = m_\sigma^2|\sigma|^2 + \lambda_{\sigma H}|\sigma|^2|H|^2 + \lambda_\sigma|\sigma|^4 . \tag{6.34}$$

This model contains an additional complex scalar, $\sigma = (\rho + i\theta)/\sqrt{2}$, charged under both the global $U(1)_L$ symmetry and the same discrete symmetry $\mathcal{Z}_2$ responsible for the stability of the DM candidate. $V(\sigma, H)$ is the most general scalar potential preserving the global $U(1)_L$ symmetry. Conversely to the case with the real scalar in Model A1, now i) f can always be taken real by re-phasing σ, and ii) the new Yukawa interaction preserves lepton number. It is worth to consider three versions of this model depending on the status of lepton number, namely:

- **Model A2a.** Lepton number is preserved, therefore m_N term in the Lagrangian is forbidden and the sterile neutrino is the right-handed companion of the left-handed SM neutrino. In this case, neutrinos are of Dirac type. Only the portal operator $\mathcal{O}_1$ is generated (see Table 6.3) and DM annihilations are p-wave, see *e.g.* Equation (6.19). Therefore, we can lower the value for DM mass because ID bounds do not apply (see the lower limit for m_χ in Figure 6.3).

  In this case, neutrinos are Dirac particles, and DD and ID are suppressed. If no signal is observed neither in DM searches nor in neutrinoless double beta decay experiments, this would remain a valid option.

- **Model A2b.** Lepton number is violated only by the mass term m_N which is included now in the Lagrangian. The rest of the terms in the Lagrangian preserve lepton number. Therefore, only the portal operator $\mathcal{O}_1$ is generated (see Table 6.3).

- **Model A2c.** The Lagrangian of the model reads

$$\mathcal{L}_{\text{A2c}} = \mathcal{L}_{\text{A2}}|_{m_N=0} - \left[\frac{1}{2}\mu_\sigma^2\,\sigma^2 + \text{H.c.}\right], \tag{6.35}$$

  and lepton number is softly broken by the μ_σ^2 term in the scalar potential. Moreover, the Yukawa coupling f can always be taken real: the mass term for the sterile neutrino is absent in the Lagrangian, therefore we can re-phase N_R (and also l and e_R) to absorb the phase of the Yukawa coupling. From the EFT approach, we also expect portal operators that violate lepton number. In particular, after integrating out the complex scalar, $\mathcal{O}_1$ and $\mathcal{O}_2$ are generated, with the latter being proportional to the term in the scalar potential that breaks lepton number, namely μ_σ^2 (see Table 6.3). Moreover, in Section 6.4.2 we will discuss in detail an interesting feature of the model: m_N is generated at one loop.

We detail in Appendix C.2 the calculation of the matching conditions for the Wilson coefficients.

6.3.2 Models B

Model B1

The Lagrangian of the model reads

$$\mathcal{L}_{\text{B1}} = \mathcal{L}_4 + \frac{1}{2}\left(\partial_\mu\phi\right)\left(\partial^\mu\phi\right) - V(\phi,H) - \left[f\overline{N_R^c}N_R\,\phi + g\overline{\chi_L^c}\chi_L\,\phi + \text{H.c.}\right], \tag{6.36}$$

with the following scalar potential:

$$V(\phi,H) = \frac{1}{2}m_\phi^2\,\phi^2 + \mu_\phi\phi^3 + \lambda_\phi\,\phi^4 + \mu_{\phi H}\phi|H|^2 + \lambda_{\phi H}\phi^2|H|^2\,. \tag{6.37}$$

This model contains an additional real scalar, ϕ, which is not charged under the discrete symmetry $\mathcal{Z}_2$. $V(\phi,H)$ is the most general scalar potential one can write, with no linear term in ϕ, as it can always be removed by a shift of the new scalar field. Regarding the new Yukawa couplings f and g, they are complex, in general.

As can be seen from Table 6.3, $\mathcal{O}_2$ and $\mathcal{O}_3$ operators are generated after integrating out the scalar mediator ϕ. Moreover, the relation $c_2 = -2c_3^*$ is satisfied for g real, and since $c_1 = 0$, this scenario yields p-wave DM annihilation cross section. See *e.g.* Equation (6.13).

In addition to the portal operators, there are new operators generated after integrating out the heavy mediator ϕ, namely:

$$\mathcal{O}_{NH} = (\overline{N_R^c} N_R)(H^\dagger H)\,, \tag{6.38}$$

$$\mathcal{O}_{\chi H} = (\overline{\chi_L^c} \chi_L)(H^\dagger H)\,, \tag{6.39}$$

$$\mathcal{O}_4 = (\overline{N_R^c} N_R)(\overline{N_R} N_R^c) = \frac{1}{2}(\overline{N_R}\gamma_\mu N_R)(\overline{N_R}\gamma^\mu N_R)\,, \tag{6.40}$$

$$\mathcal{O}_5 = (\overline{\chi_L^c} \chi_L)(\overline{\chi_L} \chi_L^c) = \frac{1}{2}(\overline{\chi_L}\gamma_\mu \chi_L)(\overline{\chi_L}\gamma^\mu \chi_L)\,. \tag{6.41}$$

On the one hand, the Wilson coefficients for the first two $D = 5$ operators $\mathcal{O}_{NH}$ and $\mathcal{O}_{\chi H}$ are proportional to the coupling $\mu_{\phi H}$, see *e.g.* Table 6.3. Therefore, we can control them via this coupling, and make the portal operators to be the dominant ones. Let us mention that, after SSB of the EW symmetry, $\mathcal{O}_{NH}$ contributes to the neutrino mass m_N, and also to the Higgs boson decay $h \to NN$, if $m_N < m_h/2$. The phenomenology associated to this operator has been analysed in detail in the literature, see *e.g.* Refs. [248–252]. In addition, $\mathcal{O}_{\chi H}$ is responsible for the fermionic Higgs portal [253–255], and also contributes to the DM Majorana mass, m_χ.

On the other hand, $D = 6$ operators $\mathcal{O}_4$ and $\mathcal{O}_5$ generate four-fermion self-interactions.[8]

We detail in Appendix C.3 the calculation of the matching conditions for the Wilson coefficients.

Model B2: global $U(1)_{B-L}$

The Lagrangian of the model reads

$$\mathcal{L}_{\text{B2}} = \mathcal{L}_4|_{m_N = m_\chi = 0} + \left(\partial_\mu \sigma\right)^* \left(\partial^\mu \sigma\right) - V(\sigma, H) - \left[f \overline{N_R^c} N_R \sigma + g \overline{\chi_L} \chi_L^c \sigma + \text{H.c.}\right], \tag{6.42}$$

with $V(\sigma, H)$ given in Equation (6.34). This model contains a complex scalar, σ, which is not charged under the discrete symmetry $\mathcal{Z}_2$. One can consider a global $U(1)$ symmetry, which could be identify with lepton number, or $U(1)_{B-L}$.[9] This global symmetry is preserved by the Lagrangian if we assign the following lepton charges to the new particles: $L(N_R) = L(\chi_L^c) = 1$ and $L(\sigma) = -2$. Note that the Yukawa couplings f and g can be taken real.

In this scenario, the SSB of the global $U(1)_{B-L}$ via the VEV of the new scalar, v_σ, yields Majorana mass terms for the chiral fermions, namely

$$m_N = \sqrt{2} f v_\sigma \quad \text{and} \quad m_\chi = \sqrt{2} g v_\sigma\,. \tag{6.43}$$

Now we can write the complex scalar σ in the exponential parameterisation as

$$\sigma = \frac{1}{\sqrt{2}} \left(v_\sigma + s\right) e^{iJ/v_\sigma}\,, \tag{6.44}$$

[8] Note that the operators $(\overline{N_R^c} N_R)(\overline{N_R^c} N_R)$ and $(\overline{\chi_L^c} \chi_L)(\overline{\chi_L^c} \chi_L)$, which are also obtained after integrating out ϕ, vanish for one generation of N_R and χ_L.

[9] $U(1)_{B-L}$ is an anomaly-free global symmetry of the SM, but there are others such as the differences of flavour lepton numbers *e.g.* $L_\mu - L_\tau$, which can also be gauged [256]. However, flavour symmetries have strong implications for neutrino masses and mixings.

being s the radial mode, and J the Goldstone boson (the Majoron). The latter can be completely removed from the scalar potential, and it only enters in the Lagrangian through the kinetic term of the complex scalar:

$$\left(\partial_\mu \sigma\right)^* \left(\partial^\mu \sigma\right) = \frac{1}{2}\left(\partial s\right)^2 + \frac{1}{2}\left(\partial J\right)^2 + \frac{1}{v_\sigma} s \left(\partial J\right)^2 + \frac{1}{2v_\sigma^2} s^2 \left(\partial J\right)^2 . \tag{6.45}$$

Note that we can also remove the Majoron from the Yukawa interactions in Equation (6.42) with a re-phasing of the fields which have an associated non-zero lepton number, namely $\Psi = N_R$, χ_L^c, l and e_R, as

$$\Psi \to e^{-iJ/(2v_\sigma)} \Psi \, . \tag{6.46}$$

In view of that, we get from the kinetic terms of Ψ the following derivative interactions with the Majoron:[10]

$$\mathcal{O}_{\Psi J} = (\overline{\Psi} \gamma^\mu \Psi)(\partial_\mu J) \qquad \text{with} \qquad \frac{c_{\Psi J}}{\Lambda} = \frac{1}{2v_\sigma} \, . \tag{6.47}$$

On the other hand, from the EFT approach, we obtain, after integrating out the heavy radial mode to $\mathcal{O}(1/m_s^2)$, the following operators: portal operators $\mathcal{O}_2$ and $\mathcal{O}_3$, self-interactions $\mathcal{O}_4$ and $\mathcal{O}_5$, and the operators $\mathcal{O}_{NH}$ and $\mathcal{O}_{\chi H}$. We detail in Appendix C.3 the calculation of the matching conditions for the Wilson coefficients summarised in Table 6.3.

Let us stress that in this model, the DM annihilation cross section $\chi\chi \to NN$ is p-wave, since $c_2 = -2c_3^*$ and $c_1 = 0$, see *e.g.* Equation (6.13).

As in Model B1, the Wilson coefficients for the operators $\mathcal{O}_{NH}$ and $\mathcal{O}_{\chi H}$ are proportional to a free parameter of the scalar potential, namely the Higgs portal coupling $\lambda_{\sigma H}$. Therefore, we can control these operators via this coupling, and make the portal operators to be the dominant ones, *i.e.* taking $\lambda_{\sigma H} \ll 1$.

Apart from the aforementioned effective operators obtained after integrating out s, we also get a $D = 6$ operator involving the Higgs boson and the Majoron, namely

$$\mathcal{O}_{HJ} = |H|^2 \left(\partial J\right)^2 \qquad \text{with} \qquad \frac{c_{HJ}}{\Lambda^2} = -\frac{\lambda_{\sigma H}}{m_s^2} = -\frac{\lambda_{\sigma H}}{2\lambda_\sigma v_\sigma^2} \, . \tag{6.48}$$

This is basically the same effective operator that was discussed in the last section of Chapter 5, see *e.g.* Equation (5.63).

Finally, corrections to the mass and the quartic coupling of the Higgs boson are generated:

$$\delta m_H^2 = \frac{1}{2} \lambda_{\sigma H} v_\sigma^2 \qquad \text{and} \qquad \delta\lambda_H = -\frac{\lambda_{\sigma H}^2}{4\lambda_\sigma} \, . \tag{6.49}$$

Therefore, the parameters of the SM scalar potential are redefined as[11]

$$m_H^2 \to m_H^2 + \delta m_H^2 \qquad \text{and} \qquad \lambda_H \to \lambda_H + \delta\lambda_H \, . \tag{6.50}$$

[10] We clearly see in this representation that the Goldstone boson couples derivatively.

[11] Note the change of notation with respect to Equation (1.11), namely $\phi \to H$, $\mu^2 \to m_H^2$ and $\lambda \to \lambda_H$.

Note also that the $D = 6$ operator $|H|^6$ is absent at tree level due to a peculiar cancellation in the scalar potential. See details in the last part of Appendix C.3. This feature was already noticed in Ref. [257].

6.3.3 Models C

Model C1

Motivated by the Fierz transformed version of $\mathcal{O}_1$ in Equation (6.5), one can introduce a heavy vector boson, Z'_μ, which after being integrated out can generate the aforementioned operator. Therefore, we can write the following Lagrangian

$$\mathcal{L}_{\text{C1}} = \mathcal{L}_4 - \frac{1}{4} Z'_{\mu\nu} Z'^{\mu\nu} + \frac{1}{2} m^2_{Z'} Z'_\mu Z'^\mu + g_N \overline{N_R} \gamma^\mu N_R Z'_\mu + g_\chi \overline{\chi_L} \gamma^\mu \chi_L Z'_\mu \,, \tag{6.51}$$

with $Z'_{\mu\nu} = \partial_\mu Z'_\nu - \partial_\nu Z'_\mu$ the field strength tensor, and real couplings g_N and g_χ, without loss of generality. Note that we do not include kinetic mixing among Z' and Z, $\epsilon Z'_{\mu\nu} Z^{\mu\nu}$, and mass mixing, $\delta m^2 Z'_\mu Z^\mu$, because we are interested in the neutrino portal regime.

Then, after integrating out the heavy vector boson, we get the following operators: portal operator $\mathcal{O}_1$ and the self-interactions $\mathcal{O}_4$ and $\mathcal{O}_5$. We detail in Appendix C.4 the calculation of the matching conditions for the Wilson coefficients summarised in Table 6.3.

However, this scenario is a kind of toy model in the sense that, to have a UV-complete gauge-invariant model, both the chiral fermions N_R and χ_L should be charged under the same gauge symmetry, namely $U(1)_{B-L}$. This scenario will be analysed in Model C2, which is precisely a gauged version of Model B2.

Model C2: gauged $U(1)_{B-L}$

As mentioned in the last paragraph, this scenario is the gauged version of Model B2. To promote the global symmetry $U(1)_{B-L}$ to a local symmetry, we need three right-handed neutrinos to cancel gauge anomalies.[12] In our model, these three new neutral chiral fermions are $N_R^{1,2}$ and χ_L^c, with their corresponding charges under $B - L$ listed in Table 6.4.[13] Regarding the masses of the two sterile neutrinos, we assume that i) one of them is lighter than DM particles, and ii) the other has a mass similar to the scale of $U(1)_{B-L}$ symmetry breaking, v_σ.

Therefore, the Lagrangian of the model reads

$$\mathcal{L}_{\text{C2}} = \mathcal{L}_{\text{B2}} - \frac{1}{4} Z'_{\mu\nu} Z'^{\mu\nu} \,, \tag{6.52}$$

but with the covariant derivatives in the Lagrangian $\mathcal{L}_{\text{B2}}$ in Equation (6.42) modified to consider the new term associated with the gauge symmetry, namely

$$D_\mu = D_\mu^{\text{SM}} - i g' Q_{B-L} Z'_\mu \,, \tag{6.53}$$

[12] See *e.g.* the related discussion in Section 30.4 in Ref. [258].

[13] For gauge anomalies cancellation is important to have $L(N_R^{1,2}) = L(\chi_L^c) = 1$.

	Q	u_R	d_R	l	e_R	$N_R^{1,2}$	χ_L	σ
$U(1)_{B-L}$	$+1/3$	$+1/3$	$+1/3$	-1	-1	-1	$+1$	$+2$

Table 6.4: *$B-L$ charges of the particles in Model C2. Q and l are the SM lepton and quark $SU(2)_L$ doublets, and u_R, d_R and e_R are the SM fermion singlets. $N_R^{1,2}$ are right-handed neutrinos, χ_L is a fermionic DM candidate, and σ is a complex scalar.*

where g' and Q_{B-L} are the new gauge coupling and the $B-L$ charge of the field D_μ acts upon, respectively, and $D_\mu^{\rm SM}$ is given in Equation (1.3).

Moreover, the SSB of the $U(1)_{B-L}$ through the VEV of the complex scalar, v_σ, yields the mass terms for N_R, χ_L and Z', namely

$$m_N = \sqrt{2} f v_\sigma, \quad m_\chi = \sqrt{2} g v_\sigma \quad \text{and} \quad m_{Z'} = 2 g' v_\sigma \,. \tag{6.54}$$

We assume that $m_N < m_\chi < m'_Z$ which implies that $f < g < \sqrt{2} g'$.

From the EFT approach, we can integrate out the Z' and the real part of the scalar, s, if one assumes that v_σ is larger than the EW scale, and also considering not too small values for g' and λ_σ. We detail in Appendix C.4 the computation of the matching conditions for the Wilson coefficients summarised in Table 6.3.

On the one hand, similarly to Model B2, $c_2 = -2c_3^*$ and therefore operators $\mathcal{O}_2$ and $\mathcal{O}_3$ only contribute to the p-wave term of the DM annihilation cross section $\chi\chi \to NN$, see *e.g.* Equation (6.13). Notice also that the Wilson coefficients c_4 and c_5 are zero if $\lambda_\sigma = f^2$ and $\lambda_\sigma = g^2$, respectively; see *e.g.* Table 6.3.

On the other hand, it is interesting to note that we also find the following operators:

$$\mathcal{O}_{\psi\psi} = (\overline{\psi}\gamma_\mu\psi)(\overline{\psi}\gamma^\mu\psi)\,, \tag{6.55}$$
$$\mathcal{O}_{N\psi} = (\overline{N_R}\gamma_\mu N_R)(\overline{\psi}\gamma^\mu\psi)\,, \tag{6.56}$$
$$\mathcal{O}_{\chi\psi} = (\overline{\chi_L}\gamma_\mu\chi_L)(\overline{\psi}\gamma^\mu\psi)\,, \tag{6.57}$$

which describe four-fermion interactions. Here, ψ are the SM fermions, $\psi = l$, e_R, Q, u_R, d_R, and the associated Wilson coefficients are

$$\frac{c_{\psi\psi}}{\Lambda^2} = -\frac{g'^2 Q_\psi^2}{2m_{Z'}^2}\,, \tag{6.58}$$
$$\frac{c_{N\psi}}{\Lambda^2} = -\frac{g'^2 Q_N Q_\psi}{m_{Z'}^2}\,, \tag{6.59}$$
$$\frac{c_{\chi\psi}}{\Lambda^2} = -\frac{g'^2 Q_\chi Q_\psi}{m_{Z'}^2}\,. \tag{6.60}$$

The $B-L$ charges of the fields Q_ψ, Q_N and Q_χ are given in Table 6.4.

	A1	A2a	A2b	A2c	B1	B2	C1	C2
s-wave $\langle\sigma v\rangle_{\chi\chi\to NN}$	✓	✗	✓	✓	$*$	✗	✓	✓
DD @ tree level	✗	✗	✗	✗	✓	✓	✗	✓
Self-interactions	✗	✗	✗	✗	✓	✓	✓	✓

Table 6.5: *Summary of the DM phenomenology associated to the UV models analysed in Section 6.3. Note that for p-wave DM annihilation cross section, ID constraints can be easily avoided. The asterisk $*$ in Model B1 implies that, if the coupling g is real, $\langle\sigma v\rangle_{\chi\chi\to NN}$ is p-wave.*

6.4 Phenomenology of the UV models

In this section we analyse the phenomenology of the UV models introduced in the previous part. As has been mentioned during this chapter, in particular in Section 6.2, we are interested in the secluded regime via the portal operators, where the DM annihilations $\chi\chi \to NN$ set the relic abundance via the usual freeze-out mechanism. Therefore, we need that sterile neutrinos were in thermal equilibrium with the SM particles in the Early Universe through some interactions among both sectors. In the Lagrangians of the UV completions there are terms that could play the role of keeping these sectors in thermal equilibrium, namely the Higgs portal term for Models A and B, and/or the kinetic mixing for Models C. Regarding this, in the numerical analysis we ensure the kinetic equilibrium with a small value of the Higgs portal coupling, $10^{-6} \lesssim \lambda_{\phi H} \lesssim\sim 10^{-3}$.[14] For Models A, these values for the coupling do not spoil the DM abundance with other processes involving SM particles. Conversely, for Models B2 and C2, once both σ and H develop VEVs, the two scalars do mix, and the relic abundance around the Higgs boson resonance, $m_\chi \simeq m_h/2$, would be spoiled for values $\lambda_{\sigma H}$ of $\mathcal{O}\left(10^{-3}\right)$, see *e.g.* Ref. [207]. A detailed calculation of the DM abundance near the Higgs boson resonance is beyond the scope of this work.

In the first part of the section, we give some generic phenomenological features of the considered UV models, summarised in Table 6.5. Then, we select some renormalisable models for a detailed analysis of their phenomenology, namely Models A2b, A2c and B1. Finally, we discuss the sterile neutrino mass generation at one loop in Model A2c.

Models A

In these models, the presence of non-zero Higgs portal coupling could yield i) invisible Higgs boson decays, $h \to \chi\chi$, if $m_\chi < m_h/2$, and ii) DD signals at one loop. However, constraints from both processes are evaded due to the small value of the coupling and/or the loop suppression. Similarly, there are contributions to DD signals at one loop due to the Z boson, in addition to invisible Z boson decays, $Z \to \chi\chi$, if $m_\chi < m_Z/2$. Both processes are suppressed due to the presence of the (small)

[14] See the discussion in Appendix A in Ref. [2].

neutrino Yukawa coupling. See a detailed analysis of the aforementioned one-loop processes in Ref. [259].

Let us remark that in Model A2a, ID bounds are avoided due to the p-wave nature of the DM annihilations, and in Model A2c the sterile neutrino mass is generated at one loop. We will comment on the latter in Section 6.4.2.

Models B

In Model B1, we can have mixing between the scalar ϕ and the Higgs field due to the $\mu_{\phi H}$ term in the potential in Equation (6.37) when there is SSB of the EW symmetry. Therefore, this mixing will produce i) DD signals at tree level, and ii) invisible Higgs boson decays, $h \to \chi\chi$, if $m_\chi < m_h/2$. However, in the numerical analysis we take $\mu_{\phi H} = 0$ to ensure the neutrino portal regime.

On the other hand, depending on the values of the couplings f and g, we get the following results:

- Model B1 yields p-wave DM annihilation cross section $\chi\chi \to NN$ for g real. This is related to the fact that s-wave DM annihilations requires a pseudo-scalar coupling between DM and mediators,[15] which is given by the imaginary part of g.
- Model B2 yields p-wave DM annihilation cross section $\chi\chi \to NN$, because the couplings f and g are real. Therefore, ID constraints are evaded.

Let us also mention that Models B have N and χ self-interactions. With respect to the DM ones, in our numerical analysis the cross section $\chi\chi \leftrightarrow \chi\chi$ is well below the current limits [177]. For instance, for Model B1 we have checked that $\sigma_{\chi\chi\to\chi\chi}/m_\chi \lesssim 10^{-6}\,\mathrm{cm}^2/\mathrm{g}$ in the considered parameter space.

Models C

On the one hand, Model C1 is not UV-complete. Moreover, if there is kinetic mixing in the Lagrangian,[16] additional processes such as invisible Z boson decay, $Z \to \chi\chi$, would be generated if $m_\chi < m_Z/2$.

On the other hand, Model C2 generates interactions between DM and SM particles, as can be seen from Equation (6.57). Therefore, the parameter space of this model is very constrained [261].

6.4.1 Phenomenology of selected models

The phenomenology of Models A1, B2 and C2 has been analysed in detail in Refs. [225, 226, 228, 238], [262] and [261], respectively. Moreover, Model C1 is not UV-complete.

[15] See *e.g.* Ref. [260].

[16] Note that the kinetic mixing $\epsilon Z'_{\mu\nu} Z^{\mu\nu}$, even if absent at tree level in the Lagrangian, will be induced at one loop. Apart from the loop factors, it will also be suppressed due to the (small) Yukawa neutrino coupling.

In view of that, we focus on the phenomenology of Models A2b, A2c and B1 in what follows.

First, we present the expressions for the a and b coefficients in Equation (6.20) for the selected models. We will use the notation $r_i \equiv m_i/m_\chi$.

Model A2b

For one generation of N_R and χ_L, the coupling f can always be taken real, see *e.g.* Section 6.3.1. In this case, we get:

$$a = \frac{f^4}{16\pi m_\chi^2} \frac{r_N^2\sqrt{1-r_N^2}}{\left(1+r_\sigma^2-r_N^2\right)^2}\,. \tag{6.61}$$

Model A2c

In this scenario, as in Model A2b, for one generation of N_R and χ_L the coupling f can always be taken real. Then, we obtain:

$$a = \frac{f^4}{64\pi m_\chi^2} \frac{\sqrt{1-r_N^2}\left(r_\rho^2-r_\theta^2-\left(2+r_\rho^2+r_\theta^2\right)r_N+2r_N^3\right)^2}{\left(1+r_\rho^2-r_N^2\right)^2\left(1+r_\theta^2-r_N^2\right)^2}\,. \tag{6.62}$$

Model B1

In this model, as discussed in Section 6.3.2, the couplings f and g are complex, in general. Therefore we take $f = f_r + if_i$ and $g = g_r + ig_i$, and obtain the following expressions for the coefficients:

$$a = \frac{4g_i^2}{\pi m_\chi^2} \frac{\sqrt{1-r_N^2}}{\left(r_\phi^2-4\right)^2}\left[f_i^2+f_r^2\left(1-r_N^2\right)\right], \tag{6.63}$$

$$\begin{aligned} b = \frac{2}{\pi m_\chi^2\left(r_\phi^2-4\right)^3\sqrt{1-r_N^2}} \Bigg\{ & f_i^2\left[g_i^2\left(16+r_N^2\left(r_\phi^2-20\right)\right)+2g_r^2\left(1-r_N^2\right)\left(r_\phi^2-4\right)\right] \\ & + f_r^2\left(1-r_N^2\right)\left[g_i^2\left(16+r_N^2\left(3r_\phi^2-28\right)\right)+2g_r^2\left(1-r_N^2\right)\left(r_\phi^2-4\right)\right]\Bigg\}. \end{aligned} \tag{6.64}$$

From these equations, we consider the following particular cases:

- Real f and g, yielding

$$a = 0\,, \quad b = \frac{4f_r^2g_r^2}{\pi m_\chi^2}\frac{\left(1-r_N^2\right)^{3/2}}{\left(r_\phi^2-4\right)^2}\,. \tag{6.65}$$

- Purely imaginary f and g, for which

$$a = \frac{4 f_i^2 g_i^2}{\pi m_\chi^2} \frac{\sqrt{1 - r_N^2}}{\left(r_\phi^2 - 4\right)^2} \,. \tag{6.66}$$

Let us remark that the DM annihilation cross section is s-wave for all the selected models with one exception: Model B1 with real couplings.

In the following, we discuss Figure 6.5, which contains the numerical analysis of the selected models, namely Models A2b (top left panel), A2c (top right panel) and B1 with real and imaginary couplings (bottom left and right panels, respectively). For each model, the red line is the mass of the mediator as a function of the DM mass which reproduces the observed relic abundance: we use the coefficients a and b in Equations (6.61–6.66), substitute back their expressions in $\langle \sigma v \rangle$ given in Equation (6.20), and equate the $\langle \sigma v \rangle$ to either the value extracted from Fig. 1 or Fig. 4 in Ref. [246], depending on the s-wave or p-wave nature of the DM annihilation cross section, respectively.[17] Moreover, the blue line represents the corresponding EFT for each UV model, using the matching conditions given in Table 6.3. It is interesting to note that we have compared our analytical results with numerical scans using `micrOMEGAs` [218, 263], and we have found perfect agreement between them.

Before analysing the available parameter space of the selected models, let us mention that regions in red correspond to values of the relic abundance that would overclose the Universe, *i.e.* $\Omega_{\rm DM} h^2 > 0.12$. In addition, we also include ID constraints from Ref. [226], namely:

- *Planck* cosmic microwave background (CMB) measurements, represented by the blue hatched regions. This analysis sets bounds on the DM annihilation into SM particles. The resulting particles in these annihilations produce an homogenisation of the CMB power spectra, and modifies the ionisation history of the Universe.

- *Fermi* analysis of dwarf spheroidal galaxies (dSphs), represented by the orange hatched regions. If there is no significant excess above the astrophysical background in gamma-ray flux (with photon energies in the 500 MeV–500 GeV range) coming from these galaxies, we can derive bounds on the DM annihilation cross section.

Finally, we analyse the available parameter space for the selected models, which corresponds to the white regions in Figure 6.5.

- **Model A2b.** We take $f = 1$ and $m_N = 2\,\text{GeV}$, which is the lowest sterile neutrino mass allowed by BBN, see *e.g.* Figure 6.2. The EFT computation is valid for $m_\chi \lesssim m_\sigma/4$, and there is an available region of the parameter space with $100\,\text{GeV} \lesssim m_\chi \lesssim 300\,\text{GeV}$ and $200\,\text{GeV} \lesssim m_\sigma \lesssim 300\,\text{GeV}$.

[17] Note that, as has been already mentioned, there are special regions of the parameter space where we use the general expression for $\langle \sigma v \rangle$ in Equation (6.21), namely near mass thresholds and resonances.

- **Model A2c.** We take $f = 1$ and $\mu_\sigma^2 = 10^4\,\text{GeV}$. In this model, the mass of the sterile neutrino is generated radiatively, and depends on μ_σ^2. We discuss this feature in Section 6.4.2. Therefore, the chosen value for μ_σ^2 is motived to have $m_N \gtrsim 2\,\text{GeV}$ in the parameter space that we are considering. Regarding this, the black dotted lines are the contours of m_N in GeV. In this case, the brown region is excluded by BBN. The EFT computation is valid for $m_\chi \lesssim m_\theta/4$, and there is an available region of the parameter space with $100\,\text{GeV} \lesssim m_\chi \lesssim 800\,\text{GeV}$ and $300\,\text{GeV} \lesssim m_\theta \lesssim 800\,\text{GeV}$. This region corresponds to masses of the sterile neutrino between 2 and 10 GeV.

- **Model B1.** In this model, we take $m_N = 2\,\text{GeV}$ and consider real and imaginary couplings. In both cases, the EFT computation is valid for $m_\chi \lesssim m_\phi/6$, and the resonance in the results for the UV model can not be reproduced by the EFT, as expected.

  On the one hand, for real couplings $f_r = g_r = 1$, the DM annihilation cross section is p-wave, and therefore ID bounds can be easily avoided. There is an available region of the parameter space with $2\,\text{GeV} \lesssim m_\chi \lesssim 10\,\text{TeV}$ and $2\,\text{GeV} \lesssim m_\phi \lesssim 20\,\text{TeV}$.

  On the other hand, for imaginary couplings $f_i = g_i = 1$, there is an available region of the parameter space with $30\,\text{GeV} \lesssim m_\chi \lesssim 50\,\text{TeV}$ and $1\,\text{TeV} \lesssim m_\phi \lesssim 100\,\text{TeV}$.

Let us remind that, in our numerical analysis, we are assuming thermal equilibrium among the dark sector, sterile neutrinos, and the SM particles. Related to this assumption, in Appendix A in Ref. [2] we analysed i) the case where particles in the dark sector evolve out of thermal equilibrium (including decays of particles in the Boltzmann equations), and ii) the case where they kinetically decouple from the SM particles before freeze-out. Finally, we concluded that there are not significant deviations from the results obtained assuming thermal and kinetic equilibrium in almost all of the parameter space considered in the numerical analysis shown in Figure 6.5.

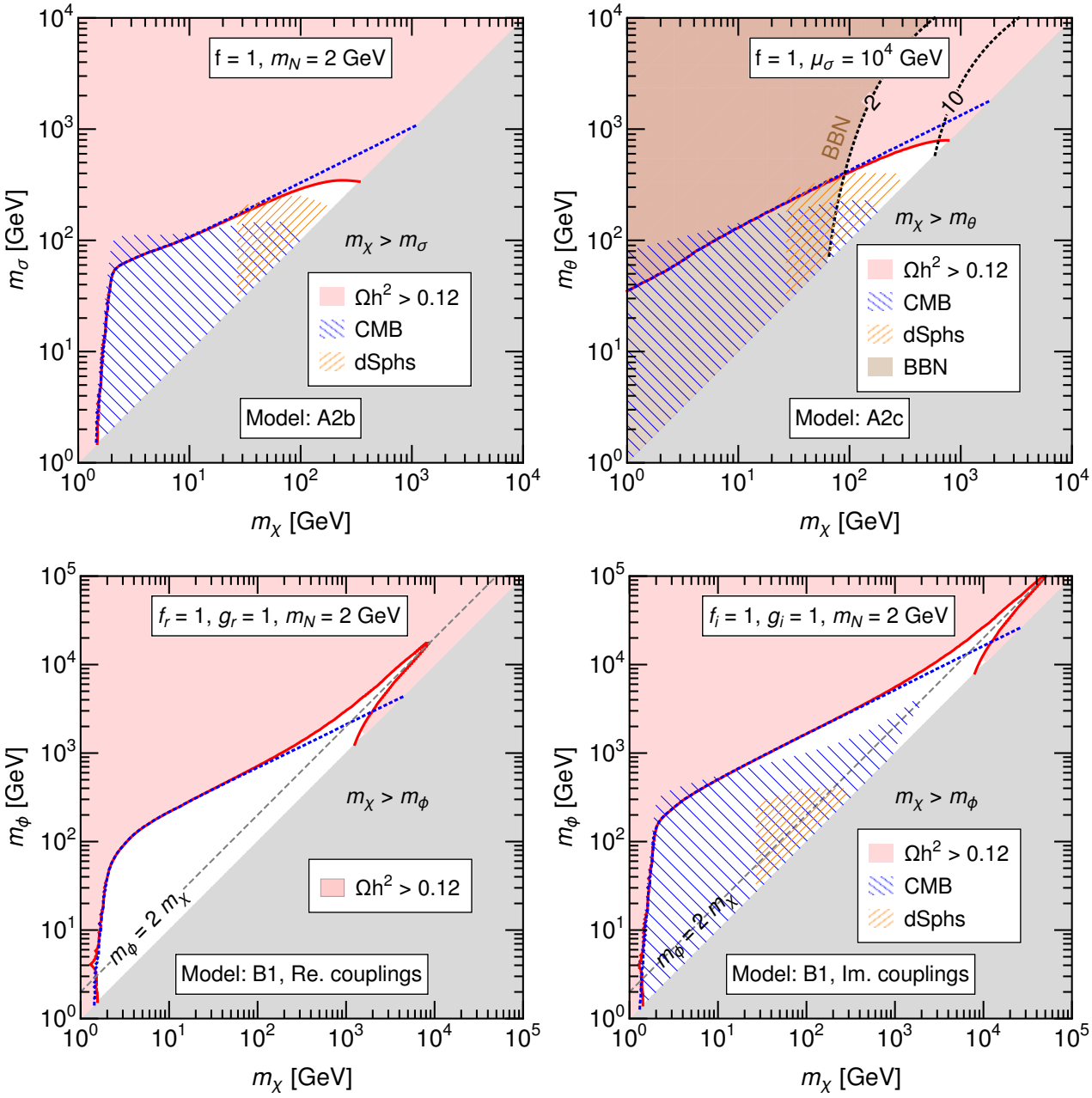

Figure 6.5: *Mass of the mediator as a function of the DM mass, where red line stands for the observed relic abundance for the selected models, namely A2b (top left panel), A2c (top right panel) and B1 with real and imaginary couplings (bottom left and right panels, respectively). The EFT results for each UV completion is depicted as blue dotted lines. The values of the fixed parameters are specified in the upper region of the plots. We also include experimental constraints form ID and BBN. See details in the text.*

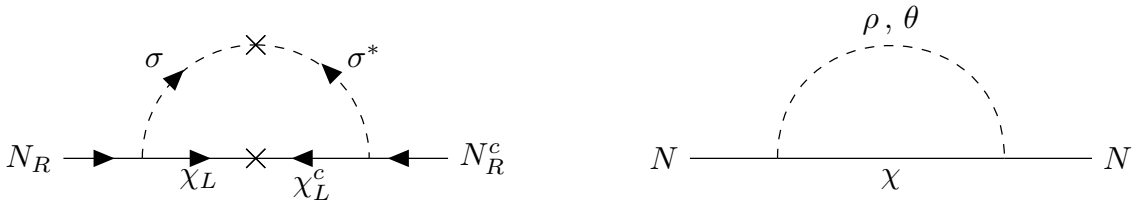

Figure 6.6: *On the left (right) panel, one-loop contribution to the sterile neutrino mass in Model A2c in the weak (mass) basis. Note that the symbol $\times$ stands for the mass insertions μ_σ^2 and m_χ.*

6.4.2 Model A2c and neutrino masses

In Model A2c the sterile neutrino mass is zero at tree level, and the global $U(1)_L$ symmetry, the lepton number, is softly broken by the μ_σ^2 term in the Lagrangian in Equation (6.35). This term, which we take real and positive,[18] yields a mass splitting of the real and the imaginary parts of the complex scalar, ρ and θ, such that $m_\rho > m_\theta$, see *e.g.* Equation (C.16). In addition, the complex scalar is also charged under the $\mathcal{Z}_2$ symmetry. Therefore, the DM candidate will be the lightest of the two fields charged under $\mathcal{Z}_2$, namely χ or θ. In our analysis we do not discuss the pseudo-scalar DM case.

Let us remark that one can include other terms in the Lagrangian that break lepton number, *e.g.* $\lambda'_{\sigma H}\sigma^2|H|^2$ or even a Majorana mass term for N_R, although they are harder in the sense of operators of higher dimension. Moreover, even if these terms are zero at tree level, they are generated at one loop. On the one hand, one can estimate the contribution to the $\sigma^2|H|^2$ term as:

$$\lambda'_{\sigma H} \simeq \frac{\lambda_{\sigma H}\,\lambda_\sigma\,\mu_\sigma^2}{(4\pi)^2 m_\sigma^2}\,. \tag{6.67}$$

On the other hand, the mass splitting between ρ and θ generates a one-loop finite contribution to the sterile neutrino mass, as depicted in Figure 6.6. For a similar mechanism see Ref. [264].

We give in Appendix C.5 the details of the computation of m_N at one loop, where we consider n_N generations of N_R and n_χ generations of χ_L. In addition, we go to the χ_L basis in which m_χ is diagonal with positive and real elements m_{χ_k}. We get the following result for the sterile neutrino mass:

$$(m_N)_{ij} = \sum_{k=1}^{n_\chi} \frac{f_{ik}^* f_{jk}^* m_{\chi_k}}{32\pi^2} F\left(m_\rho^2, m_\theta^2, m_{\chi_k}^2\right)\,, \tag{6.68}$$

where the loop function $F(x,y,z)$ is given in Equation (C.106).

[18] Therefore in this case the f and g couplings are complex (in general) for more than one generations of N_R and χ_L.

Moreover, we can get the expression for the sterile neutrino mass matrix in the limit $m_{\chi_k} \ll m_\rho, m_\theta$ and $m_\rho \simeq m_\theta \simeq m_\sigma$:[19]

$$(m_N)_{ij} \approx \frac{\mu_\sigma^2}{(4\pi)^2 m_\sigma^2} \sum_{k=1}^{n_\chi} f_{ik}^* f_{jk}^* m_{\chi_k} \,. \tag{6.69}$$

Finally, let us comment on an interesting feature regarding the mass of the right-handed neutrinos depending on the number of generations:

- For $n_N = 3$ and $n_\chi = 1$, only one of the eigenvalues of m_N is different from zero. This can be understood from the fact that $m_N \simeq f^* f^\dagger$, see *e.g.* Equation (6.68)
- For $n_N = 3$ and $n_\chi = 2$, only two of the eigenvalues of m_N are non-zero. In fact, two massive neutrinos is the minimal number to explain neutrino data, as was already briefly commented in Section 1.3.
- For $n_N = 3$ and $n_\chi = 3$, we get three massive right-handed neutrinos.
- For $n_N = 1$ and $n_\chi = 1$, and assuming $m_N \gg m_{\rm D}$, we get the following expression for the coupling f:

$$f = 4\pi \frac{y_\nu \, v_h}{\sqrt{m_\nu \, m_\chi \, F(m_\rho^2, m_\theta^2, m_\chi^2)}} \,, \tag{6.70}$$

  where m_ν is the mass of the light (active) neutrino, $m_\nu \simeq 0.05\,\text{eV}$, and v_h is the VEV of the Higgs field, $v_h = 246\,\text{GeV}$. See the details of this computation in Appendix C.5, where we also derive the expression for the coupling f in the general case of more than one generation of N_R and χ_L in Equation (C.115).

[19] Note that one can estimate this result by means of dimensional analysis and symmetry arguments.

Part IV

Final remarks and conclusions

Conclusions

In this section, we summarise the main results presented in the thesis. As has been argued in Chapter 1, the SM describes with a great accuracy a large number of experimental observations related to particle physics. However, there are several open problems that remain unsolved within this theoretical framework, and a couple of them have been the main topics of the thesis, namely: the discrepancies in the AMM of electrons and muons, and DM.

First, in Chapter 2 we reviewed the basic concepts of spin and the AMM of charged leptons, a_l. In particular, we analysed the main contributions to the AMM in the SM, which can be divided in three types, namely the QED, the QCD or hadronic, and the EW contributions. We also emphasized the main role of the fine-structure constant, α, in the determination of the contribution coming from QED, which can be expressed as a power series expansion in α. Therefore, the fine-structure constant can be understood as an input parameter for the SM prediction of AMMs. For electrons, the $a_e^{\rm SM}$ and its uncertainty is dominated by the QED contribution, whereas for muons, the QCD contribution, calculated using lattice techniques, governs the uncertainty in the theoretical estimation of $a_\mu^{\rm SM}$.

Moreover, we have analysed the discrepancies in the electron and the muon AMMs, and their relation with the considered value of the fine-structure constant. In particular, we have summarised in Table 2.2 the values for the discrepancy in the electron AMM considering different experimental measurements of the fine-structure constant. Note that, with the most recent value of α, the sign of the discrepancy has been reversed, changing from negative to positive. In fact, if we take the last experimental determination of α from the Laboratoire Kastler Brossel (LKB), see $\alpha_{\rm Rb}^{(\rm LKB,\,2020)}$ in Table 2.2, the discrepancy for electrons reads $\Delta a_e^{(\rm LKB)} = (0.48 \pm 0.30) \times 10^{-12}$, at the level of $1.6\,\sigma$. The positive sign of this quantity has motivated us to analyse the impact of new (light) scalars, ρ, that couple to electrons and yield a relevant contribution to the electron AMM. As we have mentioned in the last paragraph, the fine-structure constant is an input parameter for the determination of AMMs. However, we can reverse the roles and use the electron AMM in order to get the value of α. In that case, we have studied, in the first part of Chapter 3, how robust is the extraction of the fine-structure constant from the electron AMM assuming new scalars that couple to electrons. After imposing different experimental bounds on the coupling of scalars

to electrons, h_e, we concluded that there are two relevant regions of the parameter space of scalars where their presence could pollute the extraction of α from a_e. In particular, couplings in the interval $10^{-4} \lesssim h_e \lesssim 10^{-2}$ for m_ρ between 1 and 60 MeV, and couplings $h_e \gtrsim 0.2$ for $m_\rho > 100\,\text{GeV}$. If future experiments can constrain these regions of interest, and rule out the full parameter space plotted in the bottom panel in Figure 3.2, one can safely ensure that the extraction of the fine-structure constant from the electron AMM will be robust, in the sense that new scalars which couple to electrons could not spoil the extraction of α.

In the last part of Chapter 3, however, we have taken the value of the fine-structure constant measured by the Berkeley group, see $\alpha_{\text{Cs}}^{(\text{Berkeley, 2018})}$ in Table 2.2, which yields $\Delta a_e^{(\text{Berkeley})} = -(0.88 \pm 0.36) \times 10^{-12}$, at the level of $-2.4\,\sigma$. We have assumed this strategy because the last measurement of α done by LKB is not consistent with previous results obtained by the same experimental group, see *e.g.* in Figure 2.3 the value and the error bars of the points in blue. In this scenario, we have studied the parameter space of scalars (ρ) and pseudo-scalars (θ) that couple to charged leptons and can explain the discrepancies in both the electron and the muon AMM. First, we have considered NP contributions to AMM generated at one loop, and both anomalies can be explained for m_ρ and m_θ between 10 and 100 MeV, and couplings $h_e \sim \mathcal{O}(10^{-4})$ and $h_\mu \sim \mathcal{O}(10^{-3})$, see Figure 3.6. Moreover, we have considered the case where the electron AMM receives contributions at two loops (with only taus running into the loop), and the available parameter space is enlarged with respect to the previous case, allowing higher NP masses and couplings, see Figure 3.9. It is interesting to note that, forthcoming results from the Belle-II experiment can be used to test several regions of the aforementioned parameter space, see *e.g.* Figures 3.5 and 3.8.

Now, we summarise the results regarding the second topic of the thesis, DM. First, we have reviewed its evidences and main properties in Chapter 4. It is well known that neutral scalars, with the appropriated symmetries that prevent their decays, could provide suitable DM candidates. Therefore, inspired by the analysis done in the first part of the thesis regarding scalars, in Chapter 5 we studied how a complex scalar singlet can yield a suitable candidate for DM. Here, we have considered that the complex scalar is charged under a global $U(1)$ symmetry, which is broken both explicitly and spontaneously. This scenario yields a pNGB as the DM candidate. Moreover, the explicit symmetry breaking terms in the Lagrangian must preserve the discrete symmetry DCP, which stabilises the DM particle. We have analysed the possible discrete symmetries of complex scalars in the first part of the chapter. Then, we have considered models with just one explicit symmetry breaking term, labelled as *minimal models*, namely the linear, the quadratic, the cubic and the quartic models. They are motivated by either being the softest possible symmetry breaking term, or by a discrete symmetry which is preserved. In particular, the $\mathcal{Z}_2$, $\mathcal{Z}_3$ and $\mathcal{Z}_4$ symmetries in the quadratic, the cubic and the quartic model, respectively. In addition, all the models preserve DCP, which is responsible of the DM stability.

From the phenomenological point of view, the *minimal models* are characterised by four parameters, namely: the pseudo-scalar and scalar masses, m_θ and m_ρ, the mixing between the CP-even scalars ρ and Higgs, s_α, and the VEV of the complex scalar, v_s.

The region of the parameter space of the complex scalar that is able to reproduce the observed relic abundance is significantly enlarged with respect to the case with just real scalars. We have found that the observed DM abundance is reproduced in the following annihilation channels: i) being at a resonance with the Higgs boson, h, and/or ρ, ii) FDM, where the h and/or ρ pairs in the final state are slightly heavier than the DM, and iii) direct annihilations into lighter pairs of h and/or ρ. The case where $m_\theta \gtrsim m_\rho$ is an example of SDM.

Regarding the numerical results, we have shown that the *minimal models* can be distinguished if a signal in DD experiments is observed. Moreover, if one can measure the DM mass (for instance, by a gamma ray line in ID) we can extract information about the underlying symmetry of the model.

In the last part of Chapter 5, we have explored the possibility of taking more than one symmetry breaking term in the Lagrangian. In this case, one needs to require that DCP is preserved after SSB, which yields several restrictions for all possible pair combinations of the symmetry breaking terms that appear in the *minimal models*. We concluded that, taking two symmetry breaking terms in the Lagrangian enlarges the allowed parameter space in the region between the *minimal models*.

Finally, we have considered the case where the explicit symmetry term is small compared to the scale of SSB of the $U(1)$. In this scenario, after integrating out the heavy new CP-even scalar, we have derived an effective Lagrangian, which contains the Higgs portal term and also a derivative Higgs portal.

Last but not least, in Chapter 6 we analysed the DM phenomenology associated to the SM extended with right-handed neutrinos, N_R (sterile neutrinos), and a Majorana fermion, χ, which is charged under a discrete symmetry, $\mathcal{Z}_2$. This symmetry stabilises it, and yields a suitable DM candidate. In our setup, the DM abundance is obtained by the freeze-out of the annihilations $\chi\chi \to NN$. In the first part of the chapter, we have studied three possible four-fermion operators that relate DM and sterile neutrinos, which we called *portal operators*: the LNC operator $\mathcal{O}_1$, and the operators $\mathcal{O}_2$ and $\mathcal{O}_3$, which can either preserve or violate lepton number; see Table 6.1 for the definition of the operators. In particular, the s-wave part of the DM annihilation cross section for $\mathcal{O}_1$ is proportional to m_N^2, and therefore, it is suppressed for small sterile neutrino masses.

Furthermore, we have analysed the possible UV completions of the *portal operators*, finding different models depending on the channel that governs the DM annihilations. In Models A, the heavy mediator is a real or complex scalar charged under $\mathcal{Z}_2$, and it propagates in the t-channel. Conversely, in Models B and C, the heavy mediators are real or complex scalars and also vector bosons that propagate in s-channels. Within each category, we have considered different scenarios. In particular, in Model A2a, $m_N = 0$ and light neutrinos are Dirac. Moreover, DM annihilations are p-wave and ID bounds from annihilations to neutrinos are avoided. This scenario yields light DM, $m_\chi \sim \mathcal{O}(100)\,\text{MeV}$, but it is difficult to test because neutrinos are Dirac, and therefore DD and ID are suppressed. If no signal is observed neither in DM searches nor in neutrinoless double beta decay experiments, this model would still be a valid option. Models A2b and A2c contain a complex scalar, σ, but the former has a Ma-

jorana mass term for sterile neutrinos, which violates lepton number, whereas the latter has $m_N = 0$, and the lepton number is softly broken by the $\mu_\sigma^2 \sigma^2$ term in the Lagrangian. This model generates the sterile neutrino mass at one loop. Moreover, Model B2 (C2) contains a complex scalar which develops a VEV and spontaneously breaks in two units the global (local) $U(1)_{B-L}$ symmetry of the Lagrangian.

For all the UV completions, we have detailed the computation of the matching conditions in dedicated appendices. Models A are called *genuine* in the sense that they only generate the *portal operators*, but the rest of the models give rise to more operators at $D \leqslant 6$, including, among others, four-fermion self-interactions of χ and N.

In the last part of Chapter 6, we have focused on the DM phenomenology of Models A2b, A2c and B1 with real and imaginary couplings. In Model A2b (A2c) the observed DM abundance can be reproduced for m_χ between 100 and 300 (800) GeV. Note that in Model A2c, the mass of sterile neutrinos generated radiatively is fixed in terms of the rest of the parameters of the model, and the region of the parameter space where the observed DM abundance is reproduced corresponds to m_N between 2 and 10 GeV. In Model B1, the DM annihilation cross section is p-wave for real coupling of DM to scalar mediators. In that case, ID bounds are evaded and the observed relic abundance is reproduced for m_χ between 2 GeV and 10 TeV. Conversely, for imaginary coupling of DM to scalar mediators, the DM annihilation cross section is s-wave and the observed relic abundance is reproduced for m_χ between 30 GeV and 50 TeV.

To summarise, neutral scalars can explain the discrepancies in the AMM of charged leptons and provide a suitable DM candidate. It would be interesting to consider scenarios where they can explain both simultaneously (and also the mass of active neutrinos).

Bibliography

[1] L. Coito, C. Faubel, J. Herrero-Garcia and A. Santamaria, *Dark matter from a complex scalar singlet: the role of dark CP and other discrete symmetries*, *JHEP* **11** (2021) 202 [2106.05289]. Back to page i or 89

[2] L. Coito, C. Faubel, J. Herrero-García, A. Santamaria and A. Titov, *Sterile neutrino portals to Majorana dark matter: effective operators and UV completions*, 2203.01946. Back to page i, 117 or 121

[3] C. Faubel, L. Coito, J. Herrero-García and A. Santamaria, *Dark matter from a complex scalar singlet and the role of dark CP*, *J. Phys. Conf. Ser.* **2156** (2021) 012031. Back to page i

[4] L. Coito, C. Faubel, J. Herrero garcia and A. Santamaria, *Dark matter from a complex scalar singlet and and preservation of its stabilising symmetry*, *PoS* **PANIC2021** (2022) 055. Back to page i

[5] L. Coito, C. Faubel and A. Santamaria, *Composite Higgs bosons from neutrino condensates in an inverted seesaw scenario*, *Phys. Rev. D* **101** (2020) 075009 [1912.10001]. Back to page i

[6] S. L. Glashow, *Partial-symmetries of weak interactions*, *Nuclear Physics* **22** (1961) 579. Back to page 3

[7] P. W. Higgs, *Broken symmetries and the masses of gauge bosons*, *Phys. Rev. Lett.* **13** (1964) 508. Back to page 3 or 6

[8] F. Englert and R. Brout, *Broken symmetry and the mass of gauge vector mesons*, *Phys. Rev. Lett.* **13** (1964) 321. Back to page 3 or 6

[9] G. S. Guralnik, C. R. Hagen and T. W. B. Kibble, *Global conservation laws and massless particles*, *Phys. Rev. Lett.* **13** (1964) 585. Back to page 3

[10] P. W. Higgs, *Spontaneous symmetry breakdown without massless bosons*, *Phys. Rev.* **145** (1966) 1156. Back to page 3

[11] T. W. B. Kibble, *Symmetry breaking in non-abelian gauge theories*, *Phys. Rev.* **155** (1967) 1554. Back to page 3

[12] S. Weinberg, *A model of leptons*, *Phys. Rev. Lett.* **19** (1967) 1264. Back to page 3

[13] A. Salam, *Weak and Electromagnetic Interactions*, *Conf. Proc. C* **680519** (1968) 367. Back to page 3

[14] M. Y. Han and Y. Nambu, *Three-triplet model with double* SU(3) *symmetry*, *Phys. Rev.* **139** (1965) B1006. Back to page 3

[15] H. Fritzsch, M. Gell-Mann and H. Leutwyler, *Advantages of the color octet gluon picture*, *Physics Letters B* **47** (1973) 365. Back to page 3

[16] M. Gell-Mann, *Quarks*, *Acta Phys. Austriaca Suppl.* **9** (1972) 733. Back to page 3

[17] H. Fritzsch and M. Gell-Mann, *Current algebra: Quarks and what else?*, *eConf* **C720906V2** (1972) 135 [hep-ph/0208010]. Back to page 3

[18] A. Pich, *The Standard Model of Electroweak Interactions*, in *2010 European School of High Energy Physics*, pp. 1–50, 1, 2012, 1201.0537. Back to page 3

[19] A. Pich, *Aspects of quantum chromodynamics*, in *ICTP Summer School in Particle Physics*, pp. 53–102, 6, 1999, hep-ph/0001118. Back to page 3

[20] J. Goldstone, *Field Theories with Superconductor Solutions*, *Nuovo Cim.* **19** (1961) 154. Back to page 7

[21] ATLAS collaboration, G. Aad et al., *Observation of a new particle in the search for the Standard Model Higgs boson with the ATLAS detector at the LHC*, *Phys. Lett. B* **716** (2012) 1 [1207.7214]. Back to page 9 or 12

[22] CMS collaboration, S. Chatrchyan et al., *Observation of a New Boson at a Mass of 125 GeV with the CMS Experiment at the LHC*, *Phys. Lett. B* **716** (2012) 30 [1207.7235]. Back to page 9 or 12

[23] PARTICLE DATA GROUP collaboration, P. A. Zyla et al., *Review of Particle Physics*, *PTEP* **2020** (2020) 083C01. Back to page 9, 12, 28, 34, 46, 47, 49 or 83

[24] L. Wolfenstein, *Parametrization of the kobayashi-maskawa matrix*, *Phys. Rev. Lett.* **51** (1983) 1945. Back to page 11

[25] CKMFITTER GROUP collaboration, J. Charles, A. Hocker, H. Lacker, S. Laplace, F. R. Le Diberder, J. Malcles et al., *CP violation and the CKM matrix: Assessing the impact of the asymmetric B factories*, *Eur. Phys. J. C* **41** (2005) 1 [hep-ph/0406184]. Back to page 11

[26] A. Hocker, H. Lacker, S. Laplace and F. Le Diberder, *A New approach to a global fit of the CKM matrix*, *Eur. Phys. J. C* **21** (2001) 225 [hep-ph/0104062]. Back to page 11

[27] UTFIT collaboration, M. Bona et al., *The 2004 UTfit collaboration report on the status of the unitarity triangle in the standard model*, *JHEP* **07** (2005) 028 [hep-ph/0501199]. Back to page 11

[28] UTFIT collaboration, M. Bona et al., *Model-independent constraints on $\Delta F = 2$ operators and the scale of new physics*, *JHEP* **03** (2008) 049 [0707.0636]. Back to page 11

[29] LHCB collaboration, R. Aaij et al., *Test of lepton universality with $B^0 \to K^{*0}\ell^+\ell^-$ decays*, *JHEP* **08** (2017) 055 [1705.05802]. Back to page 13

[30] LHCB collaboration, R. Aaij et al., *Test of lepton universality with $\Lambda_b^0 \to pK^-\ell^+\ell^-$ decays*, *JHEP* **05** (2020) 040 [1912.08139]. Back to page 13

[31] LHCB collaboration, R. Aaij et al., *Test of lepton universality in beauty-quark decays*, *Nature Phys.* **18** (2022) 277 [2103.11769]. Back to page 13

[32] LHCB collaboration, R. Aaij et al., *Tests of lepton universality using $B^0 \to K_S^0\ell^+\ell^-$ and $B^+ \to K^{*+}\ell^+\ell^-$ decays*, 2110.09501. Back to page 13

[33] W. Altmannshofer and P. Stangl, *New physics in rare B decays after Moriond 2021*, *Eur. Phys. J. C* **81** (2021) 952 [2103.13370]. Back to page 13

[34] G. Isidori, D. Lancierini, P. Owen and N. Serra, *On the significance of new physics in $b \to s\ell^+\ell^-$ decays*, *Phys. Lett. B* **822** (2021) 136644 [2104.05631]. Back to page 13

[35] HFLAV collaboration, Y. S. Amhis et al., *Averages of b-hadron, c-hadron, and τ-lepton properties as of 2018*, *Eur. Phys. J. C* **81** (2021) 226 [1909.12524]. Back to page 13

[36] F. U. Bernlochner, M. F. Sevilla, D. J. Robinson and G. Wormser, *Semitauonic b-hadron decays: A lepton flavor universality laboratory*, *Rev. Mod. Phys.* **94** (2022) 015003 [2101.08326]. Back to page 13

[37] W. Altmannshofer and J. Zupan, *Snowmass White Paper: Flavor Model Building*, in *2022 Snowmass Summer Study*, 3, 2022, 2203.07726. Back to page 13 or 14

[38] SUPERNOVA COSMOLOGY PROJECT collaboration, S. Perlmutter et al., *Measurements of Ω and Λ from 42 high redshift supernovae*, *Astrophys. J.* **517** (1999) 565 [astro-ph/9812133]. Back to page 13

[39] SUPERNOVA SEARCH TEAM collaboration, A. G. Riess et al., *Observational evidence from supernovae for an accelerating universe and a cosmological constant*, *Astron. J.* **116** (1998) 1009 [astro-ph/9805201]. Back to page 13

[40] H. Ishimori, T. Kobayashi, H. Ohki, Y. Shimizu, H. Okada and M. Tanimoto, *Non-Abelian Discrete Symmetries in Particle Physics*, *Prog. Theor. Phys. Suppl.* **183** (2010) 1 [1003.3552]. Back to page 14

[41] S. F. King and C. Luhn, *Neutrino Mass and Mixing with Discrete Symmetry*, *Rept. Prog. Phys.* **76** (2013) 056201 [1301.1340]. Back to page 14

[42] W. Grimus and P. O. Ludl, *Finite flavour groups of fermions*, *J. Phys. A* **45** (2012) 233001 [1110.6376]. Back to page 14

[43] R. D. Peccei and H. R. Quinn, *CP Conservation in the Presence of Instantons*, *Phys. Rev. Lett.* **38** (1977) 1440. Back to page 14

[44] R. D. Peccei and H. R. Quinn, *Constraints Imposed by CP Conservation in the Presence of Instantons*, *Phys. Rev. D* **16** (1977) 1791. Back to page 14

[45] S. Weinberg, *A New Light Boson?*, *Phys. Rev. Lett.* **40** (1978) 223. Back to page 14

[46] F. Wilczek, *Problem of Strong P and T Invariance in the Presence of Instantons*, *Phys. Rev. Lett.* **40** (1978) 279. Back to page 14

[47] W. Pauli, *Dear radioactive ladies and gentlemen*, *Phys. Today* **31N9** (1978) 27. Back to page 15

[48] C. D. Ellis and W. A. Wooster, *The $\beta-$ray type of disintegration*, *Mathematical Proceedings of the Cambridge Philosophical Society* **22** (1925) 849–860. Back to page 16

[49] F. Reines and C. L. Cowan, *Detection of the free neutrino*, *Phys. Rev.* **92** (1953) 830. Back to page 15

[50] F. Reines, C. L. Cowan, F. B. Harrison, A. D. McGuire and H. W. Kruse, *Detection of the free antineutrino*, *Phys. Rev.* **117** (1960) 159. Back to page 15

[51] C. L. Cowan, F. Reines, F. B. Harrison, H. W. Kruse and A. D. McGuire, *Detection of the free neutrino: A Confirmation*, *Camb. Monogr. Part. Phys. Nucl. Phys. Cosmol.* **14** (2000) 38. Back to page 15

[52] B. T. Cleveland, T. Daily, R. Davis, Jr., J. R. Distel, K. Lande, C. K. Lee et al., *Measurement of the solar electron neutrino flux with the Homestake chlorine detector*, *Astrophys. J.* **496** (1998) 505. Back to page 15

[53] E. Majorana, *Teoria simmetrica dell'elettrone e del positrone*, *Nuovo Cim.* **14** (1937) 171. Back to page 16

[54] P. Minkowski, *$\mu \to e\gamma$ at a Rate of One Out of 10^9 Muon Decays?*, *Phys. Lett. B* **67** (1977) 421. Back to page 17

[55] M. Gell-Mann, P. Ramond and R. Slansky, *Complex Spinors and Unified Theories*, *Conf. Proc. C* **790927** (1979) 315 [1306.4669]. Back to page 17

[56] T. Yanagida, *Horizontal gauge symmetry and masses of neutrinos*, *Conf. Proc. C* **7902131** (1979) 95. Back to page 17

[57] R. N. Mohapatra and G. Senjanovic, *Neutrino Mass and Spontaneous Parity Nonconservation*, *Phys. Rev. Lett.* **44** (1980) 912. Back to page 17

[58] W. Konetschny and W. Kummer, *Nonconservation of Total Lepton Number with Scalar Bosons*, *Phys. Lett. B* **70** (1977) 433. Back to page 17

[59] T. P. Cheng and L.-F. Li, *Neutrino Masses, Mixings and Oscillations in SU(2) x U(1) Models of Electroweak Interactions*, *Phys. Rev. D* **22** (1980) 2860. Back to page 17

[60] G. Lazarides, Q. Shafi and C. Wetterich, *Proton Lifetime and Fermion Masses in an SO(10) Model*, *Nucl. Phys. B* **181** (1981) 287. Back to page 17

[61] M. Magg and C. Wetterich, *Neutrino Mass Problem and Gauge Hierarchy*, *Phys. Lett. B* **94** (1980) 61. Back to page 17

[62] J. Schechter and J. W. F. Valle, *Neutrino Masses in SU(2) x U(1) Theories*, *Phys. Rev. D* **22** (1980) 2227. Back to page 17

[63] R. Foot, H. Lew, X. G. He and G. C. Joshi, *Seesaw Neutrino Masses Induced by a Triplet of Leptons*, *Z. Phys. C* **44** (1989) 441. Back to page 17

[64] E. Ma and D. P. Roy, *Heavy triplet leptons and new gauge boson*, *Nucl. Phys. B* **644** (2002) 290 [hep-ph/0206150]. Back to page 17

[65] R. N. Mohapatra and J. W. F. Valle, *Neutrino Mass and Baryon Number Nonconservation in Superstring Models*, *Phys. Rev. D* **34** (1986) 1642. Back to page 17

[66] A. Zee, *Quantum Numbers of Majorana Neutrino Masses*, *Nucl. Phys. B* **264** (1986) 99. Back to page 17

[67] K. Babu, *Model of "calculable" majorana neutrino masses*, *Physics Letters B* **203** (1988) 132. Back to page 17

[68] E. Ma, *Verifiable radiative seesaw mechanism of neutrino mass and dark matter*, *Phys. Rev. D* **73** (2006) 077301 [hep-ph/0601225]. Back to page 17 or 177

[69] Y. Cai, J. Herrero-Garca, M. A. Schmidt, A. Vicente and R. R. Volkas, *From the trees to the forest: a review of radiative neutrino mass models*, *Front.in Phys.* **5** (2017) 63 [1706.08524]. Back to page 17

[70] S. Weinberg, *Phenomenological Lagrangians*, *Physica A* **96** (1979) 327. Back to page 18

[71] H. Georgi, *Effective field theory*, *Ann. Rev. Nucl. Part. Sci.* **43** (1993) 209. Back to page 18

[72] J. Wudka, *Electroweak effective Lagrangians*, *Int. J. Mod. Phys. A* **9** (1994) 2301 [hep-ph/9406205]. Back to page 18, 30 or 40

[73] A. Pich, *Effective field theory: Course*, in *Les Houches Summer School in Theoretical Physics, Session 68: Probing the Standard Model of Particle Interactions*, pp. 949–1049, 6, 1998, hep-ph/9806303. Back to page 18 or 20

[74] E. Rutherford, *The scattering of alpha and beta particles by matter and the structure of the atom*, *Phil. Mag. Ser. 6* **21** (1911) 669. Back to page 25

[75] N. Bohr, *On the Constitution of Atoms and Molecules*, *Phil. Mag. Ser. 6* **26** (1913) 1. Back to page 25

[76] S. A. Goudschmidt and G. H. Uhlenbeck, *Spinning electrons and the structure of spectra*, *Nature* **117** (1926) 264. Back to page 26

[77] S. Pakvasa, *The Stern-Gerlach Experiment and the Electron Spin*, 1805.09412. Back to page 25

[78] O. Stern, *Z. Phys.* **7** (1921) 249. Back to page 26

[79] W. Gerlach and O. Stern, *Experimental proof of the magnetic moment of the silver atom*, *Z. Phys.* **8** (1922) 110. Back to page 26

[80] W. Gerlach and O. Stern, *Experimental test of the applicability of the quantum their to the magnetic field*, *Z. Phys.* **9** (1922) 349. Back to page 26

[81] W. Gerlach and O. Stern, *The Magnetic Moment of Silver Atoms*, *Z. Phys.* **9** (1922) 353. Back to page 26

[82] W. Gerlach and O. Stern, *Ann. Phys.* **74** (1924) 673. Back to page 26

[83] T. E. Phipps and J. B. Taylor, *The magnetic moment of the hydrogen atom*, *Phys. Rev.* **29** (1927) 309. Back to page 26

[84] A. K. Compton, *Jour. Franklin. Inst.* **192** (1921) 145. Back to page 26

[85] G. E. Uhlenbeck and S. Goudsmit, *Naturwissenschaften* **47** (1925) 953. Back to page 26

[86] P. A. M. Dirac, *The quantum theory of the electron*, *Proc. Roy. Soc. Lond. A* **117** (1928) 610. Back to page 27

[87] P. A. M. Dirac, *The Quantum theory of electron. 2.*, *Proc. Roy. Soc. Lond. A* **118** (1928) 351. Back to page 27

[88] J. D. Bjorken and S. D. Drell, *Relativistic Quantum Mechanics*, International Series In Pure and Applied Physics. McGraw-Hill, New York, 1965. Back to page 27

[89] A. Pais, M. Jacob, D. I. Olive and M. F. Atiyah, *Paul Dirac: the man and his work*. Cambridge U. Press, New York, ed. P. Goddard, 1998. Back to page 27

[90] M. Kobayashi and T. Maskawa, *CP Violation in the Renormalizable Theory of Weak Interaction*, *Prog. Theor. Phys.* **49** (1973) 652. Back to page 28

[91] M. J. Booth, *The Electric dipole moment of the W and electron in the Standard Model*, hep-ph/9301293. Back to page 28

[92] M. Pospelov and A. Ritz, *Electric dipole moments as probes of new physics*, *Annals Phys.* **318** (2005) 119 [hep-ph/0504231]. Back to page 28

[93] J. S. Schwinger, *On Quantum electrodynamics and the magnetic moment of the electron*, *Phys. Rev.* **73** (1948) 416. Back to page 30

[94] A. Gérardin, *The anomalous magnetic moment of the muon: status of Lattice QCD calculations*, *Eur. Phys. J. A* **57** (2021) 116 [2012.03931]. Back to page 31

[95] C. Aubin, T. Blum, C. Tu, M. Golterman, C. Jung and S. Peris, *Light quark vacuum polarization at the physical point and contribution to the muon $g-2$*, *Phys. Rev. D* **101** (2020) 014503 [1905.09307]. Back to page 31

[96] C. Aubin, T. Blum, M. Golterman and S. Peris, *The muon anomalous magnetic moment with staggered fermions: is the lattice spacing small enough?*, 2204.12256. Back to page 31

[97] A. Czarnecki, B. Krause and W. J. Marciano, *Electroweak corrections to the muon anomalous magnetic moment*, *Phys. Rev. Lett.* **76** (1996) 3267 [hep-ph/9512369]. Back to page 32

[98] C. Gnendiger, D. Stöckinger and H. Stöckinger-Kim, *The electroweak contributions to $(g-2)_\mu$ after the Higgs boson mass measurement*, *Phys. Rev. D* **88** (2013) 053005 [1306.5546]. Back to page 32

[99] T. Aoyama, T. Kinoshita and M. Nio, *Theory of the Anomalous Magnetic Moment of the Electron*, *Atoms* **7** (2019) 28. Back to page 32

[100] P. J. Mohr, D. B. Newell and B. N. Taylor, *Codata recommended values of the fundamental physical constants: 2014*, *Rev. Mod. Phys.* **88** (2016) 035009. Back to page 33 or 44

[101] R. Bouchendira, P. Clade, S. Guellati-Khelifa, F. Nez and F. Biraben, *New determination of the fine structure constant and test of the quantum electrodynamics*, *Phys. Rev. Lett.* **106** (2011) 080801 [1012.3627]. Back to page 33

[102] R. H. Parker, C. Yu, W. Zhong, B. Estey and H. Müller, *Measurement of the fine-structure constant as a test of the Standard Model*, *Science* **360** (2018) 191 [1812.04130]. Back to page 33 or 37

[103] L. Morel, Z. Yao, P. Cladé and S. Guellati-Khélifa, *Determination of the fine-structure constant with an accuracy of 81 parts per trillion*, *Nature* **588** (2020) 61. Back to page 33, 34 or 36

[104] D. Hanneke, S. Fogwell and G. Gabrielse, *New Measurement of the Electron Magnetic Moment and the Fine Structure Constant*, *Phys. Rev. Lett.* **100** (2008) 120801 [0801.1134]. Back to page 33 or 34

[105] S. Eidelman, M. Giacomini, F. V. Ignatov and M. Passera, *The tau lepton anomalous magnetic moment*, *Nucl. Phys. B Proc. Suppl.* **169** (2007) 226 [hep-ph/0702026]. Back to page 34

[106] T. Aoyama et al., *The anomalous magnetic moment of the muon in the Standard Model*, *Phys. Rept.* **887** (2020) 1 [2006.04822]. Back to page 35

[107] MUON G-2 collaboration, B. Abi et al., *Measurement of the Positive Muon Anomalous Magnetic Moment to 0.46 ppm*, *Phys. Rev. Lett.* **126** (2021) 141801 [2104.03281]. Back to page 35, 35 or 36

[108] G. Colangelo et al., *Prospects for precise predictions of a_μ in the Standard Model*, 2203.15810. Back to page 35

[109] A. Keshavarzi, K. S. Khaw and T. Yoshioka, *Muon $g-2$: A review*, *Nucl. Phys. B* **975** (2022) 115675 [2106.06723]. Back to page 35

[110] MUON G-2 collaboration, G. W. Bennett et al., *Final Report of the Muon E821 Anomalous Magnetic Moment Measurement at BNL*, *Phys. Rev. D* **73** (2006) 072003 [hep-ex/0602035]. Back to page 36

[111] M. Lindner, M. Platscher and F. S. Queiroz, *A Call for New Physics : The Muon Anomalous Magnetic Moment and Lepton Flavor Violation*, *Phys. Rept.* **731** (2018) 1 [1610.06587]. Back to page 36

[112] P. Athron, C. Balázs, D. H. J. Jacob, W. Kotlarski, D. Stöckinger and H. Stöckinger-Kim, *New physics explanations of a_μ in light of the FNAL muon $g-2$ measurement*, *JHEP* **09** (2021) 080 [2104.03691]. Back to page 36

[113] V. Brdar, S. Jana, J. Kubo and M. Lindner, *Semi-secretly interacting Axion-like particle as an explanation of Fermilab muon $g-2$ measurement*, *Phys. Lett. B* **820** (2021) 136529 [2104.03282]. Back to page 36 or 36

[114] M. Pospelov, *Secluded U(1) below the weak scale*, *Phys. Rev. D* **80** (2009) 095002 [0811.1030]. Back to page 36, 42 or 151

[115] A. Greljo, Y. Soreq, P. Stangl, A. E. Thomsen and J. Zupan, *Muonic force behind flavor anomalies*, *JHEP* **04** (2022) 151 [2107.07518]. Back to page 36

[116] M. Bauer, M. Neubert, S. Renner, M. Schnubel and A. Thamm, *Axionlike Particles, Lepton-Flavor Violation, and a New Explanation of a_μ and a_e*, *Phys. Rev. Lett.* **124** (2020) 211803 [1908.00008]. Back to page 36 or 37

[117] H. Davoudiasl and W. J. Marciano, *Tale of two anomalies*, *Phys. Rev. D* **98** (2018) 075011 [1806.10252]. Back to page 36, 37, 59 or 59

[118] W. J. Marciano, A. Masiero, P. Paradisi and M. Passera, *Contributions of axionlike particles to lepton dipole moments*, *Phys. Rev. D* **94** (2016) 115033 [1607.01022]. Back to page 36 or 37

[119] M. A. Buen-Abad, J. Fan, M. Reece and C. Sun, *Challenges for an axion explanation of the muon $g-2$ measurement*, *JHEP* **09** (2021) 101 [2104.03267]. Back to page 36

[120] D. Buttazzo, P. Panci, D. Teresi and R. Ziegler, *Xenon1T excess from electron recoils of non-relativistic Dark Matter*, *Phys. Lett. B* **817** (2021) 136310 [2011.08919]. Back to page 36

[121] S.-F. Ge, X.-D. Ma and P. Pasquini, *Probing the dark axion portal with muon anomalous magnetic moment*, *Eur. Phys. J. C* **81** (2021) 787 [2104.03276]. Back to page 36

[122] R. Capdevilla, D. Curtin, Y. Kahn and G. Krnjaic, *Systematically testing singlet models for $(g-2)_\mu$*, *JHEP* **04** (2022) 129 [2112.08377]. Back to page 36

[123] R. Capdevilla, D. Curtin, Y. Kahn and G. Krnjaic, *No-lose theorem for discovering the new physics of $(g-2)_\mu$ at muon colliders*, *Phys. Rev. D* **105** (2022) 015028 [2101.10334]. Back to page 36

[124] N. V. Krasnikov, *Implications of last NA64 results and the electron g_e-2 anomaly for the X(16.7) boson survival*, *Mod. Phys. Lett. A* **35** (2020) 2050116 [1912.11689]. Back to page 37

[125] H.-S. Lee, *Muon $g-2$ anomaly and dark leptonic gauge boson*, *Phys. Rev. D* **90** (2014) 091702 [1408.4256]. Back to page 37

[126] A. Crivellin, M. Hoferichter and P. Schmidt-Wellenburg, *Combined explanations of $(g-2)_{\mu,e}$ and implications for a large muon EDM*, *Phys. Rev. D* **98** (2018) 113002 [1807.11484]. Back to page 37

[127] E. J. Chun and T. Mondal, *Explaining $g-2$ anomalies in two Higgs doublet model with vector-like leptons*, *JHEP* **11** (2020) 077 [2009.08314]. Back to page 37

[128] J. Liu, C. E. M. Wagner and X.-P. Wang, *A light complex scalar for the electron and muon anomalous magnetic moments*, *JHEP* **03** (2019) 008 [1810.11028]. Back to page 37, 49 or 58

[129] S. Gardner and X. Yan, *Light scalars with lepton number to solve the $(g-2)_e$ anomaly*, *Phys. Rev. D* **102** (2020) 075016 [1907.12571]. Back to page 37

[130] L. Darmé, F. Giacchino, E. Nardi and M. Raggi, *Invisible decays of axion-like particles: constraints and prospects*, *JHEP* **06** (2021) 009 [2012.07894]. Back to page 37

[131] L. Delle Rose, S. Khalil and S. Moretti, *Explaining electron and muon $g-2$ anomalies in an Aligned 2-Higgs Doublet Model with right-handed neutrinos*, *Phys. Lett. B* **816** (2021) 136216 [2012.06911]. Back to page 37

[132] M. Endo and W. Yin, *Explaining electron and muon $g-2$ anomaly in SUSY without lepton-flavor mixings*, *JHEP* **08** (2019) 122 [1906.08768]. Back to page 37

[133] I. Doršner, S. Fajfer and S. Saad, *$\mu \to e\gamma$ selecting scalar leptoquark solutions for the $(g-2)_{e,\mu}$ puzzles*, *Phys. Rev. D* **102** (2020) 075007 [2006.11624]. Back to page 37

[134] K.-F. Chen, C.-W. Chiang and K. Yagyu, *An explanation for the muon and electron $g-2$ anomalies and dark matter*, *JHEP* **09** (2020) 119 [2006.07929]. Back to page 37

[135] C. Boehm, X. Chu, J.-L. Kuo and J. Pradler, *Scalar dark matter candidates revisited*, *Phys. Rev. D* **103** (2021) 075005 [2010.02954]. Back to page 37

[136] S. N. Gninenko, N. V. Krasnikov and V. A. Matveev, *Search for dark sector physics with NA64*, *Phys. Part. Nucl.* **51** (2020) 829 [2003.07257]. Back to page 37

[137] S. Jana, P. K. Vishnu, W. Rodejohann and S. Saad, *Dark matter assisted lepton anomalous magnetic moments and neutrino masses*, *Phys. Rev. D* **102** (2020) 075003 [2008.02377]. Back to page 37

[138] S. Jana, V. P. K. and S. Saad, *Resolving electron and muon $g-2$ within the 2HDM*, *Phys. Rev. D* **101** (2020) 115037 [2003.03386]. Back to page 37

[139] C. Cornella, P. Paradisi and O. Sumensari, *Hunting for ALPs with Lepton Flavor Violation*, *JHEP* **01** (2020) 158 [1911.06279]. Back to page 37

[140] G. F. Giudice, P. Paradisi and M. Passera, *Testing new physics with the electron g-2*, *JHEP* **11** (2012) 113 [1208.6583]. Back to page 40, 43, 151 or 152

[141] A. Czarnecki and W. J. Marciano, *The Muon anomalous magnetic moment: A Harbinger for 'new physics'*, *Phys. Rev. D* **64** (2001) 013014 [hep-ph/0102122]. Back to page 40

[142] E. Hardy and R. Lasenby, *Stellar cooling bounds on new light particles: plasma mixing effects*, *JHEP* **02** (2017) 033 [1611.05852]. Back to page 45

[143] S. Knapen, T. Lin and K. M. Zurek, *Light Dark Matter: Models and Constraints*, *Phys. Rev. D* **96** (2017) 115021 [1709.07882]. Back to page 45, 45, 50, 50, 50, 50 or 50

[144] C. Delaunay, C. Frugiuele, E. Fuchs and Y. Soreq, *Probing new spin-independent interactions through precision spectroscopy in atoms with few electrons*, *Phys. Rev. D* **96** (2017) 115002 [1709.02817]. Back to page 46

[145] J. D. Bjorken, S. Ecklund, W. R. Nelson, A. Abashian, C. Church, B. Lu et al., *Search for Neutral Metastable Penetrating Particles Produced in the SLAC Beam Dump*, *Phys. Rev. D* **38** (1988) 3375. Back to page 46

[146] E. M. Riordan et al., *A Search for Short Lived Axions in an Electron Beam Dump Experiment*, *Phys. Rev. Lett.* **59** (1987) 755. Back to page 46

[147] M. Davier, J. Jeanjean and H. Nguyen Ngoc, *Search for Axions in Electron Bremsstrahlung*, *Phys. Lett. B* **180** (1986) 295. Back to page 46

[148] M. Davier and H. Nguyen Ngoc, *An Unambiguous Search for a Light Higgs Boson*, *Phys. Lett. B* **229** (1989) 150. Back to page 46

[149] M. Battaglieri et al., *The Heavy Photon Search Test Detector*, *Nucl. Instrum. Meth. A* **777** (2015) 91 [1406.6115]. Back to page 46

[150] B. Batell, N. Lange, D. McKeen, M. Pospelov and A. Ritz, *Muon anomalous magnetic moment through the leptonic Higgs portal*, *Phys. Rev. D* **95** (2017) 075003 [1606.04943]. Back to page 46, 50, 50 or 58

[151] E. Goudzovski et al., *New Physics Searches at Kaon and Hyperon Factories*, 2201.07805. Back to page 46

[152] G. Krnjaic, G. Marques-Tavares, D. Redigolo and K. Tobioka, *Probing Muonphilic Force Carriers and Dark Matter at Kaon Factories*, *Phys. Rev. Lett.* **124** (2020) 041802 [1902.07715]. Back to page 46

[153] J. Bijnens, G. Ecker and J. Gasser, *Radiative semileptonic kaon decays*, *Nucl. Phys. B* **396** (1993) 81 [hep-ph/9209261]. Back to page 47

[154] I. Alikhanov and E. A. Paschos, *Searching for new light gauge bosons at e^+e^- colliders*, *Phys. Rev. D* **97** (2018) 115004 [1710.10131]. Back to page 47

[155] F. Abu-Ajamieh, *Probing Scalar and Pseudoscalar Solutions of the g - 2 Anomaly*, *Adv. High Energy Phys.* **2020** (2020) 1751534 [1810.08891]. Back to page 48, 48 or 59

[156] J. L. Rainbolt and M. Schmitt, *Branching fraction for Z decays to four leptons and constraints on new physics*, *Phys. Rev. D* **99** (2019) 013004 [1805.05791]. Back to page 49

[157] A. Anastasi et al., *Limit on the production of a low-mass vector boson in $e^+e^- \to U\gamma$, $U \to e^+e^-$ with the KLOE experiment*, *Phys. Lett. B* **750** (2015) 633 [1509.00740]. Back to page 49

[158] D. S. M. Alves and N. Weiner, *A viable QCD axion in the MeV mass range*, *JHEP* **07** (2018) 092 [1710.03764]. Back to page 49

[159] BABAR collaboration, J. P. Lees et al., *Search for a Dark Photon in e^+e^- Collisions at BaBar*, *Phys. Rev. Lett.* **113** (2014) 201801 [1406.2980]. Back to page 50

[160] BABAR collaboration, J. P. Lees et al., *Search for Invisible Decays of a Dark Photon Produced in e^+e^- Collisions at BaBar*, *Phys. Rev. Lett.* **119** (2017) 131804 [1702.03327]. Back to page 50

[161] BABAR collaboration, J. P. Lees et al., *Search for a Dark Leptophilic Scalar in e^+e^- Collisions*, *Phys. Rev. Lett.* **125** (2020) 181801 [2005.01885]. Back to page 50

[162] BELLE-II collaboration, T. Abe et al., *Belle II Technical Design Report*, 1011.0352. Back to page 50

[163] BELLE-II collaboration, W. Altmannshofer et al., *The Belle II Physics Book*, *PTEP* **2019** (2019) 123C01 [1808.10567]. Back to page 50 or 58

[164] M. A. Corona, M. Cadeddu, N. Cargioli, F. Dordei, C. Giunti, Y. F. Li et al., *Probing light mediators and $(g-2)_\mu$ through detection of coherent elastic neutrino nucleus scattering at COHERENT*, 2202.11002. Back to page 50

[165] B. Batell, A. Freitas, A. Ismail and D. Mckeen, *Flavor-specific scalar mediators*, *Phys. Rev. D* **98** (2018) 055026 [1712.10022]. Back to page 50, 58, 58, 58 or 58

[166] NA64 collaboration, Y. M. Andreev et al., *Constraints on New Physics in Electron $g-2$ from a Search for Invisible Decays of a Scalar, Pseudoscalar, Vector, and Axial Vector*, *Phys. Rev. Lett.* **126** (2021) 211802 [2102.01885]. Back to page 50

[167] N. Chen, B. Wang and C.-Y. Yao, *The collider tests of a leptophilic scalar for the anomalous magnetic moments*, 2102.05619. Back to page 50

[168] BABAR collaboration, J. P. Lees et al., *Search for a muonic dark force at BABAR*, *Phys. Rev. D* **94** (2016) 011102 [1606.03501]. Back to page 58

[169] ATLAS collaboration, G. Aad et al., *Measurements of Four-Lepton Production at the Z Resonance in pp Collisions at $\sqrt{s}$ =7 and 8 TeV with ATLAS*, *Phys. Rev. Lett.* **112** (2014) 231806 [1403.5657]. Back to page 58

[170] CMS collaboration, A. M. Sirunyan et al., *Search for an $L_\mu - L_\tau$ gauge boson using $Z\to 4\mu$ events in proton-proton collisions at $\sqrt{s} = 13$ TeV*, *Phys. Lett. B* **792** (2019) 345 [1808.03684]. Back to page 58

[171] V. C. Rubin and W. K. Ford, Jr., *Rotation of the Andromeda Nebula from a Spectroscopic Survey of Emission Regions*, *Astrophys. J.* **159** (1970) 379. Back to page 66

[172] V. C. Rubin, N. Thonnard and W. K. Ford, Jr., *Rotational properties of 21 SC galaxies with a large range of luminosities and radii, from NGC 4605 /R = 4kpc/ to UGC 2885 /R = 122 kpc/*, *Astrophys. J.* **238** (1980) 471. Back to page 66

[173] F. Zwicky, *On the Masses of Nebulae and of Clusters of Nebulae*, *Astrophys. J.* **86** (1937) 217. Back to page 66

[174] D. Clowe, M. Bradac, A. H. Gonzalez, M. Markevitch, S. W. Randall, C. Jones et al., *A direct empirical proof of the existence of dark matter*, *Astrophys. J. Lett.* **648** (2006) L109 [astro-ph/0608407]. Back to page 68

[175] PLANCK collaboration, N. Aghanim et al., *Planck 2018 results. VI. Cosmological parameters*, *Astron. Astrophys.* **641** (2020) A6 [1807.06209]. Back to page 67

[176] S. W. Randall, M. Markevitch, D. Clowe, A. H. Gonzalez and M. Bradac, *Constraints on the Self-Interaction Cross-Section of Dark Matter from Numerical Simulations of the Merging Galaxy Cluster 1E 0657-56*, *Astrophys. J.* **679** (2008) 1173 [0704.0261]. Back to page 68

[177] S. Tulin and H.-B. Yu, *Dark Matter Self-interactions and Small Scale Structure*, *Phys. Rept.* **730** (2018) 1 [1705.02358]. Back to page 68, 89 or 118

[178] S. D. McDermott, H.-B. Yu and K. M. Zurek, *Turning off the Lights: How Dark is Dark Matter?*, *Phys. Rev. D* **83** (2011) 063509 [1011.2907]. Back to page 68 or 68

[179] C. Kouvaris, *Composite Millicharged Dark Matter*, *Phys. Rev. D* **88** (2013) 015001 [1304.7476]. Back to page 68

[180] A. D. Dolgov, S. L. Dubovsky, G. I. Rubtsov and I. I. Tkachev, *Constraints on millicharged particles from Planck data*, *Phys. Rev. D* **88** (2013) 117701 [1310.2376]. Back to page 68

[181] M. R. Lovell, C. S. Frenk, V. R. Eke, A. Jenkins, L. Gao and T. Theuns, *The properties of warm dark matter haloes*, *Mon. Not. Roy. Astron. Soc.* **439** (2014) 300 [1308.1399]. Back to page 68

[182] F. Chadha-Day, J. Ellis and D. J. E. Marsh, *Axion dark matter: What is it and why now?*, *Sci. Adv.* **8** (2022) abj3618 [2105.01406]. Back to page 69

[183] V. Silveira and A. Zee, *SCALAR PHANTOMS*, *Phys. Lett. B* **161** (1985) 136. Back to page 72

[184] J. McDonald, *Gauge singlet scalars as cold dark matter*, *Phys. Rev. D* **50** (1994) 3637 [hep-ph/0702143]. Back to page 72 or 72

[185] M. W. Goodman and E. Witten, *Detectability of Certain Dark Matter Candidates*, *Phys. Rev. D* **31** (1985) 3059. Back to page 72

[186] M. Pospelov and A. Ritz, *Higgs decays to dark matter: beyond the minimal model*, *Phys. Rev. D* **84** (2011) 113001 [1109.4872]. Back to page 72

[187] Y. Cai, X.-G. He and B. Ren, *Low Mass Dark Matter and Invisible Higgs Width In Darkon Models*, *Phys. Rev. D* **83** (2011) 083524 [1102.1522]. Back to page 72

[188] M. C. Bento, O. Bertolami and R. Rosenfeld, *Cosmological constraints on an invisibly decaying Higgs boson*, *Phys. Lett. B* **518** (2001) 276 [hep-ph/0103340]. Back to page 72

[189] C. P. Burgess, M. Pospelov and T. ter Veldhuis, *The Minimal model of nonbaryonic dark matter: A Singlet scalar*, *Nucl. Phys. B* **619** (2001) 709 [hep-ph/0011335]. Back to page 72

[190] A. Beniwal, J. Herrero-García, N. Leerdam, M. White and A. G. Williams, *The ScotoSinglet Model: a scalar singlet extension of the Scotogenic Model*, *JHEP* **21** (2020) 136 [2010.05937]. Back to page 72

[191] GAMBIT collaboration, P. Athron et al., *Global analyses of Higgs portal singlet dark matter models using GAMBIT*, *Eur. Phys. J. C* **79** (2019) 38 [1808.10465]. Back to page 72

[192] J. M. Cline, K. Kainulainen, P. Scott and C. Weniger, *Update on scalar singlet dark matter*, *Phys. Rev. D* **88** (2013) 055025 [1306.4710]. Back to page 72, 81, 84 or 85

[193] M. R. Buckley, D. Feld and D. Goncalves, *Scalar Simplified Models for Dark Matter*, *Phys. Rev. D* **91** (2015) 015017 [1410.6497]. Back to page 72

[194] J. A. Casas, D. G. Cerdeño, J. M. Moreno and J. Quilis, *Reopening the Higgs portal for single scalar dark matter*, *JHEP* **05** (2017) 036 [1701.08134]. Back to page 72, 73 or 75

[195] A. Albert et al., *Towards the next generation of simplified Dark Matter models*, *Phys. Dark Univ.* **16** (2017) 49 [1607.06680]. Back to page 72

[196] S. Bhattacharya, P. Poulose and P. Ghosh, *Multipartite Interacting Scalar Dark Matter in the light of updated LUX data*, *JCAP* **04** (2017) 043 [1607.08461]. Back to page 72

[197] A. Drozd, B. Grzadkowski and J. Wudka, *Multi-Scalar-Singlet Extension of the Standard Model - the Case for Dark Matter and an Invisible Higgs Boson*, *JHEP* **04** (2012) 006 [1112.2582]. Back to page 72

[198] Q.-H. Cao, E. Ma, J. Wudka and C. P. Yuan, *Multipartite dark matter*, 0711.3881. Back to page 72

[199] T. Alanne, N. Benincasa, M. Heikinheimo, K. Kannike, V. Keus, N. Koivunen et al., *Pseudo-Goldstone dark matter: gravitational waves and direct-detection blind spots*, *JHEP* **10** (2020) 080 [2008.09605]. Back to page 75, 78, 81, 81 or 96

[200] C. Arina, *Review on Dark Matter Tools*, *PoS* **TOOLS2020** (2021) 001 [2012.09462]. Back to page 75

[201] M. Mühlleitner, M. O. P. Sampaio, R. Santos and J. Wittbrodt, *ScannerS: Parameter Scans in Extended Scalar Sectors*, 2007.02985. Back to page 75

[202] C. Gross, O. Lebedev and T. Toma, *Cancellation Mechanism for Dark-Matter–Nucleon Interaction*, *Phys. Rev. Lett.* **119** (2017) 191801 [1708.02253]. Back to page 75, 81 or 81

[203] R. Coimbra, M. O. P. Sampaio and R. Santos, *ScannerS: Constraining the phase diagram of a complex scalar singlet at the LHC*, *Eur. Phys. J. C* **73** (2013) 2428 [1301.2599]. Back to page 75

[204] J. Elias-Miro, J. R. Espinosa, G. F. Giudice, H. M. Lee and A. Strumia, *Stabilization of the Electroweak Vacuum by a Scalar Threshold Effect*, *JHEP* **06** (2012) 031 [1203.0237]. Back to page 75

[205] H. E. Haber and Z. Surujon, *A Group-theoretic Condition for Spontaneous CP Violation*, *Phys. Rev. D* **86** (2012) 075007 [1201.1730]. Back to page 75

[206] O. Lebedev, *The Higgs Portal to Cosmology*, 2104.03342. Back to page 79

[207] T. Binder, T. Bringmann, M. Gustafsson and A. Hryczuk, *Early kinetic decoupling of dark matter: when the standard way of calculating the thermal relic density fails*, *Phys. Rev. D* **96** (2017) 115010 [1706.07433]. Back to page 80 or 117

[208] T. Binder, T. Bringmann, M. Gustafsson and A. Hryczuk, *DRAKE: Dark matter Relic Abundance beyond Kinetic Equilibrium*, 2103.01944. Back to page 80 or 80

[209] T. Abe, *The early kinetic decoupling and a pseudo-Nambu Goldstone dark matter model*, 2106.01956. Back to page 80

[210] C. Arina, A. Beniwal, C. Degrande, J. Heisig and A. Scaffidi, *Global fit of pseudo-Nambu-Goldstone Dark Matter*, *JHEP* **04** (2020) 015 [1912.04008]. Back to page 80 or 88

[211] D. Azevedo, M. Duch, B. Grzadkowski, D. Huang, M. Iglicki and R. Santos, *Testing scalar versus vector dark matter*, *Phys. Rev. D* **99** (2019) 015017 [1808.01598]. Back to page 80

[212] S. Abe, G.-C. Cho and K. Mawatari, *Probing a degenerate-scalar scenario in a pseudoscalar dark-matter model*, 2101.04887. Back to page 81

[213] S. Glaus, M. Mühlleitner, J. Müller, S. Patel, T. Römer and R. Santos, *Electroweak Corrections in a Pseudo-Nambu Goldstone Dark Matter Model Revisited*, *JHEP* **12** (2020) 034 [2008.12985]. Back to page 81

[214] K. Ishiwata and T. Toma, *Probing pseudo Nambu-Goldstone boson dark matter at loop level*, *JHEP* **12** (2018) 089 [1810.08139]. Back to page 81

[215] D. Azevedo, M. Duch, B. Grzadkowski, D. Huang, M. Iglicki and R. Santos, *One-loop contribution to dark-matter-nucleon scattering in the pseudo-scalar dark matter model*, *JHEP* **01** (2019) 138 [1810.06105]. Back to page 81

[216] XENON collaboration, E. Aprile et al., *Dark Matter Search Results from a One Ton-Year Exposure of XENON1T*, *Phys. Rev. Lett.* **121** (2018) 111302 [1805.12562]. Back to page 82, 86, 88 or 88

[217] CMS collaboration, A. M. Sirunyan et al., *Search for invisible decays of a Higgs boson produced through vector boson fusion in proton-proton collisions at* $\sqrt{s} = 13$ *TeV*, *Phys. Lett. B* **793** (2019) 520 [1809.05937]. Back to page 83

[218] G. Bélanger, F. Boudjema, A. Goudelis, A. Pukhov and B. Zaldivar, *micrOMEGAs5.0 : Freeze-in*, *Comput. Phys. Commun.* **231** (2018) 173 [1801.03509]. Back to page 83 or 120

[219] M. W. Winkler, *Decay and detection of a light scalar boson mixing with the Higgs boson*, *Phys. Rev. D* **99** (2019) 015018 [1809.01876]. Back to page 83, 83 or 85

[220] XENON collaboration, E. Aprile et al., *Physics reach of the XENON1T dark matter experiment*, *JCAP* **04** (2016) 027 [1512.07501]. Back to page 86, 88 or 88

[221] FERMI-LAT, DES collaboration, A. Albert et al., *Searching for Dark Matter Annihilation in Recently Discovered Milky Way Satellites with Fermi-LAT*, *Astrophys. J.* **834** (2017) 110 [1611.03184]. Back to page 88

[222] R. Balkin, M. Ruhdorfer, E. Salvioni and A. Weiler, *Dark matter shifts away from direct detection*, *JCAP* **11** (2018) 050 [1809.09106]. Back to page 97

[223] M. Ruhdorfer, E. Salvioni and A. Weiler, *A Global View of the Off-Shell Higgs Portal*, *SciPost Phys.* **8** (2020) 027 [1910.04170]. Back to page 97

[224] M. Pospelov, A. Ritz and M. B. Voloshin, *Secluded WIMP Dark Matter*, *Phys. Lett. B* **662** (2008) 53 [0711.4866]. Back to page 100 or 100

[225] M. Escudero, N. Rius and V. Sanz, *Sterile Neutrino portal to Dark Matter II: Exact Dark symmetry*, *Eur. Phys. J. C* **77** (2017) 397 [1607.02373]. Back to page 100, 102, 103 or 118

[226] B. Batell, T. Han and B. Shams Es Haghi, *Indirect Detection of Neutrino Portal Dark Matter*, *Phys. Rev. D* **97** (2018) 095020 [1704.08708]. Back to page 100, 102, 118 or 120

[227] M. G. Folgado, G. A. Gómez-Vargas, N. Rius and R. Ruiz De Austri, *Probing the sterile neutrino portal to Dark Matter with γ rays*, *JCAP* **08** (2018) 002 [1803.08934]. Back to page 100

[228] P. Bandyopadhyay, E. J. Chun, R. Mandal and F. S. Queiroz, *Scrutinizing Right-Handed Neutrino Portal Dark Matter With Yukawa Effect*, *Phys. Lett. B* **788** (2019) 530 [1807.05122]. Back to page 100 or 118

[229] B. Bertoni, S. Ipek, D. McKeen and A. E. Nelson, *Constraints and consequences of reducing small scale structure via large dark matter-neutrino interactions*, *JHEP* **04** (2015) 170 [1412.3113]. Back to page 100

[230] B. Batell, T. Han, D. McKeen and B. Shams Es Haghi, *Thermal Dark Matter Through the Dirac Neutrino Portal*, *Phys. Rev. D* **97** (2018) 075016 [1709.07001]. Back to page 100

[231] M. Blennow, E. Fernandez-Martinez, A. Olivares-Del Campo, S. Pascoli, S. Rosauro-Alcaraz and A. V. Titov, *Neutrino Portals to Dark Matter*, *Eur. Phys. J. C* **79** (2019) 555 [1903.00006]. Back to page 100

[232] V. Gonzalez Macias and J. Wudka, *Effective theories for Dark Matter interactions and the neutrino portal paradigm*, *JHEP* **07** (2015) 161 [1506.03825]. Back to page 101

[233] V. González-Macías, J. I. Illana and J. Wudka, *A realistic model for Dark Matter interactions in the neutrino portal paradigm*, *JHEP* **05** (2016) 171 [1601.05051]. Back to page 101

[234] M. Duch, B. Grzadkowski and J. Wudka, *Classification of effective operators for interactions between the Standard Model and dark matter*, *JHEP* **05** (2015) 116 [1412.0520]. Back to page 101 or 102

[235] J. C. Criado, A. Djouadi, M. Perez-Victoria and J. Santiago, *A complete effective field theory for dark matter*, *JHEP* **07** (2021) 081 [2104.14443]. Back to page 101

[236] J. Aebischer, W. Altmannshofer, E. E. Jenkins and A. V. Manohar, *Dark Matter Effective Field Theory and an Application to Vector Dark Matter*, 2202.06968. Back to page 101

[237] M. C. Gonzalez-Garcia, A. Santamaria and J. W. F. Valle, *Isosinglet Neutral Heavy Lepton Production in Z Decays and Neutrino Mass*, *Nucl. Phys. B* **342** (1990) 108. Back to page 102 or 103

[238] Y.-L. Tang and S.-h. Zhu, *Dark Matter Relic Abundance and Light Sterile Neutrinos*, *JHEP* **01** (2017) 025 [1609.07841]. Back to page 103 or 118

[239] M. Chianese and S. F. King, *The Dark Side of the Littlest Seesaw: freeze-in, the two right-handed neutrino portal and leptogenesis-friendly fimpzillas*, *JCAP* **09** (2018) 027 [1806.10606]. Back to page 103

[240] M. Chianese, B. Fu and S. F. King, *Minimal Seesaw extension for Neutrino Mass and Mixing, Leptogenesis and Dark Matter: FIMPzillas through the Right-Handed Neutrino Portal*, *JCAP* **03** (2020) 030 [1910.12916]. Back to page 103

[241] L. Bian and Y.-L. Tang, *Thermally modified sterile neutrino portal dark matter and gravitational waves from phase transition: The Freeze-in case*, *JHEP* **12** (2018) 006 [1810.03172]. Back to page 103

[242] P. Bandyopadhyay, E. J. Chun and R. Mandal, *Feeble neutrino portal dark matter at neutrino detectors*, *JCAP* **08** (2020) 019 [2005.13933]. Back to page 103

[243] A. Alloul, N. D. Christensen, C. Degrande, C. Duhr and B. Fuks, *FeynRules 2.0 - A complete toolbox for tree-level phenomenology*, *Comput. Phys. Commun.* **185** (2014) 2250 [1310.1921]. Back to page 104

[244] T. Hahn and M. Perez-Victoria, *Automatized one loop calculations in four-dimensions and D-dimensions*, *Comput. Phys. Commun.* **118** (1999) 153 [hep-ph/9807565]. Back to page 104

[245] P. Gondolo and G. Gelmini, *Cosmic abundances of stable particles: Improved analysis*, *Nucl. Phys. B* **360** (1991) 145. Back to page 106, 107 or 107

[246] T. Bringmann, P. F. Depta, M. Hufnagel and K. Schmidt-Hoberg, *Precise dark matter relic abundance in decoupled sectors*, *Phys. Lett. B* **817** (2021) 136341 [2007.03696]. Back to page 106, 107 or 120

[247] M. Claudson, L. J. Hall and I. Hinchliffe, *COSMOLOGICAL BARYON GENERATION AT LOW TEMPERATURES*, *Nucl. Phys. B* **241** (1984) 309. Back to page 107

[248] M. L. Graesser, *Broadening the Higgs boson with right-handed neutrinos and a higher dimension operator at the electroweak scale*, *Phys. Rev. D* **76** (2007) 075006 [0704.0438]. Back to page 113

[249] M. L. Graesser, *Experimental Constraints on Higgs Boson Decays to TeV-scale Right-Handed Neutrinos*, 0705.2190. Back to page 113

[250] A. Aparici, K. Kim, A. Santamaria and J. Wudka, *Right-handed neutrino magnetic moments*, *Phys. Rev. D* **80** (2009) 013010 [0904.3244]. Back to page 113

[251] A. Caputo, P. Hernandez, J. Lopez-Pavon and J. Salvado, *The seesaw portal in testable models of neutrino masses*, *JHEP* **06** (2017) 112 [1704.08721]. Back to page 113

[252] J. M. Butterworth, M. Chala, C. Englert, M. Spannowsky and A. Titov, *Higgs phenomenology as a probe of sterile neutrinos*, *Phys. Rev. D* **100** (2019) 115019 [1909.04665]. Back to page 113

[253] L. Lopez-Honorez, T. Schwetz and J. Zupan, *Higgs portal, fermionic dark matter, and a Standard Model like Higgs at 125 GeV*, *Phys. Lett. B* **716** (2012) 179 [1203.2064]. Back to page 113

[254] M. A. Fedderke, J.-Y. Chen, E. W. Kolb and L.-T. Wang, *The Fermionic Dark Matter Higgs Portal: an effective field theory approach*, *JHEP* **08** (2014) 122 [1404.2283]. Back to page 113

[255] GAMBIT collaboration, P. Athron et al., *Global analyses of Higgs portal singlet dark matter models using GAMBIT*, *Eur. Phys. J. C* **79** (2019) 38 [1808.10465]. Back to page 113

[256] X. G. He, G. C. Joshi, H. Lew and R. R. Volkas, *New-Z′ phenomenology*, *Phys. Rev. D* **43** (1991) 22. Back to page 113

[257] M. Gorbahn, J. M. No and V. Sanz, *Benchmarks for Higgs Effective Theory: Extended Higgs Sectors*, *JHEP* **10** (2015) 036 [1502.07352]. Back to page 115

[258] M. D. Schwartz, *Quantum Field Theory and the Standard Model*. Cambridge University Press, 3, 2014. Back to page 115

[259] J. Herrero-Garcia, E. Molinaro and M. A. Schmidt, *Dark matter direct detection of a fermionic singlet at one loop*, *Eur. Phys. J.* **C78** (2018) 471 [1803.05660]. Back to page 118

[260] A. Berlin, D. Hooper and S. D. McDermott, *Simplified Dark Matter Models for the Galactic Center Gamma-Ray Excess*, *Phys. Rev. D* **89** (2014) 115022 [1404.0022]. Back to page 118

[261] M. Escudero, S. J. Witte and N. Rius, *The dispirited case of gauged U(1)$_{B-L}$ dark matter*, *JHEP* **08** (2018) 190 [1806.02823]. Back to page 118 or 118

[262] M. Escudero, N. Rius and V. Sanz, *Sterile neutrino portal to Dark Matter I: The $U(1)_{B-L}$ case*, *JHEP* **02** (2017) 045 [1606.01258]. Back to page 118

[263] G. Belanger, F. Boudjema, A. Pukhov and A. Semenov, *MicrOMEGAs: A Program for calculating the relic density in the MSSM*, *Comput. Phys. Commun.* **149** (2002) 103 [hep-ph/0112278]. Back to page 120

[264] A. Ahriche, S. M. Boucenna and S. Nasri, *Dark Radiative Inverse Seesaw Mechanism*, *Phys. Rev. D* **93** (2016) 075036 [1601.04336]. Back to page 123

[265] J. Kumar and D. Marfatia, *Matrix element analyses of dark matter scattering and annihilation*, *Phys. Rev. D* **88** (2013) 014035 [1305.1611]. Back to page 161 or 162

[266] M. E. Peskin and D. V. Schroeder, *An Introduction to quantum field theory*. Addison-Wesley, Reading, USA, 1995. Back to page 179

APPENDIX A

Light scalars and the AMM of charged leptons

In this part we summarise the details of the relevant computations regarding the Chapter 3.

A.1 New contributions to the AMM

Here we present the contributions from scalars, ρ, pseudo-scalars, θ and vector bosons, V, to the AMM of charged leptons. Their interactions with charged leptons, f, are described by the following Lagrangians:

$$\mathcal{L}_{\rho,\theta} = h_f \overline{f} f \rho + i h_f \overline{f} \gamma_5 f \theta \,, \tag{A.1}$$

$$\mathcal{L}_V = \kappa \, J^{\mu}_{\rm em} V_{\mu} \,, \tag{A.2}$$

with the electromagnetic current $J^{\mu}_{\rm em}$ given in Equation (2.8). For completeness, we consider NP contributions to the AMM generated both at one and two-loop level, see *e.g.* Figure A.1. From the interaction Lagrangians in Equations (A.1) and (A.2), the one-loop contributions to the AMM can be written as [114, 140]:

$$a_f^{(1)} = \frac{h_f^2}{(4\pi)^2} \, I_f^{(1)}(m_f, m_\rho, m_\theta) \,, \tag{A.3}$$

$$a_{f,V}^{(1)} = \frac{\alpha}{2\pi} \, \kappa^2 \, I_V^{(1)} \left(\frac{m_f^2}{m_V^2} \right) \,, \tag{A.4}$$

where the loop functions are given by the following expressions

$$I_f^{(1)}(m_f, m_\rho, m_\theta) = I_\rho^{(1)} \left(\frac{m_f^2}{m_\rho^2} \right) + I_\theta^{(1)} \left(\frac{m_f^2}{m_\theta^2} \right) \,, \tag{A.5}$$

with

$$I_\rho^{(1)}(r) = \; 2r\int_0^1 dx \frac{x^2(2-x)}{1-x+x^2 r}\,, \tag{A.6}$$

$$I_\theta^{(1)}(r) = -2r\int_0^1 dx \frac{x^3}{1-x+x^2 r}\,, \tag{A.7}$$

$$I_V^{(1)}(r) = \; 2r\int_0^1 dx \frac{x^2(1-x)}{1-x+x^2 r}\,. \tag{A.8}$$

On the other hand, the two-loop contribution (Barr-Zee type diagrams) to the AMM due to scalars and pseudo-scalars depicted on the right-hand side of Figure A.1 is given by [140]:

$$a_f^{(\mathrm{BZ})} = -\frac{h_f^2}{(4\pi)^2}\frac{\alpha}{\pi}\sum_k \frac{m_f}{m_k}\frac{h_k}{h_f} I^{(\mathrm{BZ})}(m_k, m_\rho, m_\theta)\,, \tag{A.9}$$

where we have defined the loop functions as

$$I^{(\mathrm{BZ})}(m_k, m_\rho, m_\theta) = I_\rho^{(\mathrm{BZ})}\left(\frac{m_k^2}{m_\rho^2}\right) - I_\theta^{(\mathrm{BZ})}\left(\frac{m_k^2}{m_\theta^2}\right)\,. \tag{A.10}$$

Here, the corresponding contributions from scalars and pseudo-scalars are

$$I_\rho^{(\mathrm{BZ})}(r) = 2r\int_0^1 dx \frac{1-2x(1-x)}{x(1-x)-r}\ln\frac{x(1-x)}{r}\,, \tag{A.11}$$

$$I_\theta^{(\mathrm{BZ})}(r) = 2r\int_0^1 dx \frac{1}{x(1-x)-r}\ln\frac{x(1-x)}{r}\,. \tag{A.12}$$

In Equations (A.9) and (A.10) the letter k stands for particles that run inside the loop. Finally, the NP (scalar and pseudo-scalar) contribution to the AMM up to the two-loop level will be the sum of Equations (A.3) and (A.9), namely:

$$a_f^{(2)} = \frac{h_f^2}{(4\pi)^2}\left(I_f^{(1)}(m_f, m_\rho, m_\theta) - \frac{\alpha}{\pi}\sum_k \frac{m_f}{m_k}\frac{h_k}{h_f} I^{(\mathrm{BZ})}(m_k, m_\rho, m_\theta)\right)\,. \tag{A.13}$$

Note that in the last equation we have assumed that scalars and pseudo-scalars couple to charged fermions with the same coupling, *i.e.* $h_{f,\rho} = h_{f,\theta} \equiv h_f$.

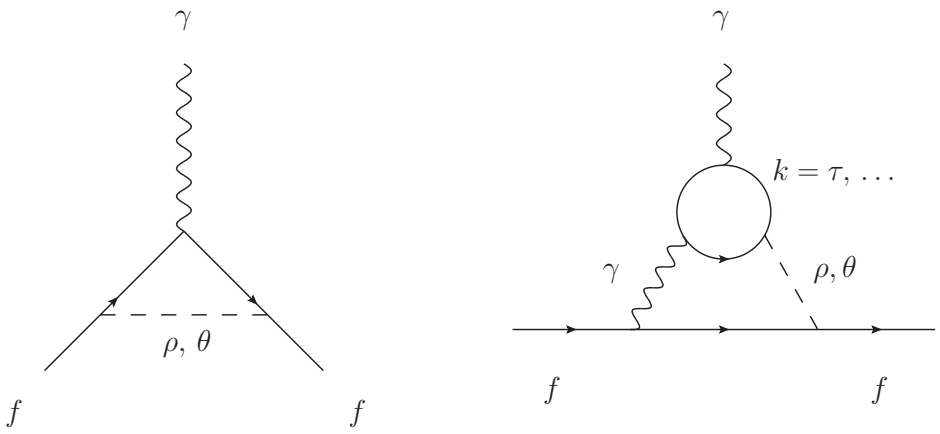

Figure A.1: *One-loop (left) and two-loop (right) contribution to the AMM of charged lepton f due to scalars and pseudo-scalars, ρ and θ, respectively.*

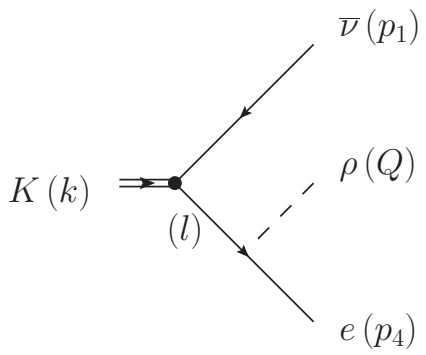

Figure A.2: *Feynman diagram of the kaon decay to electron and neutrino with the emission of the new scalar, ρ, due to the interaction given in Equation* (3.14). *l represents the momentum of the internal propagator, $l = k - p_1$.*

A.2 Rare kaon decay width calculation

The rare kaon decay process involving the scalar ρ depicted in Figure A.2, namely $K \to e\nu\rho$, is described by the following matrix element:

$$i\mathcal{M} = i\,\frac{A}{l^2 - m_e^2}\,\overline{u}_{p_4}(\not{l} + m_e)\,\not{k}\,P_L\,v_{p_1}\,, \tag{A.14}$$

where P_L is the usual left-handed chiral projector, $P_L = (1-\gamma_5)/2$, l stands for the momentum of the internal propagator, namely $l = k - p_1$, and $\overline{u}$, v are Dirac spinor fields. In order to simplify the notation, we have defined

$$A \equiv h_e\,\frac{2G_F\,\sin\theta_C\,f_K}{\sqrt{2}}\,, \tag{A.15}$$

with G_F the Fermi coupling constant, θ_C the Cabbibo angle and f_K the kaon form factor. The differential decay width is given by

$$d\Gamma = \frac{1}{2M_K}\overline{\sum_{\text{spin}}}\,|\mathcal{M}|^2\,d\phi_3\,, \tag{A.16}$$

where M_K is the kaon mass, and we are summing over the spins of the final particles and averaging on the spin of the initial particle. The 3-body phase space is defined as follows:

$$d\phi_3 \equiv \frac{1}{(2\pi)^5}\frac{d^3\vec{p}_1}{2E_1}\frac{d^3\vec{Q}}{2E_Q}\frac{d^3\vec{p}_4}{2E_4}\delta^{(4)}(k - p_1 - Q - p_4)\,. \tag{A.17}$$

Moreover, the rare kaon decay process can be split into two terms in order to simplify the computation. In particular, one can express the Equation (A.17) as a product of two 2-body phase space factors, namely

$$d\phi_3 = \frac{1}{2\pi}\,dl^2\,d\phi_2(k; p_1, l)\,d\phi_2(l; Q, p_4)\,, \tag{A.18}$$

where the 2-body phase space for the decay process $a \to bc$ is given by

$$d\phi_2(a;b,c) = \frac{1}{(2\pi)^2}\frac{d^3\vec{b}}{2E_b}\frac{d^3\vec{c}}{2E_c}\delta^{(4)}(a-b-c)\,. \tag{A.19}$$

Using Equations (A.14), (A.16) and (A.18) we can obtain the following differential decay width for the rare kaon decay:[1]

$$\begin{aligned} d\Gamma = \; & \frac{A^2}{2M_K(2\pi)}\frac{1}{(l^2-m_e^2)^2}\,dl^2\,d\phi_2(k;p_1,l)\,d\phi_2(l;Q,p_4) \\ & \cdot\left[\frac{1}{2l^2}(l^2+m_e^2-m_\rho^2)\cdot B + m_e\cdot C\right], \end{aligned} \tag{A.20}$$

with B and C given by:

$$B = \mathrm{Tr}\left\{\not{l}\,(\not{l}+m_e)\,\not{k}\,P_L\,\not{p}_1\,\not{k}\,(\not{l}+m_e)\right\}, \tag{A.21}$$

$$C = \mathrm{Tr}\left\{(\not{l}+m_e)\,\not{k}\,P_L\,\not{p}_1\,\not{k}\,(\not{l}+m_e)\right\}. \tag{A.22}$$

In addition, we define the following dimensionless quantities:

$$x \equiv \left(\frac{l}{M_K}\right)^2, \quad \omega \equiv \left(\frac{m_e}{M_K}\right)^2 \quad \text{and} \quad y \equiv \left(\frac{m_\rho}{M_K}\right)^2. \tag{A.23}$$

These definitions will be useful to simplify the notation in the derivation of the decay width from Equation (A.20). Finally, we get for the decay width:

$$\Gamma(K\to e\nu\rho) = h_e^2\,\frac{M_K^3 G_F^2\sin^2\theta_C f_K^2}{2^8\,3\,\pi^3}\,F(\omega,y)\,, \tag{A.24}$$

where the function $F(\omega,y)$ is given by

$$F(\omega,y) = 3\int_{(\sqrt{\omega}+\sqrt{y})^2}^{1} f(x,\omega,y)\,dx\,, \tag{A.25}$$

with the following function in the integrand:

$$f(x,\omega,y) = \frac{(x-1)^2(\omega^2-y(\omega+x)+6\,\omega\,x+x^2)\sqrt{\omega^2-2\,\omega\,(x+y)+(x-y)^2}}{x(\omega-x)^2}\,. \tag{A.26}$$

Now from Equation (A.24), and using that the decay width of the process $K\to e\nu$ is

$$\Gamma(K\to e\nu) = \frac{M_K^3 G_F^2\sin^2\theta_C f_K^2}{2^3\,\pi}\,\omega(1-\omega)^2\,, \tag{A.27}$$

one can get the following expression for the branching ratio of the decay $K\to e\nu\rho$:

$$\mathrm{BR}(K\to e\nu\rho) = \frac{\Gamma(K\to e\nu\rho)}{\Gamma(K\to e\nu)}\,\mathrm{BR}(K\to e\nu) = \frac{h_e^2}{96\,\pi^2}\,\frac{F(\omega,y)}{\omega(1-\omega)^2}\,\mathrm{BR}(K\to e\nu)\,. \tag{A.28}$$

[1] We are neglecting neutrino masses.

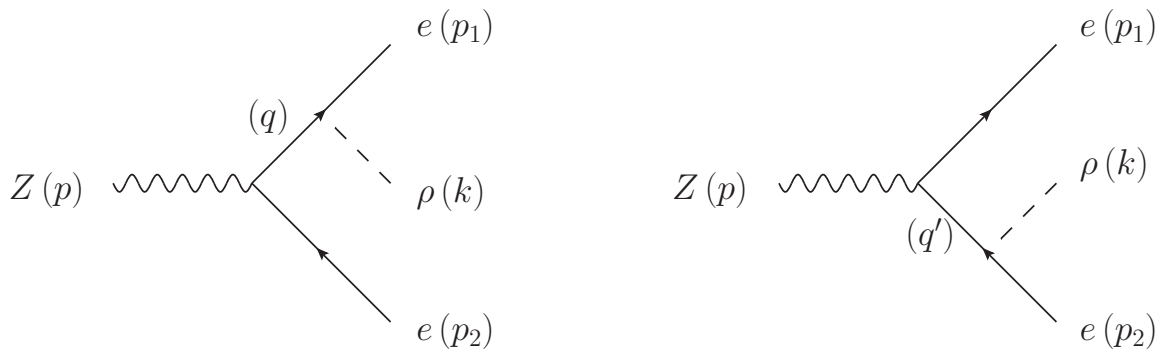

Figure A.3: *Feynman diagrams of the Z boson decay to electrons with the emission of the new scalar, ρ, due to the interaction given in Equation* (3.14). *$q = p - p_2$ and $q' = p - p_1$ represent the momentum of the internal propagators.*

A.3 Rare Z boson decay width calculation

The rare Z boson decay process involving the scalar ρ depicted in Figure A.3, namely $Z \to ee\rho$, is described by the following matrix elements:

$$i\mathcal{M}_A = -\,i\,h_e \frac{e}{2\sin\theta_W\cos\theta_W}\,\frac{1}{q^2 - m_e^2}\,\overline{u}_{p_1}(\not{q} + m_e)\not{\epsilon}(g_V^e - g_A^e\gamma_5)v_{p_2}\,, \tag{A.29}$$

$$i\mathcal{M}_B = \;\;i\,h_e \frac{e}{2\sin\theta_W\cos\theta_W}\,\frac{1}{q'^2 - m_e^2}\,\overline{u}_{p_1}\not{\epsilon}(g_V^e - g_A^e\gamma_5)(\not{q}' - m_e)v_{p_2}\,, \tag{A.30}$$

which are associated to the left and right-hand side Feynman diagrams in the aforementioned figure, respectively. Here, $q = p - p_2$ and $q' = p - p_1$ are the momentum of the internal propagators, θ_W is the Weinberg angle and $g_{V,A}^e$ are the vector and axial couplings of the electron to the Z boson, respectively. The differential decay width is given by

$$d\Gamma = \frac{1}{2M_Z}\overline{\sum_{spin}}\,|\mathcal{M}|^2\,d\phi_3\,, \tag{A.31}$$

with $|\mathcal{M}|^2 = |\mathcal{M}_A + \mathcal{M}_B|^2$ and the 3-body phase space, $d\phi_3$, defined as in Equation (A.17) but changing the corresponding momenta. Similarly to the rare kaon decay computation discussed in Appendix A.2, we can split the differential decay width as a product of two 2-body phase space terms. However, now we have an interference term due to the sum of the two diagrams depicted in Figure A.3. Finally, we get the following expression for the rare Z boson decay width:

$$\Gamma(Z \to ee\rho) = h_e^2\,\frac{\alpha}{2^5\,3^2\,\pi^2}M_Z\,\left[G(\omega, y) + I(\omega, y)\right]\,, \tag{A.32}$$

where M_Z is the Z boson mass, α the fine-structure constant, $\alpha = e^2/(4\pi)$, and we have defined $\omega = (m_e/M_Z)^2$ and $y = (m_\rho/M_Z)^2$. Moreover, the functions $G(\omega, y)$

and $I(\omega, y)$ are given by

$$G(\omega, y) = \int_{(\sqrt{\omega}+\sqrt{y})^2}^{(1-\sqrt{\omega})^2} g(x, \omega, y)\, dx\,, \tag{A.33}$$

$$I(\omega, y) = \int_{4\omega}^{(1-\sqrt{y})^2} dz \int_{\eta^-}^{\eta^+} f(z, \eta, \omega, y)\, d\eta\,, \tag{A.34}$$

with

$$\eta^{\pm} = y + \omega - \frac{1}{2z}\left((z-1+y)z \mp \lambda^{1/2}(z,1,y)\lambda^{1/2}(z,\omega,\omega)\right)\,. \tag{A.35}$$

Here we have used the so called Källén function:

$$\lambda(a,b,c) = a^2 + b^2 + c^2 - 2(ab + ac + bc)\,. \tag{A.36}$$

The integrands in Equations (A.33) and (A.34) are given by the following complicated functions:

$$\begin{aligned} g(x,\omega,y) =& -\frac{\lambda^{1/2}(1,\omega,x)\lambda^{1/2}(x,\omega,y)}{x^2(x-\omega)^2} \\ & \Big\{\omega^4 + \omega^3\,(4x - y + 1) - \omega^2\left(10x^2 - x\,(y+31) + y + 2\right) \\ & + \omega\left(4x^3 + x^2\,(y+31) - 2x\,(7y+6) + 2y\right) + x\left(x^2 + x - 2\right)(x-y)\Big\}\,, \\ f(z,\eta,\omega,y) =& \frac{2}{(\omega-\eta)(\omega-z+y-\eta+1)}\Big\{4\omega^3 + \omega^2\,(-3z + 4y - 8\eta + 34) \\ & + \omega\left(z^2 + z\,(-3y + 2\eta - 9) - 4y\eta + 2\,(y-3)\,y + 4\eta^2\right) \\ & + y\,(-\eta z + 2z + 2\eta - 2) + (z-2)\,\eta\,(z + \eta - 1)\Big\}\,. \end{aligned} \tag{A.37}$$

Now from Equation (A.32), and using that the decay width of the process $Z \to ee$ is

$$\Gamma(Z \to ee) = \frac{\alpha}{12 s_W^2 c_W^2}(g_V^2 + g_A^2) M_Z\,(1-4\omega)^{3/2} \simeq \frac{\alpha}{3^2} M_Z\,(1-4\omega)^{3/2}\,, \tag{A.38}$$

one can get the following expression for the branching ratio of the decay $Z \to ee\rho$:

$$\mathrm{BR}(Z \to ee\rho) = \frac{h_e^2}{32\,\pi^2}\frac{[G(\omega,y) + I(\omega,y)]}{(1-4\omega)^{3/2}}\,\mathrm{BR}(Z \to ee)\,. \tag{A.39}$$

APPENDIX B

Dark Matter from a complex scalar singlet

In this part we summarise the details of the relevant computations regarding the Chapter 5.

Relevant interactions for the *minimal models*

For the analysis of the DM phenomenology of the *minimal models*, it is useful to write the relevant part of the Lagrangian interaction as:

$$-\mathcal{L} \supset \frac{1}{2}\left(\beta_{h\theta\theta}\theta^2 + \beta_{h\rho\rho}\rho^2\right) h + \frac{1}{2}\beta_{\rho\theta\theta}\theta^2\rho\,. \tag{B.1}$$

The expressions for the β_i coefficients are given in Table B.1 for each *minimal model*.

	Linear	Quadratic
$\beta_{h\theta\theta}$	$\frac{s_\alpha\left(m_\theta^2 - m_h^2\right)}{v_s}$	$-\frac{m_h^2 s_\alpha}{v_s}$
$\beta_{\rho\theta\theta}$	$-\frac{c_\alpha\left(m_\theta^2 - m_\rho^2\right)}{v_s}$	$\frac{m_\rho^2 c_\alpha}{v_s}$
$\beta_{h\rho\rho}$	$c_\alpha s_\alpha\left(\frac{s_\alpha\left(m_h^2 + 2m_\rho^2\right)}{v} - \frac{c_\alpha\left(m_h^2 - 3m_\theta^2 + 2m_\rho^2\right)}{v_s}\right)$	$-\frac{c_\alpha s_\alpha\left(m_h^2 + 2m_\rho^2\right)\left(v c_\alpha - s_\alpha v_s\right)}{v v_s}$

	Cubic	Quartic
$\beta_{h\theta\theta}$	$-\frac{s_\alpha\left(m_h^2 + m_\theta^2\right)}{v_s}$	$-\frac{s_\alpha\left(m_h^2 + 2m_\theta^2\right)}{v_s}$
$\beta_{\rho\theta\theta}$	$\frac{c_\alpha\left(m_\rho^2 + m_\theta^2\right)}{v_s}$	$\frac{c_\alpha\left(m_\rho^2 + 2m_\theta^2\right)}{v_s}$
$\beta_{h\rho\rho}$	$\frac{1}{3}c_\alpha s_\alpha\left(\frac{3s_\alpha\left(m_h^2 + 2m_\rho^2\right)}{v} - \frac{c_\alpha\left(3m_h^2 + m_\theta^2 + 6m_\rho^2\right)}{v_s}\right)$	$-\frac{c_\alpha s_\alpha\left(m_h^2 + 2m_\rho^2\right)\left(v c_\alpha - s_\alpha v_s\right)}{v v_s}$

Table B.1: *Expressions for the β_i coefficients particularised for the minimal models in terms of the physical parameters. Note that $\beta_{\rho\theta\theta}$ can be obtained from $\beta_{h\theta\theta}$ by means of the following substitutions: $s_\alpha \to -c_\alpha$ and $m_h^2 \to m_\rho^2$.*

APPENDIX C

Sterile neutrino portals to Majorana DM

In this part we summarise the details of the relevant computations regarding the Chapter 6.

C.1 Alternative discussion on DM annihilations

The relic abundance is set by DM annihilations $\chi\chi \to NN$, with χ and N being Majorana fermions.

On the one hand, the initial state i formed by a (identical) pair of Majorana particles has an anti-symmetric wave function defined by

$$(-1)^{L^i}(-1)^{S^i+1} = -1\,, \tag{C.1}$$

with the spin and the orbital angular momentum of the pair denoted by S^i and L^i, respectively. Therefore, we derive that $L^i + S^i$ must be even. Moreover, regarding the final pair f, if we take the z-axis to lie along the direction of motion of the outgoing particles we have $L_z^f = 0$, see *e.g.* Ref. [265], then $J_z^f = S_z^f$. Here J stands for the total angular momentum.

On the other hand, we can analyse the final state generated by the portal operators in Equations (6.5)–(6.7), with some considerations regarding the mass of the sterile neutrinos.

- **Operator $\mathcal{O}_1$.** For $m_N = 0$, N_R can be described by a Weyl fermion. The operator generates a pair $\overline{N_R}\,, N_R$, with opposite helicities, namely $+1/2$ $(-1/2)$ for N_R $(\overline{N_R})$. In this case, the spins are aligned and $\left|S_z^f\right| = 1$. Moreover, from the conservation of the total angular momentum we get $\left|J_z^i\right| = \left|J_z^f\right| = 1$. Since $L^i + S^i$ must be even, the lowest order combination that can realise $\left|J_z^i\right| = 1$ is $S^i = L^i = 1$. This selection for the orbital angular momentum of the initial pair leads

to p-wave suppressed DM annihilation cross section, see *e.g.* Equations (6.15) and (6.16).

For $m_N \neq 0$, there can be a helicity flip thanks to a sterile neutrino mass insertion, and we can get also the possibility $S_z^f = 0$. This scenario yields the s-wave proportional to m_N^2, in agreement with Equation (6.13).

- **Operator $\mathcal{O}_2$ ($\mathcal{O}_3$).** For $m_N = 0$, this operator generates a pair $N_R\,, N_R$ ($\overline{N_R}\,, \overline{N_R}$), both states with the same helicity. In this case, the spins are anti-aligned and $S_z^f = 0$. Moreover, from the conservation of the total angular momentum we get $J_z^i = J_z^f = 0$, and at the lowest order we have $S^i = L^i = 0$. This selection for the orbital angular momentum of the initial pair leads to s-wave DM annihilation cross section, in agreement with Equations (6.15).

Let us now try to understand the fact that the s-wave vanishes if $c_1 = 0$ and $c_2 = -2c_3^*$, see *e.g.* Equation (6.13). For this, it is interesting to express the Lagrangian in Equation (6.4) in terms of fermion bilinears, which have definite transformation properties under parity. Then, we can write

$$\begin{aligned}\mathcal{L}_6 =& \frac{1}{4\Lambda^2}\Bigg\{ \frac{c_1}{2}\,(\overline{\chi}\gamma_\mu\gamma_5\chi)(\overline{N}\gamma^\mu\gamma_5 N) \\ &+ (2\,\mathrm{Re}\,c_3 - \mathrm{Re}\,c_2)\,(\overline{\chi}\chi)(\overline{N}N) + (2\,\mathrm{Im}\,c_3 + \mathrm{Im}\,c_2)\,(\overline{\chi}\chi)(i\overline{N}\gamma_5 N) \\ &+ (\mathrm{Re}\,c_2 + 2\,\mathrm{Re}\,c_3)\,(i\overline{\chi}\gamma_5\chi)(i\overline{N}\gamma_5 N) + (\mathrm{Im}\,c_2 - 2\,\mathrm{Im}\,c_3)\,(i\overline{\chi}\gamma_5\chi)(\overline{N}N)\Bigg\}\,. \end{aligned} \tag{C.2}$$

Moreover, a state formed by a pair of Majorana particles has parity P given by

$$P = (-1)^{L+1}\,, \tag{C.3}$$

with L being the orbital angular momentum of the pair. Now, regarding the bilinears in Equation (C.2) we have:

- **Bilinear $\overline{\chi}\chi$.** It annihilates a pair of DM particles with $P = +1$, which at the lowest order corresponds to $L = 1$, see *e.g.* Ref. [265].[1] This selection for the orbital momentum implies that the DM annihilation cross section is p-wave.
- **Bilinear $i\overline{\chi}\gamma_5\chi$.** It annihilates a pair of DM particles with $L = 0$, which corresponds to s-wave DM annihilation cross section.
- **Bilinear $\overline{\chi}\gamma_\mu\gamma_5\chi$.** Its zeroth component has $P = -1$, whereas the spatial components have $P = +1$, so the bilinear contributes to both s- and p-waves.

Therefore, we conclude that for having p-wave DM annihilation cross section, the terms in the Lagrangian in Equation (C.2) which involves the bilinears $i\overline{\chi}\gamma_5\chi$ and $\overline{\chi}\gamma_0\gamma_5\chi$ should be absent. This restriction on the bilinears in the Lagrangian yields $c_1 = 0$ and $c_2 = -2c_3^*$.

[1] The same conclusion can be obtained using $CP = (-1)^{S+1} = 1$ and the antisymmetry of the wave function, which together imply $L = S = 1$.

C.2 Integrating out heavy mediators in Models A

Model A2

The Lagrangian of the model can be written as

$$\mathcal{L}_{\text{A2}} \supset \left(\partial_\mu \sigma\right)^* \left(\partial^\mu \sigma\right) - m_\sigma^2 \left|\sigma\right|^2 - \frac{1}{2}\mu_\sigma^2 \left(\sigma^2 + \sigma^{*2}\right) - f\overline{N}\left[\sigma P_L + \sigma^* P_R\right]\chi\,, \tag{C.4}$$

where we have also added the lepton number violating term in the scalar potential from Model A2c in Equation (6.35), μ_σ^2, to get the most general expressions after integrating out the complex scalar σ. Therefore, to obtain the Wilson coefficient for Models A2a and A2b, we take $\mu_\sigma^2 = 0$. Note that we have not included the λ_σ and $\lambda_{\sigma H}$ terms in the scalar potential in Equation (6.34) since they would lead to higher-dimensional operators we are not interested in.

Now, using the EoM for σ and σ^* we get

$$\left(\partial^2 + m_\sigma^2\right)\sigma^* + f\overline{N}P_L\chi + \mu_\sigma^2\sigma = 0\,, \tag{C.5}$$

$$\left(\partial^2 + m_\sigma^2\right)\sigma + f\overline{N}P_R\chi + \mu_\sigma^2\sigma^* = 0\,. \tag{C.6}$$

In addition, assuming that the momentum of the complex scalar, corresponding to the derivative, is much smaller than its mass (for the EFT approach to hold), we obtain the following expressions for the complex scalar field:

$$\sigma^* \simeq -\frac{f}{m_\sigma^2}\overline{N}P_L\chi - \frac{\mu_\sigma^2}{m_\sigma^2}\sigma\,, \tag{C.7}$$

$$\sigma \simeq -\frac{f}{m_\sigma^2}\overline{N}P_R\chi - \frac{\mu_\sigma^2}{m_\sigma^2}\sigma^*\,. \tag{C.8}$$

Substituting back Equation (C.7) into (C.8) and vice versa, one gets

$$\sigma^* \simeq -\frac{f}{m_\sigma^2}\overline{N}P_L\chi + \frac{f\mu_\sigma^2}{m_\sigma^4}\overline{N}P_R\chi + \frac{\mu_\sigma^4}{m_\sigma^4}\sigma^*\,, \tag{C.9}$$

$$\sigma \simeq -\frac{f}{m_\sigma^2}\overline{N}P_R\chi + \frac{f\mu_\sigma^2}{m_\sigma^4}\overline{N}P_L\chi + \frac{\mu_\sigma^4}{m_\sigma^4}\sigma\,. \tag{C.10}$$

We will keep only the terms $\mathcal{O}\left(1/m_\sigma^4\right)$. Since at leading order σ goes as $\mathcal{O}\left(1/m_\sigma^2\right)$, we can safely drop the last term in both equations. Now, we can rewrite the Lagrangian in Equation (C.4) as:

$$\begin{aligned}\mathcal{L}_{\text{A2}} \supset\ & \frac{1}{2}\partial_\mu\left(\sigma\partial_\mu\sigma^* + \sigma^*\partial_\mu\sigma\right) - \frac{1}{2}f\overline{N}\left[\sigma P_L + \sigma^* P_R\right]\chi \\ & - \frac{1}{2}\sigma\left[\left(\partial^2 + m_\sigma^2\right)\sigma^* + f\overline{N}P_L\chi + \mu_\sigma^2\sigma\right] \\ & - \frac{1}{2}\sigma^*\left[\left(\partial^2 + m_\sigma^2\right)\sigma + f\overline{N}P_R\chi + \mu_\sigma^2\sigma^*\right]\,.\end{aligned} \tag{C.11}$$

Moreover, in the last equation we can omit the total derivative term in the first line, whereas the second and the third ones are zero by Equations (C.5) and (C.6). Therefore we get the Lagrangian

$$\mathcal{L}_{\text{A2}} \supset -\frac{1}{2} f \overline{N} \left[\sigma P_L + \sigma^* P_R\right] \chi \,, \tag{C.12}$$

which after substituting back the expressions for the complex scalar field in Equations (C.9) and (C.10) (neglecting their last terms) yields the following effective interactions:

$$\begin{aligned} \mathcal{L}_{\text{A2}}^{\text{eff}} = \; & \frac{f^2}{m_\sigma^2} \left(\overline{N} P_L \chi\right) \left(\overline{\chi} P_R N\right) \\ & - \frac{f^2 \mu_\sigma^2}{2 m_\sigma^4} \left(\overline{N} P_L \chi\right) \left(\overline{N} P_L \chi\right) - \frac{f^2 \mu_\sigma^2}{2 m_\sigma^4} \left(\overline{N} P_R \chi\right) \left(\overline{N} P_R \chi\right) \,. \end{aligned} \tag{C.13}$$

Finally, this effective Lagrangian can be expressed in terms of the portal operators as:

$$\mathcal{L}_{\text{A2}}^{\text{eff}} = \frac{f^2}{m_\sigma^2} \mathcal{O}_1 - \frac{f^2 \mu_\sigma^2}{2 m_\sigma^4} \left[\mathcal{O}_2 + \mathcal{O}_2{}^\dagger\right] \,. \tag{C.14}$$

Alternatively, one can express the complex scalar in terms of its real and imaginary parts, *i.e.* $\sigma = (\rho + i\theta)/\sqrt{2}$. Then, the Lagrangian in Equation (C.4) reads

$$\begin{aligned} \mathcal{L}_{\text{A2}} \supset \; & \frac{1}{2} \left(\partial_\mu \rho\right)^2 - \frac{1}{2} m_\rho^2 \rho^2 + \frac{1}{2} \left(\partial_\mu \theta\right)^2 - \frac{1}{2} m_\theta^2 \theta^2 \\ & - \frac{1}{\sqrt{2}} f \left[\overline{N} P_L \chi + \overline{N} P_R \chi\right] \rho - \frac{i}{\sqrt{2}} f \left[\overline{N} P_L \chi - \overline{N} P_R \chi\right] \theta \,, \end{aligned} \tag{C.15}$$

where

$$m_\rho^2 = m_\sigma^2 + \mu_\sigma^2 \qquad \text{and} \qquad m_\theta^2 = m_\sigma^2 - \mu_\sigma^2 \,. \tag{C.16}$$

Using the Lagrangian in Eq. (C.15), we obtain the EoM for ρ and θ:

$$\partial^2 \rho + m_\rho^2 \rho + \frac{1}{\sqrt{2}} f \left[\overline{N} P_L \chi + \overline{N} P_R \chi\right] = 0 \,, \tag{C.17}$$

$$\partial^2 \theta + m_\theta^2 \theta + \frac{i}{\sqrt{2}} f \left[\overline{N} P_L \chi - \overline{N} P_R \chi\right] = 0 \,. \tag{C.18}$$

Neglecting the derivative terms, we have

$$\rho \simeq -\frac{1}{\sqrt{2} m_\rho^2} f \left[\overline{N} P_L \chi + \overline{N} P_R \chi\right] \,, \tag{C.19}$$

$$\theta \simeq -\frac{i}{\sqrt{2} m_\theta^2} f \left[\overline{N} P_L \chi - \overline{N} P_R \chi\right] \,. \tag{C.20}$$

Now, we can rewrite the Lagrangian in Equation (C.15) as:

$$\begin{aligned}\mathcal{L}_{\text{A2}} \supset & -\frac{1}{2}\rho\left[\partial^2\rho + m_\rho^2\rho + \frac{1}{\sqrt{2}}f\left[\overline{N}P_L\chi + \overline{N}P_R\chi\right]\right] \\ & -\frac{1}{2}\theta\left[\partial^2\theta + m_\theta^2\theta + \frac{i}{\sqrt{2}}f\left[\overline{N}P_L\chi - \overline{N}P_R\chi\right]\right] \\ & -\frac{1}{2\sqrt{2}}f\left[\overline{N}P_L\chi + \overline{N}P_R\chi\right]\rho - \frac{i}{2\sqrt{2}}f\left[\overline{N}P_L\chi - \overline{N}P_R\chi\right]\theta\,. \end{aligned} \tag{C.21}$$

In the last equation, the first and the second lines are zero by Equations (C.17) and (C.18), and also substituting back the expressions for ρ and θ in Equations (C.19) and (C.20) we get the following effective Lagrangian

$$\begin{aligned}\mathcal{L}_{\text{A2}}^{\text{eff}} = & \frac{f^2}{2}\left(\frac{1}{m_\rho^2} + \frac{1}{m_\theta^2}\right)\left(\overline{N}P_L\chi\right)\left(\overline{\chi}P_R N\right) \\ & + \frac{f^2}{4}\left(\frac{1}{m_\rho^2} - \frac{1}{m_\theta^2}\right)\left[\left(\overline{N}P_L\chi\right)\left(\overline{N}P_L\chi\right) + \left(\overline{N}P_R\chi\right)\left(\overline{N}P_R\chi\right)\right]\,, \end{aligned} \tag{C.22}$$

which can be expressed in terms of the portal operators:

$$\mathcal{L}_{\text{A2}}^{\text{eff}} = \frac{f^2}{2}\left(\frac{1}{m_\rho^2} + \frac{1}{m_\theta^2}\right)\mathcal{O}_1 + \frac{f^2}{4}\left(\frac{1}{m_\rho^2} - \frac{1}{m_\theta^2}\right)\left[\mathcal{O}_2 + \mathcal{O}_2{}^\dagger\right]\,. \tag{C.23}$$

Finally, assuming $\mu_\sigma^2/m_\sigma^2 \ll 1$, we can expand

$$\frac{1}{m_\rho^2} = \frac{1}{m_\sigma^2} - \frac{\mu_\sigma^2}{m_\sigma^4} + \mathcal{O}\left(\frac{1}{m_\sigma^6}\right) \qquad \text{and} \qquad \frac{1}{m_\theta^2} = \frac{1}{m_\sigma^2} + \frac{\mu_\sigma^2}{m_\sigma^4} + \mathcal{O}\left(\frac{1}{m_\sigma^6}\right)\,. \tag{C.24}$$

Substituting these expressions in Equation (C.23) we recover Equation (C.14).

C.3 Integrating out heavy mediators in Models B

Model B1

The Lagrangian of the model can be written as

$$\begin{aligned}\mathcal{L}_{\text{B1}} \supset\ & \frac{1}{2}\left(\partial_\mu\phi\right)\left(\partial^\mu\phi\right) - \frac{1}{2}m_\phi^2\phi^2 \\ & - \phi\left[f\overline{N}P_R N + g\overline{\chi}P_L\chi + f^*\overline{N}P_L N + g^*\overline{\chi}P_R\chi + \mu_{\phi H}\left|H\right|^2\right]. \end{aligned} \tag{C.25}$$

Note that we have included the $\mu_{\phi H}$ term in the scalar potential in Equation (6.37) because it will generate $D = 5$ operators. Now, using the EoM for the scalar ϕ we get

$$\left(\partial^2 + m_\phi^2\right)\phi + \left[f\overline{N}P_R N + g\overline{\chi}P_L\chi + f^*\overline{N}P_L N + g^*\overline{\chi}P_R\chi + \mu_{\phi H}\left|H\right|^2\right] = 0\,. \tag{C.26}$$

In addition, assuming that the momentum of the real scalar, corresponding to the derivative, is much smaller than its mass (for the EFT approach to hold), we obtain the following expressions for the scalar field:

$$\phi \simeq -\frac{1}{m_\phi^2}\left[f\overline{N}P_R N + g\overline{\chi}P_L\chi + f^*\overline{N}P_L N + g^*\overline{\chi}P_R\chi + \mu_{\phi H}\left|H\right|^2\right]. \tag{C.27}$$

Now, we can rewrite the Lagrangian in Equation (C.25) as:

$$\begin{aligned}\mathcal{L}_{\text{B1}} \supset\ & \frac{1}{2}\partial_\mu\left(\phi\partial_\mu\phi\right) \\ & - \frac{1}{2}\phi\left[\left(\partial^2 + m_\phi^2\right)\phi + \left[f\overline{N}P_R N + g\overline{\chi}P_L\chi + f^*\overline{N}P_L N + g^*\overline{\chi}P_R\chi + \mu_{\phi H}\left|H\right|^2\right]\right] \\ & - \frac{1}{2}\phi\left[f\overline{N}P_R N + g\overline{\chi}P_L\chi + f^*\overline{N}P_L N + g^*\overline{\chi}P_R\chi + \mu_{\phi H}\left|H\right|^2\right]. \end{aligned} \tag{C.28}$$

Moreover, in the last equation we can omit the total derivative term in the first line, whereas the second line is zero by Equation (C.26). Therefore we get the Lagrangian

$$\mathcal{L}_{\text{B1}} \supset -\frac{1}{2}\phi\left[f\overline{N}P_R N + g\overline{\chi}P_L\chi + f^*\overline{N}P_L N + g^*\overline{\chi}P_R\chi + \mu_{\phi H}\left|H\right|^2\right], \tag{C.29}$$

which after substituting back the expressions for the real scalar field in Equation (C.27) yields the following effective interactions:

$$\begin{aligned}\mathcal{L}_{\text{B1}}^{\text{eff}} = & \left[\frac{fg}{m_\phi^2}\left(\overline{N}P_R N\right)\left(\overline{\chi}P_L\chi\right) + \frac{fg^*}{m_\phi^2}\left(\overline{N}P_R N\right)\left(\overline{\chi}P_R\chi\right) + \text{H.c.}\right] \\ & + \left[\frac{f^2}{2m_\phi^2}\left(\overline{N}P_R N\right)^2 + \frac{g^2}{2m_\phi^2}\left(\overline{\chi}P_L\chi\right)^2 + \text{H.c.}\right] \\ & + \frac{\left|f\right|^2}{m_\phi^2}\left(\overline{N}P_R N\right)\left(\overline{N}P_L N\right) + \frac{\left|g\right|^2}{m_\phi^2}\left(\overline{\chi}P_L\chi\right)\left(\overline{\chi}P_R\chi\right) \\ & + \left[\frac{f\mu_{\phi H}}{m_\phi^2}\left(\overline{N}P_R N\right) + \frac{g\mu_{\phi H}}{m_\phi^2}\left(\overline{\chi}P_L\chi\right) + \text{H.c.}\right]\left|H\right|^2 + \frac{\mu_{\phi H}^2}{2m_\phi^2}\left|H\right|^4. \end{aligned} \tag{C.30}$$

The second line vanishes identically because we only consider one generation of N_R and χ_L, whereas the last term in the last line is just a correction to the quartic coupling of the Higgs field.

Finally, this effective Lagrangian can be expressed in terms of the operators defined in Table 6.1 using also the Fierz transformed version of $\mathcal{O}_2$ in Equation (6.6). Therefore, we get:

$$\begin{aligned}\mathcal{L}_{\text{B1}}^{\text{eff}} = & \left[\frac{fg}{m_\phi^2}\mathcal{O}_3 - \frac{2fg^*}{m_\phi^2}\mathcal{O}_2{}^\dagger + \text{H.c.}\right] + \frac{|f|^2}{m_\phi^2}\mathcal{O}_4 + \frac{|g|^2}{m_\phi^2}\mathcal{O}_5 \\ & + \left[\frac{f\mu_{\phi H}}{m_\phi^2}\mathcal{O}_{NH} + \frac{g\mu_{\phi H}}{m_\phi^2}\mathcal{O}_{\chi H} + \text{H.c.}\right] . \end{aligned} \tag{C.31}$$

Model B2

The scalar potential of the model is

$$V = V(\sigma, H) + V_{\text{SM}} , \tag{C.32}$$

with $V(\sigma, H)$ given in Equation (6.34), and we have also explicitly written the SM scalar potential

$$V_{\text{SM}} = m_H^2 |H|^2 + \lambda_H |H|^4 . \tag{C.33}$$

Then, using the exponential parameterisation for the complex scalar σ in Equation (6.44), and after minimising the potential V, one gets:

$$V = \frac{1}{2}m_s^2 s^2 \left(1 + \frac{s}{v_\sigma} + \frac{s^2}{4v_\sigma^2}\right) + \frac{1}{2}\lambda_{\sigma H} v_\sigma^2 \left(1 + \frac{s}{v_\sigma}\right)^2 |H|^2 . \tag{C.34}$$

In the minimisation of the potential we get $m_\sigma^2 \simeq -\lambda_\sigma v_\sigma^2$ (assuming $\lambda_\sigma \gg \lambda_{\sigma H}$), and the expression for the mass of the radial mode is $m_s^2 = 2\lambda_\sigma v_\sigma^2$. In our EFT approach, we are interested in the effective operators generated when the heavy mediator s is integrated out. Regarding this, we assume that its mass is larger than the EW scale, and therefore in the following we work in the unbroken phase of the EW symmetry.

On the other hand, from the kinetic term of the complex scalar σ we have:

$$|\partial\sigma|^2 = \frac{1}{2}(\partial s)^2 + \frac{1}{2}(\partial J)^2 + \frac{s}{v_\sigma}\left(1 + \frac{s}{2v_\sigma}\right)(\partial J)^2 , \tag{C.35}$$

and the Lagrangian of the model, keeping only the dominant pieces in $1/v_\sigma$, yields

$$\begin{aligned}\mathcal{L}_{\text{B2}} \supset & \frac{1}{2}(\partial s)^2 - \frac{1}{2}m_s^2 s^2 + \frac{s}{v_\sigma}(\partial J)^2 - \lambda_{\sigma H} v_\sigma |H|^2 s \\ & - \frac{(v_\sigma + s)}{\sqrt{2}}\left[f\overline{N_R^c}N_R + g\overline{\chi_L}\chi_L^c + \text{H.c.}\right] , \end{aligned} \tag{C.36}$$

where we have removed the Majoron from the Yukawa interaction by means of the chiral fermion fields redefinition in Equation (6.46). Now, using the EoM for s, given by

$$\left(\partial^2 + m_s^2\right) s - \frac{(\partial J)^2}{v_\sigma} + \lambda_{\sigma H} v_\sigma \left|H\right|^2 + \frac{1}{\sqrt{2}}\left[f\overline{N_R^c} N_R + g\overline{\chi_L}\chi_L^c + \text{H.c.}\right] = 0\,, \tag{C.37}$$

we can get the following expression for the field s:

$$s \simeq \frac{1}{m_s^2}\left[\frac{(\partial J)^2}{v_\sigma} - \lambda_{\sigma H} v_\sigma \left|H\right|^2 - \frac{1}{\sqrt{2}}\left[f\overline{N_R^c} N_R + g\overline{\chi_L}\chi_L^c + \text{H.c.}\right]\right]. \tag{C.38}$$

In the last equation we apply that the momentum of s, corresponding to the derivative, is assumed to be much smaller than its mass.

Moreover, we can rewrite the Lagrangian in Equation (C.36) as

$$\begin{aligned}\mathcal{L}_{\text{B2}} \supset\ & \frac{1}{2}\partial_\mu\left(s\partial_\mu s\right) - \frac{1}{2}s\left[-\frac{(\partial J)^2}{v_\sigma} + \lambda_{\sigma H} v_\sigma \left|H\right|^2 + \frac{1}{\sqrt{2}}\left[f\overline{N_R^c} N_R + g\overline{\chi_L}\chi_L^c + \text{H.c.}\right]\right] \\ & - \frac{1}{2}s\left[\left(\partial^2 + m_s^2\right) s - \frac{(\partial J)^2}{v_\sigma} + \lambda_{\sigma H} v_\sigma \left|H\right|^2 + \frac{1}{\sqrt{2}}\left[f\overline{N_R^c} N_R + g\overline{\chi_L}\chi_L^c + \text{H.c.}\right]\right] \\ & - \frac{v_\sigma}{\sqrt{2}}\left[f\overline{N_R^c} N_R + g\overline{\chi_L}\chi_L^c + \text{H.c.}\right]. \end{aligned} \tag{C.39}$$

In the last equation we can omit the total derivative term in the first line, whereas the second line is zero by Equation (C.37). In addition, the third line gives the masses for the new chiral fermions, namely

$$\mathcal{L}_{\text{B2}}^{\text{mass}} \supset -\left[\frac{1}{2} m_N \overline{N_R^c} N_R + \frac{1}{2} m_\chi \overline{\chi_L}\chi_L^c + \text{H.c.}\right], \tag{C.40}$$

with

$$m_N = \sqrt{2} f v_\sigma \quad \text{and} \quad m_\chi = \sqrt{2} g v_\sigma\,. \tag{C.41}$$

In view of that, the relevant part of the Lagrangian for obtaining the effective interactions is

$$\mathcal{L}_{\text{B2}} \supset \frac{1}{2}s\left[\frac{(\partial J)^2}{v_\sigma} - \lambda_{\sigma H} v_\sigma \left|H\right|^2 - \frac{1}{\sqrt{2}}\left[f\overline{N_R^c} N_R + g\overline{\chi_L}\chi_L^c + \text{H.c.}\right]\right], \tag{C.42}$$

which after substituting back the expressions for the radial part s in Equation (C.38)

yields the following effective interactions:

$$\begin{aligned}\mathcal{L}^{\text{eff}}_{\text{B2}} = & \left[\frac{fg}{2m_s^2}\left(\overline{N_R^c}N_R\right)\left(\overline{\chi_L}\chi_L^c\right) + \frac{fg}{2m_s^2}\left(\overline{N_R^c}N_R\right)\left(\overline{\chi_L^c}\chi_L\right) + \text{H.c.}\right] \\ & + \frac{f^2}{2m_s^2}\left(\overline{N_R^c}N_R\right)\left(\overline{N_R}N_R^c\right) + \frac{g^2}{2m_s^2}\left(\overline{\chi_L}\chi_L^c\right)\left(\overline{\chi_L^c}\chi_L\right) \\ & + \frac{\lambda_{\sigma H}v_\sigma}{\sqrt{2}m_s^2}\left[f\overline{N_R^c}N_R + g\overline{\chi_L}\chi_L^c + \text{H.c.}\right]|H|^2 \\ & - \frac{1}{\sqrt{2}m_s^2 v_\sigma}\left[f\overline{N_R^c}N_R + g\overline{\chi_L}\chi_L^c + \text{H.c.}\right](\partial J)^2 \\ & + \frac{1}{2m_s^2 v_\sigma^2}(\partial J)^4 + \frac{\lambda_{\sigma H}^2 v_\sigma^2}{2m_s^2}|H|^4 - \frac{\lambda_{\sigma H}}{m_s^2}(\partial J)^2|H|^2\,. \end{aligned} \tag{C.43}$$

Finally, this effective Lagrangian can be expressed in terms of the operators defined in Table 6.1 using also the Fierz transformed version of $\mathcal{O}_2$ in Equation (6.6). Therefore, we get:

$$\begin{aligned}\mathcal{L}^{\text{eff}}_{\text{B2}} = & \left[-\frac{fg}{m_s^2}\mathcal{O}_2{}^\dagger + \frac{fg}{2m_s^2}\mathcal{O}_3 + \text{H.c.}\right] + \frac{f^2}{2m_s^2}\mathcal{O}_4 + \frac{g^2}{2m_s^2}\mathcal{O}_5 \\ & + \left[\frac{f\lambda_{\sigma H}v_\sigma}{\sqrt{2}m_s^2}\mathcal{O}_{NH} + \frac{g\lambda_{\sigma H}v_\sigma}{\sqrt{2}m_s^2}\mathcal{O}_{\chi H}{}^\dagger + \text{H.c.}\right] \\ & - \frac{1}{\sqrt{2}m_s^2 v_\sigma}\left[f\overline{N_R^c}N_R + g\overline{\chi_L}\chi_L^c + \text{H.c.}\right](\partial J)^2 \\ & + \frac{1}{2m_s^2 v_\sigma^2}(\partial J)^4 + \frac{\lambda_{\sigma H}^2 v_\sigma^2}{2m_s^2}|H|^4 - \frac{\lambda_{\sigma H}}{m_s^2}(\partial J)^2|H|^2\,. \end{aligned} \tag{C.44}$$

Note the presence of higher dimension operators: i) the third line describes interactions between the new fermions and the Majoron, $D = 7$ operators, and ii) the first operator in the last line describes Majoron self-interactions, $D = 8$ operator.

Moreover, we also have effective $D = 5$ operators resulting from the fermion field redefinition in Equation (6.46). Once this transformation has been done, the Majoron appears in the kinetic terms of the fermions, namely

$$\begin{aligned} i\overline{\Psi}\not{\partial}\Psi \quad \to \quad & ie^{iJ/(2v_\sigma)}\overline{\Psi}\not{\partial}\left(e^{-iJ/(2v_\sigma)}\Psi\right) = i\overline{\Psi}\gamma^\mu\left(\frac{-i}{2v_\sigma}(\partial_\mu J)\,\Psi + \partial_\mu\Psi\right) = \\ & = i\overline{\Psi}\not{\partial}\Psi + \frac{1}{2v_\sigma}(\overline{\Psi}\gamma^\mu\Psi)(\partial_\mu J) \\ & = i\overline{\Psi}\not{\partial}\Psi + \frac{1}{2v_\sigma}\mathcal{O}_{\Psi J}\,. \end{aligned} \tag{C.45}$$

Finally, let us show a peculiar cancellation regarding the operator $|H|^6$. For this discussion, the relevant terms from the scalar potential in Equation (C.34) are

$$V \supset \frac{1}{2}\frac{m_s^2}{v_\sigma}s^3 + \frac{1}{2}\lambda_{\sigma H}|H|^2 s^2\,. \tag{C.46}$$

Now, we substitute back the expression for s given in Equation (C.38), and keep only the relevant terms for the discussion. Finally, we get:

$$V \supset \frac{1}{2}\frac{m_s^2}{v_\sigma}\left(-\frac{\lambda_{\sigma H}^3 v_\sigma^3}{m_s^6}\left|H\right|^6\right) + \frac{1}{2}\lambda_{\sigma H}\left|H\right|^2\left(\frac{\lambda_{\sigma H}^2 v_\sigma^2}{m_s^4}\left|H\right|^4\right) = 0\,. \tag{C.47}$$

Therefore, the $|H|^6$ operator is not generated in this model.

C.4 Integrating out heavy mediators in Models C

Model C1

The Lagrangian of the model reads

$$\mathcal{L}_{\text{C1}} \supset -\frac{1}{4} Z'_{\mu\nu} Z'^{\mu\nu} + \frac{1}{2} m^2_{Z'} Z'_\mu Z'^\mu + g_N \overline{N_R} \gamma^\mu N_R Z'_\mu + g_\chi \overline{\chi_L} \gamma^\mu \chi_L Z'_\mu \,, \tag{C.48}$$

with $Z'_{\mu\nu} = \partial_\mu Z'_\nu - \partial_\nu Z'_\mu$ the field strength tensor. Now, using the EoM for Z'_μ we get

$$g_N \overline{N_R} \gamma^\mu N_R + g_\chi \overline{\chi_L} \gamma^\mu \chi_L + m^2_{Z'} Z'^\mu - \partial_\nu \left(Z'^{\mu\nu} \right) = 0 \,, \tag{C.49}$$

where the last term can be written as

$$\partial_\nu \left(Z'^{\mu\nu} \right) = \partial_\nu \left(\partial^\mu Z'^\nu - \partial^\nu Z'^\mu \right) = \partial^\mu \left(\partial Z' \right) - \partial^2 Z'^\mu \,. \tag{C.50}$$

Therefore, the EoM for Z'_μ reads

$$\left(\partial^2 + m^2_{Z'} \right) Z'^\mu - \partial^\mu \left(\partial Z' \right) + g_N \overline{N_R} \gamma^\mu N_R + g_\chi \overline{\chi_L} \gamma^\mu \chi_L = 0 \,. \tag{C.51}$$

In addition, assuming that the momentum of the vector boson, corresponding to the derivative, is much smaller than its mass (for the EFT approach to hold), we obtain from the EoM the following expression for Z'^μ:

$$Z'^\mu \simeq -\frac{1}{m^2_{Z'}} \left[g_N \overline{N_R} \gamma^\mu N_R + g_\chi \overline{\chi_L} \gamma^\mu \chi_L \right] \,. \tag{C.52}$$

Now, we can rewrite the Lagrangian in Equation (C.48) as:

$$\begin{aligned} \mathcal{L}_{\text{C1}} \supset & -\frac{1}{4} \left[\partial_\mu (Z'_\nu Z'^{\mu\nu}) - \partial_\nu (Z'_\mu Z'^{\mu\nu}) \right] \\ & + \frac{1}{2} \left[\left(\partial^2 + m^2_{Z'} \right) Z'^\mu - \partial^\mu \left(\partial Z' \right) + g_N \overline{N_R} \gamma^\mu N_R + g_\chi \overline{\chi_L} \gamma^\mu \chi_L \right] Z'_\mu \\ & + \frac{1}{2} Z'_\mu \left(g_N \overline{N_R} \gamma^\mu N_R + g_\chi \overline{\chi_L} \gamma^\mu \chi_L \right) \,. \end{aligned} \tag{C.53}$$

In the last equation we can neglect the total derivative terms in the first line, whereas the second line is zero by Equation (C.51). Therefore we get the Lagrangian

$$\mathcal{L}_{\text{C1}} \supset \frac{1}{2} Z'_\mu \left(g_N \overline{N_R} \gamma^\mu N_R + g_\chi \overline{\chi_L} \gamma^\mu \chi_L \right) \,, \tag{C.54}$$

which after substituting back the expressions for the heavy vector boson field in Equation (C.52) yields the following effective interactions:

$$\begin{aligned} \mathcal{L}^{\text{eff}}_{\text{C1}} = & -\frac{g_N^2}{2m^2_{Z'}} \left(\overline{N_R} \gamma^\mu N_R \right) \left(\overline{N_R} \gamma_\mu N_R \right) - \frac{g_\chi^2}{2m^2_{Z'}} \left(\overline{\chi_L} \gamma^\mu \chi_L \right) \left(\overline{\chi_L} \gamma_\mu \chi_L \right) \\ & - \frac{g_N g_\chi}{m^2_{Z'}} \left(\overline{N_R} \gamma^\mu N_R \right) \left(\overline{\chi_L} \gamma_\mu \chi_L \right) \,. \end{aligned} \tag{C.55}$$

Finally, this effective Lagrangian can be expressed in terms of the operators defined in Table 6.1 using also the Fierz transformed version of $\mathcal{O}_1$, $\mathcal{O}_4$ and $\mathcal{O}_5$ given in Equations (6.5), (6.40) and (6.41), respectively. Therefore, we get:

$$\mathcal{L}_{\text{C1}}^{\text{eff}} = -\frac{g_N^2}{m_{Z'}^2}\mathcal{O}_4 - \frac{g_\chi^2}{m_{Z'}^2}\mathcal{O}_5 + \frac{2g_N g_\chi}{m_{Z'}^2}\mathcal{O}_1\,. \tag{C.56}$$

Model C2

This is the gauged version of Model B2, with the covariant derivate defined in Equation (6.53). From the EFT point of view, it is convenient to go to the unitary gauge, and then σ in Equation (6.44) is real in each point of spacetime, and the Majoron J disappears from the theory. This can also be seen in the following way.

The Lagrangian of the model is given by

$$\mathcal{L}_{\text{C2}} = \mathcal{L}_{\text{kin}} - \left[f\overline{N_R^c}N_R\sigma + g\overline{\chi_L}\chi_L^c\sigma + \text{H.c.}\right] + \left|D_\mu\sigma\right|^2 - V(\sigma,H) - \frac{1}{4}Z'_{\mu\nu}Z'^{\mu\nu}\,, \tag{C.57}$$

with $V(\sigma,H)$ given in Equation (6.34), and $\mathcal{L}_{\text{kin}}$ containing the kinetic terms

$$\mathcal{L}_{\text{kin}} = \overline{N_R}i\not{D}N_R + \overline{\chi_L}i\not{D}\chi_L + \overline{\psi}i\not{D}\psi\,, \tag{C.58}$$

with $\psi = l,\, e_R,\, Q,\, u_R,\, d_R$. Using the exponential parameterisation for σ in Equation (6.44), we clearly see that the kinetic term of the complex scalar involves the Majoron. However, if the vector boson Z'_μ transforms like

$$Z'_\mu \to Z'_\mu + \alpha\partial_\mu J\,, \tag{C.59}$$

we can remove the Majoron from the kinetic term of the complex scalar choosing a specific value for the coefficient α, which we assume to be real. Then, from the kinetic term of the complex scalar we obtain

$$\begin{aligned}\left|D_\mu\sigma\right|^2 = \;& \frac{1}{2}\left(\partial s\right)^2 + \frac{1}{2}m_{Z'}^2 Z'_\mu Z'^\mu\left(1+\frac{s}{v_\sigma}\right)^2 \\ & + \frac{1}{2}\left(\partial J\right)^2\left(1+\frac{s}{v_\sigma}\right)^2\left[1 + m_{Z'}^2\alpha^2 - 2g'Q_\sigma v_\sigma\,\alpha\right] \\ & + \left(\partial_\mu J\right)Z'^\mu\left(1+\frac{s}{v_\sigma}\right)^2\left[m_{Z'}^2\,\alpha - g'Q_\sigma v_\sigma\right]\,,\end{aligned} \tag{C.60}$$

with $m_{Z'} = g'Q_\sigma v_\sigma$, and Q_σ the $B-L$ charge of the complex scalar given in Table (6.4). In the last equation, we can remove the terms that involve the Majoron J if

$$\alpha = \frac{1}{g'Q_\sigma v_\sigma}\,. \tag{C.61}$$

Having this in mind, and after minimising the scalar potential and re-phasing the fields as in Equation (6.46) to remove the Majoron from the Yukawa interactions, we obtain the following Lagrangian from Equation (C.57):

$$\begin{aligned}\mathcal{L}_{\text{C2}} = &-\frac{1}{4}Z'_{\mu\nu}Z'^{\mu\nu} + \overline{N_R}i\partial\!\!\!/ N_R + \overline{\chi_L}i\partial\!\!\!/\chi_L + \overline{\psi_1}i\partial\!\!\!/\psi_1 + \overline{\psi_2}iD\!\!\!/\psi_2 \\ &+ \frac{(\partial_\mu J)}{2v_\sigma}\overline{N_R}\gamma^\mu N_R\left(1+\frac{2Q_N}{Q_\sigma}\right) + \frac{(\partial_\mu J)}{2v_\sigma}\overline{\chi_L}\gamma^\mu\chi_L\left(-1+\frac{2Q_\chi}{Q_\sigma}\right) \\ &+ \frac{(\partial_\mu J)}{2v_\sigma}\overline{\psi_1}\gamma^\mu\psi_1\left(1+\frac{2Q_{\psi_1}}{Q_\sigma}\right) \\ &+ g'Z'^\mu\left(Q_N\overline{N_R}\gamma_\mu N_R + Q_\chi\overline{\chi_L}\gamma_\mu\chi_L\right) - \frac{s}{\sqrt{2}}\left[f\overline{N_R^c}N_R + g\overline{\chi_L}\chi_L^c + \text{H.c.}\right] \\ &- \left[\frac{1}{2}m_N\overline{N_R^c}N_R + \frac{1}{2}m_\chi\overline{\chi_L}\chi_L^c + \text{H.c.}\right] + \frac{1}{2}m_{Z'}^2Z'_\mu Z'^\mu\left(1+\frac{s}{v_\sigma}\right)^2 \\ &+ \frac{1}{2}(\partial s)^2 - \frac{1}{2}m_s^2s^2\left(1+\frac{s}{v_\sigma}+\frac{s^2}{4v_\sigma^2}\right) - \frac{1}{2}\lambda_{\sigma H}v_\sigma^2\left(1+\frac{s}{v_\sigma}\right)^2|H|^2\,, \end{aligned} \tag{C.62}$$

with

$$m_N = \sqrt{2}fv_\sigma \quad \text{and} \quad m_\chi = \sqrt{2}gv_\sigma\,. \tag{C.63}$$

Note that now $\psi_1 = l$, e_R and $\psi_2 = Q$, u_R, d_R. We can check that the terms $(\partial_\mu J)\,\overline{N_R}\gamma^\mu N_R$, $(\partial_\mu J)\,\overline{\chi_L}\gamma^\mu\chi_L$ and $(\partial_\mu J)\,\overline{\psi_1}\gamma^\mu\psi_1$ vanish due to the $B-L$ charge of the fields, see *e.g.* Table 6.4. However, regarding the latter term, what happens for ψ_2? In this case, one can always make a field redefinition in such a way that the terms with $(\partial_\mu J)$ vanishes. For instance, for the quark doublet we can transform the field as

$$Q \to Qe^{-iJa/v_\sigma}\,, \tag{C.64}$$

with a an arbitrary number. With this redefinition of the quark doublet, we get from its kinetic term

$$\overline{Q}iD\!\!\!/Q = \overline{Q}i\partial\!\!\!/Q + g'Q_QZ'_\mu\overline{Q}\gamma^\mu Q + \frac{(\partial_\mu J)}{v_\sigma}\overline{Q}\gamma^\mu Q\left(a+\frac{Q_Q}{Q_\sigma}\right)\,. \tag{C.65}$$

Therefore, if $a = -Q_Q/Q_\sigma$ the last term vanishes. Similar procedure can also be done for u_R and d_R with different a for each one.

Having all these considerations in mind, the Lagrangian in Equation (C.62) yields

$$\begin{aligned}\mathcal{L}_{\text{C2}} = &-\frac{1}{4}Z'_{\mu\nu}Z'^{\mu\nu} + \overline{N_R}i\partial\!\!\!/ N_R + \overline{\chi_L}i\partial\!\!\!/\chi_L + \overline{\psi}i\partial\!\!\!/\psi \\ &+ g'Z'^\mu\left(Q_N\overline{N_R}\gamma_\mu N_R + Q_\chi\overline{\chi_L}\gamma_\mu\chi_L + Q_\psi\overline{\psi}\gamma_\mu\psi\right) - \frac{s}{\sqrt{2}}\left[f\overline{N_R^c}N_R + g\overline{\chi_L}\chi_L^c + \text{H.c.}\right] \\ &- \left[\frac{1}{2}m_N\overline{N_R^c}N_R + \frac{1}{2}m_\chi\overline{\chi_L}\chi_L^c + \text{H.c.}\right] + \frac{1}{2}m_{Z'}^2Z'_\mu Z'^\mu\left(1+\frac{s}{v_\sigma}\right)^2 \\ &+ \frac{1}{2}(\partial s)^2 - \frac{1}{2}m_s^2s^2\left(1+\frac{s}{v_\sigma}+\frac{s^2}{4v_\sigma^2}\right) - \frac{1}{2}\lambda_{\sigma H}v_\sigma^2\left(1+\frac{s}{v_\sigma}\right)^2|H|^2\,. \end{aligned} \tag{C.66}$$

Now, we proceed with the integration out of the heavy mediators of the model, namely s and Z'. Focusing first on s, and using its EoM given by[2]

$$\left(\partial^2 + m_s^2\right) s + \lambda_{\sigma H} v_\sigma \left|H\right|^2 - \frac{m_{Z'}^2}{v_\sigma} Z'_\mu Z'^\mu + \frac{1}{\sqrt{2}} \left[f \overline{N_R^c} N_R + g \overline{\chi_L} \chi_L^c + \text{H.c.}\right] = 0\,, \quad \text{(C.67)}$$

we can get the following expression for the field s:

$$s \simeq -\frac{1}{m_s^2} \left[\lambda_{\sigma H} v_\sigma \left|H\right|^2 - \frac{m_{Z'}^2}{v_\sigma} Z'_\mu Z'^\mu + \frac{1}{\sqrt{2}} \left[f \overline{N_R^c} N_R + g \overline{\chi_L} \chi_L^c + \text{H.c.}\right]\right]. \quad \text{(C.68)}$$

In the last equation we apply that the momentum of s, corresponding to the derivative, is assumed to be much smaller than its mass (for the EFT approach to hold).

Moreover, we can rewrite the Lagrangian in Equation (C.66) as

$$\begin{aligned}
\mathcal{L}_{\text{C2}} \supset\ & \frac{1}{2}\partial_\mu \left(s \partial_\mu s\right) - \frac{1}{4} Z'_{\mu\nu} Z'^{\mu\nu} + \frac{1}{2} m_{Z'}^2 Z'_\mu Z'^\mu \\
& - \frac{s}{2} \left[\left(\partial^2 + m_s^2\right) s + \lambda_{\sigma H} v_\sigma \left|H\right|^2 - \frac{m_{Z'}^2}{v_\sigma} Z'_\mu Z'^\mu + \frac{1}{\sqrt{2}} \left[f \overline{N_R^c} N_R + g \overline{\chi_L} \chi_L^c + \text{H.c.}\right]\right] \\
& + g' Z'^\mu \left(Q_N \overline{N_R} \gamma_\mu N_R + Q_\chi \overline{\chi_L} \gamma_\mu \chi_L + Q_\psi \overline{\psi} \gamma_\mu \psi\right) \\
& - \frac{s}{2} \left[\lambda_{\sigma H} v_\sigma \left|H\right|^2 - \frac{m_{Z'}^2}{v_\sigma} Z'_\mu Z'^\mu + \frac{1}{\sqrt{2}} \left[f \overline{N_R^c} N_R + g \overline{\chi_L} \chi_L^c + \text{H.c.}\right]\right]. \quad \text{(C.69)}
\end{aligned}$$

In the last equation we can omit the total derivative term in the first line, whereas the second line is zero by Equation (C.67). Therefore, the relevant part of the Lagrangian for obtaining the effective interactions after substituting back the expression for s given in Equation (C.68) is:

$$\begin{aligned}
\mathcal{L}_{\text{C2}}^{\text{eff}} \supset\ & \frac{1}{2m_s^2} \left[\lambda_{\sigma H} v_\sigma \left|H\right|^2 - \frac{m_{Z'}^2}{v_\sigma} Z'_\mu Z'^\mu + \frac{1}{\sqrt{2}} \left[f \overline{N_R^c} N_R + g \overline{\chi_L} \chi_L^c + \text{H.c.}\right]\right]^2 \\
& - \frac{1}{4} Z'_{\mu\nu} Z'^{\mu\nu} + \frac{1}{2} m_{Z'}^2 Z'_\mu Z'^\mu \\
& + g' Z'^\mu \left(Q_N \overline{N_R} \gamma_\mu N_R + Q_\chi \overline{\chi_L} \gamma_\mu \chi_L + Q_\psi \overline{\psi} \gamma_\mu \psi\right). \quad \text{(C.70)}
\end{aligned}$$

Once we have eliminated s from the interactions, let us proceed with the heavy vector boson. Now, from the EoM for Z'_μ given by

$$\begin{aligned}
& m_{Z'}^2 Z'_\mu \left\{1 - \frac{2}{m_s^2 v_\sigma} \left[\lambda_{\sigma H} v_\sigma \left|H\right|^2 + \frac{1}{\sqrt{2}} \left[f \overline{N_R^c} N_R + g \overline{\chi_L} \chi_L^c + \text{H.c.}\right]\right]\right\} \\
& \qquad + g' \left(Q_N \overline{N_R} \gamma_\mu N_R + Q_\chi \overline{\chi_L} \gamma_\mu \chi_L + Q_\psi \overline{\psi} \gamma_\mu \psi\right) - \partial_\nu Z'^{\mu\nu} = 0\,, \quad \text{(C.71)}
\end{aligned}$$

[2] We keep only the leading terms in $1/v_\sigma$.

we can get the following expression for Z'_μ:

$$Z'_\mu \simeq -\frac{g'}{m^2_{Z'}} \left(Q_N \overline{N_R} \gamma_\mu N_R + Q_\chi \overline{\chi_L} \gamma_\mu \chi_L + Q_\psi \overline{\psi} \gamma_\mu \psi \right) . \tag{C.72}$$

In the last equation we apply that the momentum of the vector boson, corresponding to the derivative, is assumed to be much smaller than its mass.

Now, we can write the Lagrangian in Equation (C.70) as[3]

$$\begin{aligned} \mathcal{L}^{\text{eff}}_{\text{C2}} \supset & -\frac{1}{4}\left[\partial_\mu (Z'_\nu Z'^{\mu\nu}) - \partial_\nu (Z'_\mu Z'^{\mu\nu})\right] + \frac{1}{2}\left[\,\text{EoM}\,\right] Z'_\mu \\ & + \frac{\lambda^2_{\sigma H} v^2_\sigma}{2 m^2_s} |H|^4 + \frac{\lambda_{\sigma H} v_\sigma}{\sqrt{2} m^2_s} |H|^2 \left[f \overline{N^c_R} N_R + g \overline{\chi_L} \chi^c_L + \text{H.c.} \right] \\ & + \frac{1}{4 m^2_s} \left[f \overline{N^c_R} N_R + g \overline{\chi_L} \chi^c_L + \text{H.c.} \right]^2 \\ & + \frac{1}{2} Z'^\mu \left(Q_N \overline{N_R} \gamma_\mu N_R + Q_\chi \overline{\chi_L} \gamma_\mu \chi_L + Q_\psi \overline{\psi} \gamma_\mu \psi \right) . \end{aligned} \tag{C.73}$$

Regarding the first line in the last equation, we can neglect the total derivative terms, whereas the term written as $[\,\text{EoM}\,]$ is zero due to Equation (C.71). Therefore, we get the Lagrangian

$$\begin{aligned} \mathcal{L}^{\text{eff}}_{\text{C2}} \supset \; & \frac{\lambda^2_{\sigma H} v^2_\sigma}{2 m^2_s} |H|^4 + \frac{\lambda_{\sigma H} v_\sigma}{\sqrt{2} m^2_s} |H|^2 \left[f \overline{N^c_R} N_R + g \overline{\chi_L} \chi^c_L + \text{H.c.} \right] \\ & + \frac{1}{4 m^2_s} \left[f \overline{N^c_R} N_R + g \overline{\chi_L} \chi^c_L + \text{H.c.} \right]^2 \\ & + \frac{1}{2} Z'^\mu \left(Q_N \overline{N_R} \gamma_\mu N_R + Q_\chi \overline{\chi_L} \gamma_\mu \chi_L + Q_\psi \overline{\psi} \gamma_\mu \psi \right) . \end{aligned} \tag{C.74}$$

Finally, after substituting back in the last effective Lagrangian the expression for Z'^μ given in Equation (C.72), we obtain the following operators up to $D = 6$:

- From the first line in Equation (C.74), apart from the correction to the quartic coupling of the Higgs field, we get the $D = 5$ operators:

$$\frac{f \lambda_{\sigma H} v_\sigma}{\sqrt{2} m^2_s} \mathcal{O}_{NH} + \frac{g \lambda_{\sigma H} v_\sigma}{\sqrt{2} m^2_s} \mathcal{O}^\dagger_{\chi H} + \text{H.c.} \,. \tag{C.75}$$

- From the second line in Equation (C.74), we get the $D = 6$ operators:

$$\left[-\frac{f g}{m^2_s} \mathcal{O}_2{}^\dagger + \frac{f g}{2 m^2_s} \mathcal{O}_3 + \text{H.c.} \right] + \frac{f^2}{2 m^2_s} \mathcal{O}_4 + \frac{g^2}{2 m^2_s} \mathcal{O}_5 \,. \tag{C.76}$$

[3] We keep only terms at leading order in $1/v_\sigma$, and neglect the ones that would generate higher-dimensional operators.

- From the third line in Equation (C.74), we get the $D = 6$ operators:

$$-\frac{g'^2}{m_{Z'}^2}\left[Q_N^2\mathcal{O}_4 + Q_\chi^2\mathcal{O}_5 + \frac{Q_\psi^2}{2}\mathcal{O}_{\psi\psi} - 2Q_N Q_\chi \mathcal{O}_1 + Q_N Q_\psi \mathcal{O}_{N\psi} + Q_\chi Q_\psi \mathcal{O}_{\chi\psi}\right]. \tag{C.77}$$

See also Table 6.1 for the definition of the operators.

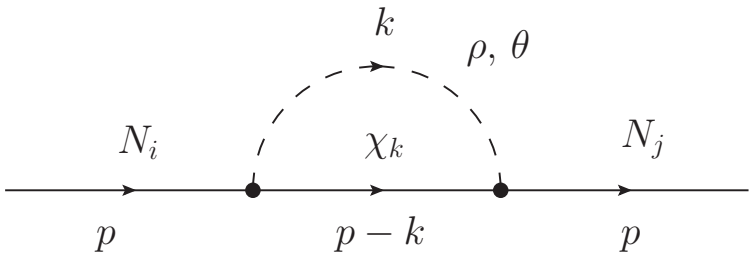

Figure C.1: *Radiative generation of m_N in Model A2c. Note that the arrows indicate the flux of momentum.*

C.5 Sterile neutrino mass in Model A2c

Computation of the sterile neutrino mass at one loop

The relevant part of the Lagrangian in Equation (6.33) for the computation of the sterile neutrino mass at one loop is

$$-\mathcal{L}_{\text{A2}} \supset \mathcal{L}_N = \overline{N_R} f \chi_L \sigma + \overline{\chi_L} f^\dagger N_R \sigma^* \,, \tag{C.78}$$

where we assume n_N and n_χ generations of N_R and χ_L, respectively. Therefore, f is a $n_N \times n_\chi$ complex matrix, in general, and we also work in the χ_L basis in which m_χ is diagional, with real and positive entries m_{χ_k}. Note that this computation of the sterile neutrino mass at one loop is analogous to that of the Scotogenic model [68].

The Lagrangian in Equation (C.78) can be written in terms of the real and imaginary parts of the complex scalar, $\sigma = (\rho + i\theta)/\sqrt{2}$, as

$$\mathcal{L}_N = \frac{\rho}{\sqrt{2}} \overline{\chi} \left(f^T P_L + f^\dagger P_R \right) N + \frac{i\theta}{\sqrt{2}} \overline{\chi} \left(f^T P_L - f^\dagger P_R \right) N \,, \tag{C.79}$$

where N and χ are the Majorana fields in Equation (6.3), and $P_{L,R}$ are the usual chiral projectors given in Equation (6.25).

The real and the imaginary parts of the complex scalar generate a contribution to the sterile neutrino self-energy, as can be seen in Figure C.1. This basically gives

$$-i \left\{ \left[\sum(p) \right]^{(\rho)} + \left[\sum(p) \right]^{(\theta)} \right\} \equiv \left[-i \sum(p) \right]^{(\rho+\theta)} \,, \tag{C.80}$$

and the radiative correction to m_N can be calculated from the last equation by means of

$$m_N = \left[\sum(p = 0) \right]^{(\rho+\theta)} \,. \tag{C.81}$$

One the one hand, the ρ contribution is given by

$$\begin{aligned} \left[-i \sum(p) \right]^{(\rho)} = \left(\frac{-i}{\sqrt{2}} \right)^2 \left(f P_L + f^* P_R \right)_{jk} \int \frac{d^4k}{(2\pi)^4} \frac{i(\not{p} - \not{k} + m_{\chi_k})}{(p-k)^2 - m_{\chi_k}^2} \frac{i}{k^2 - m_\rho^2} \\ \left(f^T P_L + f^\dagger P_R \right)_{ki} \,. \end{aligned} \tag{C.82}$$

Doing some algebra, this contribution can be written as

$$\left[-i\sum(p)\right]^{(\rho)} = \frac{A}{2} I_1 + \frac{B}{2} m_{\chi_k} I_2 \,, \tag{C.83}$$

with

$$A = f_{jk} f_{ik}^* P_R + f_{jk}^* f_{ik} P_L \,, \tag{C.84}$$

$$B = f_{jk} f_{ik} P_L + f_{jk}^* f_{ik}^* P_R \,, \tag{C.85}$$

$$I_1 = \int \frac{d^4k}{(2\pi)^4} \frac{(\not{p} - \not{k})}{(k^2 - m_\rho^2)\left[(p-k)^2 - m_{\chi_k}^2\right]} \,, \tag{C.86}$$

$$I_2 = \int \frac{d^4k}{(2\pi)^4} \frac{1}{(k^2 - m_\rho^2)\left[(p-k)^2 - m_{\chi_k}^2\right]} \,. \tag{C.87}$$

$$\tag{C.88}$$

Now, changing the variable of integration $k \to k' + p$ in the integral I_1 in Equation (C.86) we get

$$I_1 = -\int \frac{d^4k'}{(2\pi)^4} \frac{\not{k}'}{\left[(k'+p)^2 - m_\rho^2\right](k'^2 - m_{\chi_k}^2)} \,, \tag{C.89}$$

which after introducing a Feynman parameter to combine the two propagators reads

$$I_1 = -\int_0^1 dx \int \frac{d^4\hat{k}}{(2\pi)^4} \frac{(\hat{\not{k}} - x\not{p})}{(\hat{k}^2 - L_\rho^2(p))^2} \,, \tag{C.90}$$

with

$$\hat{k} = k' + xp \quad \text{and} \quad L_\rho^2(p) = x\left[(x-1)p^2 - m_{\chi_k}^2 + m_\rho^2\right] + m_{\chi_k}^2 \,. \tag{C.91}$$

The part proportional to $\hat{\not{k}}$ in the integral in Equation (C.90) vanishes because it is odd in $\not{k}$, and therefore we end up with the following integral:

$$I_1 = \not{p} \int_0^1 x\, dx \int \frac{d^4\hat{k}}{(2\pi)^4} \frac{1}{(\hat{k}^2 - L_\rho^2(p))^2} \,. \tag{C.92}$$

To compute the integral in $\not{k}$, we consider

$$I = \int \frac{d^d\hat{k}}{(2\pi)^d} \frac{1}{(\hat{k}^2 - L_\rho^2(p))^2} \quad \text{with} \quad d = 4 - \epsilon \,. \tag{C.93}$$

Therefore, in the limit $\epsilon \to 0$ we recover the original integral in $\hat{k}$. In this case, the f coupling in the Lagrangian in Equation (C.78) has some residual part from this generalisation to d dimensions. In fact, from the mass terms of the fermions and the scalar, we can check that now the dimension of the coupling is

$$[f] = \mu^0\, \mu^{\epsilon/2} \,, \tag{C.94}$$

with μ having dimensions of mass. In view of that, we can redefine the f coupling in the Lagrangian in Equation (C.78) as

$$f \to f^{(4)}\,\mu^{\epsilon/2}\,, \tag{C.95}$$

where the superscript refers to $d = 4$. With this redefinition of the coupling, the terms A and B in Equations (C.84) and (C.85) have now the $f^{(4)}$, although for simplifying the notation the superscript will be omitted in what follows. Moreover, we can insert the μ term which arises after the redefinition in Equation (C.95) in the integral I given in Equation (C.93), which can be computed using the standard results for this kind of integrals, see *e.g.* Appendix A.4 in Ref. [266]:

$$I = \mu^{\epsilon}\int \frac{d^d\hat{k}}{(2\pi)^d}\frac{1}{(\hat{k}^2 - L_\rho^2(p))^2} = \frac{i}{(4\pi)^2}(4\pi)^{\epsilon/2}\Gamma\left(\frac{\epsilon}{2}\right)\left(\frac{L_\rho^2(p)}{\mu^2}\right)^{-\epsilon/2}. \tag{C.96}$$

Using the expansion of the Euler gamma function near the pole

$$\Gamma\left(\frac{\epsilon}{2}\right) \simeq \frac{2}{\epsilon} - \gamma + \mathcal{O}(\epsilon)\,, \tag{C.97}$$

and also that

$$x^{\epsilon} = e^{\epsilon \ln x} \xrightarrow[\epsilon\to 0]{} \simeq 1 + \epsilon \ln x\,, \tag{C.98}$$

we can express the Equation (C.96) as:

$$I = \frac{i}{16\pi^2}\left(\frac{2}{\hat{\epsilon}} - \ln\frac{L_\rho^2(p)}{\mu^2}\right). \tag{C.99}$$

Here we have defined

$$\frac{2}{\hat{\epsilon}} \equiv \frac{2}{\epsilon} - \gamma + \ln 4\pi\,, \tag{C.100}$$

where γ is the Euler-Mascheroni constant. Note that the arbitrary mass scale μ compensates the dimension of L_ρ^2 in the logarithm of Equation (C.99).

Finally, we substitute back these results in Equation (C.83) yielding

$$\left[-i\sum(p)\right]^{(\rho)} = \frac{i}{32\pi^2}\left[\int_0^1 dx\,(A\not{p}x + Bm_{\chi_k})\left(\frac{2}{\hat{\epsilon}} - \ln\frac{L_\rho^2(p)}{\mu^2}\right)\right]. \tag{C.101}$$

Similarly, one can compute the contribution from θ:

$$\left[-i\sum(p)\right]^{(\theta)} = \frac{i}{32\pi^2}\left[\int_0^1 dx\,(A\not{p}x - Bm_{\chi_k})\left(\frac{2}{\hat{\epsilon}} - \ln\frac{L_\theta^2(p)}{\mu^2}\right)\right]. \tag{C.102}$$

Finally, the sum of both the ρ and the θ contributions is:

$$\left[-i\sum(p)\right]^{(\rho+\theta)} = \frac{i}{32\pi^2}\left\{\int_0^1 dx\left[A\not{p}x\left(\frac{4}{\hat{\epsilon}} - \ln\frac{L_\rho^2(p)\,L_\theta^2(p)}{\mu^4}\right) + Bm_{\chi_k}\ln\frac{L_\theta^2(p)}{L_\rho^2(p)}\right]\right\}. \tag{C.103}$$

As stated in Equation (C.81), the mass for the sterile neutrino generated radiatively is given by

$$\left[\sum(p=0)\right]^{(\rho+\theta)} = \frac{Bm_{\chi_k}}{32\pi^2}\int_0^1 dx \ln\frac{L_\rho^2(0)}{L_\theta^2(0)}\,. \tag{C.104}$$

The integral in x can be easily computed yielding

$$\int_0^1 dx \ln\frac{L_\rho^2(0)}{L_\theta^2(0)} = F\left(m_\rho^2, m_\theta^2, m_{\chi_k}^2\right)\,, \tag{C.105}$$

where we have defined the loop function $F(x,y,z)$ as

$$F(x,y,z) = \frac{x}{x-z}\log\left(\frac{x}{z}\right) - \frac{y}{y-z}\log\left(\frac{y}{z}\right). \tag{C.106}$$

Let us remark that our convention for the sterile neutrino mass term in the Lagrangian is $m_N\overline{N_R^c}N_R$, therefore we have to choose the P_R term in B in Equation (C.85). Finally, substituting back in Equation (C.104) the results from (C.85) and (C.105) , we get the following expression for the sterile neutrino mass:

$$(m_N)_{ij} = \sum_{k=1}^{n_\chi}\frac{f_{ik}^* f_{jk}^* m_{\chi_k}}{32\pi^2}F\left(m_\rho^2, m_\theta^2, m_{\chi_k}^2\right)\,. \tag{C.107}$$

From the definition of $F(x,y,z)$ in Equation (C.106) we clearly see that for $\mu_\sigma^2 = 0$, and hence $m_\rho^2 = m_\theta^2$, this function vanishes. Therefore, the sterile neutrino mass matrix generated at one loop is zero if lepton number is conserved $(\mu_\sigma^2 = 0)$.

Generalised Casas-Ibarra parameterisation

In Model A2c, the mass term for N is generated at one loop, as discussed in Section. 6.4.2. Therefore, we can write the Majorana mass term for electrically neutral fermions as

$$\mathcal{M}_\nu^{1-\text{loop}} = \begin{pmatrix} \overline{\nu_L} & \overline{N_R^c} & \overline{\chi_L} \end{pmatrix} \begin{pmatrix} 0 & m_\text{D} & 0 \\ m_\text{D}^T & m_N & 0 \\ 0 & 0 & m_\chi \end{pmatrix} \begin{pmatrix} \nu_L^c \\ N_R \\ \chi_L^c \end{pmatrix} , \tag{C.108}$$

with m_N being generated at one loop. In the limit of $m_N \gg m_\text{D}$, the expression for the active neutrino masses is given by

$$m_\nu \simeq -m_\text{D} m_N^{-1} m_\text{D}^T , \tag{C.109}$$

with $m_\text{D} = y_\nu v_h/\sqrt{2}$. The mass matrix m_ν can be diagonalised by means of the so called PMNS matrix U_PMNS:

$$U_\text{PMNS}^T \, \kappa \, U_\text{PMNS} = D_\kappa , \tag{C.110}$$

with $\kappa = 2m_\nu/v_h^2$ and D_κ the diagonal matrix with the active neutrino mass eigenstates in its diagonal. From Equations (C.109) and (C.110), working in the basis where m_N is diagonal, we get

$$\left(m_N^{-1/2} \, y_\nu^T \, U_\text{PMNS} \, D_{\sqrt{\kappa^{-1}}}\right)^T \left(m_N^{-1/2} \, y_\nu^T \, U_\text{PMNS} \, D_{\sqrt{\kappa^{-1}}}\right) = 1 \quad \rightarrow \quad \mathcal{R}^T \, \mathcal{R} = 1 , \tag{C.111}$$

where we use the notation $D_{\sqrt{A}} = \sqrt{D_A}$. Therefore, from the last equation one can derive the following expression for the neutrino mass matrix m_N:

$$m_N^{1/2} = y_\nu^T \, U_\text{PMNS} \, D_{\sqrt{\kappa^{-1}}} \, \mathcal{R}^T , \tag{C.112}$$

with $\mathcal{R}$ being an arbitrary orthogonal matrix. Now, we can express m_N using the general formula in Equation (C.107) (also working in the basis where m_χ is diagonal) as:

$$m_N = \frac{f^* \, \tilde{m}_\chi \, f^\dagger}{2(4\pi)^2} , \tag{C.113}$$

with

$$\tilde{m}_\chi \equiv m_{\chi_k} F\left(m_\rho^2, m_\theta^2, m_{\chi_k}^2\right) , \tag{C.114}$$

and the function $F(x, y, z)$ defined in Equation (C.106). From Equations (C.112) and (C.113) we obtain the following expression for the coupling f in terms of the neutrino-related observables:

$$f^\dagger = 4\pi \sqrt{2} \, (\tilde{m}_\chi)^{-1/2} \, \mathcal{Q}^T \left(\mathcal{R} \, D_{\sqrt{\kappa^{-1}}} \mathcal{U}^T \, y_\nu\right) , \tag{C.115}$$

with $\mathcal{Q}$ being an arbitrary orthogonal matrix. In the case of only one generation of neutrinos, this coupling can be written as

$$f = 4\pi \frac{y_\nu \, v_h}{\sqrt{m_\nu \, \tilde{m}_\chi}} , \tag{C.116}$$

where m_ν is the mass of the light (active) neutrino, $m_\nu \simeq 0.05\,\text{eV}$, and v_h is the VEV of the Higgs field, $v_h = 246\,\text{GeV}$.